Exploring the mitochondrial function in muscle and molecular dysregulation in cerebellum in a mouse model for ARCA2, a recessive ataxia with coenzyme Q10 deficiency

Tiphaine Jaeg

UNIVERSITÉ DE STRASBOURG

ÉCOLE DOCTORALE DES SCIENCES DE LA VIE ET DE LA SANTE

Institut de Génétique et Biologie Moléculaire et Cellulaire

THÈSE présentée par :

Tiphaine JAEG

soutenue le : **03 octobre 2017**

pour obtenir le grade de : **Docteur de l'université de Strasbourg**

Discipline/ Spécialité : Aspects moléculaires et cellulaires de la biologie

Exploring the mitochondrial function in muscle and molecular dysregulation in cerebellum in a mouse model for ARCA2, a recessive ataxia with coenzyme Q_{10} deficiency

THÈSE dirigée par :
Dr PUCCIO Hélène — Directrice de Recherche, IGBMC, Inserm U964, UMR 7104 CNRS, Université de Strasbourg

RAPPORTEURS :
Dr RÖTIG Agnès — Directrice de Recherche, Institut Imagine, Inserm U1163
Dr QUINZII Catarina — MD PhD, Assistant Professor, Columbia University Medical Center

AUTRES MEMBRES DU JURY :
Dr DUPUIS Luc — Directeur de recherche, Inserm U1118, Université de Strasbourg

---

MEMBRE INVITE
Dr ISOPE Philippe — Directeur de recherche, INCI, CNRS UPR 3212

Try to leave this world a little better than you found it and, when your turn comes to die, you can die happy in feeling that at any rate you have not wasted your time but have done your best

Robert Baden-Powell

Acknowledgements

I would like to dedicate these first line to Hélène Puccio, my PhD supervisor who accepted to host me in her lab starting from September 2013. Thanks for the freedom you gave me and all what I learned during these four years.

Thanks to the Dr. Luc Dupuis, Philippe Isope and Yvon Trottier who helped us decide what should be the best path to pursue with. Also, a big thank for having evaluated my work at key moments of my thesis which helped me go further.

I would like to thank the Dr. Agnès Rötig, Catarina Quinzii, Luc Dupuis and Philippe Isope for having accepted to evaluate my work, and taken part of their time to read through this manuscript.

I thank Laurence, for the help she has provided me for experiments. Thank for having explained me patiently some assays, how to handle mice, how to deal with mice colonies and how to build cohorts. Thanks also for having accepted to generate and genotype so many mice for the purpose of my experiments. I'm really grateful.

Thanks to Floriana, Leïla and Pankaj with whom I worked with, trying to unravel the cause of ARCA2 and who have cheered me up and shared doubts, questions, ideas about this hard but fascinating project.

Thanks to all the lab members, for the nice discussions we had and all what I learned from you! For sharing protocols, benches, and brainstorming for new experiments and troubleshooting.

Thanks to Nadège and Aurélie, for their kindness and benevolence. You laugh and smiles each day made my everyday life so much nicer! I also greatly appreciated all the little things you did to make my life easier and to help me take decisions for certain experiments.

I now have to dedicate an entire paragraph to Charline, so here you are ;-p! Thanks for having shared the back of the lab with me. I will never forget how we cheered each other up, and for our numerous discussions. Thanks for having been there, with me, late in the lab and for all our debates and brainstorming about protocols, new experimental design, publications and so on. Thanks for having wondered about me and make me realize I needed to slow down at some points to be able to achieve this PhD. Thanks for the numerous giggles that made life in the lab so much nicer and gave me energy to work more and persevere. And a simple big thank for your smiles.

Samantha and Arielle, this PhD would not have been the same without you! We shared our doubts, rejoice, questions… You were always around, even late in the cell culture room or the lab, sharing chocolate or motivation to cheer up. I will never forget these precious moments so thanks!

Thanks also to Angélique, Francesca, Florent, Aurore, Léa, Mélanie, with whom I sometimes ate, and often met in the corridors, thanks for the long discussions, your advices and tips! And thanks for your friendship.

Thanks to the IGBMC platforms and services for all the help provided. Thanks to Nadia, Jean-Luc and Josiane for the electron microscopy. Thanks to Betty, Marion and all the girls from the cell culture facility. A big thanks to Marc, Marcel and Yves who helped me with microscopy. A huge thanks to Pascal for his patience and time, explaining microscopy, building macros to help the little PhD student I was.

Thanks also to Frédéric Doussau, for teaching me how to perform organotypic cultures, immunofluorescence with them, and all the nice ideas he shared.

Thanks to Paulo and Francine, who simplified our PhD lifes. A special thanks to Paulo for having supervised the organization of the PhD retreat. And thanks to Arielle, Samantha, Damola, Hichem, Federica, Tajith and Tiago for the nice PhD retreat we have built up.

Merci à tous les Openlabistes, avec qui j'ai partagé cette belle aventure. Je vous suis reconnaissante pour les parfois longues discussions dans la voiture, direction les interventions, à refaire le monde et surtout la biologie, à essayer de tourner et retourner les problèmes sur lesquels nous bloquions pour nos sujets de thèse. Merci pour vos remarques et idées ! Et merci pour les bons moments passés à expliquer la science simplement.

Merci à ma famille et tous mes amis et qui m'ont encouragé et soutenu tout au long de cette thèse.

Merci à Maëlyne, Soléane, Auxence et Isaure, de m'avoir fait voir la beauté de la vie, d'avoir échangé autant de tendresse, de sourires, d'avoir joué et rit. Pour tous ces moments hors du temps avec vous qui m'ont permis de prendre du recul, de réaliser que la vie est un magnifique cadeau, et m'ont permis de persévérer : MERCI.

A Fanny et Lowik, sans vous la vie aurait beaucoup moins de saveur. Si je réussi cette thèse, c'est en partie grâce à vous. Merci pour les questions et remarques qui m'ont déstabilisé mais qui m'ont permis de me remettre en question et d'avancer. Fanny, merci de comprendre la petite biologiste que je suis et d'avoir partagé tous ces trucs et astuces. Ton soutien a été précieux, tout comme ton sourire et ta joie qui m'ont fait garder le sourire et souvent reprendre des forces. Lowik, tu as le don pour amuser la galerie, semer une bonne ambiance, lancer des phrases cinglantes qui titillent mais permettent de repenser les choses autrement. Merci d'être toi, de rester toujours disponible pour moi et de m'avoir aidé à surmonter ce beau défi, notamment en nous proposant de belles sorties, pique-nique… pour que je puisse faire des pauses et reprendre des forces.

A mes parents, sans qui je ne serais pas là aujourd'hui. Papa et Maman, merci pour votre patience et votre amour. Merci d'être toujours là pour moi tout en me laissant libre. Merci pour vos encouragements, et d'avoir réussi à trouver les mots pour m'aider à surmonter les épreuves et les découragements. Merci de m'avoir forcé à réfléchir, à voir les choses différemment, à sortir de ma zone de confort, à me dépasser et surtout à me poser les bonnes questions au bon moment. Merci d'avoir accepté mes choix, et de m'aider à aller jusqu'au bout. Vous m'avez aidé à murir et vous continuez inlassablement de la faire. Vous avez grandement participé à la réussite de ma thèse (et de beaucoup d'autres belles réussites !).

Enfin je dédie ces dernières lignes à Guillaume, mon mari. Merci de m'accompagner tous les jours sur les chemins de la vie. Merci d'avoir accepté de partager ma vie, et de m'avoir encouragé à faire cette thèse. Merci pour ta patience, surtout lorsque je te disais, j'essaye de ne pas rentrer trop tard et que je n'y arrivais pas. Merci de m'avoir demandé en mariage et d'avoir accepté de m'épouser dans une période où je n'étais pas très présente. Tu es resté là discrètement à mes côtés, sans faillir et j'espère pouvoir en faire autant pour toi. Merci pour tes sourires, tes blagues qui ont toujours su dissiper les nuages et me permettre d'entrevoir la vie et cette thèse beaucoup plus positivement. Merci de m'avoir encouragé tout au long de ces 4 années et de m'avoir sans cesse motivé à aller jusqu'au bout. Tu as ta part dans l'accomplissement de cette thèse !

TABLE OF CONTENT

LIST OF FIGURES

LIST OF TABLES

ABBREVIATIONS

2-DG	2-Deoxy-D-glucose
4-HB	4-hydroxybenzoate
ABL	Abetalipoproteinemia
ADCK	aarF domain-containing protein kinases
ADP	Adenosine diphosphate
AM	Amygdala nuclei
AOA1 and AOA2	Ataxia-oculomotor apraxia 1 and 2
ARCA1 and 3	Autosomal recessive cerebellar ataxia type 1 and 3
ARCA2	Autosomal Recessive Cerebellar Ataxia type 2
ARSACS	Autosomal recessive spastic ataxia of Charlevoix-Saguenay
AT	Ataxia-telangiectasia
ATLD1	Ataxia-telangiectasia-like disorder 1
ATP	Adenosine triphosphate
AVED	Ataxia with vitamin E deficiency
BAT	Brown adipose tissue
BNHS	Boucher-Neuhauser syndrome
cc	Corpus callosum
CoQ	Coenzyme Q
CTX	Cerebrotendinous xanthomatosis
D3V	Dorsal third ventricle
DAPI	4',6-diamidino-2-phenylindole
del	Deletion
DG	Dentate gyrus
dhc	Dorsal hippocampal commissure
DMQ	demethoxyubiquinone
E17.5	Embryonic day 17.5
EAOH	Early-onset ataxia with oculomotor apraxia and hypoalbuminemia
ECAR	Extracellular acidification rate
ER	Endoplamic reticulum
FAD	Flavin adenine dinucleotide
FCCP	Carbonyl cyanide-p-trifluoromethoxyphenylhydrazone
fi	Fimbria hippocampus
FRDA	Friedreich's ataxia
fs	Frameshift mutations
FXTAS	Fragile X tremor-ataxia syndrome
GABA	Gama-aminobutyric acid
GFP	Green fluorescent protein
HAB	3-hexaprenyl-4-aminobenzoic acid
Hb	Habenular nucleus
HBB	3-hexaprenyl-4-hydroxybenzoic acid
HDL	High density lipoprotein

HMG-CoA	3-hydroxy-3-methylglutaryl-coenzyme A
HP	Hippocampus
ic	Internal capsule
ins	Insertion
IOSCA	Infantile onset spinocerebellar ataxia
KO	Knock-out
LDL	Low density lipoprotein
LV	Lateral ventricles
M1	Motor cortex
MIRAS	Mitochondrial recessive ataxia syndrome
Mol	Molecular layer of the hippocampus
MSS	Marinesco-Sjogren syndrome
mt	Mammillothalamic tract
NAD	Nicotinamide adenine dinucleotide
NGS	Normal goat serum
NMDA	N-methyl-D-aspartate
NOX	NADH-oxidase
NPC	Niemann-Pick type C
OCR	Oxygen consumption rate
Oligo	Oligomycin
opt	Optic tract
Or	Hippocampal oriens layer
OXPHOS	Oxidative phosphorylation
P0	Post-natal day 0
pABA	para-aminobenzoic acid
PHARC	Polyneuropathy, hearing loss, ataxia, retinitis pigmentosa, and cataract
PHB	Polyprenyl-4-OH-benzoate
PHYH	phytanoyl-CoA hydroxylase
Pir	Piriform cortex
PP	Pyrophosphate
PTP	permeability transition pore
PTZ	Pentylenetetrazole
qRT-PCR	Real-time quantitative reverse transcription PCR
Rad	Hippocampal stratum radiatum layer
ROS	Reactive oxygen species
Rot/Ant	Rotenone / Antimycine A
RSGc	Retrosplenial granular cortex
S2	Secondary somatosensory cortex
SANDO	Sensory ataxic neuropathy, dysarthria, and ophthalmoparesis
SCA	autosomal dominant spinocerebllar ataxia
SCAN1	Spinocerebellar ataxia, autosomal recessive with axonal neuropathy
SCAR	autosomal recessive spinocerebllar ataxia
SD	Standard deviation

SESAME syndrome	Syndrome with seizures, sensorineural deafness, ataxia, mental retardation, and electrolyte imbalance
shRNA	Short hairpin RNA
SQRDL	Sulfide-quinone oxidoreductase
TBA	Total brain area
TILpy	Total internal hippocampal pyramidal cell layer
UCP	Uncoupling protein
WAT	White adipose tissue
WT	Wild-type
XLSA	X-linked sideroblastic anemia and ataxia

INTRODUCTION

Introduction

This PhD work has been in the continuity of the ARCA2 (Autosomal Recessive Cerebellar Ataxia type 2) mouse model characterization which was previously performed by Floriana Licitra (Licitra, 2013). Her results, and more recent data that we obtained, led to a publication (Stefely et al., 2016). The genetic causes for ARCA2 were discovered in 2008 (Lagier-Tourenne et al., 2008; Mollet et al., 2008) and a mouse model was generated shortly afterwards. It is a constitutive knock-out mouse, deleted in the ARCA2 causing gene: COQ8A (previously named ADCK3 and CABC1).

As the ARCA2 mouse model recapitulated most of the patient's symptoms, the aim of my project was to gain insight into the pathophysiological mechanisms leading to the different phenotypes observed in this model organism.

ARCA2 is also part of the Coenzyme Q (CoQ) deficiencies. Therefore, ataxias are first going to be introduced, followed by cerebellar structures and functions, coenzyme Q functions and biosynthesis, and finally the ARCA2 disease with the observed phenotypes and COQ8A function.

I. Ataxia

The name ataxia comes from ancient Greek, “α”: without /negative and “τάξις”: order, and means the absence of order. It is a syndrome defined by the loss of coordination and balance observed in patients. Various types of ataxia exist, and they are usually classified according to their causes. These causes are broad and range from genetic mutations to infections, including nutritional deficiencies or additional symptoms of other diseases (Van Gaalen et al., 2014; Manto and Marmolino, 2009). Therefore, different classes are defined to differentiate them. A common classification divides ataxias in three categories: acquired, inherited and sporadic.

Sporadic ataxias are mainly defined as ataxias for which genetic or acquired etiology are lacking and with a late onset (Klockgether, 2010; Klockgether et al., 1990).

Acquired ataxias conversely distinguished by the fact that they ensue from toxicity, environmental factors or effects of another disease. It is a heterogeneous group with broad causes. One of the well-known cause of acquired ataxia is chronic alcoholism (Jaatinen and Rintala, 2008). Alcohol, like heavy metals, chemotherapy or anti-epileptic drugs are part of the molecules responsible for toxic ataxias (Nachbauer et al., 2015). Infections, by human immunodeficiency virus, or in case of encephalitis or Creutzfeldt-Jakob diseases are other causes of acquired ataxias (Akbar and Ashizawa, 2015). Furthermore, acquired ataxias can also arise from autoimmune diseases (e.g.: anti glutamic acid decarboxylase antibodies or gluten), focal lesions (e.g.: strokes, anoxia, tumors, trauma), amino acid or vitamin deficiency (e.g.: vitamin B1, B12 or E) (Akbar and Ashizawa, 2015). This shows that ataxia can be induced by a large variety of threats and defects.

Finally, the hereditary ataxias are due to genetic causes and are also multiple. This category of ataxia is further subdivided in three major classes depending on their mode of inheritance: autosomal dominant (SCA), autosomal recessive (SCAR), and the X-linked forms of ataxia. To these types, the episodic (EA which are periodic) and the spastic (SPAX) ataxia are added within the classification of the inherited ataxias (Bird, 2016).

Additional symptoms, like dysarthria and dysphagia (respectively speech and swallowing difficulties) are often found is ataxic patients when the disease progresses. However, what invariably characterizes ataxia is the implication of cerebellum or its afferent or efferent connections (Klockgether, 2007). These neurodegenerative diseases, induced by a defect in cerebellar structures in combination or not

with extra-cerebellar lesions, are therefore named spinocerebellar ataxias (Manto and Marmolino, 2009).

Autosomal recessive ataxias are more frequent than the dominants forms, with a mean prevalence estimated around 3.5:100,000 for the recessive ataxias and around 2.5:100,000 for the autosomal dominant forms (Ruano et al., 2014). These prevalences vary depending on the continents, and even on the countries, probably due to founder mutations localization. The prevalence is calculated as a mean of the prevalence for each disease but specific ataxias, like SCA3 for the dominant forms, and FRDA for the recessive forms, are more frequent. In the case of a dominant ataxia one of the parents is affected but might not be aware or having declared the symptoms when this person has a child, or even at the onset of the child disease, whereas for recessive forms both parents are asymptomatic carriers of a mutation.

1. Autosomal dominant ataxia

The autosomal dominant forms of ataxias mostly have an insidious onset in adulthood (around 35 years old) and the diseases are slowly progressive (Paulson, 2009). Up to date forty-three autosomal dominant ataxias were discovered and they have already been extensively classified (Akbar and Ashizawa, 2015; Bird, 2016). Some of these spinocerebellar ataxias (SCA) have specific symptoms, enabling to discriminate them. This is the case for SCA7 characterized by retinal degeneration (Sailer and Houlden, 2012). Unfortunately, for most of the SCA, the associated phenotypes are common, so genetic testing is needed for determination of the specific gene responsible for the disease.

Autosomal dominant ataxias can be further sub-classified according to the type of mutations inducing the diseases. Part of the SCA are due to nucleotide repeat expansions and the others, to conventional mutations (Akbar and Ashizawa, 2015). Regarding repeat expansions, two different cases emerged: repeats in exons (CAG repeat), leading to polyglutamine expansion, so protein gain of function (for SCA1-3, 6, 7, 17 and DRPLA) or repeats in introns, resulting in RNA gain of function or chromatin modification (SCA 8, 10, 12, 31, 36) (Loureiro et al., 2016; Sailer and Houlden, 2012). For polyglutamine expansions, genetic anticipation is observed: the longer the repeat is, the earlier the disease declares and the more severe it is (Durr, 2010).

Numbering of the SCA was performed according to the chronology of discovery but diseases are gradually being grouped when the same gene was described and assigned for different SCA. This is the case for SCA19 and 22 which are already considered as the same ataxia, as they both arise from

mutations in *KCND3*. It could also be performed for SCA15, 16 and 29 which are induced by mutations in *ITPR1* although the resulting additional symptoms are different (Bird, 2016).

All episodic ataxias described so far and one spastic ataxia (SPAX1) are also due to autosomal dominant mutations (Bird, 2016). At later course, episodic ataxias might be constant but they are first periodic, with transient episodes of incoordination and imbalance (Akbar and Ashizawa, 2015). This periodicity differentiates them from the spinocerebellar ataxias for which the symptoms are uninterrupted and slightly progressive.

2. X-linked ataxias

Few ataxias occur with a X-linked inheritance. Some X-linked ataxias had previously been described but the precise genetic affection could not be determined (Farlow et al., 1987; Schmidley et al., 1987). More recently, six genes have been implicated in these X-linked cerebellar ataxias with the most frequent disease being Fragile X tremor-ataxia syndrome (FXTAS) (Bird, 2016). FXTAS, like some SCA, is due to a repeat expansion in a non-coding DNA region (5' UTR). This disease has the particularity of being due to a *FMR1* premutation. This premutation is an expansion comprising between 55 and 200 repeats and induces a RNA gain of function. In contrast, larger expansions (>200 CGG repeats) induce silencing of the *FMR1* gene, so a loss of function and cause the Fragile X syndrome (Amiri et al., 2008; Oostra and Willemsen, 2009). Two other X-linked ataxias, XLSA (X-linked sideroblastic anemia and ataxia) and SCAX1 are due to mutations in transporters. XLSA is due to mutations in *Abcb7*, coding for a mitochondrial ATP-binding cassette transporter implicated in iron homeostasis, and SCAX1 results from mutations in *Atp2b3*, coding for a plasma membrane calcium ATPase (Bekri et al., 2000; Zanni et al., 2012).

3. Autosomal recessive ataxias

Autosomal recessive ataxias typically begin during childhood or early adulthood, with fewer cases of later onset. They are characterized by a gait and balance defect persistent and progressively worsening (Anheim et al., 2012). Unlike for the SCA, a number has not been assigned each time a new recessive ataxia was discovered. Recessive ataxias are usually classified according to the prevalence of the disease, the other clinical features, or the type of nervous system dysfunction. In an attempt to homogenize classification, a similar system as the SCA is gradually being used, with the acronym SCAR for "SpinoCerebellar Ataxia autosomal Recessive". Yet, not all recessive ataxias have been assigned a

SCAR number. In particular, the most frequent recessive ataxias do not have a SCAR number, whereas the rare ones, with only a few reported families, do. Likewise another acronym: ARCA for "Autosomal Recessive Cerebellar Ataxia" was employed to name three ataxias with pure cerebellar affection, including ARCA2, also named SCAR9 (Sailer and Houlden, 2012).

Like for the SCA, genetic testing is needed to determine which gene is mutated and define the precise disease. Indeed, different mutations, in the same gene, can lead to different age of onset, progression severity and different additional symptoms (Anheim et al., 2012). Furthermore, different recessive ataxias display common clinical features, and some other diseases have ataxia has one of their prominent or secondary feature, which makes it difficult for clinicians to rapidly determine the specific ataxia without a multiple-gene panel test.

As mentioned previously different types of classification are used for recessive ataxias. One of them is based on the affected part of the nervous system and results in three main groups (Anheim et al., 2012). These three groups are listed here and examples of such ataxias are given (and in gray: examples of recessive disorders with ataxia as a prominent feature).

- **Pure cerebellar ataxia (without neuropathy)**

  Autosomal recessive cerebellar ataxia type 1, 2 and 3 (ARCA1 to ARCA3)

  Niemann-Pick type C disease

- **Cerebellar ataxia with pure sensory neuropathy (proprioceptive affection)**

  Friedreich's ataxia (FRDA)

  Ataxia with vitamin E deficiency (AVED)

  Sensory ataxic neuropathy, dysarthria, and ophthalmoparesis (SANDO)

  Infantile onset spinocerebellar ataxia (IOSCA)

  Abetalipoproteinemia (ABL)

- **Cerebellar ataxia with sensorimotor axonal neuropathy (proprioceptive and motor affection)**

  Ataxia-telangiectasia (AT)

  Ataxia and oculomotor apraxia (AOA 1 and 2)

  Autosomal recessive spastic ataxia of Charlevoix-Saguenay (ARSACS)

  Spinocerebellar ataxia with neuropathy (SCAN1)

  Refsum disease (RD)

  Cerebrotendinous xanthomatosis (CTX)

Most of the ataxic patients present cerebellar atrophy, except FRDA and some other pure sensory neuropathy ataxic patients for which an atrophy of the spinal cord is usually observed (Anheim et al., 2012).

The most common recessive ataxias are FRDA, AOA1, AOA2 and AT (Bird, 2016). ARCA2, also known as SCAR9, is a rare form of recessive degenerative ataxia, with approximately 35 reported patients up to date. This disease will be further described later, in a separate section (IV).

Like other types of ataxias, recessive ataxias are heterogeneous, complex and comprise a wide range of deregulated pathways. These pathways can also be used to further sub-classify recessive ataxias in six groups: DNA repair defects, abnormal protein folding, metabolic defect, mitochondrial dysfunction, trafficking and other functions (Manto and Marmolino, 2009; Vermeer et al., 2011). This classification is not redundant with the classification according to nervous system affection, as ataxias with the same type of pathway involved do not lead to the same type of degeneration.

	Ataxia	Gene	Protein	Function
DNA repair defect				
	AT	*ATM*	ATM	DNA repair and cell cycle checkpoint controller
	ATLD1	*MRE11A*	MRE11	DNA repair
	AOA1 (or EAOH)	*APTX*	Aprataxin	single-stranded DNA repair
	AOA2	*SETX*	Senataxin	RNA/DNA helicase
	SCAN1	*TDP1*	Tyrosyl-DNA phosphodiesterase 1	DNA repair
	SCAR23	*TDP2*	Tyrosyl-DNA phosphodiesterase 2	DNA repair
Mitochondrial dysfunction				
	FRDA	*FXN*	Frataxin	Iron-sulphur biogenesis
	IOSCA	*TWNK (or C10orf2)*	Twinkle	Mitochondrial DNA helicase
	SANDO (MIRAS)	*POLG*	DNA polymerase subunit γ-1	Mitochondrial DNA replication
	ARCA2 (SCAR9)	*COQ8A (or ADCK3)*	COQ8A (or ADCK3)	CoQ biosynthesis
	SCAR2	*PMPCA*	Mitochondrial-processing peptidase subunit α	Mitochondrial presequences cleavage

Table 1: Autosomal recessive spinocerebellar ataxia according to the mutated gene functions (based on Beaudin et al., 2017).

AT: ataxia-telangiectasia; ATLD1: ataxia-telangiectasia-like disorder 1; AOA1 and 2: ataxia-oculomotor apraxia 1 and 2; EAOH: early-onset ataxia with oculomotor apraxia and hypoalbuminemia; SCAN1: Spinocerebellar ataxia, autosomal recessive with axonal neuropathy; FRDA: Friedreich's ataxia; IOSCA: infantile onset spinocerebellar ataxia; SANDO: sensory ataxic neuropathy, dysarthria, and ophthalmoparesis; MIRAS: mitochondrial recessive ataxia syndrome, ARCA2: autosomal recessive cerebellar ataxia type 2; SCAR2-23: spinocerebellar ataxia type 2-23.

	Ataxia	Gene	Protein	Function
Protein misfolding				
	ARSACS	*SACS*	Sacsin	Protein folding and quality control
	MSS	*SIL1*	SIL1	Protein translocation and folding
	SCAR16	*STUB1*	E3 ubiquitin-protein ligase CHIP	Misfolded protein degradation
Metabolic defect				
	AVED	*TTPA*	Alpha-tocopherol transfer protein	Vitamin E transport
	CTX	*CYP27A1*	Sterol 26-hydroxylase	Sterol synthesis
	Refsum disease	*PHYH*	phytanoyl-CoA dioxygenase	Peroxisomal fatty-acid oxidation
	BNHS	*PNPLA6*	Neuropathy target esterase	Fatty acid synthesis
	ABL	*MTP*	Microsomal triglyceride transfer protein large subunit	Lipid transport
Trafficking				
	ARCA1 (SCAR8)	*SYNE1*	Nesprin-1	Cytoskeleton-organelle binding
	SCAR15 (Salih ataxia)	*RUBCN (or KIAA0226)*	Run domain Beclin-1-interacting and cysteine-rich domain-containing protein	Endocytosis
	SCAR11	*SYT14*	Synaptotagmin-14	Putative role in exocytosis and vesicular trafficking
	SCAR14	*SPTBN2*	Spectrin β chain, non-erythrocytic 2	Membrane cytoskeleton and membrane protein trafficking
	SCAR20	*SNX14*	Sorting nexin-14	Intracellular trafficking
	SCAR21	*SCYL1*	N-terminal kinase-like protein	Regulation of retrograde Golgi-ER trafficking
Other functions				
	ARCA3 (SCAR10)	*ANO10 (or TMEM16K)*	Anoctamin-10	Calcium signaling
	SESAME syndrome	*KCNJ10*	ATP-sensitive inward rectifier potassium channel 10	Potassium buffering
	SCAR13	*GRM1*	Metabotropic glutamate receptor 1	Neurotransmitter receptor
	SCAR18	*GRID2*	Ionotropic glutamate receptor, δ-2	Neurotransmitter receptor
	SCAR19	*SLC9A1*	Sodium/hydrogen exchanger 1	pH homeostasis

Table 1: Autosomal recessive spinocerebellar ataxia according to the mutated gene functions (continued).

ARSACS: autosomal recessive spastic ataxia of Charlevoix-Saguenay; MSS: Marinesco-Sjogren syndrome; AVED: ataxia with vitamin E deficiency; CTX: cerebrotendinous xanthomatosis; BNHS: Boucher-Neuhauser syndrome; ABL: abetalipoproteinemia ; ARCA1 and 3: autosomal recessive cerebellar ataxia type 1 and 3; BNHS: Boucher-Neuhauser syndrome; ABL: abetalipoproteinemia; SESAME syndrome: seizures, sensorineural deafness, ataxia, mental retardation, and electrolyte imbalance; SCAR2-23: spinocerebellar ataxia type 2-23.

DNA repair defect is one of the pathological mechanism leading to recessive ataxias. This defect comprises mutations in genes necessary to sense, excise and repair DNA damage (Filla and De Michele, 2011). Two categories can be distinguished: single- and double-strand break DNA repair defects. On

the one side, ataxia with oculomotor apraxia type 1 (AOA1) and spinocerebellar ataxia with neuropathy 1 (SCAN1) are part of the single strand break DNA repair defects. AOA1 is due to mutations in the gene coding for aprataxin, a protein involved in the single-strand DNA repair complex (Sano et al., 2004); whereas SCAN1 is due to mutations in the gene coding for TDP1, a tyrosyl-DNA phosphodiesterase, which repairs DNA single-strand breaks (El-Khamisy et al., 2005). On the other side, ataxia–telangiectasia (AT), ataxia–telangiectasia-like disorder (ATLD1) and spinocerebellar recessive ataxia 23 (SCAR23) fall into the double-strand DNA repair defects. ATM, defective in case of AT, phosphorylates substrates involved in DNA repair and cell cycle control (Cortez et al., 1999; Janssen et al., 2011); MRE11, defective in case of ATLD1, has exo- and endo-nuclease activity notably implicated in DNA repair during replication (Costanzo et al., 2001; Garcia et al., 2011; Paull and Gellert, 1998); and TDP2, defective in case of SCAR23, is a 5-prime tyrosyl-DNA phosphodiesterase, which repairs DNA double-strand breaks generated by topoisomerase II during transcription (Gómez-Herreros et al., 2014; Ledesma et al., 2009). AOA2 results from loss of function of senataxin, a RNA/DNA helicase, implicated in R-loop resolution for transcriptional termination (Suraweera et al., 2009; Zhao et al., 2015), and is also considered as part of the DNA repair defects.

Recessive ataxias can also be due to abnormal protein folding. Sacsin, which loss of function induces the autosomal recessive spastic ataxia of Charlevoix-Saguenay (ARSACS), was suggested to act in the ubiquitin-proteasome system in neurons (Parfitt et al., 2009), although more recent data proposed a role in intermediate filament organization but in patient's fibroblasts (Duncan et al., 2017). Marinesco-Sjögren syndrome (MSS) is caused by mutations in SIL1, a protein involved in protein translocation and folding in the endoplasmic reticulum (Anttonen et al., 2005; Buchkremer et al., 2016); and SCAR16 is due to mutations in CHIP or STUB1, an E3 ubiquitin-protein ligase, implicated in protein degradation (Narayan et al., 2015; Sha et al., 2017). All three proteins, sacsin, SIL1 and STIB1, were found to directly or indirectly interact with HSP70, a cellular proteostasis chaperone, in part implicated in recognition and refolding of misfolded or aggregated proteins (Radons, 2016).

Deregulations in cellular metabolism can also lead to recessive ataxias. The range of metabolisms affected is wide and include vitamin, sterols, fatty acid and other lipids synthesis or transport. Ataxia with vitamin E deficiency (AVED) is induced by low levels of α-tocopherol (vitamin E), due to loss of function of the α -tocopherol transfer protein (α-TTP), a protein which regulates vitamin E secretion in plasma (Kono et al., 2013). Cerebrotendinous xanthomatosis (CTX) results from cholesterol and cholestanol deposit due to CYP27A1 deficiency. CYP27A1 (cytochrome P450 27A1), also named sterol 27-hydroxylase, catalyzes the hydroxylation of different sterols, such as cholesterol, for their

elimination (Mast et al., 2017; Milagre et al., 2012). Refsum disease is induced by increased phytanic acid (a branched-chain fatty acid) levels, led by the deficiency in phytanoyl-CoA hydroxylase (PHYH), as PHYH catalyzes the first step of phytanic acid alpha-oxidation for its degradation (Jansen et al., 1997; McDonough et al., 2005). Boucher-Neuhauser syndrome (BNHS) is caused by mutations in *PNPLA6*, a gene encoding a patatin-like phospholipase domain-containing protein 6, also named neuropathy target esterase. The PNPLA6 protein acts both in de-esterification of phosphatidylcholine into fatty acids and glycerophosphocholine (a precursor for acetylcholine biosynthesis), and in the catalysis of 2-arachidonoyl lysophosphatidylinositol (Synofzik et al., 2014), both being part of fatty acid synthesis. Abetalipoproteinemia (ABL), characterized by hypocholesterolemia and malabsorption of lipids, ensue from mutations in the *MTP* gene, encoding the microsomal triglyceride transfer protein (MTP). MTP catalyzes the transport of triglyceride, cholesteryl ester, and phospholipid (Khatun et al., 2013; Lee and Hegele, 2014). All these ataxias are therefore due to altered lipid metabolism. Furthermore, other recessive diseases with defective lipid metabolism, like Niemann-Pick type C (NPC), or PHARC (polyneuropathy, hearing loss, ataxia, retinitis pigmentosa, and cataract) appear with ataxia as one of the clinical manifestation. Niemann-Pick type C is a lipid storage disorder, due to *NPC1* or *NPC2* mutations (Vance, 2006). Both proteins, encoded by these genes, are intracellular cholesterol transporter, egressing cholesterol from endosomes and lysosomes (Infante et al., 2008). PHARC, resembling Refsum disease, is due to a defect in endocannabinoid metabolism, led by mutations in *ABHD12* (Fiskerstrand et al., 2010).

Another mechanism altered in some cases of recessive ataxias is trafficking, although this category is broad, ranging from exo- and endocytosis to protein trafficking. SCAR8, is due to loss of function of nesprin-1, a protein linking the nuclear envelope to the cytoskeleton (King et al., 2014). SCAR14, is due to deficiency in SPTBN2 (βIII-spectrin) which is involved in protein trafficking through interaction with the dynactin complex (Clarkson et al., 2010). Mutations in *SCYL1*, induce SCAR21, and SCYL1 is suggested to be an accessory factor of coatomer I (COPI) complex which mediates retrograde Golgi to endoplamic reticulum (ER) trafficking (Burman et al., 2008; Schmidt et al., 2015). Salih ataxia results from mislocalization of RUBCN, a protein with an inhibitory role on autophagosome and late endosome maturation (Assoum et al., 2013; Sun et al., 2010). Mutations in *SNX14*, inducing SCAR20, lead to lysosome-autophagosome dysfunction (Akizu et al., 2015). *SYT14*, mutated in SCAR11, encodes synaptotagmin 14, a member of a family of protein known to be involved in membrane trafficking and exocytosis of secretory vesicles (Doi et al., 2011). Albeit precise implications of some of these proteins still need to be explored, all of them seem to be involved in vesicles or proteins transport which might be linked to other functions such as protein degradation.

Defective mitochondrial proteins also induce, in some cases, recessive ataxias. Both nuclear and mitochondrial DNA mutations can lead to ataxia but the focus will be put here on nuclear encoded genes. The most frequent recessive ataxia is Friedreich's ataxia (FRDA) due to mutations in the gene encoding frataxin. FRDA pathogenicity arise from trinucleotide repeat expansion, which lead to a loss of function through transcriptional silencing (Campuzano et al., 1996; Groh et al., 2014; Punga and Bühler, 2010). Frataxin is a mitochondrial protein implicated in iron-sulfur cluster biogenesis, and iron-sulfur clusters are cofactors necessary for the function of a variety of protein including proteins of the respiratory chain complex, in DNA repair or metabolism (Colin et al., 2013; Schmucker et al., 2011). Infantile onset spinocerebellar ataxia (IOSCA) and sensory ataxic neuropathy, dysarthria, and ophthalmoparesis (SANDO, also called MIRAS: mitochondrial recessive ataxia syndrome) are both due to dysfunctional mitochondrial replication machinery. The mutated genes encode, in IOSCA, a mitochondrial DNA helicase and, in SANDO, a mitochondrial DNA polymerase (Ropp and Copeland, 1996; Sen et al., 2012). SCAR2 arise from mutations of PMPCA, the α-mitochondrial processing peptidase which participates in the cleavage of mitochondrial precursor proteins for their maturation (Jobling et al., 2015). ARCA2 is characterized by reduced levels of coenzyme Q (CoQ), due to mutations in *COQ8A* (also named *ADCK3* and *CABC1*). COQ8A was recently shown to stabilize CoQ biosynthesis complex (Stefely et al., 2016). Although these are all mitochondrial proteins, their functions are diverse which could bring to reclassify them in other categories, like for SANDO and IOSCA which could be merged with DNA defects if this category was broaden to all types of DNA defects not only nuclear DNA repair defects. ARCA2 could also be added in the metabolism defect group, as CoQ is deficient.

Finally, some other recessive ataxias have mutations in genes for which a function was ascribed. In ARCA3, SESAME syndrome and SCAR19, ionic channels are affected, via a calcium-activated chloride channel, an inwardly rectifying potassium channel and a sodium/hydrogen exchanger, respectively (Guissart et al., 2015; Hartzell et al., 2009; Sala-Rabanal et al., 2010). Regarding SCAR13 and 18, both emerge from mutations in glutamate receptors. GRM1 (mGluR1): the metabotropic glutamate receptor 1 is mutated in SCAR13, whereas GRID2: the ionotropic glutamate receptor δ-2 is mutated in SCAR18 (Guergueltcheva et al., 2012; Hills et al., 2013). These last proteins, ions channels and neurotransmitter receptors, are interesting in regards to the alteration of Purkinje neurons firing occurring in ataxias.

These classifications are not set but are dynamic, as new genes responsible for ataxia continue to be discovered. Discovery of new genes with ataxia as the main clinical feature might also induce the creation of new groups or sub-categories. New families, with already known recessive ataxias, also

continue to come into the clinic, with new or previously described mutations in identified genes, helping clinicians to get a better insight in each of these diseases. Furthermore, some genes functions are more deeply explored which can broaden the spectra of pathophysiological mechanisms implicated. All in all, the general view on ataxia might evolve as the knowledge on each specific ataxia increases. A global understanding will perhaps point towards few common secondary pathomechanism leading to ataxia.

4. Treatable ataxias

Some of the ataxias, for which genetic mutations were identified and gene functions elucidated, can be treated with specific drugs. This is the case for ataxia with vitamin E deficiency, where alpha-tocopherol (vitamin E) can be administered orally to patients. Unfortunately, the maximal efficacy of this treatment is in presymptomatic stages or when very mild signs appear, so early diagnosis is needed (Braga Neto et al., 2016). For abetalipoproteinemia, alpha-tocopherol can also be given to patients. Regarding cerebrotendinous xanthomatosis and Niemann–Pick type C disease, chenodeoxycholic acid and miglustat can be prescribed respectively, to treat patients (Anheim et al., 2012). Another treatment consists in limiting certain food intake, like with a phytanic acid–free diet that will improve Refsum's disease (Braga Neto et al., 2016). It is therefore necessary to identify these types of ataxias rapidly to be able to prevent further decline and try to improve the patient clinical state.

For Coenzyme Q (CoQ) deficiencies, a supplementation with CoQ might be useful and can lead to transient clinical improvement (Anheim et al., 2012). Unfortunately, although ARCA2 is due to a deficit in a gene coding for a regulator of CoQ biosynthesis, CoQ supplementation did not improve the ataxic phenotypes for all the patients in whom it has been tested (Mignot et al., 2013).

Finally, for most ataxias, the only treatment available so far is nonspecific, and relies on physiotherapy, to help patients compensate by reinforcing certain muscles and practicing to delay speech loss for example. New methods might emerge, like cerebellar transcranial direct current stimulation (ctDCS) to modulate cerebellum excitability (Grimaldi et al., 2016) but further testing is needed and different ataxias might need specific stimulations in regards to the affected mechanisms. Lastly, gene therapy is being developed, in particular for Friedreich's ataxia (Perdomini et al., 2014). Results are encouraging but this therapy will only be available for the most frequent ataxias, as they are the only one for which clinical studies can be performed. For most recessive ataxias, a better understanding of the cellular and global dysregulations is therefore needed to be able to find drugs to alleviate patient's symptoms.

II. Cerebellum

Most ataxias are due to cerebellar affection (Anheim et al., 2012). Cerebellum means little brain in Latin. It is part of the hindbrain, with the pons and medulla oblongata, and is located at the back of the cranium under the occipital and temporal lobes of the cerebral cortex. It constitutes approximately one tenth of human brain's volume but contains more neurons than the rest of the brain (Andersen et al., 1992).

1. Structure

a. Topographical anatomy

The cerebellum was found to have a stereotyped structure which is similar in all mammals (Larsell, 1952). The cerebellar cortex, as the cerebral cortex is highly convoluted. Along the mediolateral axis, the cerebellum can be divided into three major regions: the midline part of the cerebellum is called the vermis (worm in Latin, due to its shape), and laterally are two hemispheres. The intermediate zones in between the vermis and the hemispheres are called the paravermis (Figure 1). Two lateral extensions of the hemispheres: the parafloculi and the floculi, extend outward and under the cerebellum (White and Sillitoe, 2013).

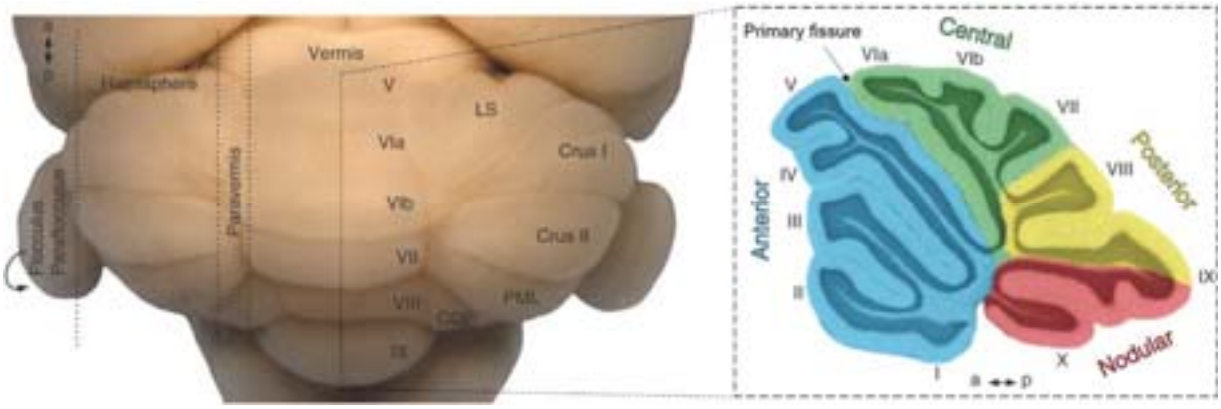

Figure 1 : Cerebellar structure in mice, adapted from (White and Sillitoe, 2013)***.***

a↔p: antero↔posterior axis. Left panel: dorsal view of a mouse cerebellum, with the vermis, paravermis, hemispheres and laterally the parafloculi and floculi. LS: lobulus simplex; PML: paramedian lobule; COP: copula pyramidis. Right panel: cerebellar sagittal section cut through the vermis with the 10 lobules (I-X). Color: transverse zones, blue: anterior domain, green: central domain, yellow: posterior domain, red: nodular domain.

Along the antero-posterior axis of the cerebellum, several fissures separate ten folia. These folia were defined as lobules by Larsell and Bolk, who labeled each lobule with a Roman number (I to X) (Bolk, 1906; Larsell, 1952). These lobules were studied and numbered in sagittal cut of the vermis. Certain

lobules were then grouped into transverse zones according to the expression pattern of certain genes (CaBP, zebrin II and Pcp2) (Ozol et al., 1999). The anterior domain of the cerebellum is separated from the central, posterior and nodular zones, by the primary fissure (Voogd and Glickstein, 1998).

b. Cellular level

At the cellular level, a uniform organization is repeated throughout the cerebellar cortex (Ramnani, 2006). The cerebellar cortex is divided into three different cellular layers: the molecular layer, the Purkinje cell layer and the granular layer (Sillitoe et al., 2012).

The outermost layer, which is the molecular layer, is composed of stellate and basket cells: two types of interneurons, of Purkinje neuron's dendritic tree and of parallel fibers: the axons of the granules cells. Just beneath is the Purkinje cell layer, which comprises the monolayer of Purkinje neurons soma (giving the name of this layer), cell bodies of Candelabrum cells and Bergmann glia. Finally, the innermost layer, the granular layer, is composed of granule cells soma, Golgi cells, Lugaro interneurons, and unipolar brush cells (Figure 2) (Sillitoe et al., 2012).

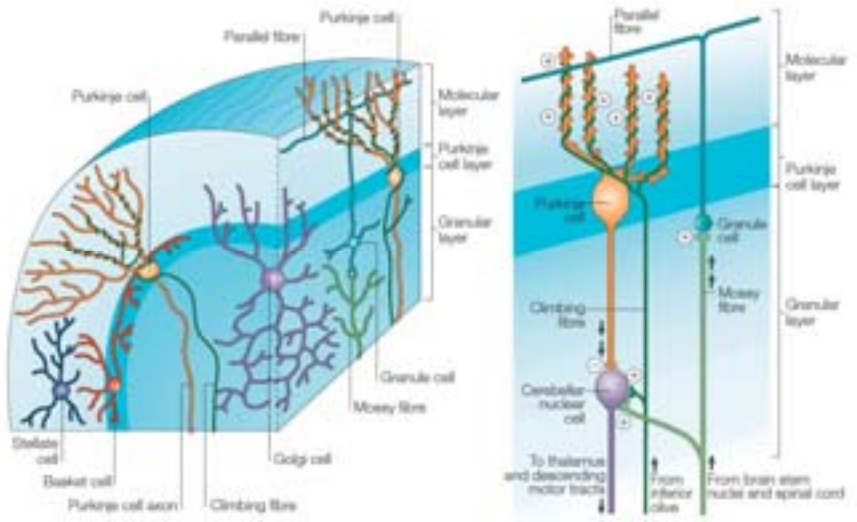

Figure 2 : Cerebellar cortex structure, adapted from (Apps and Garwicz, 2005).

Scheme of neurons and their localization on a sagittal plane. Left panel, orange: Purkinje neurons, dark blue: stellate cell, red: basket cell, purple: Golgi cell, light blue: granule cell. Right panel: excitatory synapses from the inferior olivary and the granule cells with Purkinje neurons and inhibitory output signal from the Purkinje neurons to the cerebellar nuclear cells, and excitatory output from inferior olive and mossy fibers.

The stellate and basket cells are inhibitory interneurons, which project their axons on the Purkinje neuron's dendritic tree, leading to feed-forward inhibition of these Purkinje neurons. More specifically, the axons of the basket cells contact the proximal portion of the Purkinje dendrites and envelop their soma by the formation a "basket" like shape, that gave their name. One basket cell can contact up to ten Purkinje neurons. Both types of interneurons receive excitatory input from granules cells through parallel fibers (Sillitoe et al., 2012). Candelabrum cells are also inhibitory neurons, but their soma is in the Purkinje cell layer, in between the Purkinje cell bodies. They only have one or two thick dendrites which extend through the entire molecular layer and their axon also branches in the molecular layer (Schmahmann, 2007; Sillitoe et al., 2012).

The major type of neurons in the cerebellum are the Purkinje neurons. In human cerebellum, the number of these neurons is estimated to 15 million. They were first characterized by Jan Evangelista Purkinje in 1837, before being extensively studied (Glickstein et al., 2009). The Purkinje neurons are among the largest neurons in the central nervous system. Their cell soma has a pear shape and a diameter of around 35µm. The dendritic tree usually starts with two proximal dendrites that branch multiple times to give rise to a 400µm long dendritic tree in the sagittal plane, that is only 15-20µm thick in the transverse plane, in the molecular layer. Purkinje neurons compute afferent information from different sources, as they receive input from different neurons but the main excitatory synaptic connections are through the parallel fibers formed by the granules cells on the distal dendritic spines, and the climbing fibers emerging from the inferior olive onto the proximal part of the dendrites (Figure 2). The Purkinje myelinated axon extends in the granular layer and terminates in the cerebellar nuclei. Purkinje neurons use gama-aminobutyric acid (GABA) neurotransmitter and are therefore inhibitory. These neurons are critical for the function of cerebellum, as they are the sole output of the cerebellar cortex (Schmahmann, 2007; Sillitoe et al., 2012; Voogd and Glickstein, 1998).

Purkinje cells are the bigger neurons in the cerebellar cortex, but granules cells are the smallest and the most numerous. These granule neurons are excitatory interneurons which use glutamate as their neurotransmitter. They are densely packed in the granular layer and extend three to five dendrites in this same layer. They receive excitatory input from mossy fibers terminals (originating from the brainstem nuclei or the spinal cord) and inhibitory input from Golgi cell's axons. Granule cells project their axons in the molecular layer where they extend as parallel fibers, with a "T" shape, perpendicular to the Purkinje neurons dendritic tree. Each granule cell intersects with multiple Purkinje neurons (up to 300) and drives excitation. Each Purkinje neuron is also contacted by different granule cells. Through

the parallel fibers, granule cells also contact diverse interneurons (Schmahmann, 2007; Sillitoe et al., 2012; White and Sillitoe, 2013).

Golgi cells are inhibitory interneurons, using GABA and glycine as neurotransmitter, unlike stellate and basket cells which only deliver GABA. The soma of these Golgi neurons is localized in the granular layer, where they form inhibitory synapses with granules cell and therefore act in a feed-backward process. The Lugaro cells, also present in the granular layer, exert an inhibitory control of the other interneurons (basket, stellate and Golgi cells) by their axonal collaterals, which mostly reach the molecular layer and become parallel to parallel fibers. Finally, the unipolar brush cells are excitatory interneurons present in the granular layer. The unipolar brush cells receive the main excitatory input from vestibulocerebellar mossy fibers and their axons innervate granules cells and other unipolar brush cells. These neurons provide a feed-forward amplification of mossy fibers excitation on granule cells (Schmahmann, 2007; Sillitoe et al., 2012; White and Sillitoe, 2013).

Glial cells are also present in the cerebellum. In particular, Bergmann glia is a unique type of astrocyte which only exist in the cerebellar cortex. The progenitors of Bergmann glia, radial glia, serve for Purkinje neurons migration during development and Bergmann fibers are then needed for granule cell migration. Bergmann glia have a unipolar appearance: their soma localizes in the Purkinje cell layer and they extend in the molecular layer. These astrocytes form a glial sheath around the soma of Purkinje neurons, as well as around the synapses of the dendritic tree. A bidirectional signaling exist between these neurons and glial cell, enabling the replenishment of the neurotransmitter pool of adjacent neurons and serving in neuronal communication (Schmahmann, 2007; Sillitoe et al., 2012; White and Sillitoe, 2013).

Climbing fibers extend through the three cellular layers but they originate from the inferior olivary nuclei, in the caudal part of the brainstem. These fibers are one of the cerebellar input and synapse directly on the Purkinje dendrites. The excitatory connection between climbing fibers and Purkinje neurons is thought to be one of the most powerful, as one synaptic impulse can depolarize a Purkinje cell and evoke a train of 5-6 action potentials. A Purkinje neuron is only innervated by one climbing fiber, whereas one climbing fiber can innervate more than one Purkinje neuron. During development more climbing fibers contact a Purkinje neuron, but the exuberant fibers are eliminated before the end of the development (Armstrong, 1974; Schmahmann, 2007; Sillitoe et al., 2012; White and Sillitoe, 2013).

Mossy fibers are the other cerebellar input, and arise from cell bodies in the spinal cord and brainstem. They reach the granular layer after entering the cerebellum by one of the three peduncles. Unlike climbing fibers, mossy fibers excite Purkinje neurons indirectly, by the excitation of granule cells. Mossy fibers also synapse with unipolar brush cells and Golgi cells (Cerminara et al., 2015; Schmahmann, 2007).

The deep cerebellar nuclei is composed of 4 nuclei: the fastigial, globose, emboliform and dentate nuclei. They are present in the white matter of the cerebellum and provide the sole output of the cerebellar cortex. Indeed, Purkinje cell's axons are the only collaterals emerging from the cerebellar cortex, and they reach the cerebellar nuclei cells on which they form inhibitory synapses. One Purkinje neuron contact around 35 neurons of the deep cerebellar nuclei and one nuclear neuron receives inputs from more than 800 Purkinje cells. In these nuclei, afferent input and cerebellar cortex output are combined and integrated to be further transmitted. Excitatory output is conveyed to the thalamus, brain stem and cerebral cortex, whereas inhibitory output reaches the inferior olivary nucleus. Output from, as well as input to the cerebellum are conveyed through the cerebellar peduncles. The connection with the other regions of the central nervous system enables the control of movement and the other cerebellar functions (Schmahmann, 2007; Uusisaari and Knöpfel, 2013).

2. Functions and implications

The first hints about cerebellar functions came from the symptoms displayed when cerebellum was damaged. Indeed, an atrophy of the cerebellum often induces ataxia, a lack of steadiness and coordination, in combination with other symptoms. Thanks to neuroanatomy, neuroimaging, neuropsychology and brain stimulation, various cerebellar functions were uncovered and some can even be linked to defined cerebellar regions. The first function to be unraveled was the implication of cerebellum in motor control. The anterior part of the cerebellum (lobules I to V) and the anterior part of lobule VI could be associated with motor-related activation. Furthermore, specific lobules could even be divided according to the sensorimotor region involved: lobules II-V and VIII-IX for the lower limbs, V and VI for the upper limbs, and VI and VIII for the face (Manto et al., 2012; Sokolov et al., 2017).

So far cerebellum has been implicated in the adaptation of motor commands in a spatiotemporal manner: cerebellum coordinate and fine-tunes the timing and force to induce a proper movement. Voluntary task such as writing, walking, catching an object, eye movement pursuit, equilibrium or

posture might be affected in case of cerebellar dysfunction. More recently, modulation of non-motor functions was also assigned to the cerebellum. In particular, a contribution to language, social cognition, emotion, working memory and executive functions could be determined (Habas et al., 2009; Stoodley and Schmahmann, 2009).

More globally, the vermis or midline of the cerebellum was found to be implicated in the control of balance and eye movement, and the paravermal zone in speech. Regarding the hemispheres, an alteration induced syndromes like the incoordination of the limbs (dysmetria), and intention tremor. The control of cognitive operation seems to reside in the hemispheres but more on the posterior lobe. Overall, defects in the cerebellar function contribute to different phenotypes like ataxia, dystonia, tremor, multiple sclerosis, and autism spectrum disorders (Ito, 2008; Manto et al., 2012; Reeber et al., 2013; Sillitoe, 2012).

3. Affections

The implications of certain lobules or regions in precise functions might be explained by a defined input and output connections with a specific brain region or part of the central nervous system. Cerebellar connection with the motor cortex through lobules V, VI, HVIIB and HVIII has been reported in primates (Ramnani, 2006). Furthermore, microzones have been defined in the cerebellum, where Purkinje neurons receive inputs and send outputs to distinct population of neurons. These microzones are thought to be the fundamental functional unit (Oscarsson, 1979).

Even if the cellular organization of the cerebellum appears uniform all over this structure and that Purkinje neurons localization and branching seem similar in every lobule, Hawkes et al. were able to show that all Purkinje neurons do not express the same genes. Zebrin II, also named aldolase C, a glycolytic enzyme, was the first protein found to be differentially expressed in mouse Purkinje neurons (Hawkes et al., 1993). The expression pattern occurs in rostro-caudal stripes which are conserved in between animals and across vertebrates. Further studies enabled to show that zebrin positive and zebrin negative Purkinje neurons fire differently, with zebrin negative neurons firing more frequently (Zhou et al., 2014). A link between the zebrin stripes and the microzones of functional units has not be defined so far.

When the cerebellum is damaged, through genetic or physical insults, Purkinje neurons usually die. Thanks to mouse mutants it appeared that, for specific genetic defects, cell death occurred in a patterned way. An example is the Leaner mice, baring a homozygous mutation for CaV2.1, a P/Q type voltage gated calcium channel. Purkinje cell death appeared more rapidly in the anterior lobe and the cell loss was majorly restricted to Purkinje neurons of the zebrin II negative bands (Heckroth and Abbott, 1994; Herrup and Wilczynski, 1982). In a mouse model of Niemann Pick type C, zebrin II negative Purkinje neurons were also the first to degenerate (Sarna et al., 2003). In other cases, like the mutant mice modeling neurodegeneration or postnatal Purkinje cell degeneration, zebrin positive bands degenerated (Wassef et al., 1987). Finally, in a few cases no degenerating pattern could be observed, for example in a model of dystonia (mutated InsP3R1) (Cerminara et al., 2015; Furutama et al., 2010). The appearance of a degeneration pattern might be dependent of the function of the deleted genes.

III. Coenzyme Q

Coenzyme Q (CoQ or ubiquinone) is a lipophilic molecule ubiquitously present in membranes (Turunen et al., 2004). It is composed of a quinone head group attached to an isoprenoid side chain (itself composed of tandemly linked isoprenyl groups) (Figure 3). The length of the isoprenoid side chain varies depending on the species. In human CoQ_{10} is mostly found, with 10 isoprenyl groups tandemly bound, whereas in rats CoQ_9 is predominant, with 9 isoprenyl groups. However, in both species other forms of CoQ are also found, with CoQ_{10} representing 10-30% of total CoQ content depending on the tissue in rats, and CoQ_9 representing 2-5% of the total CoQ levels in humans (Åberg et al., 1992). In mouse, as in rats, CoQ_9 is the major form of CoQ, whereas in *Saccharomyces cerevisiae* and in *Escherichia coli*, CoQ_6 and CoQ_8 are respectively the predominant forms (Lester and Crane, 1959; Olson and Rudney, 1983).

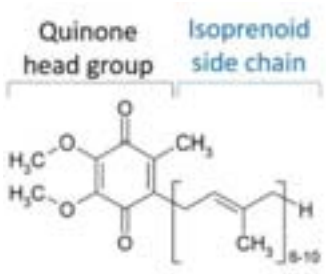

Figure 3 : Coenzyme Q (6 to 10) chemical structure.

CoQ has an intramembranous localization and therefore contributes to membranes structures. The precise CoQ orientation is still under debate due to contradictory results. Like other amphiphilic lipids, the quinone head group might localize near the polar interface of the membranes and the isoprenoid tail in the hydrophobic region (Afri et al., 2004; Lenaz et al., 1992), but it could also be that CoQ lies in the center of the lipid bilayer, parallel to the membrane plane (Hauß et al., 2005; Jemiola-Rzeminska et al., 1996) (Figure 4). CoQ diffusion rate is also debated (Galassi and Arantes, 2015), as for cholesterol its effect on membrane fluidity might depend on the surrounding lipids (Dimova, 2014).

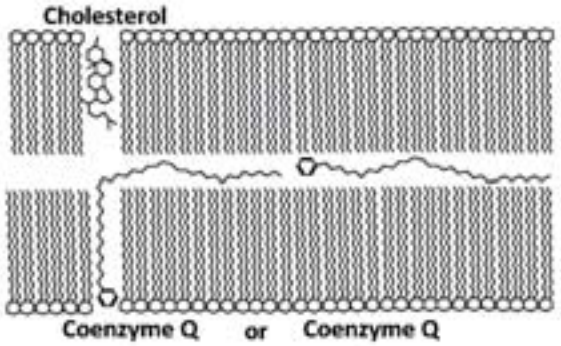

Figure 4 : Two possible coenzyme Q localization in lipid bilayers, adapted from (Turunen et al., 2004).

1. Distribution

Ubiquinone was isolated and described in 1955 by the team of Dr. Morton (Festenstein et al., 1955) and was later, in 1957, found to be present in various tissues membranes (Crane et al., 1957; Lowe et al., 1957). CoQ levels were measured in rats and post-mortem human's tissues and it appeared that the levels vary upon the organs (Table 2). The highest amount of CoQ per gram of tissue, were measured in heart, liver and kidney, both in rats and human (Åberg et al., 1992).

	Rat		*Human*	
	CoQ_9 (µg/g tissue)	CoQ_{10} (µg/g tissue)	CoQ_9 (µg/g tissue)	CoQ_{10} (µg/g tissue)
Heart	202.0 ± 18.5	16.9 ± 1.7	2.5 ± 0.3	114.0 ± 9.2
Liver	130.9 ± 14.8	21.3 ± 2.0	1.8 ± 0.2	54.9 ± 4.1
Kidney	123.9 ± 11.3	22.0 ± 1.9	3.3 ± 0.2	66.5 ± 6.6
Ventricle	55.6 ± 4.9	5.3 ± 0.5	n.d.	11.8 ± 0.8
Intestine	50.9 ± 7.2	19.0 ± 1.6	0.5 ± 0.05	11.5 ± 1.6
Colon	47.5 ± 3.9	8.4 ± 0.7	0.4 ± 0.05	10.7 ± 1.9
Thyroid	43.5 ± 3.7	6.6 ± 0.8	1.2 ± 0.2	24.7 ± 2.0
Muscle	42.6 ± 5.6	3.1 ± 0.3	1.0 ± 0.1	39.7 ± 4.3
Brain	37.4 ± 3.3	18.9 ± 1.5	1.0 ± 0.1	13.4 ± 1.0
Pancreas	37.2 ± 3.2	2.8 ± 0.3	1.6 ± 0.2	32.7 ± 2.8
Testis	32.4 ± 2.9	4.7 ± 0.5	0.4 ± 0.04	10.5 ± 1.1
Spleen	22.9 ± 2.0	9.2 ± 0.8	0.7 ± 0.09	24.6 ± 3.6
Lung	16.9 ± 1.4	2.4 ± 0.3	0.6 ± 0.08	7.9 ± 0.8

Table 2: CoQ_9 and CoQ_{10} content in rats and humans tissues, adapted from (Åberg et al., 1992)***.***

Mean values ± SD. n.d.: not determined.

CoQ levels not only vary depending on the organs, but also depending on the cellular compartments. This variation in content was shown in different cellular fractions extracted from rat liver. CoQ is present in all organellar membrane, nonetheless the highest contents were found in Golgi vesicles, lysosomes and mitochondria (Table 3) (Kalén et al., 1987).

FRACTIONS	**COQ_9 (µg/mg protein)**
Golgi vesicles	2.62 + 0.15
Lysosomes	1.86 + 0.18
Inner mitochondrial membranes	1.86 + 0.13
Mitochondria	1.40 + 0.16
Plasma membranes	0.74 + 0.07
Peroxisomes	0.29 + 0.04
Microsomes	0.15 + 0.02

Table 3 : CoQ_9 amounts in fractions extracted from rat liver, adapted from (Kalén et al., 1987).

Mean values ± SD.

2. Functions

In the 1960's, CoQ was described as having a central role in cellular respiration (Mitchell, 1961) but many other functions were discovered afterward, even though its role in oxidative phosphorylation remains the most extensively studied. On top of its function as an electron transporter in the mitochondrial respiratory chain (Schultz and Chan, 2001), CoQ also acts as an electron transporter in the plasma membrane (Gómez-Díaz et al., 1997; Kishi et al., 1999), and maybe in other cell compartment such as lysosomes (Gille and Nohl, 2000). Furthermore, it is a lipid-soluble antioxidant, a cofactor for uncoupling proteins and is implicated in the mitochondrial transition pore modulation, as well as in pyrimidine synthesis (Bentinger et al., 2010).

Three redox states exists for CoQ: ubiquinone being the fully oxidized form, ubiquinol the fully reduced form and in between ubisemiquinone (also called semiquinone) the partially reduced (Figure 5) (Mellors and Tappel, 1966; Mitchell, 1976). The cycling between the oxidized and the reduced form enable its functions as a coenzyme. This so-called Q cycle, with the exchange of up to two electrons on the quinone head group, allow ubiquinol redox functions in cellular energy production and as an antioxidant.

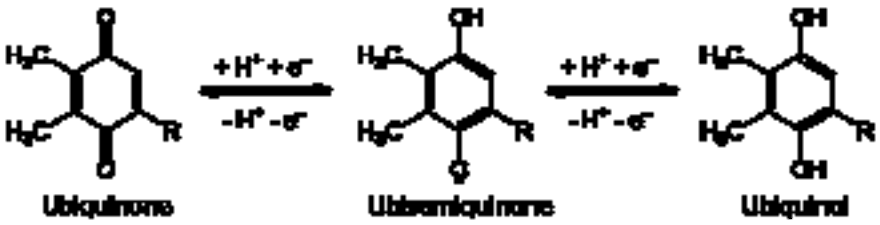

Figure 5 : Redox states of coenzyme Q.

Ubiquinone (fully oxidized), ubisemiquinone (partially reduced), ubiquinol (fully reduced); with R being the isoprenoid side chain.

a. Mitochondrial respiration

The mostly described function of CoQ is its role as an electron shuttle in the mitochondrial respiratory chain. Indeed CoQ transports electrons from complex I and II to complex III of the respiratory chain (Figure 6) (Brandt, 1999; Yu et al., 1999). This transport contributes to the generation of a membrane potential, which is coupled to oxidative phosphorylation, for ATP production. CoQ is in equilibrium between the reduced and the oxidized form. The redox cycle occurs though a two-step transfer: CoQ first receives one electrons (converting ubiquinone to ubisemiquinone), and then a second one

(converting ubisemiquinone to ubiquinol) (Alcázar-Fabra et al., 2016; Trumpower, 1981). These electrons are received from the reactions of acetyl-CoA with NADH (complex I: NADH-CoQ oxidoreductase) or succinate with $FADH_2$ (complex II: succinate-CoQ oxidoreductase), with acetyl-CoA and succinate being part of the citric acid cycle (Lenaz et al., 1993). In complex III, ubiquinol is then converted back to ubiquinone, by the reduction of cytochrome b and c, which further transfers the electrons (Lenaz and Genova, 2010; Mitchell, 1976; Slater, 1983). The electron transport chain require oxygen (in complex IV), which makes it possible to measure mitochondrial respiratory chain activity through measurement of the oxygen consumed (Fried et al., 2014; Pelletier et al., 2014). Mitochondrial respiration is also named oxidative phosphorylation (OXPHOS).

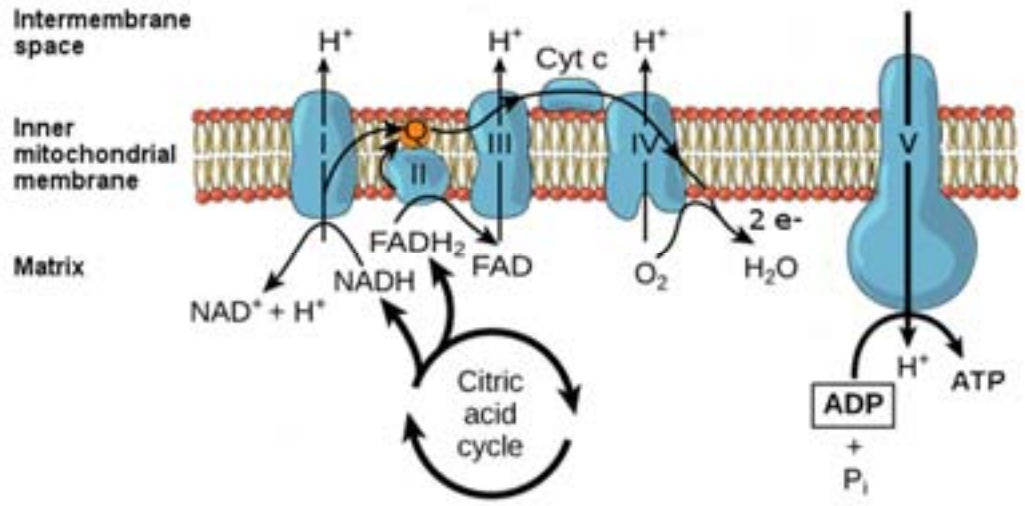

Figure 6 : Mitochondrial respiratory chain with coenzyme Q.

Q (orange): Coenzyme Q; Complex I: NADH-coenzyme Q oxidoreductase; complex II: succinate-Q oxidoreductase; complex III: Q-cytochrome c oxidoreductase; complex IV: cytochrome c oxidase; complex V: ATP synthase; Cyt c: cytochrome c; NADH and $FADH_2$ are two coenzymes which are reduced in the citric acid cycle, NAD: nicotinamide adenine dinucleotide, FAD: flavin adenine dinucleotide, ADP: adenosine diphosphate, ATP: adenosine triphosphate, Pi: inorganic phosphate.

b. Electron transport

As CoQ is present in all cellular membranes, it should therefore play a role in every compartment. Actually, CoQ acts as an electron transporter in the plasma membrane (Gómez-Díaz et al., 1997; Kishi et al., 1999). To maintain or adapt cellular pH, protons are released to the extracellular space through a Na+/H+ antiport, and CoQ participates in the activation of this antiport by transferring electrons (Crane et al., 1991). Furthermore, to maintain cellular redox homeostasis, an NADH-oxidase (NOX) oxidizes cytosolic NADH to NAD^+. CoQ shuttles the electron for this oxidation (Löw et al., 2012; Morré

and Morré, 2011). Therefore, CoQ is involved both in pH and redox homeostasis across the plasma membrane.

In mitochondria, on top of the action of CoQ in complex I and II of the mitochondrial respiration, it transfers electrons from an enzyme of the pyrimidine biosynthesis route, precisely from dihydroorotase dehydrogenase (DHOH), to the respiratory chain (Evans and Guy, 2004). Furthermore, sulfide-quinone oxidoreductase (SQRDL), another mitochondrial protein, involved in sulfide metabolism, also requires CoQ as an electron transporter (Ackermann et al., 2011).

The capacity of CoQ to shuttle electrons might also be used in lysosomes to translocate protons from the cytosol into the lysosomal lumen. This mechanisms would acidify the lysosomes, through a NADH-dependent CoQ reductase (Gille and Nohl, 2000), but further research are needed, to clarify this function. CoQ role in other cells compartments, such as Golgi vesicles, where the highest content was found, still need to be uncovered.

c. Antioxidant

Mammalian cells mostly rely on aerobic metabolism, and all cells are capable of using this type of metabolism for energy production (Böning et al., 2012). Oxygen is consumed in this respiratory metabolism, and produces reactive oxygen species (ROS). Although most of the ROS is estimated to be produced in the mitochondria, at the level of complex I and III, it can also be generated in other cells compartments such as the peroxisomes or the cytosol (Finkel and Holbrook, 2000). When ROS are excessively produced (as superoxide radicals: $O_2^{\cdot-}$, hydrogen peroxide H_2O_2 or hydroxyl groups $HO^{\cdot}$), it generates oxidative stress. These ROS can oxidize other molecules, like proteins, lipids or DNA, which can be harmful for the cells (Ernster and Forsmark-Andrée, 1993). To prevent the damages that can be caused by ROS, antioxidants are used by the cells. Ubiquinol serves as one of the antioxidants, by scavenging ROS (Mellors and Tappel, 1966; Papa and Skulachev, 1997). Other antioxidants include vitamin C and E, and enzymes such as superoxide dismutase, catalase or glutathione peroxidase (Finkel and Holbrook, 2000). CoQ, as an antioxidant, can inhibit oxidation of proteins, DNA and lipids. For lipid peroxidation, CoQ quenches the initiation of lipid radicals which prevents lipid peroxidation propagation and therefore protects from further lipid and proteins oxidations (Bentinger et al., 2010).

As for other antioxidants, CoQ needs to be regenerated to the reduced form to keep its antioxidant properties. This can be done through the NADH-CoQ reductase in the mitochondria (in respiratory

complex III), but also by enzymes in other cell compartments, such as lipoamide dehydrogenase or DT-diaphorase (Beyer et al., 1996; Xia et al., 2001).

d. Other functions

The mitochondrial permeability transition pore (PTP) has been involved in cell death induced by oxidative stress, as its inhibition led to antiapoptotic effects (Baines et al., 2005; Schinzel et al., 2005). PTP is an inner mitochondrial channel, which allows an unselective diffusion of molecules smaller than 1500 Da when opened (Zoratti and Szabò, 1995). Its's opening, upon calcium accumulation, disrupt mitochondrial structure and cause the release of proapoptotic factors (Ichas and Mazat, 1998). CoQ was first shown to block PTP opening (Fontaine et al., 1998; Papucci et al., 2003), therefore having an antiapoptotic effect. Nonetheless, more recently, its seems that CoQ modulates differently PTP depending on the cell types (Devun et al., 2010). Still CoQ is implicated in the regulation of the mitochondrial permeability transition pore but either as an inhibitor or as an activator (Belliere et al., 2012; Walter et al., 2000).

Besides its modulation role for the PTP, CoQ acts as a cofactor for mitochondrial uncouplers (Echtay et al., 2001). Uncoupling proteins, located in the inner mitochondrial membrane, allow the translocation of protons from the intermembrane space to the matrix of mitochondria. This proton translocation reduces the protons gradient and therefore the activity of oxidative phosphorylation, replacing ATP by heat production (Echtay et al., 2000). Uncoupling is mostly used in brown adipose tissue for thermogenesis (Klingenberg and Huang, 1999; Nedergaard et al., 2001).

In conclusion, CoQ functions mostly rely on its activity as an electron shuttle.

3. Biosynthesis

Although ubiquinone and ubiquinol can be taken up from diet, the major source of CoQ present in membranes is derived from *de novo* synthesis (Bentinger et al., 2003). This lipid is endogenously synthesized through a complex metabolic pathway, implicating at least 10 different enzymes (Coq1p to Coq10p in yeast). Most of the current knowledge on its biosynthesis comes from studies in yeast and bacteria with CoQ-deficient mutants (Aussel et al., 2014; Tran and Clarke, 2007). Biosynthesis in the mitochondria was extensively studied but it appears that it can also be produced in the endoplasmic reticulum (ER) and the Golgi (Kalen et al., 1990; Mugoni et al., 2013; Teclebrhan et al.,

1995). Yet, additional research is needed regarding CoQ synthesis in Golgi and ER, because only two enzymes were discovered to be implicated in this mechanism so far.

a. Mevalonate pathway

CoQ is built up starting from two precursors: a benzoquinone ring derived from phenylalanine or tyrosine and an isoprenoid chain derived from the mevalonate pathway (Laredj et al., 2014). The mevalonate pathway gives rise to different isoprenoid lipids such as ubiquinone, cholesterol and dolichol starting from acetyl-coenzyme A (Grünler et al., 1994). All these lipids are therefore linked by a unique starting point, which when deregulated, could lead to aberrant levels of specific lipid species.

Through a series of sequential reactions, starting from acetyl-CoA, farnesyl-pyrophosphate is generated by the mevalonate pathway. One of the intermediate step is the conversion of HMG-CoA (3-hydroxy-3-methylglutaryl-coenzyme A) to mevalonate, by the HMG-CoA reductase (HMGCR), which is the rate controlling enzyme of the mevalonate pathway. HMG-CoA reductase can be inhibited with drugs like statins. These inhibitors are used to reduce the rate of the mevalonate pathway, notably to treat hypercholesterolemia (Chang et al., 2017). The mevalonate then goes through a series of different steps of phosphorylation and decarboxylation to yield farnesyl pyrophosphate. Farnesyl pyrophosphate being the last common substrate for synthesis of the different isoprenoid lipids including cholesterol and CoQ (Dallner and Sindelar, 2000). It is a branching point, as the pathways are then specific for each lipid (Figure 7).

The first step dedicated to cholesterol synthesis, is performed by squalene synthase (FDFT1), catalyzing the conversion of 2 molecules of farnesyl pyrophosphate into squalene (Ortiz de Montellano et al., 1977). Regarding CoQ synthesis, the first committed step is the conversion of farnesyl pyrophosphate in polyprenyl pyrophosphate, by the trans-prenyl transferase. Polyprenyl pyrophosphate being the precursor of CoQ isoprenoid side chain (Bentinger et al., 2010).

CoQ differentiate from the other isoprenoid lipids by the addition of an nonisoprenoid moiety, a benzoate ring. This benzoquinone ring, is predominantly derived from tyrosine, through a series of steps leading to 4-hydroxybenzoate (Ernster and Dallner, 1995).

The first steps of the mevalonate pathway, from acetyl-CoA to farnesyl pyrophosphate, are thought to occur in the cytosol or have multilocal distribution, in Golgi or ER (Grünler et al., 1994), whereas the steps dedicated to CoQ biosynthesis occur in the mitochondria (Laredj et al., 2014).

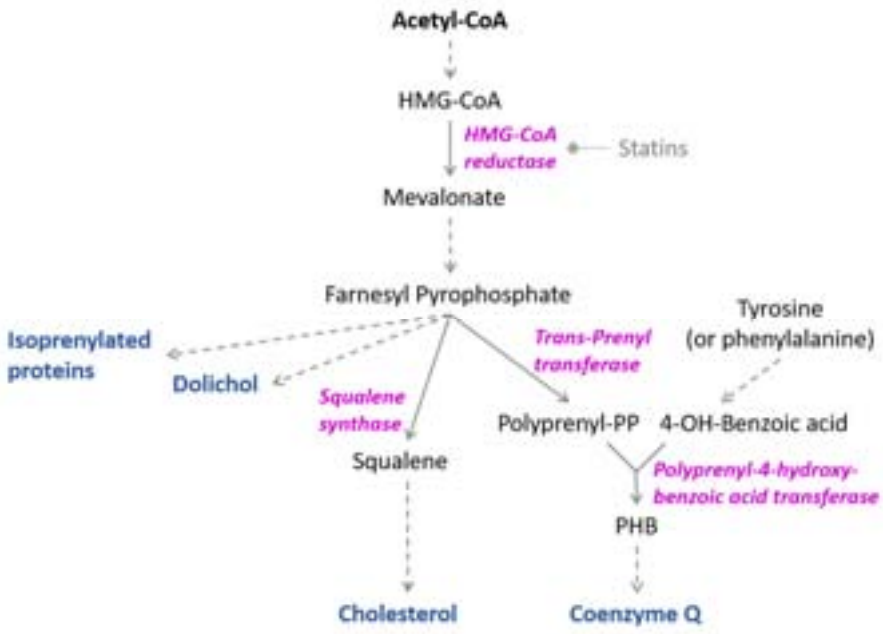

Figure 7 : Mevalonate pathway, adapted from (Bentinger et al., 2010).

Pathway enabling the production of isoprenoid products (blue). Key enzymes are depicted (purple). HMG-CoA: 3-hydroxy-3-methylglutaryl-coenzyme A; PP: pyro-phosphate; PHB: polyprenyl-4-OH-benzoate.

b. Complex Q

The focus will be put on eukaryotic biosynthesis, based on the knowledge acquired from yeast. So far, in the unicellular eukaryote *S. cerevisiae*, 13 genes (coq1-11, Yah1 and Arh1) were found to be implicated in the biosynthesis of CoQ in the mitochondria (Allan et al., 2015; Tran and Clarke, 2007). *Coq1* to *Coq9* deleted yeast strains were shown to lack CoQ_6 production and to have severe respiratory defect as these strains could not grow on non-fermentable carbons sources (Tran and Clarke, 2007). The first step, in the generation of CoQ from farnesyl pyrophosphate, is performed by the Coq1 enzyme in yeast, and Pdss1/Pdss2 in animal cells (Saiki et al., 2005). These enzymes, trans-prenyl transferase, condense the farnesyl pyrophosphate molecules to generate an isoprenoid chain with a defined length (corresponding to the final CoQ isoprenoid side chain length, so 9 or 10 in human, rats and mouse, and 6 in *S. cerevisiae*) (Okada et al., 1996). Subsequently, the isoprenoid side chain (polyprenyl pyrophosphate) and the quinone head moiety (4-hydroxybenzoate: 4-HB) are condensed to HBB (3-hexaprenyl-4-hydroxybenzoic acid) by Coq2, a polyprenyltransferase (Figure 8) (Ashby et al., 1992). In *S. cerevisiae*, para-aminobenzoic acid (pABA) was found to be an alternative quinone ring for the generation of HHB by Coq2 (Marbois et al., 2010). Afterwards, only the benzoquinone ring will be subjected a series of modifications.

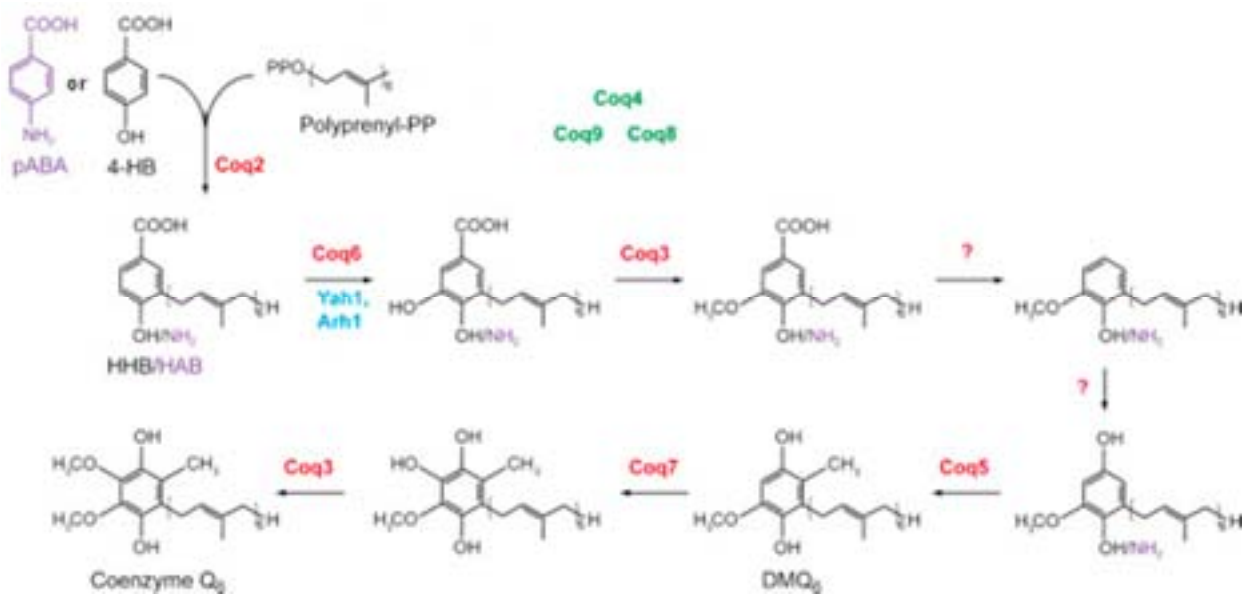

Figure 8 : Coenzyme Q biosynthesis in mitochondria of S.cerevisiae, adapted from (Laredj et al., 2014).

In red: enzymes implicated in the modifications of the benzoquinone ring, in blue: enzymes required for the modification; in green: accessory subunit with undefined functions but probably implicated in the regulation of the pathway; *pABA, para-aminobenzoic acid; 4-HB: 4-hydroxybenzoate; polyprenyl-PP: polyprenyl pyrophosphate; HHB: 3-hexaprenyl-4-hydroxybenzoic acid; HAB: 3-hexaprenyl-4-aminobenzoic acid; DMQ, demethoxyubiquinone;* Yah1: ferredoxin and Arh1: ferredoxin reductase.

The first benzoquinone ring modification, a hydroxylation of the C5 position, is catalyzed by Coq6 (Ozeir et al., 2011). Yah1 and Arh1, ferredoxin and ferredoxin reductase respectively, seem to be the enzymes providing electrons for the hydroxylation by Coq6 (Pierrel et al., 2010). The next step, an O-methylation, is carried out by Coq3 (Poon et al., 1999). A decarboxylation, and a hydroxylation are then performed, but the enzymes have not been discovered yet. Coq5 catalyzes the only C-methylation, and Coq7 the last hydroxylation, followed by the last step: a second O-methylation, again performed by Coq3 (Laredj et al., 2014; Wang and Hekimi, 2013a). The functions of these catalytic enzymes were discovered due to the accumulation of CoQ intermediates in the specific *Coq* mutants.

Coq4, Coq8 and Coq9 are three Coq proteins for which a catalytic function could not be assigned. Their molecular functions have not been identified yet but they could act as regulators of the CoQ biosynthesis. Nonetheless, Coq4 and Coq9 were suggested to play a role in the maintenance or the assembly of a CoQ biosynthesis complex (He et al., 2015; Marbois et al., 2009). Indeed, in yeast, the Coq proteins act in a biosynthesis complex, present in the mitochondrial matrix and associated to the inner mitochondrial membrane (He et al., 2014; Tran and Clarke, 2007). Some clues about the formation of a complex, came from Blue Native PAGE analysis and gel filtration which showed that Coq3 and Coq4, and Coq3, Coq4, Coq5 and Coq6 respectively, appeared together with a high molecular

mass (Marbois et al., 2005). Furthermore, in the absence of single Coq proteins, other Coq proteins were degraded, reinforcing the idea of a complex (Tran and Clarke, 2007). By tandem affinity purification, tagged Coq3, Coq4, Coq5, Coq7 and Coq9 were shown to be associated in one or more complex (Allan et al., 2015). Coq10 and Coq11, have undefined functions, but Coq11 was found to associate with the complex by tagged affinity purification (Allan et al., 2015). Coq8 was postulated as being a regulatory subunit. Coq8 deficiency in *S. cerevisiae* was shown to decrease the levels of Coq4, Coq6, Coq7 and Coq9 and to perturb Coq3, Coq5 and Coq7 phosphorylation state (Hsieh et al., 2007; Xie et al., 2011), but it is unsure if the phosphorylations are direct or indirect effects and if they influence the functioning of the biosynthesis complex. Overexpression of Coq8 in *Coq3-Coq7* and *Coq9* null mutants was shown to restore the protein levels of certain Coq protein, so it should stabilize the complex formed by the Coq3-Coq7 and Coq9 proteins (Xie et al., 2012). Furthermore, Coq8 was shown to coprecipitate with Coq6 (Allan et al., 2015). The formation of a complex and the enzymatic activities of Coq1-Coq7 are well established in yeast, but the precise functions of Coq4, Coq8 and Coq9 and the regulation of this complex remains to be determined.

The knowledge on the CoQ biosynthesis came from studies in yeast and was extrapolated to mammals, but some mechanisms might diverge. Mammalian homologues could be identified for all yeast's *Coq* genes by sequence homology, and some protein activities were confirmed by functional complementation (Wang and Hekimi, 2013a). By sequence homology, two yeast Coq proteins were each found to have 2 homologs in mice and humans. This is the case for the yeast Coq1, present in mammals as PDSS1 and PDSS2, and Coq8, having COQ8A and COQ8B orthologs in mammals.

To study the phenotypes and the implicated mechanisms in mammals, some models were generated. Knock-out mouse models of certain *Coq* genes are available: *Pdss2*, *Coq3*, *Coq4*, *Coq7* and *Coq9*, and other studies were performed in patients fibroblasts (Licitra and Puccio, 2014; López et al., 2014). *Pdss2* as well as *Coq3*, *Coq4* and *Coq7* complete knock-out mouse, are embryonic lethal (IMPC; Lapointe et al., 2012; Levavasseur et al., 2001; Lu et al., 2012), highlighting the importance of these enzymes and CoQ for normal development.

4. Deficiencies

Mutations in *PDSS1*, *PDSS2*, *COQ2*, *COQ4*, *COQ6*, COQ7, *COQ9*, *COQ8A* and *COQ8B* have been identified in humans, as leading to heterogeneous diseases with CoQ deficiencies. Surprisingly, the CoQ deficiencies in human and mice are a heterogeneous group of rare diseases with complex clinical

symptoms (Licitra and Puccio, 2014). These symptoms include 5 major phenotypes: encephalomyopathy, severe infantile multisystemic disease, isolated nephropathy, cerebellar ataxia and isolated myopathy (Quinzii et al., 2014). The CoQ deficiencies can be divided into two classes: primary CoQ deficiencies, due to mutations in genes implicated in the CoQ biosynthesis, and secondary CoQ deficiencies, due to mutations in genes not directly implicated in CoQ biosynthesis. For a number of patients, genetic diagnosis is lacking (Rahman et al., 2012). Thereby causes of CoQ deficiency cannot be determined, and suggest that other genes or conditions, not described so far, might lead to lowering of CoQ levels and broaden the spectra.

a. Primary deficiencies

Severe infantile multisystemic disease has been associated with *PDSS1*, *PDSS2, COQ2, COQ4* and *COQ9* mutations (Chung et al., 2015; Duncan et al., 2009; López et al., 2006; Mollet et al., 2007; Quinzii et al., 2006; Rötig et al., 2000). So far one patient with *PDSS1*, two with *COQ9*, four with *PDSS2*, twelve with *COQ2* and 12 with COQ4 were reported. Severe infantile multisystemic disease is characterized by a very early onset and early renal involvement, on top of additional symptoms which vary depending on the patients (for a global review see Quinzii et al., 2014).

COQ6 (monooxygenase 6) and COQ8B (ADCK4), when mutated lead to nephropathy (Ashraf et al.; Heeringa et al., 2011; Korkmaz et al., 2015). This kidney affection is characterized by a steroid-resistant nephrotic syndrome and lead to kidney failure. Nine out of the eleven reported patients bearing a *COQ6* mutation also presented with sensorineural deafness (Heeringa et al., 2011). Two patients with *COQ2* mutations were also reported with nephropathy, one without extrarenal symptoms and the other with progressive epileptic encephalopathy (Diomedi-Camassei et al., 2007). Nephropathy is also sometimes associated to severe infantile multisystemic disease although it is not the only phenotype in this type of disease (López et al., 2006).

The most represented phenotype in CoQ deficiencies is cerebellar ataxia, as the number of patients reported with this affection is greater than for the number of patients reported with other phenotypes. This cerebellar phenotype is characterized by an atrophy of the cerebellum, in association with various other symptoms such as neuropathy, muscle weakness, mental retardation seizures and hypogonadism (Quinzii et al., 2014). Nevertheless, the only primary CoQ deficiency leading to a cerebellar phenotype is due to COQ8A (ADCK3) mutations (Lagier-Tourenne et al., 2008; Mollet et al., 2008).

Isolated myopathy was not found, as such, in primary CoQ deficiencies. Regarding encephalomyopathy, a case was report for a patient with a *COQ4* mutation (Salviati et al., 2012). *COQ7* mutations were only reported in two patients so far and both have very different phenotypes. The first patient had lung hypoplasia since embryonic stages, muscular hypotonia and renal dysfunction, out of other symptoms, whereas the second patient presented with spasticity and bilateral sensorineural hearing loss (Freyer et al., 2015; Wang et al., 2017).

Most of the *COQ* mutations induce severe phenotype in the form of severe infantile multisystemic disease with a very short life expectancy. The enzymes encoded by these genes (*PDSS1*, *PDSS2, COQ2, COQ4* and *COQ9)* are therefore necessary for normal cell functioning, and CoQ seems to be essential for normal development and growth. Up to date, *COQ3* and *COQ5* mutations have not been reported. Hence, either mutations were not discovered yet, or COQ3 and COQ5 are essential and mutations lead to embryonic lethality. Regarding *COQ8A*, *COQ8B* and *COQ6*, mutations mainly induce mild or restricted phenotypes compared to mutations in other *COQ* genes. These specific phenotypes raise the question of the roles of COQ8A, COQ8B and COQ6, with a potential accessory role for COQ8A and COQ8B and possible bypass mechanisms for COQ6 functions in the first benzoquinone ring hydroxylation. Furthermore, the type of mutation in any of the *COQ* gene might define the severity of the affection.

b. Secondary deficiencies

Genes not known to be involved in CoQ biosynthesis were also described as inducing CoQ deficiencies. This is for example the case in AOA1 (ataxia with oculomotor apraxia 1), one of the recessive cerebellar ataxias, due to mutations in the aprataxin coding gene (*APTX*). Aprataxin is a protein involved in single-stranded DNA repair and most probably repairs DNA damage caused by oxidative stress, both in the nucleus and in the mitochondria (Luo et al., 2004; Sykora et al., 2012). In AOA1 patient's fibroblasts, low levels of PDSS1 were found, thereby explaining the CoQ deficiency. The PDSS1 low levels were so far explained by reduced gene transcription, and a new function of APTX as a transcriptional regulator of mitochondrial functions was proposed (Garcia-Diaz et al., 2015). CoQ deficiency was also found in case of a myopathic phenotype caused by mutations in *ETFDH*. The patients presented with exercise intolerance; and lipid accumulation as well as reduced respiratory chain activities were found in their muscles (Gempel et al., 2007). *ETFDH* encodes an inner mitochondrial membrane electron transfer flavoprotein (Watmough and Frerman, 2010). In contrast, other ETFDH mutations, inducing a myopathy, were not found to induce CoQ deficiency (Ohkuma et al., 2009). Furthermore, a patient

with a cardiofaciocutaneous syndrome, hypotonia and ataxia, due to mutations in a B-Type Raf Kinase, also presented a CoQ deficiency (Aeby et al., 2007). Finally, other mitochondrial DNA depletion, dietary insufficiency or pharmacotherapeutic agents can also lead to CoQ deficiencies (Artuch et al., 2009). Treatments with statins for example, can lower CoQ levels (Littarru and Langsjoen, 2007; Mancuso et al., 2010).

c. Treatments

Treatment with CoQ or analogs seems obvious to treat CoQ deficiencies. Unfortunately oral CoQ_{10} supplementation is not effective for all CoQ deficiencies and not all patients respond to supplementation (Hirano et al., 2012). In case of AOA1 or myopathies due to *ETFDH* mutations, which are secondary CoQ deficiencies, high dose of CoQ or riboflavin supplementation were respectively found to improve patients state (Gempel et al., 2007; Quinzii et al., 2005). The same was true for another CoQ deficiency, with undefined causes, leading to severe encephalomyopathy and renal failure, for which CoQ supplementation improved the patient's condition (Rötig et al., 2000). Although some patients with *COQ2* mutations responded well to CoQ supplementation (patients with nephrotic syndromes), and some patients with COQ8B partially responded, patients with COQ8A, *COQ9* or *PDSS2* mutations had poor or no responses (Ashraf et al., 2013; Hirano et al., 2012; Mignot et al., 2013). The lack of efficacy and the variability in responses might be explained by the poor bioavailability of CoQ_{10} orally up taken, which seems to be further prevented by the blood-brain-barrier (Bentinger et al., 2003), clarifying the absence of improvement in case of ataxia or encephalopathies. Biodistribution and availability should explain the absence of improvement albeit it does not explain why AOA1 or encephalomyopathies with unknown causes showed relieved phenotype upon treatment. Furthermore, to rescue mitochondrial defects and in particular respiratory chain activity, CoQ should reach the inner mitochondrial membrane, which was shown to be delayed compared to the uptake in other cellular membranes in fibroblasts of patients with CoQ primary deficiencies (López et al., 2010). Finally, from studies in a mouse model with COQ9 deficiency, which showed that ubiquinol is more efficient that ubiquinone to reverse the encephalopathy phenotypes and increase mitochondrial respiratory chain complexes in these mice, it seems that the molecule and the pharmacological formulation are important to increase the efficacy (García-Corzo et al., 2014). Further understanding of CoQ deficiencies and CoQ biodistribution are needed for the development of better therapies against primary CoQ deficiencies.

IV. ARCA2

ARCA2 (autosomal recessive ataxia type 2), also named SCAR9 (spinocerebellar ataxia type 9) is a rare form of degenerative ataxia, with approximately forty reported patients up to date. It is part of the autosomal recessive ataxias with cerebellar affections without neuropathy and of the recessive ataxias due to mitochondrial defects.

1. Clinical manifestation

ARCA2 patients present disparate phenotypes. The only consistent element, found in all patients (except one), is the progressive ataxia with cerebellar atrophy (Table 4). In most of the patients for which CoQ levels were measured, a mild to moderate ubiquinone (CoQ) deficiency is also observed (Horvath et al., 2012; Lagier-Tourenne et al., 2008). These symptoms are often associated with other neurological signs such as intellectual disability, epilepsy, myoclonus, tremor, exercise intolerance or muscle weakness (Mignot et al., 2013).

The onset majorly occurs during childhood or adolescence with a few exceptions of later adult onsets (patients 18 and 39 in Table 4). Most of the patients present with a slowly progressive ataxia. Some rare cases of acute worsening were reported but are most probably due to the epileptic crisis or stroke like episodes which markedly altered the patient's phenotype. A fatal outcome, due to stroke like episodes was even recorded for one patient (Hikmat et al., 2016) and few patients present severe encephalopathy with global brain degeneration (Mignot et al., 2013)

Epilepsy, seizures or stroke like episodes were reported in half of the patients (Table 4). The same frequency was observed for exercise intolerance and intellectual disability, although there is no correlation in between these symptoms. Out of the forty-two patients described in the literature, only eighteen underwent CoQ_{10} measurements. Fifteen patients had decreased levels of CoQ_{10} either in their fibroblasts (Lagier-Tourenne et al., 2008) or in their muscle with variable levels of decrease (Horvath et al., 2012; Mollet et al., 2008) and only three had unaltered levels (Horvath et al., 2012; Lagier-Tourenne et al., 2008; Mignot et al., 2013). For the patients in which CoQ_{10} levels were assessed both in fibroblast and in muscle, only the levels in muscles were found to be altered (Horvath et al., 2012). Muscles biopsies were probably performed after fibroblast sampling to look for a CoQ defect. Muscles biopsies are invasive but might be helpful for the diagnosis of the ARCA2 disease.

The disease course is not dependent on the age of onset: some very early onset lead to more severe ataxia whereas others are slowly progressive (Mignot et al., 2013). Multiple causes can induce an elevation of the lactate level but the increase of lactate reflects the usage of glycolysis by some cells (Andersen et al., 2013). Elevated lactate was not prominent in case of ARCA2, the majority of patients show normal levels (Table 4). Unlike lactate, the reduced activity of certain respiratory chain complexes was noteworthy, even if very variable from one patient to the other. This reduced activity appeared in cells derived from fourteen patients, out of the seventeen tested. The decrease in complex I, II and III activities of the respiratory chain should reflect CoQ deficiencies. Surprising results were obtained for one patient, patient 3 (Table 4), for which fibroblasts appeared to have normal CoQ_{10} content, but had mild but significantly reduced mitochondrial complex I and III activity (Lagier-Tourenne et al., 2008). Regarding other studies, for which measurements were performed both in fibroblasts and muscles, it might be that muscles of patient 3 would yield different results than the fibroblasts (Horvath et al., 2012). Thus, CoQ deficiency could be tissue specific (Mollet et al., 2008). Mitochondrial respiratory chain measurements were performed differently for each cohort, disabling comparison but overall results argue towards at least partially altered mitochondrial respiratory chain. Accordingly, altered CoQ_{10} levels and affected mitochondrial respiratory chain activity, in muscles, seem to be hallmarks for ARCA2.

2. Genetic cause

ARCA2 was found to be due to mutations in the aarF-domain-containing kinase 3 (*ADCK3*) gene (on human 1q41-42 locus), also named *CABC1* and *COQ8A* (Lagier-Tourenne et al., 2008; Mollet et al., 2008). This gene encodes a putative atypical kinase that is homologous to Coq8 in yeast and UbiB in bacteria (Lagier-Tourenne et al., 2008). Both Coq8p and UbiB proteins, encoded by these genes, were found to be implicated in the Coenzyme Q biosynthesis (Poon et al., 2000; Xie et al., 2012).

ARCA2 is the most common form of primary coenzyme Q deficiency, with at least 42 patients reported up to date (Table 4), most probably due to the milder phenotypes compared to other CoQ deficiencies (Barca et al., 2016; Blumkin et al., 2014; Gerards et al., 2010; Hikmat et al., 2016; Horvath et al., 2012; Kocak et al., 2015; Lagier-Tourenne et al., 2008; Liu et al., 2014; Malgireddy et al., 2016; Mignot et al., 2013; Mollet et al., 2008; Terracciano et al., 2012). Mutations occur all over the sequence of the gene and different types of mutations were discovered (Figure 9 and Table 4): missense mutations, nonsense mutations, frameshift mutations, two deletions, one insertion and a duplication. ARCA2 is a recessive ataxia, therefore both copies of *COQ8A* need to be mutated to induce the disease. Two cases

emerged: either patients are homozygous for a mutation or they are compound heterozygous, having a different mutation on each allele; an equal number of patient was reported in each case (Gerards et al., 2010).

No genotype-phenotype correlation could be found and this is emphasized by the fact that the same mutations led to heterogeneous phenotypes (Blumkin et al., 2014). This phenotypic variability can be seen, for example, between patients 30 and 31 in Table 4. Both patients carry the same mutation (p.L197Vfs*20), but in one case the patient did not have epilepsy nor intellectual disability (patient 30), whereas the other patient presented with epilepsy and a mild intellectual disability (patient 31) (Mignot et al., 2013). The same is true for patients 10 and 9 (compound heterozygous for p.R213W and p.G272V mutations), and other examples can be found (Table 4). Furthermore, big deletions do not lead to more severe phenotypes whereas certain point mutations do (Hikmat et al., 2016). The phenotypic variability observed, in particular for the same mutations, favors the idea of an implication of the environment and, or of genetic modulation.

All mutations are predicted to induce loss of functions. In patients' fibroblasts, Gerards et al. were able to show that the R348X and the L379X nonsense mutations induced an mRNA decay (Gerards et al., 2010). This mRNA decay mechanism degrades mRNA with premature stop codon to avoid translation of abnormal proteins, therefore preventing dominant negative or gain of functions effects (Chang et al., 2007). Lastly, Barca et al. found that, in case of the A504fs mutation, mRNA decay does not occur but COQ8A protein levels were diminished (Barca et al., 2016).

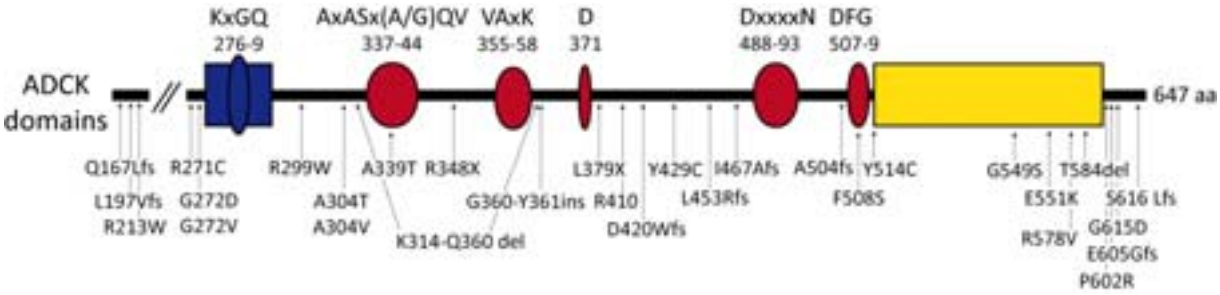

Figure 9 : Mutations found in ARCA patients, adapted from (Lagier-Tourenne et al., 2008).

Scheme of the ADCK3 human protein and the conserved kinase domains (red), a KxGQ domain conserved among the ADCK family (blue), and a domain specific to ADCK3 and ADCK4 (yellow). Underneath: mutations reported in ARCA2 patients. X: stop codon, fs: frameshift mutations, del: deletion, ins: insertion, others: point mutations with single amino acid change. For mutations, associated symptoms and reference, see Table 4. Mutations were reported in publications (Barca et al., 2016; Blumkin et al., 2014; Gerards et al., 2010; Hikmat et al., 2016; Horvath et al., 2012; Kocak et al., 2015; Lagier-Tourenne et al., 2008; Liu et al., 2014; Malgireddy et al., 2016; Mignot et al., 2013; Mollet et al., 2008; Terracciano et al., 2012).

Patient	Sex	Onset (years)	Ataxia	Cerebellar atrophy	Epilepsy or stroke like episodes	Exercise intolerance	Intellectual deficiency	CoQ_{10}	Lactate	Respiratory chain activity	Predicted aa change (homozygous for the mutation or compound heterozygous if 2 mutations are described)	Reference
5	M	4	+	+	n.d.	-	mild	↘	-	↘	p.Q167Lfs*36	1
30	F	19	+	+	-	n.d.	-	n.d.	-	-	p.L197Vfs*20	6
31	F	19	+	+	+	n.d.	mild	n.d.	-	n.d.	p.L197Vfs*20	6
9	F	1.5	+	+	+	+	mild	↘	-	-	p.R213W + p.G272V	2
10	F	1.5	+	+	-	+	-	n.d.	-	n.d.	p.R213W + p.G272V	2
29	F	1.5	+	+	+	n.d.	severe	↘	-	↘	p.R271C	6
17	F	17	+	+	+	+	-	-	n.d.	n.d.	p.R271C + p.A304T	4
11	F	3	+	+	+	+	-	↘	↗	↘	p.G272D + p.E605Gfs*125	2
19	F	1	+	+	+	+	+	n.d.	n.d.	n.d.	p.R299W	4
40	F	7	+	+	+	-	-	↘	n.d.	n.d.	p.R299W	12
27	F	4	+	+	+	n.d.	mild	n.d.	n.d.	n.d.	p.R299W + R410X	6
28	M	4	+	+	+	n.d.	mild	n.d.	-	n.d.	p.R299W + R410X	6
26	M	16	+	+	+	n.d.	-	-	n.d.	n.d.	p.R299W +L453Rfs*24	6
41	M	7	+	+	+	-	+	↘	n.d.	n.d.	p.R299W + p.F578V	12
42	F	3	+	+	+	-	+	n.d.	n.d.	n.d.	p.R299W + p.F578V	12
18	F	27	+	+	+	+	-	↘	n.d.	↘	p.A304V	4
7	F	3	+	+	-	n.d.	mild	↘	-	n.d.	p.K314_Q360del + p.G549S	1
12	M	3	+	+	+	+	mild	n.d.	n.d.	n.d.	p.R348X	3
13	M	9	+	+	-	+	mild	n.d.	n.d.	n.d.	p.R348X	3
14	M	3	+	+	+	+	mild	n.d.	n.d.	n.d.	p.R348X	3
22	F	6	+	+	+	n.d.	mild	↘	-	↘	p.R348X	5
37	M	<16	+	-	+	n.d.	n.d.	n.d.	↗	n.d.	p.R348X + p.A339T	9
15	F	2	+	+	-	+	-	n.d.	-	-	p.R348X + p.L379X	3
16	M	2	+	+	-	+	-	n.d.	-	↘	p.R348X + p.L379X	3
32	F	2	+	+	-	n.d.	-	n.d.	-	n.d.	p.Q360_Y361ins*	6
1	M	11	+	+	n.d.	-	-	n.d.	-	n.d.	p.D420Wfs*40 + p.I467Afs*22	1
2	M	4	+	+	n.d.	+	mild	n.d.	↗	n.d.	p.D420Wfs*40 + p.I467Afs*22	1
3	M	7	+	+	n.d.	+	-	-	↗	↘	p.D420Wfs*40 + p.I467Afs*22	1
4	F	8	+	+	n.d.	+	-	n.d.	↗	n.d.	p.D420Wfs*40 + p.I467Afs*22	1

Table 4 : Reported ARCA2 patients with their clinical symptoms and mutations.

Patient number assigned according to the chronology of description; n.d: not determined; +: present; - : absent (for symptoms) or unchanged (for COQ, lactate, and respiratory chain activity levels); ↘: decreased levels; ↗: increased levels; CoQ_{10} levels either determined in muscle or in fibroblasts; X: nonsense mutation; fs: frameshift mutation, del: deletion; dup: duplication. References: 1) (Lagier-Tourenne et al., 2008), 2 (Mollet et al., 2008), 3 (Gerards et al., 2010), 4 (Horvath, 2012), 5 (Terracciano et al., 2012), 6 (Mignot et al., 2013), 7 (Liu et al., 2014), 8 (Blumkin et al., 2014), 9 (Kocak et al., 2015), 10 (Barca et al., 2016), 11 (Malgireddy et al., 2016), 12 (Hikmat et al., 2016).

Patient	Sex	Onset (years)	Ataxia	Cerebellar atrophy	Epilepsy or stroke like episodes	Exercise intolerance	Intellectual deficiency	CoQ_{10}	Lactate	Respiratory chain activity	Predicted aa change (homozygous for the mutation or compound heterozygous if 2 mutations are described)	Reference
20	F	2	+	+	-	+	mild	↘	n.d.	↘	p.Y429C + ?	4
21	M	2	+	+	-	+	mild	↘	n.d.	↘	p.Y429C + ?	4
38	M	20	+	+	-	-	mild	↘	↗	↘	p.A504fs*130	10
25	M	11	+	+	-	n.d.	-	n.d.	n.d.	n.d.	p.F508S + del exon 3-15	6
8	M	2	+	+	+	+	+	↘	↗	↘	p.E551K	2
6	M	5	+	+	n.d.	n.d.	-	↘	-	↘	p.T584del + p.Y514C	1
35	F	2	+	+	-	-	+	n.d.	-	↘	p.T584del +p.P602R	8
36	F	<15	-	+	-	-	-	n.d.	n.d.	n.d.	p.T584del +p.P602R	8
23	M	2	+	+	+	n.d.	-	n.d.	-	n.d.	p.G615D	6
24	F	7	+	+	-	n.d.	-	n.d.	n.d.	n.d.	p.G615D	6
33	F	10	+	+	-	+	-	↘	n.d.	↘	p. S616Lfs*114	7
34	F	12	+	+	-	n.d.	-	n.d.	n.d.	n.d.	p. S616Lfs*114	7
39	F	<70	+	+	+	-	n.d.	n.d.	n.d.	n.d.	dup1q42.12	11
Frequency			41 /42	41 /42	20 /36	18 /27	20 /40	15 /18	7 /23	14 /17		

Table 4 (continued): Reported ARCA2 patients with their clinical symptoms and mutations.

Given the clinical heterogeneity in between patients, ARCA2 might not always be suspected. Most probably ARCA2 is underestimated, as a lot of ataxic patients and patients with CoQ deficiency are still lacking a precise diagnosis (Quinzii et al., 2014; Yubero et al., 2015). ARCA2 can, so far, only be discriminated thanks to next generation sequencing. Due to costs, not all patients have had access to this technology, or patients were tested for the most frequent genes, like frataxin (Friedreich's ataxia), aprataxin (AOA1) or ATM (ataxia-telangiectasia), when recessive ataxias were suspected (Beaudin et al., 2017). Furthermore, in suspicious cases it was difficult to screen all the potential genes (Liu et al., 2014). More ARCA2 patients might be described in the coming years as multiple-gene panel test, including the *COQ8A* gene, are now being used to determine patient's mutations. Better understanding of COQ8A function and ARCA2 pathomechanisms might improve the understanding of the clinical heterogeneity.

3. COQ8A

COQ8A functions had so far not been studied in mammals and the only clues came from its homology with the yeast Coq8p and the bacterial UbiB proteins.

a. Functions

ADCK (aarF domain-containing protein kinases) proteins, as well as Coq8 and UbiB, are part of the atypical kinase family (Leonard et al., 1998; Scheeff and Bourne, 2005). This family is composed of putative kinases that retained the 4 “universal core” motifs I, II, VIB and VII, out of the 12 motifs defining a typical protein kinase (Leonard et al., 1998; Xie et al., 2011). The conserved protein kinase domains correspond to the ATP binding and the phosphotransfer region (Lagier-Tourenne et al., 2008). The atypical kinase family comprises kinases which phosphorylate various lipids such as phosphatidyl inositol, phosphoinositide or choline (Manning et al., 2002; Walker et al., 1999).

In vertebrates, the ADCK family is composed of five paralogs (ADCK1-5), with ADCK3 (COQ8A) and ADCK4 (COQ8B) being highly similar (sharing 61% identity). The ADCK family retained the 4 universal core motifs of kinases plus the protein kinase motif III (Figure 10; conserved kinase motifs in red) (Lagier-Tourenne et al., 2008). Two aspartates, found in the kinases motifs VIB and VII, are highly conserved, they bind the magnesium ions chelated by ATP. A KxGQ domain, which seems specifically related with CoQ metabolism, is conserved among the ADCK family in the N-terminal part (Figure 10; domain in blue). The lysine residue in the KxGQ domain is highly conserved and binds the α-phosphatase. Finally, a domain specific to each vertebrate subgroup is present in C-terminus (Figure 10; domain in yellow). The first subgroup comprises ADCK1, 2 and 5 and the second subgroup COQ8A and COQ8B (Lagier-Tourenne et al., 2008).

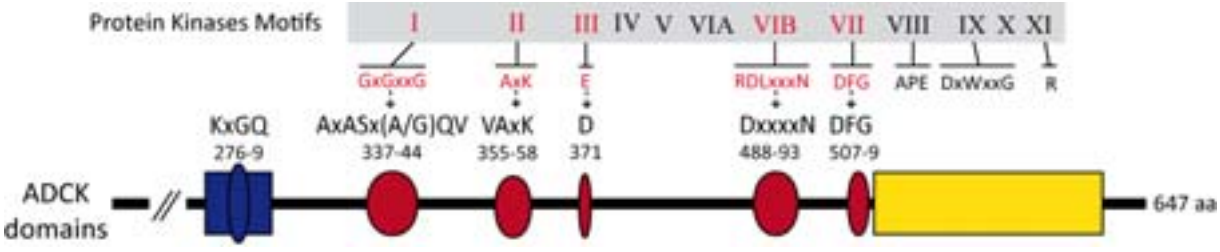

***Figure 10 : Scheme of the COQ8A/ADCK3 human protein,* adapted from** (Lagier-Tourenne et al., 2008)**.**

Conserved kinase domains (red), a KxGQ domain conserved among the ADCK family (blue), and a domain specific to ADCK3 and ADCK4 (yellow). Roman number: kinase domains; upper sequence: conserved amino acids in typical kinases and lower sequence: amino acids in the ADCK proteins with their localization in ADCK3/COQ8A.

Not much is known about the ADCK proteins and part of the knowledge comes from large scale studies in cancerous cells (Pandya et al., 2017; Šmidák et al., 2016). ADCK2 might regulate the production of reactive oxygen species in the context of cancer (Schoolmeesters et al., 2012). COQ8B was found to be overexpressed in uterine benign tumors (Lemeer et al., 2015). Moreover, COQ8B mutations in patients caused nephrotic symptoms. In COQ8B patient's fibroblasts, lower CoQ levels, as well as reduced mitochondrial respiration, were measured (Ashraf et al., 2013; Korkmaz et al., 2015). As mentioned above, COQ8A had been reported as leading to ARCA2 and, as COQ8B, to induce CoQ deficiency and mitochondrial respiratory defects when mutated (Horvath et al., 2012; Lagier-Tourenne et al., 2008; Mollet et al., 2008).

Most of the knowledge on mammalian COQ8, comes from the homology with the protein present in unicellular eukaryotes. Indeed, the yeast protein Coq8p has two homologs in human and mice: COQ8A and COQ8B, which are paralogs. Coq8p function is still controversial but it is suggested to play a role in stabilizing the supracomplex formed by the Coq proteins (Coq3-Coq7 and Coq) necessary for coenzyme Q biosynthesis in mitochondria, and to phosphorylate Coq3, Coq5 and Coq7 (He et al., 2014; Tauche et al., 2008; Xie et al., 2012).

When a truncated form of COQ8A (to be targeted in the mitochondria of *S. cerevisiae*) was expressed in yeast cells mutated in *Coq8*, COQ8A was shown to partly rescue the yeast Coq3, 5 and 7 phosphorylation state and CoQ synthesis (He et al., 2014; Xie et al., 2011). A small amount of CoQ could be produced upon expression of COQ8A in *Coq8* yeast mutants which was not the case in non-rescued *Coq8* mutant strains. Regarding the phosphorylation states, results were obtained by 2D-IEF/SDS-PAGE, comparing samples treated or not with phosphatase. According to these results, to COQ8A homology with Coq8 and UbiB and the CoQ deficiency observed in patients, mammalian COQ8A protein is suggested as being involved in the CoQ biosynthesis (Mollet et al., 2008). Regarding COQ8B, it was shown to interact with COQ6 and COQ7 (the mammalian counterparts of yeast Coq6p and coq7p) in human podocytes (Ashraf et al., 2013). Nevertheless, it is noteworthy that only COQ8A, and not COQ8B, was able to rescue the yeast *coq8* mutant (He et al., 2014). Still redundancy should occur as the yeast *Coq8* null mutant does not produce CoQ_6, whereas mammalians cells defective in either COQ8A or COQ8B do produce CoQ_{10} (Ashraf et al.; Horvath et al., 2012; Mollet et al., 2008; Tran and Clarke, 2007).

The function of COQ8A thus remains to be elucidated in mammals and the substrate of the putative kinase domain is unknown.

During my thesis, collaborators (the laboratory of Dr. Pagliarini) were able to show that a CoQ biosynthesis complex is also formed in mammals. They found that COQ3, 4, 5, 6, 7 and 9 are sufficient to form this complex in mammals, and proposed the following organization depicted in Figure 11 (Floyd et al., 2016). Collaborators were also able to show that COQ8A retained a kinase activity and can autophosphorylate (Stefely et al., 2015). Furthermore, in collaboration, we could show that COQ8A interacts with some of the COQ proteins, namely COQ4, COQ5, COQ6 and COQ7 in mammalian cells (Stefely et al., 2016). Together, we found that COQ8A specifically maintains the complex Q stability needed for CoQ biosynthesis and they found that the kinase activity is probably phosphorylating a small molecule or a lipid giving COQ8A an unorthodox protein kinase activity (Stefely et al., 2016). Finally, they determined that COQ8A and COQ8B directly interact with various COQ proteins and that these interactions are more abundant with COQ8A and reversely decreased with COQ8B in galactose conditions (Floyd et al., 2016).

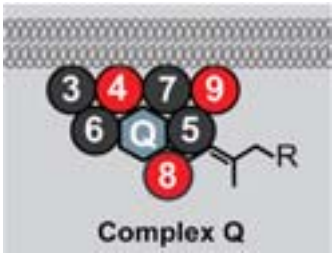

Figure 11 : Complex Q in mammalian cells, adapted from (Floyd et al., 2016).
Q: coenzyme Q, and 3-9: COQ3 to COQ9 proteins.

b. Localization

Coenzyme Q biosynthesis through the Q complex occurs in mitochondria and COQ8A was predicted as containing a mitochondrial targeting sequence. COQ8A was therefore expected to localize within the mitochondria, to be able to play its role in the stabilization of the Q complex (Pagliarini et al., 2008; Rhee et al., 2013). As no anti-COQ8A antibody was good enough to be used for immunofluorescence, tagged COQ8A were overexpressed. In our laboratory, COQ8A-GFP was overexpressed in C2C12 murine myoblasts (Licitra, 2013) and collaborators expressed COQ8A-FLAG in HEK293 human kidney embryonic epithelial cells (Stefely et al., 2016). Both studies confirmed a localization of COQ8A within the mitochondria of mammalian cells when the protein is overexpressed. Further analysis, by subfractionation of mouse mitochondria and treatment with Na_2CO_3, enabled to confirm this mitochondrial localization for mouse endogenous COQ8A, and precise a localization within the inner mitochondrial membrane with the C-terminus part facing the matrix (Stefely et al., 2016).

4. Mouse model

To better understand ARCA2 pathological mechanisms and study COQ8A functions, a constitutive Coq8a knock-out mouse model was generated (Coq8a$^{-/-}$) (Licitra, 2013; Stefely et al., 2016). These mice recapitulate most of the symptoms found in the patients, that is too say: slowly progressive ataxia, susceptibility to epilepsy, exercise intolerance, and mild CoQ deficiency. These Coq8a$^{-/-}$ mice are therefore a good model to study ARCA2 pathophysiology (Licitra, 2013; Stefely et al., 2016).

a. Cerebellar phenotype

In patients, ARCA2 is invariably defined by an ataxia with cerebellar atrophy. Similarly, Coq8a$^{-/-}$ mice were identified as being ataxic, with an onset between 5 and 10 weeks, but no cerebellar atrophy was observed. The ataxic feature was determined using the accelerating rotarod, footprint analysis and beam walking test which demonstrated a reduced coordination in mutant mice (Licitra, 2013; Stefely et al., 2016). Coq8a$^{-/-}$ mice's cerebellum had a similar size compared to WT littermates, but on histological sections, Purkinje neurons appeared shrunken in 30 weeks old mutant mice. Ultrastructural defects were also observed with dysmorphic nuclei in shrunken cells, and dilated Golgi and endoplasmic reticulum in the 30 weeks old mice's Purkinje neurons (Licitra, 2013; Stefely et al., 2016). Furthermore, Purkinje neurons normally fire spontaneously at a defined frequency and with a specific amplitude (Häusser et al., 1997). This pacemaker activity can be assessed by electrophysiology, and was found to be altered in mutant's Purkinje neurons. These neurons had a reduced firing frequency (Licitra, 2013; Stefely et al., 2016). As Purkinje neurons are the sole output of the cerebellum, ataxia is due to Purkinje neurons dysfunction in the Coq8a$^{-/-}$ mice model (Häusser et al., 1997).

b. Epilepsy and intellectual disability

Some Coq8a$^{-/-}$ mice have spontaneous seizures-like crisis (Licitra, 2013; Stefely et al., 2016). Therefore, the mice were tested for susceptibility to epilepsy. Indeed 6 month old mutant mice had increased susceptibility to epilepsy when treated with pentylenetetrazole (PTZ), a drug inducing convulsion (Licitra, 2013). This phenotype is in line with epilepsy or seizures observed in more than half of ARCA2 patients. Certain ARCA2 patients also present with intellectual disability (50% of the reported cases), so complementary neurobehavioral tests were performed on Coq8a$^{-/-}$ mice. The only manifestation in mutant mice was a mildly delayed spatial memory observed through the Morris water maze test (Licitra, 2013; Stefely et al., 2016).

c. Exercise intolerance

Coq8a$^{-/-}$ mice present with a mild CoQ_9 deficiency (the most abundant form of CoQ in mouse) in certain tissues including liver, kidney and skeletal muscles at 30 weeks of age. Furthermore, these mice had reduced maximum speed on an accelerating treadmill and a tendency towards weakened endurance without decreased muscle force (Licitra, 2013; Stefely et al., 2016). Thus, these mice seem to be exercise intolerant, like more than half of the ARCA2 patients. No histological defect could be found in the muscle, which is also the case in most of the patient's muscle biopsies (Horvath, 2012; Licitra, 2013; Mignot et al., 2013; Stefely et al., 2016). Interestingly, abnormal mitochondria were observed in Coq8a$^{-/-}$ mice quadriceps at 7 months (Licitra, 2013; Stefely et al., 2016).

d. Dyslipidemia in mouse

No deregulation in blood lipids was reported in any of the ARCA2 patients described so far (Horvath, 2012; Lagier-Tourenne et al., 2008; Mignot et al., 2013; Mollet et al., 2008). In contrast, a mild dyslipidemia with elevated levels of certain lipids (total cholesterol, HDL, LDL and free fatty acids) was measured in the blood of 25 weeks old Coq8a$^{-/-}$ mice (Licitra, 2013; Stefely et al., 2016).

All in all, Coq8a$^{-/-}$ mice appear as a good model to study ARCA2 and gain insight in COQ8A functions.

RESULTS

Results

I. Goals of my PhD project

When I started my PhD in Dr Hélène Puccio's team, a mouse model for ARCA2 had already been generated in the laboratory. One of the goals of the laboratory was to understand the pathophysiological mechanisms of the disease and study the function of COQ8A. This model was characterized by Floriana Licitra (Licitra, 2013), a previous PhD student. She was able to show that the constitutive knock-out mouse: Coq8a$^{-/-}$ (previously named Adck3$^{-/-}$) is a good model to study ARCA2. The mouse model recapitulates most of the symptoms found in the patients, that is: a slowly progressive ataxia, susceptibility to epilepsy, exercise intolerance, and mild CoQ deficiency. Moreover, a mild dyslipidemia was measured in the blood of the Coq8a$^{-/-}$ mice with an increased level of certain lipids (total cholesterol, HDL, LDL and free fatty acids).

Throughout my thesis, I have investigated different phenotypes observed in the Coq8a$^{-/-}$ mice, to try to understand the pathophysiological pathways implicated. Consequently, my thesis project was divided in different parts.

During the first year of my doctoral studies the goal was to gain insight into the mechanisms leading to two different aspects of the mouse phenotype: dyslipidemia and epilepsy. I was therefore interested in the causes of dyslipidemia and if there could be a link with the CoQ deficiency that we observe in the Coq8a$^{-/-}$ mouse model. At the same time, I also wanted to understand why patients and mice have epilepsy and if this is due to a defect in the hippocampus.

As I did not find any difference between the control and Coq8a$^{-/-}$ mice, I focused, after discussion with my mid-thesis committee, on the cerebellum and muscle, two known affected organs. I tried to elucidate why and how Purkinje neurons are degenerating in the brain and if the mitochondrial respiratory chain was altered, especially in muscles.

To study these defects, I generated cell models: organotypic cerebellar cultures and cerebellar, hippocampal and muscular primary cell cultures. These models enable to perform experiments which would have been complicated *in vivo*, such as measurement of mitochondrial respiration or addition of certain drugs. Organotypic cultures have the advantage to retain the cerebellar structure, in particular the cells organization and branching, while being an *in vitro* system, whereas the primary cultures allow to have isolated neurons and glial cells or muscle cells.

The main questions I have been trying to address during my thesis were:

1. **Is the liver affected?**
   1.1. Can a deregulation in the mevalonate pathway or the fatty acid synthesis and oxidation explain the blood dyslipidemia and the reduced levels of CoQ in this organ?
   1.2. Is there a link with the deregulation of an apoliprotein?

2. **Is COQ8A implicated in the biosynthesis of CoQ as predicted?** With which proteins does COQ8A interact?

3. **Is oxidative phosphorylation affected due to a destabilization of the CoQ biosynthesis machinery?**
   3.1. In cerebellar cells, could it lead to insufficient energy supply to neurons, contributing to the degeneration of Purkinje cells?
   3.2. In muscular cells, could a defect in mitochondrial respiration explain the exercise intolerance?

4. **Can a defect in hippocampus explain epilepsy and the delayed spatial memory?**
   4.1. Are some specific hippocampal regions degenerating?
   4.2. Is there a defect in certain neurotransmitters?

5. **What are the causes for Purkinje cells degenerations? And how early are the molecular dysregulations appearing?**
   5.1. Do Purkinje neurons degenerate in a patterned way? Are some specific ion channels deregulated?
   5.2. Which pathways are compensatory mechanisms (consequences) and which one are primary events (causes)?
   5.3. What is the link between the deregulated pathways and COQ8A?

II. Manuscript

Cerebellar Ataxia and Coenzyme Q Deficiency through Loss of Unorthodox Kinase Activity

Jonathan A. Stefely*, Floriana Licitra*, Leila Laredj, Andrew G. Reidenbach, Zachary A. Kemmerer, Anais Grangeray, Tiphaine Jaeg-Ehret, Catherine E. Minogue, Arne Ulbrich, Paul D. Hutchins, Emily M. Wilkerson, Zheng Ruan, Deniz Aydin, Alexander S. Hebert, Xiao Guo, Elyse C. Freiberger, Laurence Reutenauer, Adam Jochem, Maya Chergova, Isabel E. Johnson, Danielle C. Lohman, Matthew J.P. Rush, Nicholas W. Kwiecien, Pankaj K. Singh, Anna I. Schlagowski, Brendan J. Floyd, Ulrika Forsman, Pavel J. Sindelar, Michael S. Westphall, Fabien Pierrel, Joffrey Zoll, Matteo Dal Peraro, Natarajan Kannan, Craig A. Bingman, Joshua J. Coon, Philippe Isope, Hélène Puccio# and David J. Pagliarini#.

Molecular Cell. 2016 Aug 18;63(4):608-620. doi: 10.1016/j.molcel.2016.06.030. Epub 2016 Aug 4.

Equal contribution: * and #

For this manuscript, I contributed by verifying immunoprecipitation assays (as detailed in the “Interaction” part) and assessing COQ7 levels. I also explored mitochondrial respiration but mutant’s myoblasts respired as well as WT, so the data were not included in this publication.

Article

Molecular Cell

Cerebellar Ataxia and Coenzyme Q Deficiency through Loss of Unorthodox Kinase Activity

Graphical Abstract

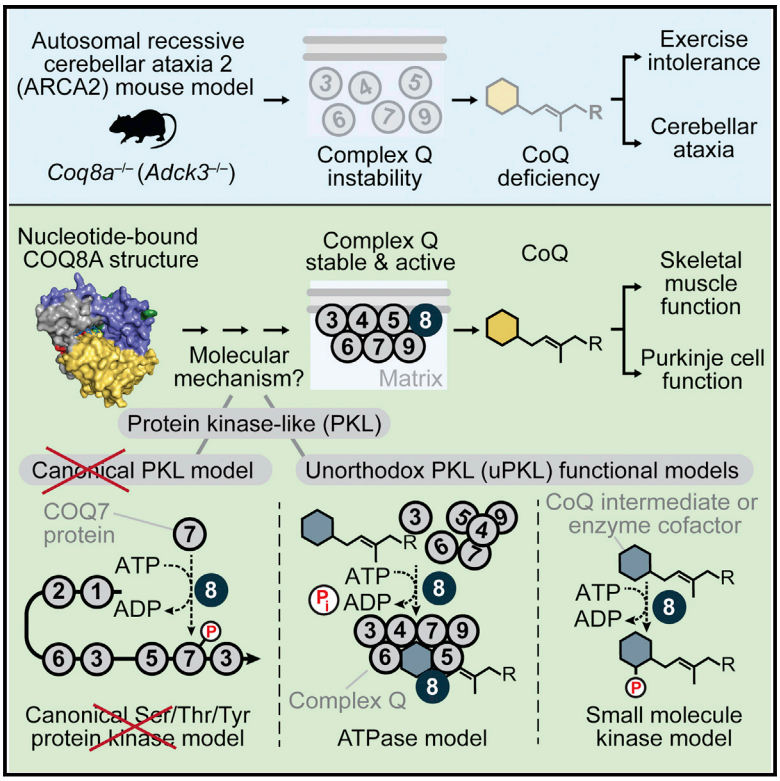

Highlights

- *Coq8a*$^{-/-}$ mice recapitulate the most frequent form of human genetic CoQ deficiency
- COQ8A maintains a mammalian coenzyme Q (ubiquinone) biosynthesis complex
- COQ8 stabilizes complex Q through unorthodox kinase-like mechanisms
- COQ8 binds lipid CoQ intermediates with a conserved structural feature (KxGQ domain)

Authors

Jonathan A. Stefely, Floriana Licitra, Leila Laredj, ..., Philippe Isope, Hélène Puccio, David J. Pagliarini

Correspondence

hpuccio@igbmc.fr (H.P.), dpagliarini@morgridge.org (D.J.P.)

In Brief

The ancient UbiB protein kinase-like (PKL) family has five human members (ADCK1–5), which are largely uncharacterized. Stefely et al. demonstrate that COQ8A (ADCK3) possesses conserved unorthodox PKL functionalities essential for maintaining a CoQ biosynthesis complex. Loss of COQ8A disrupts this complex, causing CoQ deficiency and cerebellar ataxia.

Accession Numbers

5I35

Stefely et al., 2016, Molecular Cell *63*, 608–620
August 18, 2016
http://dx.doi.org/10.1016/j.molcel.2016.06.030

CellPress

Molecular Cell
Article

Cerebellar Ataxia and Coenzyme Q Deficiency through Loss of Unorthodox Kinase Activity

Jonathan A. Stefely,[1,2,18] Floriana Licitra,[3,4,5,18] Leila Laredj,[3,4,5] Andrew G. Reidenbach,[1,2] Zachary A. Kemmerer,[1,2] Anais Grangeray,[4,6] Tiphaine Jaeg-Ehret,[3,4,5] Catherine E. Minogue,[7] Arne Ulbrich,[7] Paul D. Hutchins,[7] Emily M. Wilkerson,[7] Zheng Ruan,[8,9] Deniz Aydin,[10,11] Alexander S. Hebert,[12] Xiao Guo,[1,7] Elyse C. Freiberger,[2] Laurence Reutenauer,[3,4,5] Adam Jochem,[1] Maya Chergova,[3,4,5] Isabel E. Johnson,[1,2] Danielle C. Lohman,[1,2] Matthew J.P. Rush,[7] Nicholas W. Kwiecien,[7] Pankaj K. Singh,[3,4,5] Anna I. Schlagowski,[13] Brendan J. Floyd,[1,2] Ulrika Forsman,[14] Pavel J. Sindelar,[14,15] Michael S. Westphall,[12] Fabien Pierrel,[14,16] Joffrey Zoll,[13] Matteo Dal Peraro,[10,11] Natarajan Kannan,[8,9] Craig A. Bingman,[2] Joshua J. Coon,[7,12,17] Philippe Isope,[4,6] Hélène Puccio,[3,4,5,*] and David J. Pagliarini[1,2,*]

[1]Morgridge Institute for Research, Madison, WI 53715, USA
[2]Department of Biochemistry, University of Wisconsin–Madison, Madison, WI 53706, USA
[3]Département de Médecine Translationnelle et Neurogénétique, Institut de Génétique et de Biologie Moléculaire et Cellulaire, INSERM U596, CNRS UMR 7104, 67400 Illkirch, France
[4]Université de Strasbourg, 67081 Strasbourg, France
[5]Chaire de Génétique Humaine, Collège de France, 67404 Illkirch, France
[6]Institut des Neurosciences Cellulaires et Intégratives, CNRS UPR 3212, 67084 Strasbourg, France
[7]Department of Chemistry, University of Wisconsin–Madison, Madison, WI 53706, USA
[8]Institute of Bioinformatics
[9]Department of Biochemistry & Molecular Biology
University of Georgia, Athens, GA 30602, USA
[10]Institute of Bioengineering, School of Life Sciences, École Polytechnique Fédérale de Lausanne, 1015 Lausanne, Switzerland
[11]Swiss Institute of Bioinformatics, 1015 Lausanne, Switzerland
[12]Genome Center of Wisconsin, University of Wisconsin–Madison, Madison, WI 53706, USA
[13]Fédération de Medicine Translationnelle de Strasbourg, EA3072, Faculté de Médicine et Faculté des Sciences du Sport, Université de Strasbourg, 67084 Strasbourg, France
[14]University Grenoble Alpes, LCBM, UMR 5249, 38000 Grenoble, France
[15]Laboratoire de Chimie des Processus Biologiques, CNRS UMR 8229, Collège de France, 75252 Paris, France
[16]TIMC-IMAG, CNRS UMR 5525, UFR de Médecine, University Joseph Fourier, 38706 La Tronche, France
[17]Department of Biomolecular Chemistry, University of Wisconsin–Madison, Madison, WI 53706, USA
[18]Co-first author
*Correspondence: hpuccio@igbmc.fr (H.P.), dpagliarini@morgridge.org (D.J.P.)
http://dx.doi.org/10.1016/j.molcel.2016.06.030

SUMMARY

The UbiB protein kinase-like (PKL) family is widespread, comprising one-quarter of microbial PKLs and five human homologs, yet its biochemical activities remain obscure. COQ8A (ADCK3) is a mammalian UbiB protein associated with ubiquinone (CoQ) biosynthesis and an ataxia (ARCA2) through unclear means. We show that mice lacking COQ8A develop a slowly progressive cerebellar ataxia linked to Purkinje cell dysfunction and mild exercise intolerance, recapitulating ARCA2. Interspecies biochemical analyses show that COQ8A and yeast Coq8p specifically stabilize a CoQ biosynthesis complex through unorthodox PKL functions. Although COQ8 was predicted to be a protein kinase, we demonstrate that it lacks canonical protein kinase activity in *trans*. Instead, COQ8 has ATPase activity and interacts with lipid CoQ intermediates, functions that are likely conserved across all domains of life. Collectively, our results lend insight into the molecular activities of the ancient UbiB family and elucidate the biochemical underpinnings of a human disease.

INTRODUCTION

Coenzyme Q (CoQ; ubiquinone) is a redox-active lipid found in all domains of life and virtually all cellular membranes (Crane et al., 1957; Lester and Crane, 1959; Morton, 1958; Seshadri Sastry et al., 1961). CoQ functions as an essential component of the mitochondrial electron transport chain to enable oxidative phosphorylation, acts as a lipophilic antioxidant, and contributes to membrane structure. Yet our understanding of CoQ biosynthesis remains incomplete. In the yeast *Saccharomyces cerevisiae*, at least 11 genes (*coq1–coq9*, *yah1*, and *arh1*) are required for CoQ biosynthesis (Pierrel et al., 2010; Tran and Clarke, 2007), but the biochemical functions of Coq4p, Coq8p, and Coq9p remain unclear.

In humans, mutations in nine putative CoQ biosynthesis genes have been linked to primary CoQ deficiencies, which affect

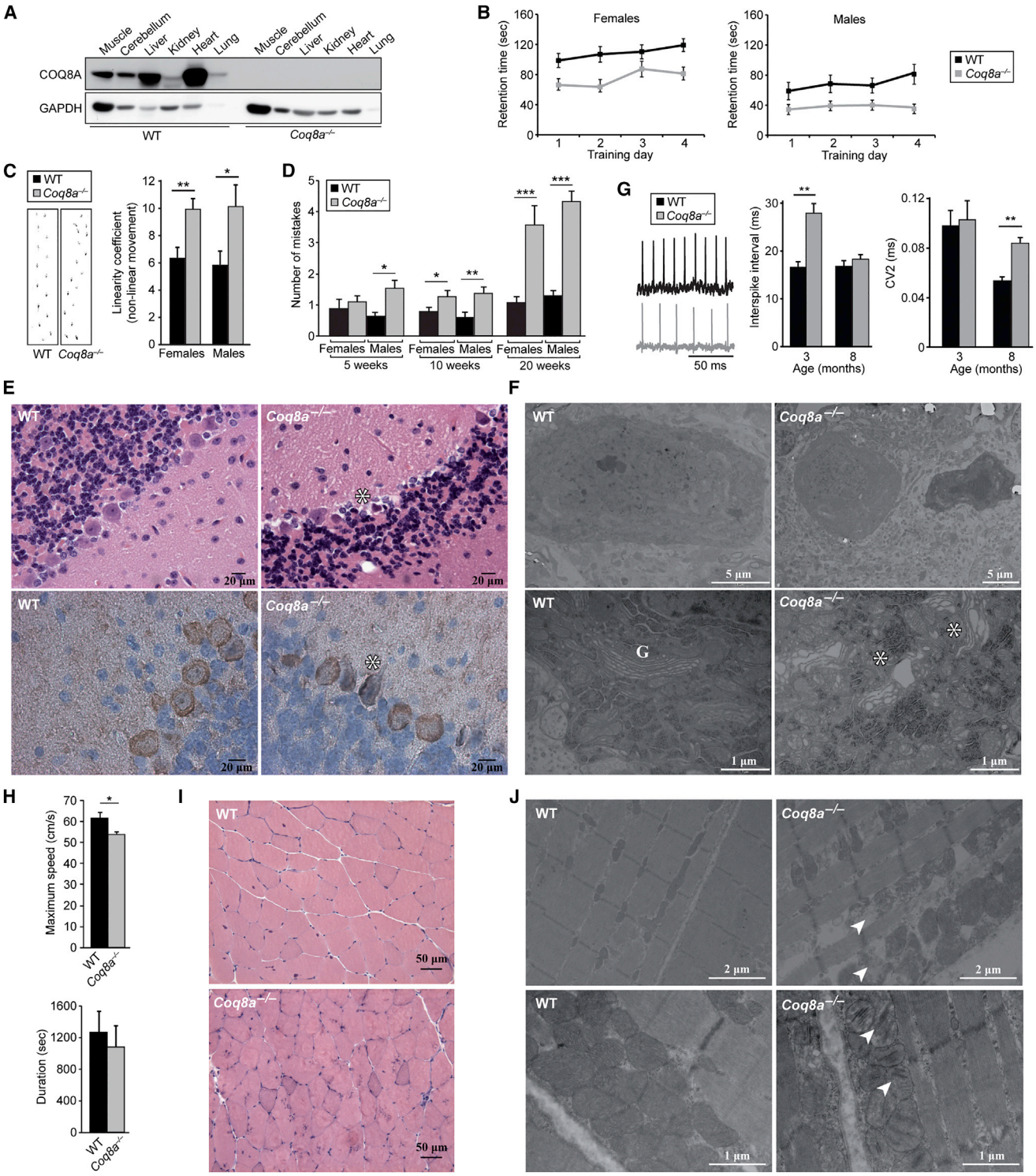

Figure 1. *Coq8a*$^{-/-}$ Mice Develop Cerebellar Ataxia and Mild Exercise Intolerance

(A) Immunoblot analysis of COQ8A abundance in 30-week-old mice.

(B) Accelerating rotarod retention times of 10-week-old mice (mean ± SEM, n = 8–12). ANOVA test $p < 0.05$.

(C) Left: representative footprints of 10-week-old mice. Right: "linearity coefficient," which is proportional to non-linear movement (mean ± SEM, n = 8–12). *$p < 0.05$, **$p < 0.01$.

(D) Number of hindlimb coordination errors (mistakes) by mice on beam test (mean ± SEM, n = 8–12). *$p < 0.05$, **$p < 0.01$, ***$p < 0.01$.

(legend continued on next page)

diverse tissues and range from severe infantile multisystemic disease to adult-onset isolated myopathy (Laredj et al., 2014; Quinzii and Hirano, 2010). Tissue specificities likely reflect cell-type-specific differences in CoQ production, uptake, and demand. Differences in clinical severity may be influenced by whether the mutated gene encodes a CoQ biosynthesis enzyme or a regulatory protein. Yet no clear explanation exists for this extreme clinical heterogeneity, in part because of the absence of suitable animal models.

The most frequent form of hereditary CoQ deficiency, autosomal-recessive cerebellar ataxia type 2 (ARCA2, SCAR9), is a rare ataxia that is due to mutations in *ADCK3*, an ortholog of yeast *coq8* (Lagier-Tourenne et al., 2008; Mollet et al., 2008). ARCA2 is characterized by slowly progressive gait abnormality, cerebellar atrophy, and moderate CoQ deficiency in skeletal muscle. More variable features include exercise intolerance, epilepsy, and intellectual deficiency. The molecular mechanisms underlying ARCA2 are obscure, largely because ADCK3 lacks a clear biochemical function.

ADCK3 belongs to the ancient UbiB family, which comprises one-quarter of all microbial protein kinase-like (PKL) genes (Kannan et al., 2007; Leonard et al., 1998; Oruganty et al., 2016) and has diverse biological functions in cell migration (Simpson et al., 2008), tumor cell viability (Brough et al., 2011; Wiedemeyer et al., 2010), and lipid metabolism (Lundquist et al., 2013; Martinis et al., 2013; Tan et al., 2013). The UbiB family has five mammalian members (ADCK1–5), which are classified as atypical kinases (Manning et al., 2002). ADCK4 is the closest homolog of ADCK3, and ADCK4 mutations cause a nephrotic syndrome associated with CoQ deficiency (Ashraf et al., 2013). On the basis of phylogenetic analyses defining ADCK3 and ADCK4 as co-orthologs of yeast Coq8p and functional studies presented in this report, we propose to rename ADCK3 and ADCK4 as COQ8A and COQ8B, respectively.

Although Coq8p and COQ8A have been linked to CoQ through genetic studies, whether these proteins act exclusively in CoQ biosynthesis is unknown. Moreover, the mild CoQ deficiency of ARCA2 has raised questions about the role of COQ8A in CoQ production. Coq8p and COQ8A localize to the matrix face of the inner mitochondrial membrane (Do et al., 2001; Pagliarini et al., 2008; Rhee et al., 2013; Tauche et al., 2008), where CoQ is produced. Additionally, using affinity enrichment mass spectrometry (AE-MS), we recently demonstrated that COQ8A and COQ8B interact with CoQ biosynthesis enzymes in a complex we term ''complex Q'' (Floyd et al., 2016 [this issue of *Molecular Cell*]), consistent with reports that yeast proteins form a similar complex (He et al., 2014). In yeast, lack of *coq8* perturbs post-translational modifications (PTMs) of Coq3p, Coq5p, and Coq7p (Xie et al., 2011), but whether this effect is direct or indirect, or whether these PTMs are important for complex Q function, is unknown.

The putative biochemical function of Coq8p, COQ8A, and the larger UbiB family is protein phosphorylation, but this idea remains largely untested and is based primarily on PKL sequence homology. Unorthodox PKL (uPKL) functions, including lipid kinase activity (Walker et al., 1999) and nucleotide-regulated conformational changes (Kung and Jura, 2016), are increasingly recognized. Moreover, 10% of the human kinome consists of pseudokinases with non-catalytic functions (Zeqiraj and van Aalten, 2010). Differentiating these diverse modes of action remains a central challenge in studying the kinome. For COQ8A in particular, unique structural features are positioned to inhibit protein kinase activity, raising the possibility of atypical functionality (Stefely et al., 2015).

Here, we show that *Coq8a* knockout (*Coq8a*$^{-/-}$) mice recapitulate the primary features of ARCA2. We trace the main pathophysiology of this disease to dysfunctional cerebellar Purkinje cells (PCs), defective skeletal muscle, and disruption of complex Q. Leveraging interspecies biochemical investigations, we provide evidence for uPKL COQ8A activity and present a new model for how COQ8A supports CoQ biosynthesis.

RESULTS

Coq8a$^{-/-}$ Mice Develop Ataxia and Seizures

To investigate COQ8A function in vivo, we generated a constitutive knockout (*Coq8a*$^{-/-}$) mouse model (Figure S1A) that showed normal Mendelian inheritance, growth, and lifespan, despite the complete absence of COQ8A in all tissues tested (Figures 1A and S1B). No overt clinical phenotypes were observed. Evaluation of standard blood parameters revealed hyperlipidemia (Figure S1C), suggesting a defect in lipid metabolism.

To assess the neurological consequences of COQ8A depletion, we conducted behavioral analyses. By 10 weeks of age, *Coq8a*$^{-/-}$ mice showed decreased performance on accelerating rotarod (Figure 1B), an increase in nonlinear movement in footprint analysis (Figure 1C), and a decrease in hindlimb coordination on the beam test that worsened with age (Figure 1D). Thus, *Coq8a*$^{-/-}$ mice develop a slowly progressive loss of coordination after birth. Epilepsy and seizures are also observed in ARCA2 patients. Consistently, *Coq8a*$^{-/-}$ mice developed occasional seizures during daily manipulation and showed increased seizure susceptibility after pentylenetetrazole injection (Figure S1D). Some ARCA2 patients also show moderate intellectual disability, although no clear genotype-phenotype correlation

(E) Hematoxylin and eosin (H&E) (top) and calbindin (bottom) staining of cerebellar sections of 15- and 40-week-old mice, respectively. *Shrunken Purkinje neurons. The scale bar represents 20 μm.

(F) Electron microscopy of 30-week-old cerebella. G, Golgi apparatus. *Dilated Golgi. The scale bars represent 5 μm (top) and 1 μm (bottom).

(G) Electrophysiological recordings of mouse PCs. ISI and CV2 (mean ± SEM) (n = 3, >40 cells/mouse). **Mann-Whitney U test $p < 0.01$.

(H) Maximum speed (top) and duration (bottom) on treadmill test by 10-month-old mice (mean ± SEM, n = 8). *$p < 0.05$.

(I) H&E-stained skeletal muscle sections of 7-month-old mice. The scale bar represents 50 μm.

(J) Electron microscopy of quadriceps showing broken mitochondria with collapsing cristae (arrows). Top: 7-month-old mice; the scale bar represents 2 μm. Bottom: 15-month-old mice; the scale bar represents 1 μm.

See also Figure S1.

exists. *Coq8a*$^{-/-}$ mice show only a slight delay in spatial memory in a Morris water maze test (Figures S1E and S1F). Collectively, these results show that the neurological phenotypes of *Coq8a*$^{-/-}$ mice recapitulate those seen in patients, and thus constitute a good model to explore ARCA2 pathophysiology.

Coq8a$^{-/-}$ PCs Are Dysfunctional

Histological analysis of the CNS revealed neither cerebellar atrophy nor gross CNS defects in *Coq8a*$^{-/-}$ mice throughout their lifespan. However, *Coq8a*$^{-/-}$ mice showed a specific defect in the cerebellar PC layer, with the presence of dark shrunken neurons and patches of gaps in calbindin staining, suggesting neuronal degeneration (Figure 1E). Ultrastructural analysis demonstrated that ~10% of *Coq8a*$^{-/-}$ PCs were dark and shrunken, with dysmorphic nuclei and abnormal membrane structures (Figure 1F). Interestingly, most *Coq8a*$^{-/-}$ PCs also displayed a dilated and fragmented Golgi apparatus and dilated cisternae of ribosome-rich endoplasmic reticulum (Figures 1F and S1G). Consistent with an important function for COQ8A in PCs, *Coq8a* mRNA is abundant in the cerebellar PC layer (Figure S1H). Yet PC mitochondria appear structurally normal (Figure S1G). *Coq8a*$^{-/-}$ cerebella also showed normal levels of PC-specific molecular markers and lacked apoptotic cells (Figures S1I and S1J), suggesting no massive PC loss, even at advanced stages of the disease.

The electrophysiological function of PCs, which normally exhibit regular pacemaking action potentials (Häusser and Clark, 1997), was assessed by measuring spontaneous firing in acute cerebellar slices (Figure 1G). PCs from 3-month-old *Coq8a*$^{-/-}$ mice exhibited a significant increase in interspike interval (ISI), while the coefficient of variation between adjacent spikes (CV2) was normal (Figure 1G). A distribution analysis demonstrated that a significant proportion of *Coq8a*$^{-/-}$ PCs have high ISI values (>40) (Figure S1K). Interestingly, 8-month-old *Coq8a*$^{-/-}$ PCs exhibited a significant increase in CV2, while the ISI was normal (Figure 1G). Thus, *Coq8a*$^{-/-}$ PCs have altered pacemaker activity, with a progressive phenotype. Together, these results show that specific PC dysfunction underlies the *Coq8a*$^{-/-}$ ataxia.

Coq8a$^{-/-}$ Mice Develop Exercise Intolerance

In addition to neurological symptoms, exercise intolerance is a common feature of ARCA2. On an accelerating treadmill, the maximum speed reached by *Coq8a*$^{-/-}$ mice was significantly decreased, and a trend toward lower endurance was observed (Figure 1H). No difference in muscle strength was observed by grip analysis (Figure S1L). Together, these data demonstrate mild exercise intolerance in *Coq8a*$^{-/-}$ mice. Consistent with an important role for COQ8A in muscle function, *COQ8A* mRNA is highly expressed in skeletal muscle (Figures S1M and S1N). Histological analyses of 7-month-old *Coq8a*$^{-/-}$ mouse skeletal muscle revealed no gross defects (Figure 1I), but ultrastructural analyses revealed abnormal mitochondrial morphology with broken or collapsed cristae and mild fiber degeneration (Figures 1J). Despite these perturbations, mtDNA levels (Figure S1O), cellular respiration (Figure S1P), and metabolites of central carbon metabolism (Figure S1Q) were found to be within wild-type (WT) ranges, further showing that the *Coq8a*$^{-/-}$ muscle phenotypes are mild, as observed in ARCA2.

Collectively, this work establishes *Coq8a*$^{-/-}$ mice as a model system that recapitulates the key features of ARCA2, deepens our understanding of its pathogenesis, and provides a foundation for molecular studies. Here, we conduct parallel studies of mammalian COQ8A and yeast Coq8p to test their functional homology and to help elucidate the biochemistry of ARCA2.

Coq8a$^{-/-}$ Mice Develop Specific CoQ Deficiency

ARCA2 patients have mild skeletal muscle CoQ_{10} deficiency, which could cause exercise intolerance. Seven-month-old *Coq8a*$^{-/-}$ mice show significant CoQ deficiencies in kidney, liver, and skeletal muscle (Figure 2A). However, CoQ levels were normal in younger mice (Figure S2A). Because the CoQ deficiency was mild in skeletal muscle and absent from whole cerebella, we used MS lipidomics to more broadly explore lipid metabolism. These analyses demonstrated that CoQ is significantly and specifically deficient in *Coq8a*$^{-/-}$ skeletal muscle (Figure 2B; Table S1). Similarly, yeast lacking *coq8* (Δ*coq8*) show specific CoQ deficiency (Figure S2B; Table S2). However, normal CoQ levels were observed in whole *Coq8a*$^{-/-}$ cerebella (Figure 2B), providing further evidence that PCs are specifically affected by loss of COQ8A. No significant difference in serum CoQ was observed (Figure 2B). Together, these results show that lack of COQ8A causes mild, tissue-specific CoQ deficiency.

COQ8A Specifically Maintains CoQ Biosynthesis Proteins

Toward understanding the molecular basis for the CoQ deficiency of *Coq8a*$^{-/-}$ mice, we quantified protein abundance changes by MS-based proteomics (Figure 2C; Table S3). Proteins of the recently defined mammalian complex Q (COQ3–9) (Floyd et al., 2016) were significantly and specifically deficient across multiple *Coq8a*$^{-/-}$ tissues, including the affected cerebellum and skeletal muscle, but also unaffected tissues to varying degrees (Figures 2C–2E, S2C, and S2D). Together with the co-purification studies by Floyd et al. (2016), these *Coq8a*$^{-/-}$ proteomics results provide further, complementary evidence to support the existence of a mammalian complex Q and its physiological significance. Immunoblot analyses of *Coq8a*$^{-/-}$ tissues from young mice (Figures 2D and S2C) and myoblasts derived from pups (Figure 2E) showed COQ7 deficiency, suggesting that complex Q dysregulation is an early feature of ARCA2. In yeast, loss of Coq8p caused a similarly specific deficiency of homologous complex Q proteins during the diauxic shift, a metabolic transition from fermentation to respiration (Figures 2F and S2E–S2H; Table S4). Together, these results show that Coq8p and COQ8A specifically maintain complex Q in yeast and mammals, respectively.

COQ8A Interacts Dynamically with Complex Q

The observed COQ8A-dependent stability of complex Q could be driven by COQ8A-complex Q protein-protein interactions. In pairwise co-expression studies in COS cells, COQ8A-FLAG robustly co-purified with COQ5-HA but not with COQ3-HA or COQ9-HA (Figure 3A). To further explore the interaction network of COQ8A, we performed AE-MS analyses of human COQ8A-FLAG expressed in HEK293 cells. Compared with MLS-GFP-FLAG, COQ8A-FLAG robustly co-purified with endogenous COQ5, COQ7, COQ6, COQ4, and COQ3 (Figures 3B, 3C, and

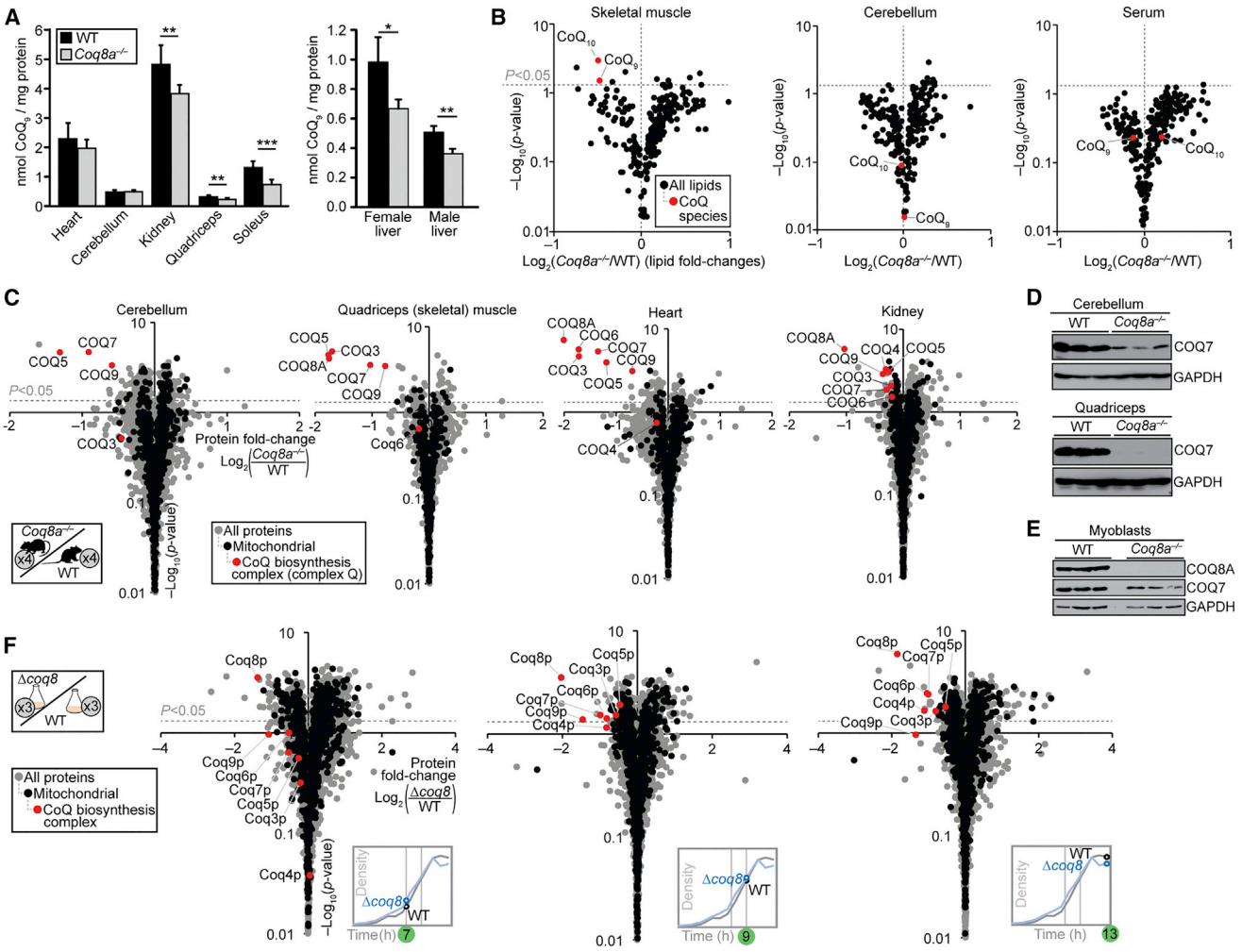

Figure 2. Loss of COQ8A or Coq8p Causes Deficiency of Complex Q and CoQ

(A) CoQ_9 content in 7-month-old mice (mean ± SD, n = 6). *p < 0.05, **p < 0.01, ***p < 0.001.

(B) Fold changes in mouse lipid abundances (log_2[*Coq8a*$^{-/-}$/WT], n = 4) versus statistical significance (–log_{10}[p value]) as quantified by LC-MS for quadriceps, cerebellum, and serum.

(C) Fold changes in mouse protein abundances (log_2[*Coq8a*$^{-/-}$/WT], n = 4) versus statistical significance as quantified by LC-MS/MS for cerebellum, quadriceps, heart, and kidney.

(D) Expression of COQ7 in cerebellum and muscles of 10-week-old mice.

(E) Expression of COQ7 in myoblasts from pups aged 7–9 days.

(F) Fold changes in yeast protein abundances (log_2[Δ*coq8*/WT], n = 3) across the diauxic shift (Figure S2E) versus statistical significance as quantified by LC-MS/MS.

See also Figure S2.

S3A). The enrichment of COQ3 was relatively weak and could be indirectly mediated by complex Q interactions. To test whether perturbation of the COQ8A active site alters these interactions, we conducted COQ8A-FLAG AE-MS experiments with two COQ8A point mutants: D507N, which disrupts Mg-nucleotide binding, and K276H, a point mutation of the UbiB family-specific KxGQ motif (Figures 3D and 3E). Both mutations altered complex Q, suggesting that the activity of COQ8A modulates the interactions between CoQ proteins. Consistently, we recently observed dynamic, metabolic state-dependent COQ8A/B-complex Q interactions (Floyd et al., 2016).

COQ8A Lacks Protein Kinase Activity in *trans*

The observed COQ8A protein interactions could fit with the prevailing model that COQ8A is a protein kinase that phosphorylates COQ proteins. To test the protein kinase hypothesis, we examined *Coq8a*$^{-/-}$ mouse phosphoproteome changes. We quantified >7,500 cerebellar phosphopeptides and >6,000 skeletal muscle phosphopeptides, but we did not detect phosphopeptides from COQ3, COQ5, or COQ7 (Figure S2I; Table S5), the hypothesized COQ8A substrates (Xie et al., 2011), despite detecting representative peptides for each protein (Figure 2C). In skeletal muscle, COQ9 pS81 and pY88 were

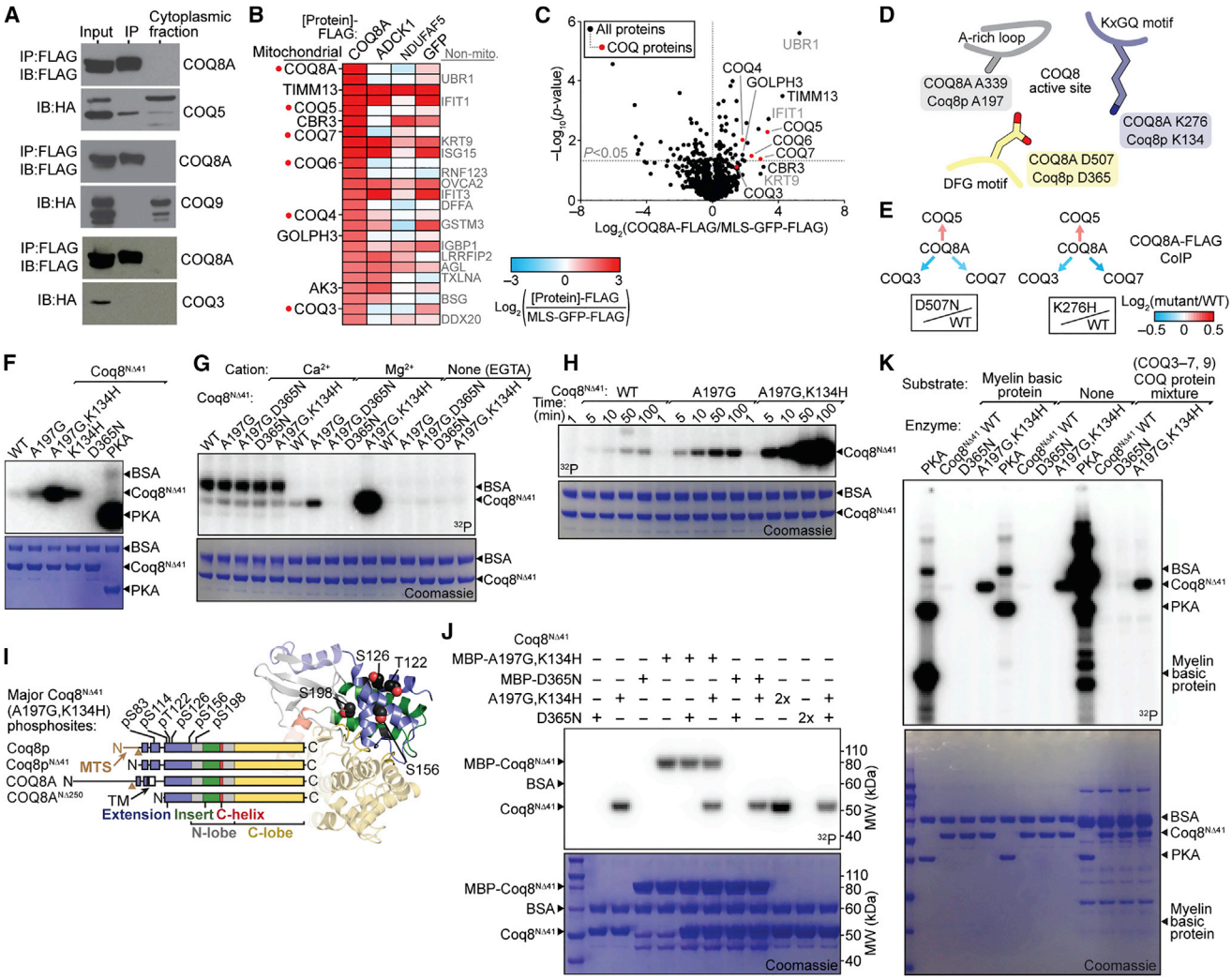

Figure 3. COQ8A Interacts with Complex Q but Lacks Protein Kinase Activity in *trans*

(A) Immunoblot (IB) analysis of interactions between COQ8A-FLAG and COQ5-HA, COQ3-HA, or COQ9-HA transfected into COS cells and immunoprecipitated (IP'd) using anti-FLAG beads.

(B) Heatmap showing the top 25 endogenous proteins most enriched by COQ8A-FLAG IP'd from HEK293 cells compared with various control IPs (mean, n = 4).

(C) Relative abundances of endogenous proteins co-purifying with COQ8A-FLAG compared with MLS-GFP-FLAG (mean, n = 4) IP'd from HEK293 cells as assessed by LC-MS/MS.

(D) Cartoon of COQ8 active site residues (based on PDB: 4PED).

(E) Relative abundances of endogenous COQ proteins co-purifying with COQ8A-FLAG ($\log_2$[mutant/WT]) IP'd from HEK293 cells as assessed by LC-MS/MS.

(F) SDS-PAGE analysis of in vitro Mg[γ-^{32}P]ATP autophosphorylation reactions with Coq8$^{N\Delta41}$ variants or PKA.

(G) Divalent cation dependence of Coq8$^{N\Delta41}$ autophosphorylation.

(H) Time course of Coq8$^{N\Delta41}$ autophosphorylation.

(I) Coq8$^{N\Delta41}$ autophosphorylation sites identified by LC-MS/MS mapped onto a homology model of Coq8p (based on COQ8A structure, PDB: 4PED).

(J) SDS-PAGE analysis of in vitro Mg[γ-^{32}P]ATP autophosphorylation reactions with combinations of Coq8$^{N\Delta41}$ variants. MBP, maltose binding protein tag.

(K) SDS-PAGE analysis of in vitro Mg[γ-^{32}P]ATP kinase reactions with PKA or Coq8$^{N\Delta41}$ and potential substrate proteins.

See also Figure S3.

observed, but were not significantly altered when normalized to protein abundance changes. Similarly, COQ9 pS81 was moderately decreased in *Coq8a*$^{-/-}$ cerebellums (*Coq8a*$^{-/-}$/WT = 0.6), likely because of the observed decrease in COQ9 abundance (Figure 2C). Likewise, in yeast, we quantified >6,000 phosphopeptides across the diauxic shift (Figures S2J and S2K; Table S6), but no phosphopeptides from Coq proteins were observed, despite detecting peptides from Coq3p–Coq9p (Figure 2F). These results suggest that complex Q proteins are not abundantly phosphorylated in vivo and led us to test the protein kinase hypothesis directly in vitro.

Mutants of a truncated COQ8A construct (COQ8A$^{N\Delta250}$) can autophosphorylate in vitro (Stefely et al., 2015), suggesting that COQ8A might act as a protein kinase in vivo. Here, we purified

the full mitochondrial form of Coq8p ($Coq8^{N\Delta41}$), which maintains its mature N terminus (Figure S3B) and thus eliminates caveats of the COQ8A truncation. Like $COQ8A^{N\Delta250}$ (Stefely et al., 2015), $Coq8^{N\Delta41}$ preferentially binds adenine nucleotides, with selectivity for ADP over ATP that can be reversed by an A-rich loop A-to-G mutation (Figures S3C and S3D). Mutating the A-rich loop or the invariant KxGQ motif enhances $Coq8^{N\Delta41}$ autophosphorylation activity, which is dependent on active site residue D365, Mg^{2+}, and time (Figures 3F–3H, S3E, and S3F). Thus, the basic biochemical properties of COQ8A and Coq8p are conserved.

Liquid chromatography tandem MS (LC-MS/MS) analyses showed that $Coq8^{N\Delta41}$ autophosphorylates residues of the KxGQ domain (Figures 3I and S3G), which occludes the canonical peptide substrate pocket. The KxGQ domain is accessible in *cis* or in *trans*, but reactions with combinations of active (WT or A197G,K134H) and inactive (D365N) $Coq8^{N\Delta41}$ showed that these Coq8p variants autophosphorylate exclusively in *cis* (Figures 3J and S3H). Similar results were observed for $COQ8A^{N\Delta250}$ (Figure S3I). Importantly, mutating $Coq8^{N\Delta41}$ autophosphorylation sites did not inhibit respiratory yeast growth (Figure S3J), showing that the autophosphorylation observed in vitro is dispensable for function in vivo.

Screening potential protein substrates for COQ8A and Coq8p further demonstrated their lack of *trans* protein kinase activity. While protein kinase A (PKA) exhibited robust protein kinase activity in *trans*, neither WT nor A197G,K134H $Coq8^{N\Delta41}$ catalyzed phosphorylation of myelin basic protein or mixtures of COQ proteins in *trans* (Figure 3K). Similar results were obtained for $COQ8A^{N\Delta250}$, which also does not catalyze phosphorylation of general protein kinase substrates (Figures S3K and S3L). Collectively, these results demonstrate that the enzymatic activities of mammalian COQ8A and yeast Coq8p are highly similar and that neither catalyzes canonical protein kinase activity. These findings argue against the protein kinase hypothesis and demand a new model for the "uPKL" functionality of COQ8.

Coq8p Catalyzes ATPase Activity with Its KxGQ Motif

To begin testing potential uPKL functions, we examined $Coq8^{N\Delta41}$ for ATPase activity, which can be considered as small-molecule "water kinase" activity. WT $Coq8^{N\Delta41}$ has ATPase activity and an A197G mutation, which enhances MgATP binding in vitro, increased the ATPase activity (Figures 4A and S4A–S4C). In contrast, K134H and A197G,K134H mutations decreased ATPase activity to a level near that of a mutant that does not bind nucleotides, D365N. Thus, Coq8p ATPase activity is enhanced by the UbiB-specific KxGQ motif. The inhibition of ATPase activity seen with the K134H mutants is in stark contrast to their dramatically enhanced autophosphorylation activity. Importantly, the K134H mutation eliminates CoQ production in vivo (Stefely et al., 2015), suggesting that, contrary to autophosphorylation, the ATPase activity is likely related to the endogenous activity of Coq8p.

To test the impact of these differential Coq8p mutations on complex Q stability in vivo, we examined Δ*coq8* yeast rescued with *coq8* variants by MS proteomics (Figures 4B and S4D). Whereas WT Coq8p rescued the abundance of complex Q proteins in vivo, the K134H mutant did not. The essentially equal need for D365 (MgATP binding) and K134 (ATPase, uPKL activity) suggests that uPKL activity stabilizes complex Q. The observation that the A197G mutation enhanced ATPase activity in vitro but decreased function in vivo could suggest that Coq8p does not act as an ATPase in vivo, but this A-rich loop perturbation likely has multifactorial effects because this loop is known to affect substrate binding and protein structure in other PKLs (Bossemeyer, 1994; Hemmer et al., 1997). Although the A-to-G mutation is useful for boosting MgATP binding in vitro, this alanine residue is highly conserved, and our results show that it does indeed support Coq8p function in vivo. More generally, these results do not necessarily demonstrate that COQ8 ATPase activity per se stabilizes complex Q in vivo, because water could mimic the hydroxyl group of another small-molecule substrate. The COQ8 ATPase activity could be more broadly indicative of small-molecule kinase activity or lipid kinase activity.

Coq8p Binds Lipid CoQ Intermediates

An interaction between COQ8A and lipids could be a feature of either lipid kinase activity or interactions with the membrane-associated complex Q. Sub-fractionation and Na_2CO_3 treatment of mouse mitochondria showed that endogenous COQ8A is partially buried in the inner mitochondrial membrane with its C terminus facing the matrix (Figure 4C). Consistently, $COQ8A^{N\Delta250}$ and $Coq8^{N\Delta41}$ bind to liposomes (Figure S4E). Thus, COQ8A interacts physically with lipid membranes.

To examine specific lipids that bind to Coq8p, we conducted LC-MS/MS analyses of lipids that co-purify with recombinant $Coq8^{N\Delta41}$ expressed in *E. coli*, which possesses a CoQ biosynthesis pathway similar to that found in eukaryotes. The *E. coli* CoQ biosynthesis intermediates octaprenylhydroxybenzoate (OHB) and octaprenylphenol (OPP) co-purified with $Coq8^{N\Delta41}$, but not with PKA, and Coq8p active site mutations decreased binding of OHB and OPP (Figure S4F). An independent set of experiments showed enrichment of OHB and OPP in samples of isolated $Coq8^{N\Delta41}$ compared with their abundance in the bacterial lysate from which they were purified (Figure 4D). Furthermore, binding of OHB, OPP, and heptaprenylphenol was decreased by Coq8p active site mutations D365N and K134H (Figures 4D and 4E). Interestingly, Coq8p did not enrich for CoQ (detected in the oxidized form in this experiment), and Coq8p active site mutations did not perturb co-purification of CoQ, suggesting that Coq8p preferentially binds CoQ biosynthesis intermediates.

Nucleotide Binding Activates COQ8A and Opens Small-Molecule Pockets

Our previous structure of apo $COQ8A^{N\Delta254}$ showed that its UbiB family specific KxGQ domain occludes the typical substrate binding pocket (Stefely et al., 2015), and no obvious hydrophobic binding pockets that could bind a lipid were present. However, nucleotide binding could open a COQ8A substrate binding pocket. To test this idea, we crystallized $COQ8A^{N\Delta254}$ R611K with adenosine 5′-(β,γ-imido)triphosphate (AMPPNP) and solved an X-ray structure at a resolution of 2.3 Å (Figure 5A; Table 1). The R611K mutant was used because we were unable to obtain WT-nucleotide co-crystals.

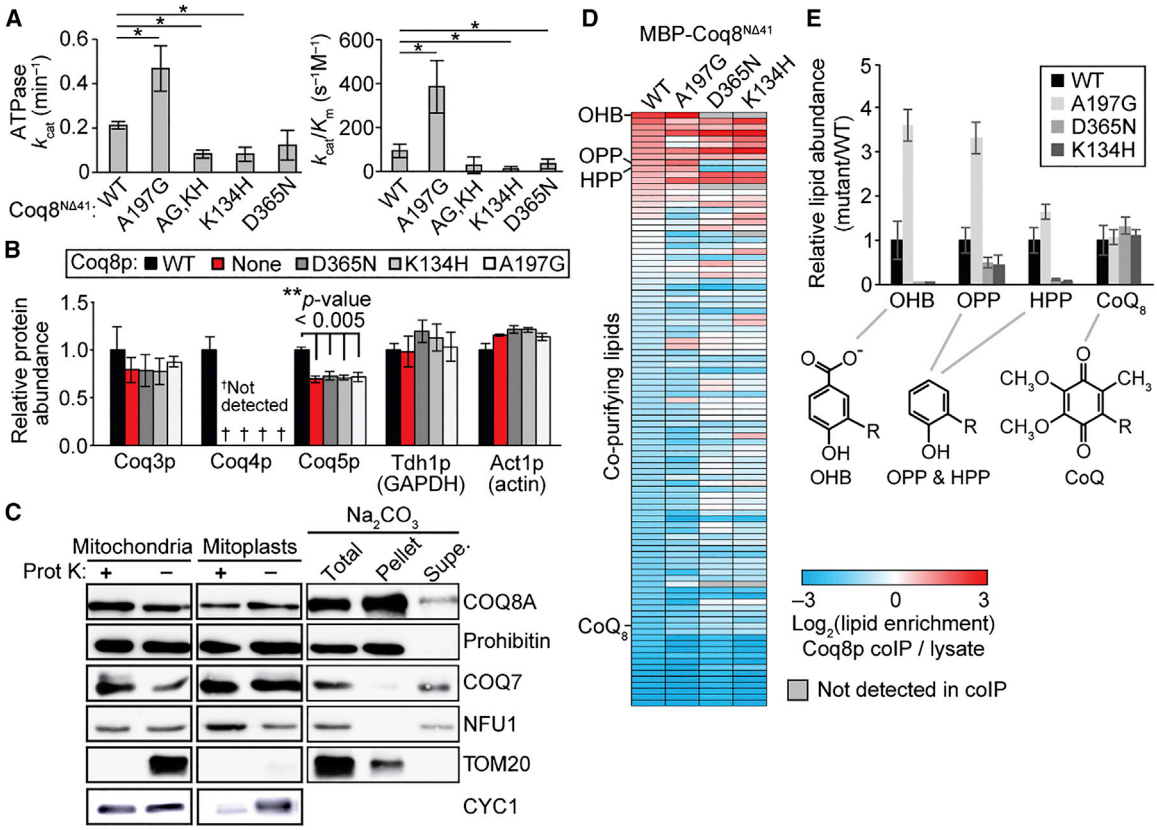

Figure 4. COQ8A and Coq8p Exhibit uPKL Activities

(A) k_{cat} and k_{cat}/K_m values for the ATPase activity of Coq8$^{N\Delta41}$ variants measured by observing production of phosphate (mean ± SD, n = 3). *p < 0.05.

(B) Relative protein abundances in Δ*coq8* yeast transformed with the indicated *coq8* (Coq8p) variants as quantified by label free quantitation LC-MS/MS analysis (mean ± SD, n = 4).

(C) Immunoblot analysis of COQ8A localization in submitochondrial fractions. Mitochondrial markers: COQ7 (inner membrane, peripheral), CYC1 (intermembrane space), NFU1 (matrix), Prohibitin (inner membrane, integral), and TOM20 (outer membrane, integral). Supe., supernatant.

(D) Heatmap showing enrichment of lipids co-purifying with MBP-Coq8$^{N\Delta41}$ variants compared with the bacterial lysate from which the proteins were purified as assessed by LC-MS (mean, n = 6).

(E) Relative abundances (mutant/WT) of CoQ biosynthesis intermediates (R, polyisoprenyl tail) co-purifying with MBP-Coq8$^{N\Delta41}$ variants as assessed by LC-MS (mean ± SD, n = 6).

See also Figure S4.

Overall, the apo and nucleotide-bound COQ8A structures are largely similar (Figures 5A, 5B, and S5A). Even with a nucleotide bound, the KxGQ motif is positioned to occlude the typical peptide substrate binding site and preclude in *trans* protein phosphorylation. Nucleotide-bound COQ8A is also structurally related to Rio family enzymes (Figures S5A and S5B), PKLs that function as ATPases (Ferreira-Cerca et al., 2012). Detailed comparisons of apo and nucleotide-bound COQ8A show that most residues deviate by only 2–3 Å, but notably larger 7–12 Å deviations of two loops in the KxGQ domain were observed: the GQα2-GQα3 loop and the GQα5-GQα6 loop ("Q switch 1" and "Q switch 2," respectively). The movement of these two COQ8A Q switches due to nucleotide binding opens two hydrophobic pockets in the KxGQ domain (KxGQ pockets 1 and 2, respectively), which are not present in the apo COQ8A structure (Figures 5A and S5D). KxGQ pocket 1 is near the putative phosphoryl acceptor substrate binding region, and it could potentially bind the kinase's substrate. In contrast, KxGQ pocket 2, which is partially formed by the "x" of the KxGQ motif, has the potential to bind an allosteric effector molecule that could communicate with the active site through the KxGQ motif.

KxGQ pocket 1 appears to be open sufficiently to accept a small-molecule kinase substrate, but other structural features also play important roles in kinase activation. Although COQ8A has intact "spine"-like structures (Figure S5E), an important feature of PKL enzyme activation (Kornev et al., 2006), the putative catalytic base D488 is locked in a salt bridge in the apo COQ8A structure (Figure S5F). To test the idea that nucleotide binding might allow D488 to move into an active conformation, we conducted 200 ns molecular dynamics (MD) simulations of apo, MgADP-bound, and MgATP-bound COQ8A. Kullback-Leibler divergence between simulations revealed clusters of residues with differential dynamics in the nucleotide pocket and the KxGQ domain (Figure S5G). In apo COQ8A, D488 remains

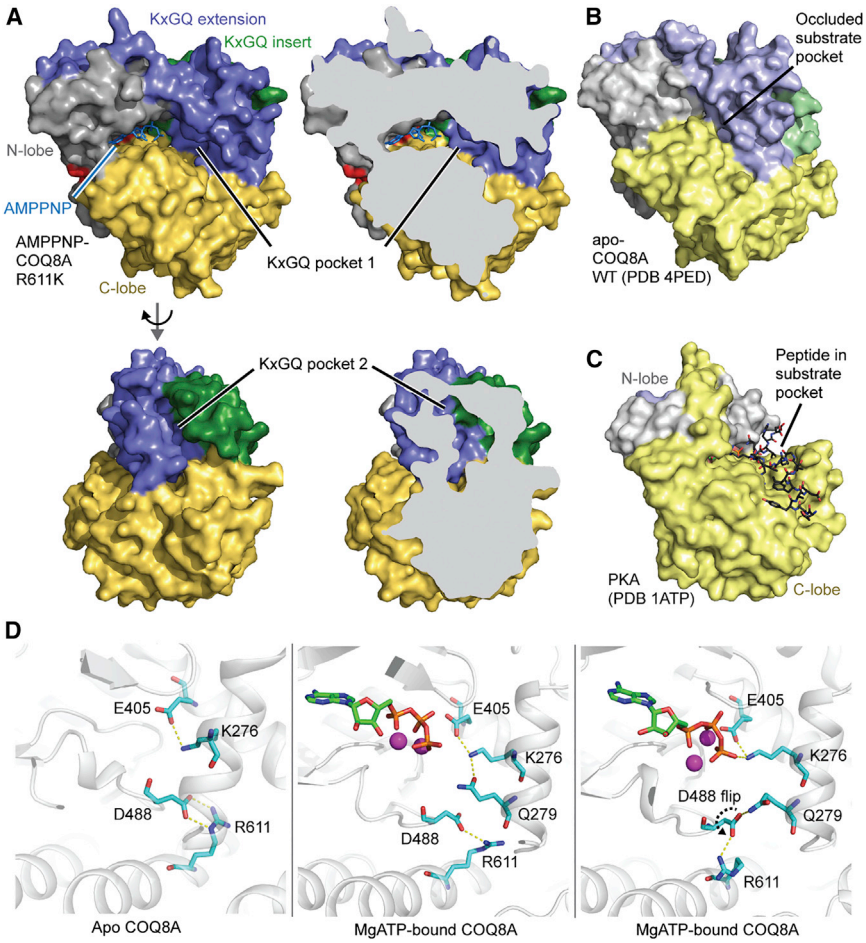

Figure 5. Structure and Dynamics of Nucleotide-Bound COQ8A

(A) Surface representations of COQ8A$^{N\Delta254}$ R611K bound to AMPPNP (PDB: 5I35), colored by domains (see Figure 3I). Two hydrophobic pockets (KxGQ pockets 1 and 2) are highlighted.

(B) Surface representation of apo COQ8A$^{N\Delta254}$ (PDB: 4PED).

(C) Surface representation of PKA (PDB: 1ATP) (Knighton et al., 1991).

(D) Representative snapshots of MD analyses of COQ8A showing interactions of D488 with either R611 or the KxGQ motif. Left: apo; middle and right: MgATP-bound.

See also Figure S5.

locked inside the protein core (Figure S5H). However, in the nucleotide-bound form, because of slight repacking of the GQα2 and GQα3 helices, D488 displays large side chain flexibility. Surprisingly, in the MgATP simulation, D488 flips from inside the hydrophobic core into a catalytically competent, solvent-exposed posture (Figure 5D), as indicated in the χ1 angle plot, which falls into two distinct ensembles (Figure S5H). This D488 flip is facilitated by hydrogen bonding with the KxGQ glutamine (Figure 5D). In addition, during our simulation, K276 can also form an ionic interaction with the γ-phosphate of ATP (Figure 5D), suggesting that the KxGQ motif may participate directly in catalyzing phosphoryl transfer. Together, these results demonstrate that COQ8A can adopt a conformation poised to catalyze phosphoryl transfer, not only in spite of the KxGQ domain's position in the typical peptide substrate pocket but likely facilitated by this very position of the KxGQ motif. Collectively, these structural observations provide further evidence for the uPKL functionality of COQ8A.

DISCUSSION

Insight into CoQ Biosynthesis

Two overarching problems continue to confound studies of CoQ biosynthesis in human health and disease. First, primary CoQ deficiencies have an extraordinary range of tissue specificities and clinical severities for unknown reasons (Laredj et al., 2014). Variable expression of COQ8A and COQ8B likely influences this clinical heterogeneity. Second, CoQ biosynthesis has many biochemical knowledge gaps, including proteins of unknown molecular function. These CoQ-associated proteins could support the pathway directly and specifically or, alternatively, indirectly as part of a broader biological function. The biochemical function of COQ8A is particularly difficult to define because, as we demonstrated here, it has complex functionalities outside of the canonical protein kinase model (Figure 6A). Completely defining the biochemistry of CoQ biosynthesis could lead to new strategies for treating CoQ deficiency.

Our results provide biological and biochemical evidence that mammalian COQ8A and yeast Coq8p function similarly by directly and specifically supporting CoQ biosynthesis through maintenance of complex Q. These results, in combination with phylogenetic analyses, led us to rename ADCK3 and ADCK4 as COQ8A and COQ8B, respectively. This nomenclature provides more functionally descriptive names and properly designates them as co-orthologs of Coq8p.

A Mouse Model of Moderate CoQ Deficiency

Generating animal models for studying CoQ deficiency is difficult because *Coq* gene knockouts are often embryonic lethal (Licitra and Puccio, 2014). Here, in contrast, we demonstrated that lack of COQ8A in mice results in a mild phenotype with progressive cerebellar ataxia, mild exercise intolerance, and moderate CoQ deficiency (Figure 6B), recapitulating the more frequent features of ARCA2 (Auré et al., 2004; Barca et al., 2016; Gerards et al., 2010; Horvath et al., 2012; Lagier-Tourenne et al., 2008; Mignot et al., 2013; Mollet et al., 2008). Thus, this work establishes *Coq8a*$^{-/-}$ mice as a valid model system for studying ARCA2 and testing potential treatments.

Table 1. X-Ray Data Collection and Refinement Statistics

Data Collection	
Space group	C 1 2 1
Cell Dimensions	
a, *b*, *c* (Å)	150.05, 59.12, 97.69
α, β, γ (°)	90, 97.69, 90
Resolution (Å)	39.42–2.30 (2.38–2.30)[a]
R_{sym}	0.088 (1.068)
$I/\sigma I$	15.6 (1.9)
Completeness (%)	99 (100)
Redundancy	7.4 (7.6)
Refinement	
Resolution (Å)	39.42–2.30
No. reflections	19,830 (1,940)
R_{work}/ R_{free}	0.184/0.259
No. Atoms	
Protein	3,105
Ligand/ion	31
Water	26
B factors	
Protein	72.4
Ligand/ion	74.8
Water	68.8
Root-Mean-Square Deviation	
Bond lengths (Å)	0.024
Bond angles (°)	2.2
Ramachandran Plot (%)	
Favored	94
Allowed	5
Outliers	1

[a]The highest resolution shell is shown in parentheses.

The pathophysiologies of cerebellar ataxias are diverse (Wolf and Koenig, 2013). Similar to other ataxia models (Custer et al., 2006; Maltecca et al., 2009; Stankewich et al., 2010), *Coq8a*$^{-/-}$ mice displayed dark degenerating PCs, while other cerebellar cells were spared. Our biochemical studies showed a deficit of complex Q proteins but normal cerebellar CoQ levels. PCs account for a small fraction (<0.1%) of cerebellar cells (Lange, 1975), and a PC-specific CoQ deficiency could be masked by other cells. Unexpectedly, *Coq8a*$^{-/-}$ PCs displayed Golgi morphology defects, but normal mitochondria. Golgi pathology is a hallmark of neurodegenerative diseases including Parkinson's disease and amyotrophic lateral sclerosis (Sundaramoorthy et al., 2015). The *Coq8a*$^{-/-}$ Golgi defects could be secondary to mitochondrial CoQ deficiency or, alternatively, due to defective Golgi CoQ biosynthesis, which is biologically important (Mugoni et al., 2013). Golgi defects could in turn disrupt intracellular protein trafficking and thus PC electrophysiology. Our *Coq8a*$^{-/-}$ mice provide a model system to study CoQ production across different organelles, cells, and tissues.

Organism-wide, loss of COQ8A has complex, tissue-specific effects. *Coq8a*$^{-/-}$ skeletal muscle is significantly deficient in complex Q and in CoQ, and *Coq8a*$^{-/-}$ mice have low exercise fitness. However, CoQ and complex Q were also affected across *Coq8a*$^{-/-}$ tissues that do not have obvious biological phenotypes. Tissue-specific variability in *COQ8A* and *COQ8B* expression could contribute to these differential effects. Indeed, the two tissues most affected by loss of COQ8A, cerebellum and skeletal muscle, show low expression of *COQ8B* (Figures S1H, S1M, and S1N). In contrast, the kidney, which is relatively unaffected by loss of COQ8A (Figure S2D), shows high *COQ8B* expression (Figures S1M and S1N). More distantly related COQ8A/B homologs (ADCK1, ADCK2, and ADCK5) could also play a role. Cell-type-specific differences in CoQ transport and uptake (Anderson et al., 2015) could further complicate the relationship between complex Q abundance and CoQ abundance. Our proteomics and phosphoproteomics results provide a resource for continued investigation of the tissue-specific effects of COQ8A deficiency.

Unorthodox Activity of UbiB Family Kinases

Initially, COQ8A was predicted to be a protein kinase with a non-essential regulatory role in CoQ biosynthesis. However, our results argue against the canonical protein kinase model and instead support a uPKL functionality for COQ8 (referring to both mammalian COQ8A/B and yeast Coq8p, which we propose to function through the same fundamental mechanisms). Thus, our work adds COQ8 to an expanding list of PKL superfamily members with non-canonical activities that are central to their biological functions (Kung and Jura, 2016).

The precise molecular mechanism by which COQ8 enhances complex Q activity to support CoQ biosynthesis is not yet fully resolved. However, our past (Stefely et al., 2015) and present work shows that COQ8's endogenous function requires adenine nucleotide binding, a conserved active site that catalyzes phosphoryl transfer, and the UbiB-specific KxGQ motif. Our results support at least two potential uPKL activities that incorporate these features (Figure 6A): (1) ATPase activity that enhances complex Q interactions or supports complex Q assembly and (2) small-molecule kinase activity that phosphorylates a complex Q component (e.g., a CoQ intermediate or cofactor), which would support both the stability and the activity of complex Q.

Rigorously defining which uPKL functional model operates in vivo will require extensive work, but our results establish biochemical uPKL activities of COQ8 that are more likely important for its endogenous function than its in vitro *cis* autophosphorylation activity. Mutating the lysine of the UbiB family-specific KxGQ motif provides a particularly informative perturbation, because it enhances *cis* autophosphorylation but inhibits other COQ8 activities, including support of in vivo respiratory metabolism, CoQ production, complex Q stability, ATPase activity (which could be indicative of small molecule kinase activity), and lipid CoQ intermediate binding.

The ability of Coq8p to bind CoQ intermediates provides an important addition to its known molecular functions. Interestingly, OPP is the intermediate that accumulates in Δ*ubiB E. coli* (Cox et al., 1969; Poon et al., 2000), which lack the prokaryotic *coq8* homolog, and hexaprenylhydroxybenzoate (an OHB analog) is the intermediate that accumulates in Δ*coq8*

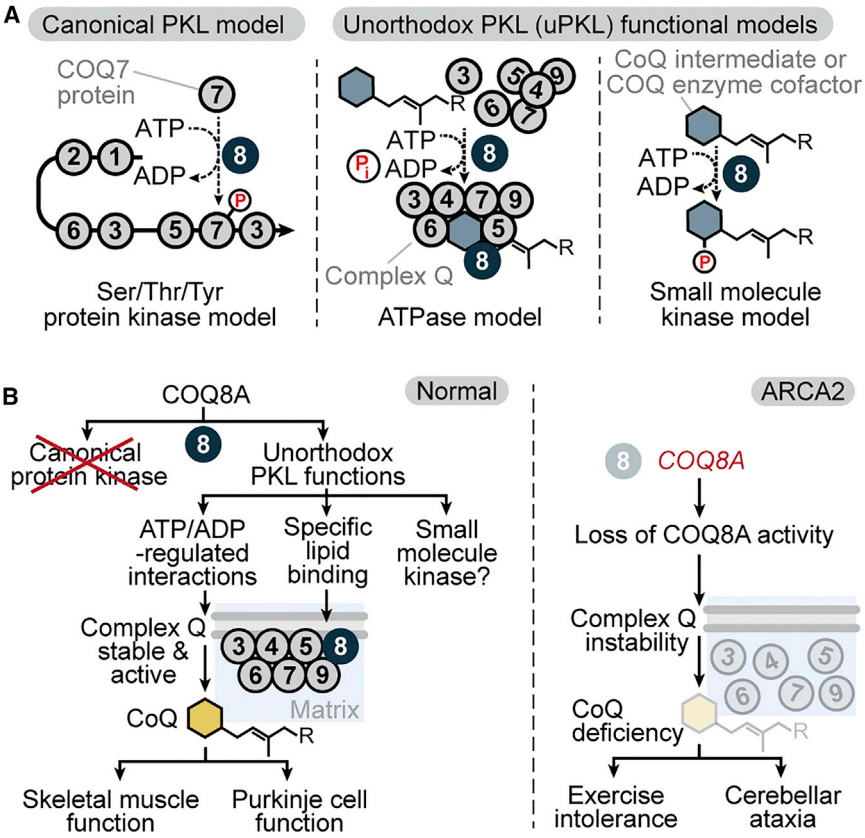

Figure 6. A Model for the Molecular Basis of COQ8 Biology

(A) Models for the molecular activity of COQ8 (COQ8A/B and Coq8p).

(B) Models for COQ8A biology and its disruption in ARCA2.

yeast. Although we have not yet observed COQ8-dependent phosphorylation of OPP or OHB, potentially because of product lability, a lipid CoQ intermediate could bind to KxGQ pocket 1 as a kinase substrate. Phosphorylation of a CoQ intermediate could potentially make it more accessible to enzymes peripherally associated with the lipid membrane or create a protecting group to maintain the intermediate in a reduced or energetically charged state for a particular biosynthetic reaction (e.g., the *C2* methylation catalyzed by COQ5). Alternatively, or in addition, an isoprenoid lipid could bind to KxGQ pocket 2 as an allosteric regulator of COQ8 activity.

Together, our work supports a model wherein the uPKL functionality of COQ8, which involves interactions with both CoQ intermediates and the protein COQ5, enhances complex Q stability and activity to support CoQ biosynthesis and various in vivo functions (e.g., skeletal muscle function and PC function in the case of COQ8A) (Figure 6B). More broadly, our work on COQ8 provides a molecular foundation for studying the larger UbiB family, which has diverse functions in lipid metabolism (Tan et al., 2013), cell migration (Simpson et al., 2008), and tumor cell viability (Brough et al., 2011; Wiedemeyer et al., 2010). Because all UbiB family members have a KxGQ motif and a predicted KxGQ domain, which we have shown to play a central role in the uPKL functions of COQ8, we predict uPKL functionality to be conserved throughout this ancient protein family.

Collectively, this work establishes a robust mammalian model system for studying neurodegeneration, muscle disorders, potential treatments, and the complex effects of CoQ deficiency on health and disease. Our studies also show that the molecular basis for the inherited disease ARCA2 involves deficiency of complex Q and CoQ due to loss of uPKL activity, which is likely conserved in homologs across all three superkingdoms of life.

EXPERIMENTAL PROCEDURES

Further details for all procedures can be found in Supplemental Experimental Procedures.

Mice and Cell Culture

Coq8a$^{-/-}$ (*Adck3*$^{-/-}$) mice deleted for exons 9–14 were generated by homologous recombination. Motor coordination was assessed by accelerating rotating rod, footprint analysis, and beam-walking tests. Memory and learning capacity were assessed with Y-Maze, object recognition, and Morris water maze tests. Physical fitness was assessed by treadmill and grip tests. Sex- and age-matched mice were used in experiments in accordance with national ethical rules. Primary myoblasts were generated from hindlimb muscle of mice aged 7–9 days.

Microscopy and PC Electrophysiology

For immunohistochemistry (IHC) and transmission electron microscopy (TEM), mice were perfused with 4% paraformaldehyde. For IHC, tissues were either frozen or paraffin embedded. For TEM, tissues were fixed in 2.5% glutaraldehyde, postfixed in 1% osmium tetroxide, and embedded in Epon. For PC electrophysiology, mice were decapitated under isoflurane anesthesia, acute 330-μm-thick cerebellar slices were prepared, and extracellular recordings of individual PCs were performed using 15–30 MΩ pipettes.

CoQ Quantitation and Lipidomics

Lipids were extracted from tissue homogenates with organic solvents. For targeted CoQ measurements, lipids were separated by LC and quantified by electrochemical detection using CoQ_8 as an internal standard. For unbiased lipidomics, lipids were separated, identified, and quantified by LC-MS/MS performed on a C18 column coupled to a Q Exactive Focus mass spectrometer by a heated ESI source.

Proteomics and Phosphoproteomics

Proteins from lysates were digested into peptides, labeled with isobaric tags, and fractionated by strong cation exchange. Phosphopeptides were enriched by immobilized metal affinity chromatography (IMAC). LC-MS/MS was performed on a C18 column coupled to an Orbitrap Elite mass spectrometer by a nanoESI source.

In Vitro Kinase and ATPase Assays

8His-MBP-[TEV]-Coq8^{NΔ41} was expressed in *E. coli* and purified using cobalt IMAC resin, tobacco etch virus (TEV) cleavage, and a second subtractive IMAC purification to remove 8His-MBP and isolate Coq8^{NΔ41}. For kinase assays, unless otherwise indicated, Coq8^{NΔ41} (4 μM), MBP-Coq8^{NΔ41} (4 μM), or PKA

(4 μM) was mixed with [γ-^{32}P]ATP (0.25 μCi/μL, 100 μM [ATP]$_{total}$), $MgCl_2$ (20 mM), and substrate proteins and incubated (30°C, 60 min) (final concentrations). Reactions were quenched with 4 × LDS buffer, [γ-^{32}P]ATP was separated from Coq8^{NΔ41} by SDS-PAGE, and the gel was stained, dried, and imaged. For ATPase assays, Coq8^{NΔ41} (2 μM) was mixed with ATP (0–2 mM) and phosphate detection reagents and incubated (22°C).

Identification of Lipids Bound to Coq8p

8His-MBP-Coq8^{NΔ41} was expressed in *E. coli* and isolated by cobalt IMAC. Lipids were extracted with $CHCl_3$/MeOH (1:1, v/v) and analyzed by unbiased LC-MS/MS.

Protein Co-immunoprecipitation

COQ8A-FLAG was expressed in HEK293 cells and immunoprecipitated with anti-FLAG M2 beads. Co-purifying proteins were digested into peptides with trypsin and analyzed by label-free quantitation LC-MS/MS.

Protein Crystallization

Crystals of selenomethionine-labeled COQ8A^{NΔ254} R611K were obtained by hanging drop vapor diffusion using 2 μl of 0.2 mM COQ8A, 2 mM AMPPNP, 4 mM $MgCl_2$ mixed with 2 μl of reservoir solution, 26% sodium acrylate 5100, 20 mM $MgCl_2$, and 100 mM NaHEPES (pH 7.5). Crystals were cryopreserved by increasing the sodium acrylate 5100 concentration to 30%.

ACCESSION NUMBERS

The accession number for the coordinates and structure factors reported in this paper is PDB: 5I35.

SUPPLEMENTAL INFORMATION

Supplemental Information includes Supplemental Experimental Procedures, five figures, and six tables and can be found with this article online at http://dx.doi.org/10.1016/j.molcel.2016.06.030.

AUTHOR CONTRIBUTIONS

J.A.S., F.L., L.L., H.P., and D.J.P. conceived of the project and its design and wrote the manuscript. All authors performed experiments and/or data analysis.

ACKNOWLEDGMENTS

We thank Nadia Messadeq, Hamid Meziane, Marie-France Champy, and the ICS facility for mouse phenotyping support; Carol Mercer for support; Bob Smith for crystallomics assistance; and Michael Becker for beamline assistance. This work was supported by Searle Scholars and Vilas Associates Awards and National Institutes of Health (NIH) grants U01GM94622, R01DK098672, R01GM112057, and R01GM115591 (to D.J.P.); the UK ataxia association, Fondation Recherche Médicale (FRM) Physiopathologie Mitochondriale DPM20121125555, and European Research Council 206634/ISCATAXIA (to H.P.); NIH Ruth L. Kirschstein National Research Service Award F30AG043282 (to J.A.S.); NIH T32GM008505 (to A.G.R.); NIH 5T32GM08349 and National Science Foundation (NSF) DGE-1256259 (to D.C.L.); NIH T32DK007665 (to B.J.F.); NIH R35GM118110 (to J.J.C.); École Polytechnique Fédérale de Lausanne and the Swiss NSF (200021_157217) (to M.D.P.); ANR grant pABACoQ (to F.P.); Institut de Génétique et de Biologie Moléculaire et Cellulaire IPP Fellowships (to F.L. and T.J.) (LabEx INRT funds, ANR-10-LABX-0030-INRT, *Investissements d'Avenir* ANR-10-IDEX-0002-02); FRM DEQ20140329514 and ANR-13-SAMA-0010-01 (to P.I.); U01GM098248 and U54GM094584 (C.A.B.); the United States Department of Energy (DE-AC02-06CH11357) (Advanced Photon Source use); the Michigan Economic Development Corporation (085P1000817) (LS-CAT); and NIH National Cancer Institute (Y1-CO-1020) and National Institute of General Medical Sciences (Y1-GM-1104) (GM/CA@APS).

Received: February 24, 2016
Revised: May 27, 2016
Accepted: June 21, 2016
Published: August 4, 2016

REFERENCES

Anderson, C.M., Kazantzis, M., Wang, J., Venkatraman, S., Goncalves, R.L., Quinlan, C.L., Ng, R., Jastroch, M., Benjamin, D.I., Nie, B., et al. (2015). Dependence of brown adipose tissue function on CD36-mediated coenzyme Q uptake. Cell Rep. *10*, 505–515.

Ashraf, S., Gee, H.Y., Woerner, S., Xie, L.X., Vega-Warner, V., Lovric, S., Fang, H., Song, X., Cattran, D.C., Avila-Casado, C., et al. (2013). ADCK4 mutations promote steroid-resistant nephrotic syndrome through CoQ10 biosynthesis disruption. J. Clin. Invest. *123*, 5179–5189.

Auré, K., Benoist, J.F., Ogier de Baulny, H., Romero, N.B., Rigal, O., and Lombès, A. (2004). Progression despite replacement of a myopathic form of coenzyme Q10 defect. Neurology *63*, 727–729.

Barca, E., Musumeci, O., Montagnese, F., Marino, S., Granata, F., Nunnari, D., Peverelli, L., DiMauro, S., Quinzii, C.M., and Toscano, A. (2016). Cerebellar ataxia and severe muscle CoQ10 deficiency in a patient with a novel mutation in ADCK3. Clin. Genet., Published online January 27, 2016. http://dx.doi.org/10.1111/cge.12742.

Bossemeyer, D. (1994). The glycine-rich sequence of protein kinases: a multifunctional element. Trends Biochem. Sci. *19*, 201–205.

Brough, R., Frankum, J.R., Sims, D., Mackay, A., Mendes-Pereira, A.M., Bajrami, I., Costa-Cabral, S., Rafiq, R., Ahmad, A.S., Cerone, M.A., et al. (2011). Functional viability profiles of breast cancer. Cancer Discov. *1*, 260–273.

Cox, G.B., Young, I.G., McCann, L.M., and Gibson, F. (1969). Biosynthesis of ubiquinone in Escherichia coli K-12: location of genes affecting the metabolism of 3-octaprenyl-4-hydroxybenzoic acid and 2-octaprenylphenol. J. Bacteriol. *99*, 450–458.

Crane, F.L., Hatefi, Y., Lester, R.L., and Widmer, C. (1957). Isolation of a quinone from beef heart mitochondria. Biochim. Biophys. Acta *25*, 220–221.

Custer, S.K., Garden, G.A., Gill, N., Rueb, U., Libby, R.T., Schultz, C., Guyenet, S.J., Deller, T., Westrum, L.E., Sopher, B.L., and La Spada, A.R. (2006). Bergmann glia expression of polyglutamine-expanded ataxin-7 produces neurodegeneration by impairing glutamate transport. Nat. Neurosci. *9*, 1302–1311.

Do, T.Q., Hsu, A.Y., Jonassen, T., Lee, P.T., and Clarke, C.F. (2001). A defect in coenzyme Q biosynthesis is responsible for the respiratory deficiency in Saccharomyces cerevisiae abc1 mutants. J. Biol. Chem. *276*, 18161–18168.

Ferreira-Cerca, S., Sagar, V., Schäfer, T., Diop, M., Wesseling, A.M., Lu, H., Chai, E., Hurt, E., and LaRonde-LeBlanc, N. (2012). ATPase-dependent role of the atypical kinase Rio2 on the evolving pre-40S ribosomal subunit. Nat. Struct. Mol. Biol. *19*, 1316–1323.

Floyd, B.J., Wilkerson, E.M., Veling, M.T., Minogue, C.E., Xia, C., Beebe, E.T., Wrobel, R.L., Cho, H., Kremer, L.S., Alston, C.L., et al. (2016). Mitochondrial protein interaction mapping identifies new regulators of respiratory chain function. Mol. Cell *63*, this issue, 621–632.

Gerards, M., van den Bosch, B., Calis, C., Schoonderwoerd, K., van Engelen, K., Tijssen, M., de Coo, R., van der Kooi, A., and Smeets, H. (2010). Nonsense mutations in CABC1/ADCK3 cause progressive cerebellar ataxia and atrophy. Mitochondrion *10*, 510–515.

Häusser, M., and Clark, B.A. (1997). Tonic synaptic inhibition modulates neuronal output pattern and spatiotemporal synaptic integration. Neuron *19*, 665–678.

He, C.H., Xie, L.X., Allan, C.M., Tran, U.C., and Clarke, C.F. (2014). Coenzyme Q supplementation or over-expression of the yeast Coq8 putative kinase stabilizes multi-subunit Coq polypeptide complexes in yeast coq null mutants. Biochim. Biophys. Acta *1841*, 630–644.

Hemmer, W., McGlone, M., Tsigelny, I., and Taylor, S.S. (1997). Role of the glycine triad in the ATP-binding site of cAMP-dependent protein kinase. J. Biol. Chem. *272*, 16946–16954.

Horvath, R., Czermin, B., Gulati, S., Demuth, S., Houge, G., Pyle, A., Dineiger, C., Blakely, E.L., Hassani, A., Foley, C., et al. (2012). Adult-onset cerebellar ataxia due to mutations in CABC1/ADCK3. J. Neurol. Neurosurg. Psychiatry *83*, 174–178.

Kannan, N., Taylor, S.S., Zhai, Y., Venter, J.C., and Manning, G. (2007). Structural and functional diversity of the microbial kinome. PLoS Biol. *5*, e17.

Knighton, D.R., Zheng, J.H., Ten Eyck, L.F., Ashford, V.A., Xuong, N.H., Taylor, S.S., and Sowadski, J.M. (1991). Crystal structure of the catalytic subunit of cyclic adenosine monophosphate-dependent protein kinase. Science *253*, 407–414.

Kornev, A.P., Haste, N.M., Taylor, S.S., and Eyck, L.F. (2006). Surface comparison of active and inactive protein kinases identifies a conserved activation mechanism. Proc. Natl. Acad. Sci. U S A *103*, 17783–17788.

Kung, J.E., and Jura, N. (2016). Structural basis for the non-catalytic functions of protein kinases. Structure *24*, 7–24.

Lagier-Tourenne, C., Tazir, M., López, L.C., Quinzii, C.M., Assoum, M., Drouot, N., Busso, C., Makri, S., Ali-Pacha, L., Benhassine, T., et al. (2008). ADCK3, an ancestral kinase, is mutated in a form of recessive ataxia associated with coenzyme Q10 deficiency. Am. J. Hum. Genet. *82*, 661–672.

Lange, W. (1975). Cell number and cell density in the cerebellar cortex of man and some other mammals. Cell Tissue Res. *157*, 115–124.

Laredj, L.N., Licitra, F., and Puccio, H.M. (2014). The molecular genetics of coenzyme Q biosynthesis in health and disease. Biochimie *100*, 78–87.

Leonard, C.J., Aravind, L., and Koonin, E.V. (1998). Novel families of putative protein kinases in bacteria and archaea: evolution of the "eukaryotic" protein kinase superfamily. Genome Res. *8*, 1038–1047.

Lester, R.L., and Crane, F.L. (1959). The natural occurrence of coenzyme Q and related compounds. J. Biol. Chem. *234*, 2169–2175.

Licitra, F., and Puccio, H. (2014). An overview of current mouse models recapitulating coenzyme q10 deficiency syndrome. Mol. Syndromol. *5*, 180–186.

Lundquist, P.K., Poliakov, A., Giacomelli, L., Friso, G., Appel, M., McQuinn, R.P., Krasnoff, S.B., Rowland, E., Ponnala, L., Sun, Q., and van Wijk, K.J. (2013). Loss of plastoglobule kinases ABC1K1 and ABC1K3 causes conditional degreening, modified prenyl-lipids, and recruitment of the jasmonic acid pathway. Plant Cell *25*, 1818–1839.

Maltecca, F., Magnoni, R., Cerri, F., Cox, G.A., Quattrini, A., and Casari, G. (2009). Haploinsufficiency of AFG3L2, the gene responsible for spinocerebellar ataxia type 28, causes mitochondria-mediated Purkinje cell dark degeneration. J. Neurosci. *29*, 9244–9254.

Manning, G., Whyte, D.B., Martinez, R., Hunter, T., and Sudarsanam, S. (2002). The protein kinase complement of the human genome. Science *298*, 1912–1934.

Martinis, J., Glauser, G., Valimareanu, S., and Kessler, F. (2013). A chloroplast ABC1-like kinase regulates vitamin E metabolism in Arabidopsis. Plant Physiol. *162*, 652–662.

Mignot, C., Apartis, E., Durr, A., Marques Lourenço, C., Charles, P., Devos, D., Moreau, C., de Lonlay, P., Drouot, N., Burglen, L., et al. (2013). Phenotypic variability in ARCA2 and identification of a core ataxic phenotype with slow progression. Orphanet J. Rare Dis. *8*, 173.

Mollet, J., Delahodde, A., Serre, V., Chretien, D., Schlemmer, D., Lombes, A., Boddaert, N., Desguerre, I., de Lonlay, P., de Baulny, H.O., et al. (2008). CABC1 gene mutations cause ubiquinone deficiency with cerebellar ataxia and seizures. Am. J. Hum. Genet. *82*, 623–630.

Morton, R.A. (1958). Ubiquinone. Nature *182*, 1764–1767.

Mugoni, V., Postel, R., Catanzaro, V., De Luca, E., Turco, E., Digilio, G., Silengo, L., Murphy, M.P., Medana, C., Stainier, D.Y., et al. (2013). Ubiad1 is an antioxidant enzyme that regulates eNOS activity by CoQ10 synthesis. Cell *152*, 504–518.

Oruganty, K., Talevich, E.E., Neuwald, A.F., and Kannan, N. (2016). Identification and classification of small molecule kinases: insights into substrate recognition and specificity. BMC Evol. Biol. *16*, 7.

Pagliarini, D.J., Calvo, S.E., Chang, B., Sheth, S.A., Vafai, S.B., Ong, S.E., Walford, G.A., Sugiana, C., Boneh, A., Chen, W.K., et al. (2008). A mitochondrial protein compendium elucidates complex I disease biology. Cell *134*, 112–123.

Pierrel, F., Hamelin, O., Douki, T., Kieffer-Jaquinod, S., Mühlenhoff, U., Ozeir, M., Lill, R., and Fontecave, M. (2010). Involvement of mitochondrial ferredoxin and para-aminobenzoic acid in yeast coenzyme Q biosynthesis. Chem. Biol. *17*, 449–459.

Poon, W.W., Davis, D.E., Ha, H.T., Jonassen, T., Rather, P.N., and Clarke, C.F. (2000). Identification of Escherichia coli ubiB, a gene required for the first monooxygenase step in ubiquinone biosynthesis. J. Bacteriol. *182*, 5139–5146.

Quinzii, C.M., and Hirano, M. (2010). Coenzyme Q and mitochondrial disease. Dev. Disabil. Res. Rev. *16*, 183–188.

Rhee, H.W., Zou, P., Udeshi, N.D., Martell, J.D., Mootha, V.K., Carr, S.A., and Ting, A.Y. (2013). Proteomic mapping of mitochondria in living cells via spatially restricted enzymatic tagging. Science *339*, 1328–1331.

Seshadri Sastry, P., Jayaraman, J., and Ramasarma, T. (1961). Distribution of coenzyme Q in rat liver cell fractions. Nature *189*, 577.

Simpson, K.J., Selfors, L.M., Bui, J., Reynolds, A., Leake, D., Khvorova, A., and Brugge, J.S. (2008). Identification of genes that regulate epithelial cell migration using an siRNA screening approach. Nat. Cell Biol. *10*, 1027–1038.

Stankewich, M.C., Gwynn, B., Ardito, T., Ji, L., Kim, J., Robledo, R.F., Lux, S.E., Peters, L.L., and Morrow, J.S. (2010). Targeted deletion of betaIII spectrin impairs synaptogenesis and generates ataxic and seizure phenotypes. Proc. Natl. Acad. Sci. U S A *107*, 6022–6027.

Stefely, J.A., Reidenbach, A.G., Ulbrich, A., Oruganty, K., Floyd, B.J., Jochem, A., Saunders, J.M., Johnson, I.E., Minogue, C.E., Wrobel, R.L., et al. (2015). Mitochondrial ADCK3 employs an atypical protein kinase-like fold to enable coenzyme Q biosynthesis. Mol. Cell *57*, 83–94.

Sundaramoorthy, V., Sultana, J.M., and Atkin, J.D. (2015). Golgi fragmentation in amyotrophic lateral sclerosis, an overview of possible triggers and consequences. Front. Neurosci. *9*, 400.

Tan, T., Ozbalci, C., Brügger, B., Rapaport, D., and Dimmer, K.S. (2013). Mcp1 and Mcp2, two novel proteins involved in mitochondrial lipid homeostasis. J. Cell Sci. *126*, 3563–3574.

Tauche, A., Krause-Buchholz, U., and Rödel, G. (2008). Ubiquinone biosynthesis in Saccharomyces cerevisiae: the molecular organization of O-methylase Coq3p depends on Abc1p/Coq8p. FEMS Yeast Res. *8*, 1263–1275.

Tran, U.C., and Clarke, C.F. (2007). Endogenous synthesis of coenzyme Q in eukaryotes. Mitochondrion *7* (*Suppl*), S62–S71.

Walker, E.H., Perisic, O., Ried, C., Stephens, L., and Williams, R.L. (1999). Structural insights into phosphoinositide 3-kinase catalysis and signalling. Nature *402*, 313–320.

Wiedemeyer, W.R., Dunn, I.F., Quayle, S.N., Zhang, J., Chheda, M.G., Dunn, G.P., Zhuang, L., Rosenbluh, J., Chen, S., Xiao, Y., et al. (2010). Pattern of retinoblastoma pathway inactivation dictates response to CDK4/6 inhibition in GBM. Proc. Natl. Acad. Sci. U S A *107*, 11501–11506.

Wolf, N.I., and Koenig, M. (2013). Progressive cerebellar atrophy: hereditary ataxias and disorders with spinocerebellar degeneration. Handb. Clin. Neurol. *113*, 1869–1878.

Xie, L.X., Hsieh, E.J., Watanabe, S., Allan, C.M., Chen, J.Y., Tran, U.C., and Clarke, C.F. (2011). Expression of the human atypical kinase ADCK3 rescues coenzyme Q biosynthesis and phosphorylation of Coq polypeptides in yeast coq8 mutants. Biochim. Biophys. Acta *1811*, 348–360.

Zeqiraj, E., and van Aalten, D.M. (2010). Pseudokinases-remnants of evolution or key allosteric regulators? Curr. Opin. Struct. Biol. *20*, 772–781.

Molecular Cell, Volume *63*

Supplemental Information

Cerebellar Ataxia and Coenzyme Q Deficiency through Loss of Unorthodox Kinase Activity

Jonathan A. Stefely, Floriana Licitra, Leila Laredj, Andrew G. Reidenbach, Zachary A. Kemmerer, Anais Grangeray, Tiphaine Jaeg-Ehret, Catherine E. Minogue, Arne Ulbrich, Paul D. Hutchins, Emily M. Wilkerson, Zheng Ruan, Deniz Aydin, Alexander S. Hebert, Xiao Guo, Elyse C. Freiberger, Laurence Reutenauer, Adam Jochem, Maya Chergova, Isabel E. Johnson, Danielle C. Lohman, Matthew J.P. Rush, Nicholas W. Kwiecien, Pankaj K. Singh, Anna I. Schlagowski, Brendan J. Floyd, Ulrika Forsman, Pavel J. Sindelar, Michael S. Westphall, Fabien Pierrel, Joffrey Zoll, Matteo Dal Peraro, Natarajan Kannan, Craig A. Bingman, Joshua J. Coon, Philippe Isope, Hélène Puccio, and David J. Pagliarini

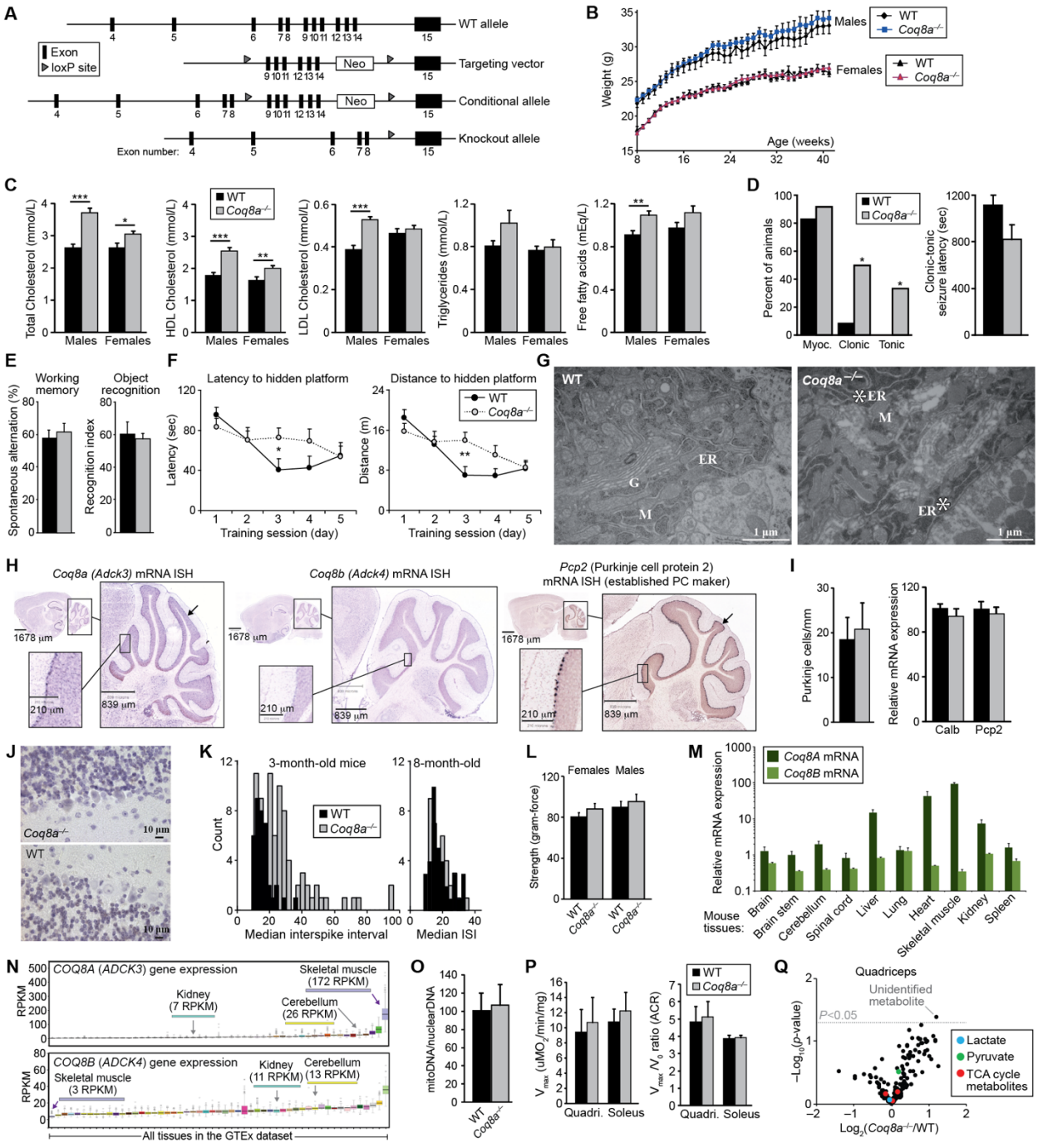

Figure S1, related to Figure 1. Generation and Characterization of *Coq8a*$^{-/-}$ Mice

(A) Scheme of constructs used to generate the *Coq8a*$^{-/-}$ mice.

(B) Body weight of WT and *Coq8a*$^{-/-}$ mice over time (mean ± SEM, n = 9).

(C) Blood lipid measurements in 25-week-old mice (mean ± SEM, n = 9).

(D) Susceptibility to epilepsy tested by PTZ injection in 6-month-old WT and *Coq8a*$^{-/-}$ mice. Left, percentage of mice that displayed myoclonic, clonic, or tonic crisis. Right, latency to clonic-tonic seizure (mean ± SEM, n = 12).

(E) Y-maze spontaneous alternation (left) and recognition memory (right) assessed in WT (black) and *Coq8a*$^{-/-}$ (gray) mice (5-month-old) (mean ± SEM, n = 12).

(F) Latency (left) and distance (right) to reach a hidden platform assessed by Morris water maze test in 5-month-old mice (mean ± SEM, n = 12).
(G) Representative electron microscopy images of WT and *Coq8a*$^{-/-}$ cerebella (30-week-old mice). G, Golgi apparatus; ER, endoplasmic reticulum; *dilated ER cisternae; scale bar, 1 μm.
(H) Allen Brain Atlas (mouse brain; http://mouse.brain-map.org) (Lein et al., 2007) in situ hybridization (ISH) images for *Coq8a*, *Coq8b*, or *Pcp2* mRNA. Arrows indicate a layer of distinct Purkinje cell bodies visible as puncta of ISH signal.
(I) Purkinje cell number in cerebellar H&E sections (left), and mRNA expression of cerebellar markers (*Calbindin* and *Pcp2*) (right) of WT (black) and *Coq8a*$^{-/-}$ (gray) mice (22-month-old) (mean ± SEM, n = 5).
(J) Representative TUNEL staining of cerebellar sections, 16-month-old mice. Scale bar 10 μm.
(K) Distribution of the median interspike intervals (ISI) of Purkinje cells recorded in acute cerebellar slices from 3-month-old (left) and 8-month-old (right) mice. Number of cells > 40.
(L) Strength of 10-week-old mice assessed by grip test (mean ± SEM, n = 8–12).
(M) Relative mRNA expression levels of *Coq8a* and *Coq8b* across various mouse tissues as quantified by RT-PCR (mean ± SEM, n = 3).
(N) mRNA expression data for *COQ8A* (*ADCK3*) and *COQ8B* (*ADCK4*) across human tissues as reported in the GTEx dataset (http://www.gtexportal.org) (Consortium, 2015). RPKM, reads per kilobase per million mapped reads.
(O) Mitochondrial content quantified as the ratio mitochondrial DNA/nuclear DNA by qRT-PCR of quadriceps muscle (18-month-old mice) (mean ± SEM, n = 7).
(P) Mitochondrial respiration (left, maximum O_2 consumption, V_{max}; right, V_{max}/V_0 ratio) of skeletal muscle fibers (10-month-old mice) (mean ± SD, n = 8).
(Q) Fold changes in mouse metabolite abundances ($\log_2$(*Coq8a*$^{-/-}$/WT), mean, n = 4) as quantified by GC-MS analysis.
For all panels: *P<0.05, **P<0.01, ***P<0.001.

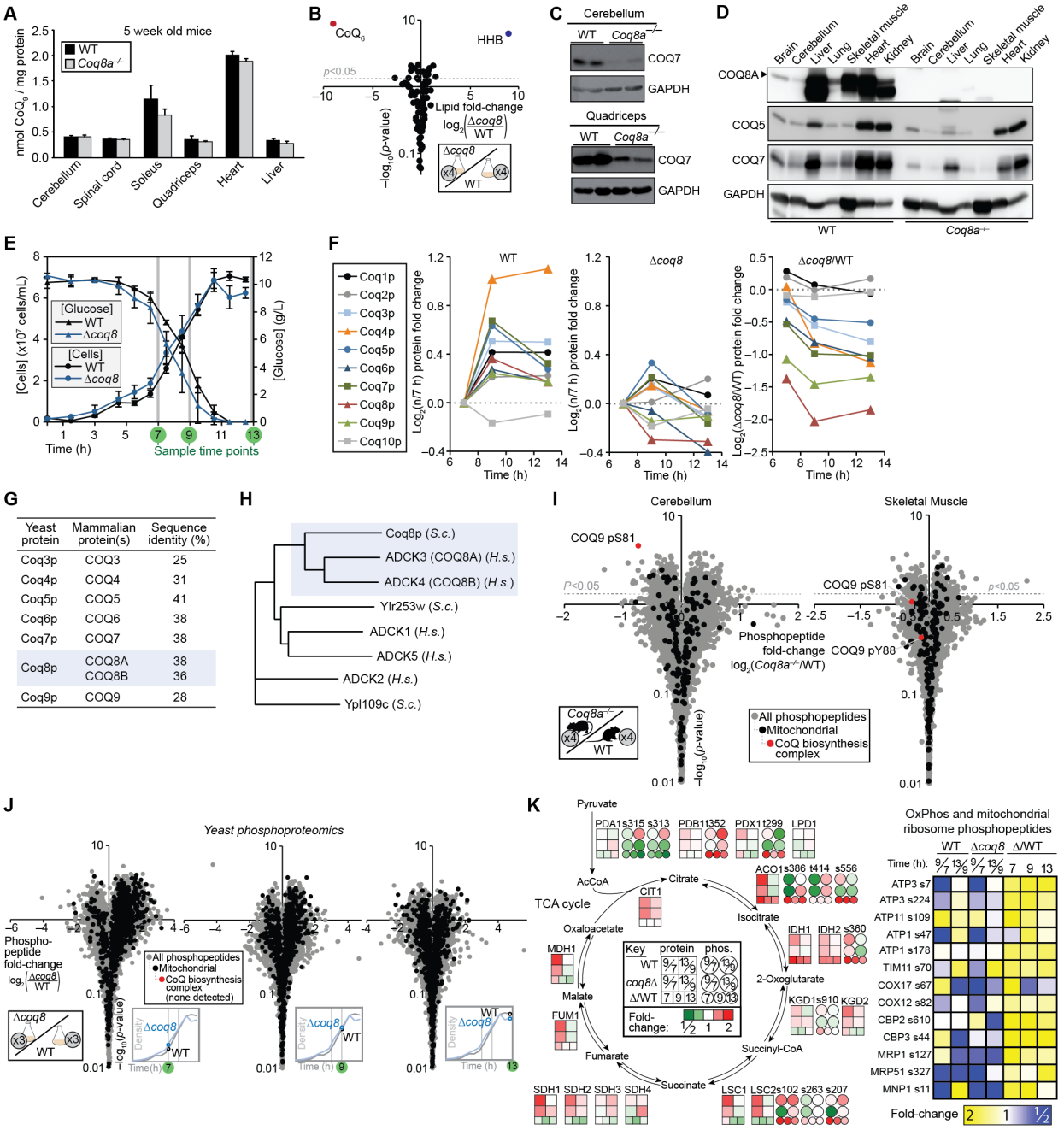

Figure S2, related to Figure 2. Loss of COQ8A or Coq8p Causes Deficiency of Complex Q and CoQ

(A) CoQ_9 abundance in WT and *Coq8a*$^{-/-}$ mice (5-week-old) (mean ± SD, n = 9).

(B) Fold changes in yeast lipid abundances ($\log_2$(Δ*coq8*/WT), mean, n = 3) as quantified by LC-MS analysis. The major yeast CoQ species (CoQ_6) is shown in red, and a CoQ biosynthesis intermediate (HHB, hexaprenylhydroxybenzoate) is shown in blue.

(C) Expression of COQ7 protein in cerebellum (top) and quadriceps (bottom) of WT and *Coq8a*$^{-/-}$ mice (2.5-week-old) as assessed by immunoblot.

(D) Immunoblot analysis of COQ8A, COQ5, and COQ7 abundances across several tissues of 30-week-old mice. Blot is representative of 3 independent biological replicates.

(E) Yeast culture (Δ*coq8* and WT) densities (mean ± SD, n = 3) and glucose concentrations (mean ± SD, n = 3) versus time. Samples were harvested for proteomics and phosphoproteomics analyses at the indicated time points (7 h, 9 h, and 13 h).
(F) Left: Fold changes in CoQ biosynthesis protein abundances in WT or Δ*coq8* yeast ($\log_2$(abundance at indicated time point/abundance at 7 h time point), mean, n = 3) versus time as determined by LC-MS/MS. Right: Fold changes in CoQ biosynthesis protein abundances ($\log_2$(Δ*coq8*/WT), mean, n = 3) at each of the 3 sample time points shown in (E).
(G) Table of yeast and mammalian complex Q proteins indicating amino acid sequence identities for homologous pairs.
(H) Phylogenetic relationship between *Homo sapiens* (*H.s.*) and yeast *Saccharomyces cerevisiae* (*S.c.*) UbiB family proteins.
(I) Fold changes in mouse cerebellum or quadriceps (skeletal muscle) phosphopeptide abundances (mean $\log_2$(*Coq8a*$^{-/-}$/WT), n = 4) versus statistical significance (–$\log_{10}$(*p*-value)) as quantified by LC-MS/MS. Phosphopeptides of mitochondrial proteins are shown in black, and all observed phosphopeptides from CoQ biosynthesis complex proteins are shown in red.
(J) Fold changes in yeast phosphopeptide abundances (mean $\log_2$(Δ*coq8*/WT), n = 3) at the 7, 9, and 13 hour time points versus statistical significance (–$\log_{10}$(*p*-value)) as quantified by LC-MS/MS. Mitochondrial phosphopeptides are shown in black. No phosphopeptides from CoQ biosynthesis complex proteins were observed. Details of the corresponding yeast growth curve and sample time points are shown in (E).
(K) Left: heat maps of fold changes in the abundances of yeast proteins and phosphopeptides (mean, n = 3) from central carbon metabolism pathways as determined by LC-MS/MS. Boxes indicate proteins, and circles indicate phosphopeptides from the protein shown immediately to the left. Right: Heat map of fold changes in the abundances of yeast proteins and phosphopeptides (mean, n = 3) from the mitochondrial ribosome and mitochondrial oxidative phosphorylation complexes as determined by LC-MS/MS.

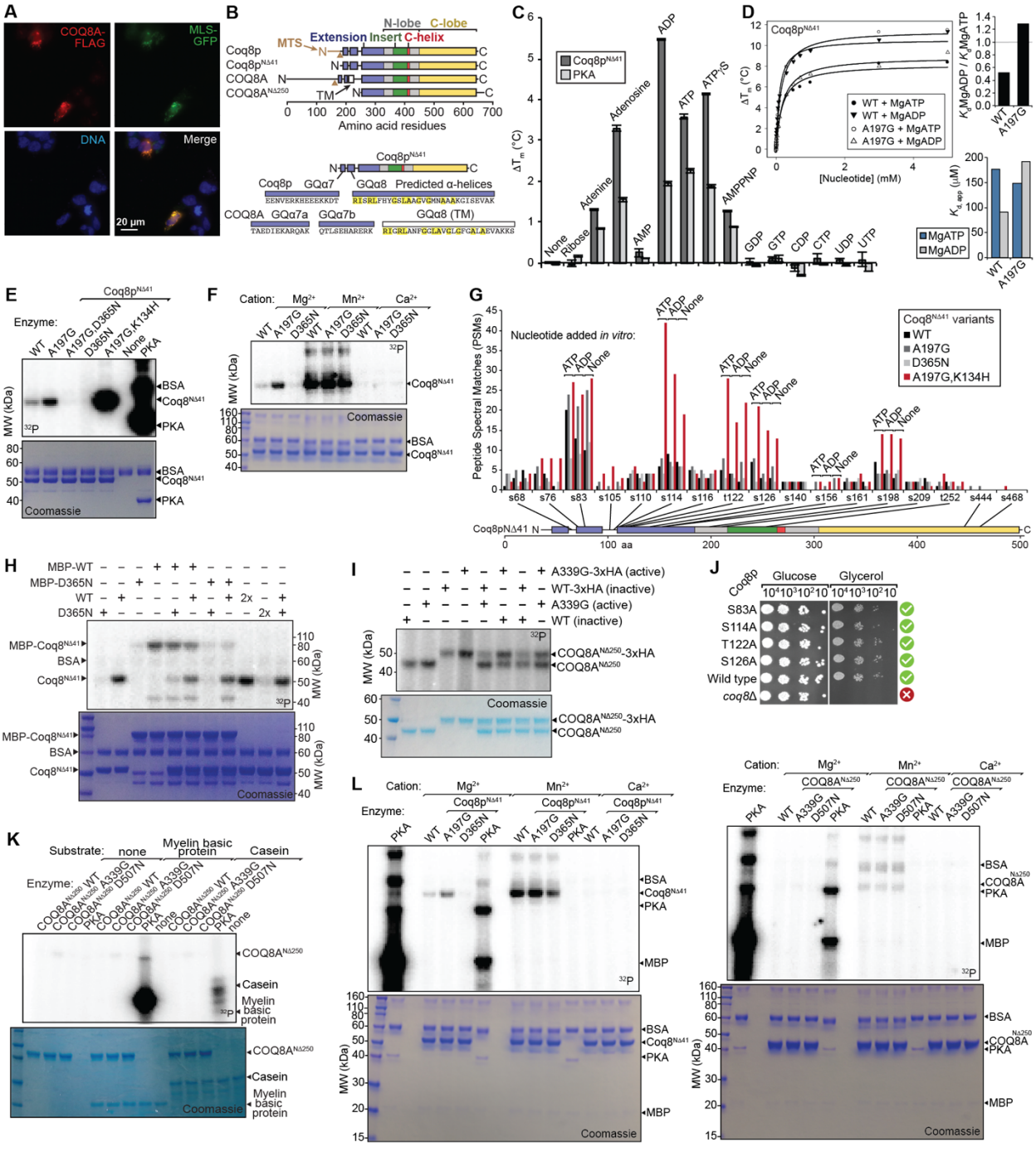

Figure S3, related to Figure 3. Biochemical Activities of COQ8A and Coq8p

(A) Fluorescence microscopy of HEK293 cells transfected with COQ8A-FLAG and MLS-GFP (mitochondrial marker) in parallel with the AE-MS experiment reported here. Nuclear DNA is visualized by Hoechst stain. Scale bar, 20 µm.

(B) Domain structures of Coq8p, COQ8A, and truncated constructs. The white box represents a single-pass transmembrane domain of COQ8A. Brown triangles represent observed N-termini of mature Coq8p and mature COQ8A. MTS, mitochondrial targeting sequence.

(C) ΔT_m of $Coq8^{N\Delta41}$ or PKA due to addition of various ligands (mean ± SD, n = 3) in the presence of Mg^{2+} as assessed by differential scanning fluorimetry (DSF).

(D) Left, nucleotide binding curves for Coq8$^{N\Delta41}$ (WT and A197G). Right, K_d^{MgATP} and K_d^{MgADP} for Coq8$^{N\Delta41}$ (WT and A197G) variants as assessed by DSF, and nucleotide selectivity of Coq8$^{N\Delta41}$ A197G compared to WT.
(E) SDS-PAGE analysis of *in vitro* Mg[γ-^{32}P]ATP autophosphorylation reactions with Coq8$^{N\Delta41}$ variants.
(F) SDS-PAGE analysis of *in vitro* [γ-^{32}P]ATP autophosphorylation reactions with Coq8$^{N\Delta41}$ variants and various divalent cations (Mg^{2+}, Mn^{2+}, or Ca^{2+}).
(G) Number of PSMs observed for Coq8$^{N\Delta41}$ phosphopeptides detected by LC-MS/MS analysis of *in vitro* MgATP autophosphorylation reactions.
(H) SDS-PAGE analysis of *in vitro* Mg[γ-^{32}P]ATP autophosphorylation reactions with the indicated combinations of Coq8$^{N\Delta41}$ variants and maltose binding protein (MBP) tagged Coq8$^{N\Delta41}$ variants.
(I) SDS-PAGE analysis of *in vitro* Mg[γ-^{32}P]ATP autophosphorylation reactions with the indicated combinations of COQ8A$^{N\Delta250}$ variants and 3xHA-tagged COQ8A$^{N\Delta250}$ variants.
(J) Serial dilutions of Δ*coq8* yeast transformed with the indicated *coq8* (Coq8p) variants grown on agar plates with glucose or glycerol.
(K) SDS-PAGE analysis of *in vitro* Mg[γ-^{32}P]ATP kinase reactions with PKA or COQ8A$^{N\Delta250}$ (WT, A339G, or D507N) and potential substrate proteins (myelin basic protein or dephosphorylated casein).
(L) SDS-PAGE analysis of *in vitro* [γ-^{32}P]ATP kinase reactions with PKA, Coq8$^{N\Delta41}$ variants, or COQ8A$^{N\Delta250}$ variants, the generic protein kinase substrate dephosphorylated myelin basic protein (MBP), and various divalent cations (Mg^{2+}, Mn^{2+}, or Ca^{2+}).

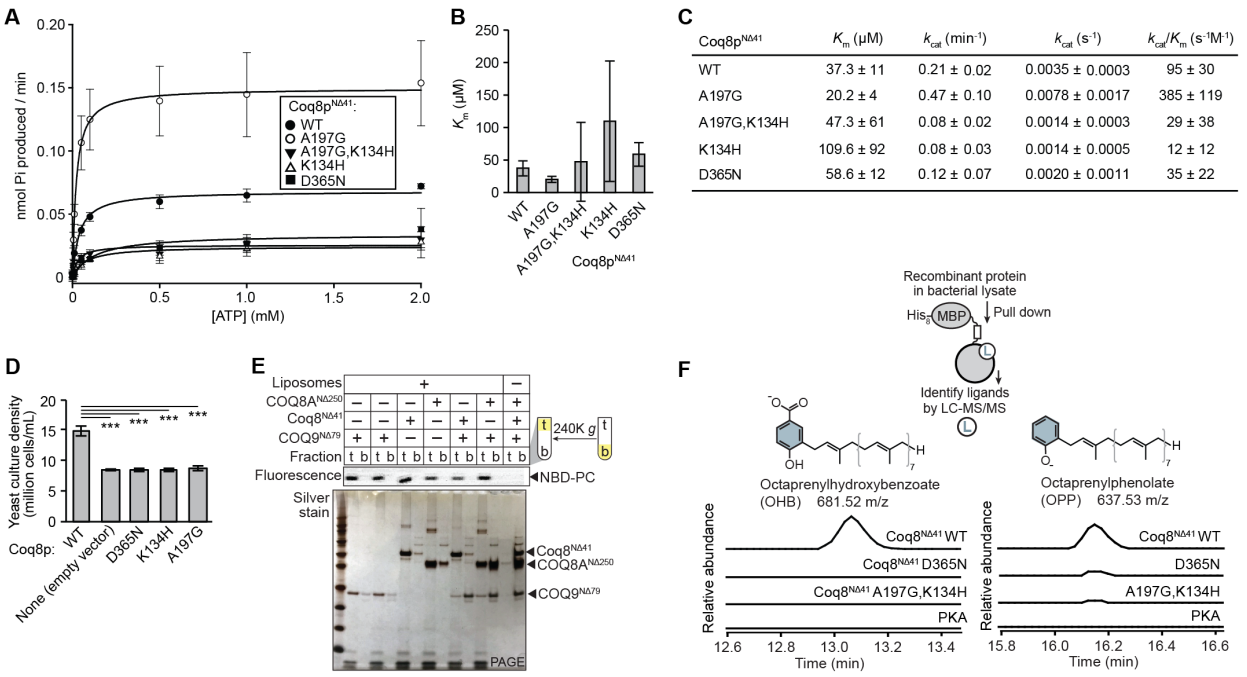

Figure S4, related to Figure 4. Unorthodox PKL Functions of COQ8A and Coq8p

(A) Kinetic curves for the ATPase activity of Coq8$^{N\Delta41}$ variants (WT and mutants) (mean ± SD, n = 3) as measured by observing production of inorganic phosphate (ELIPA assay).

(B) K_m^{MgATP} values for the ATPase activity of Coq8$^{N\Delta41}$ variants (mean ± SD, n = 3).

(C) Table of kinetic constants for the ATPase activity of Coq8$^{N\Delta41}$ variants (mean ± SD, n = 3).

(D) Densities of yeast cultures (Δ*coq8* yeast transformed with plasmids encoding the indicated Coq8p variants) at the time point of harvest for label free quantitation (LFQ) LC-MS/MS proteomics analysis (mean ± SD, n = 4). ***P<0.001.

(E) SDS-PAGE analysis of a liposome-protein co-flotation assay with the indicated proteins and liposomes generated from bacterial extract lipids. The liposomes included a fluorescent lipid marker (NBD-PC). Top (t) and bottom (b) fractions after the spin are indicated.

(F) Extracted ion chromatograms (XICs) reflecting the MS^1 precursor intensities of octaprenylhydroxybenzoate (OHB) and octaprenylphenolate (OPP) that co-purified with MBP- Coq8$^{N\Delta41}$ expressed in *E. coli*. The y-axis (reflecting precursor intensity) for each species is on the same scale across all four proteins.

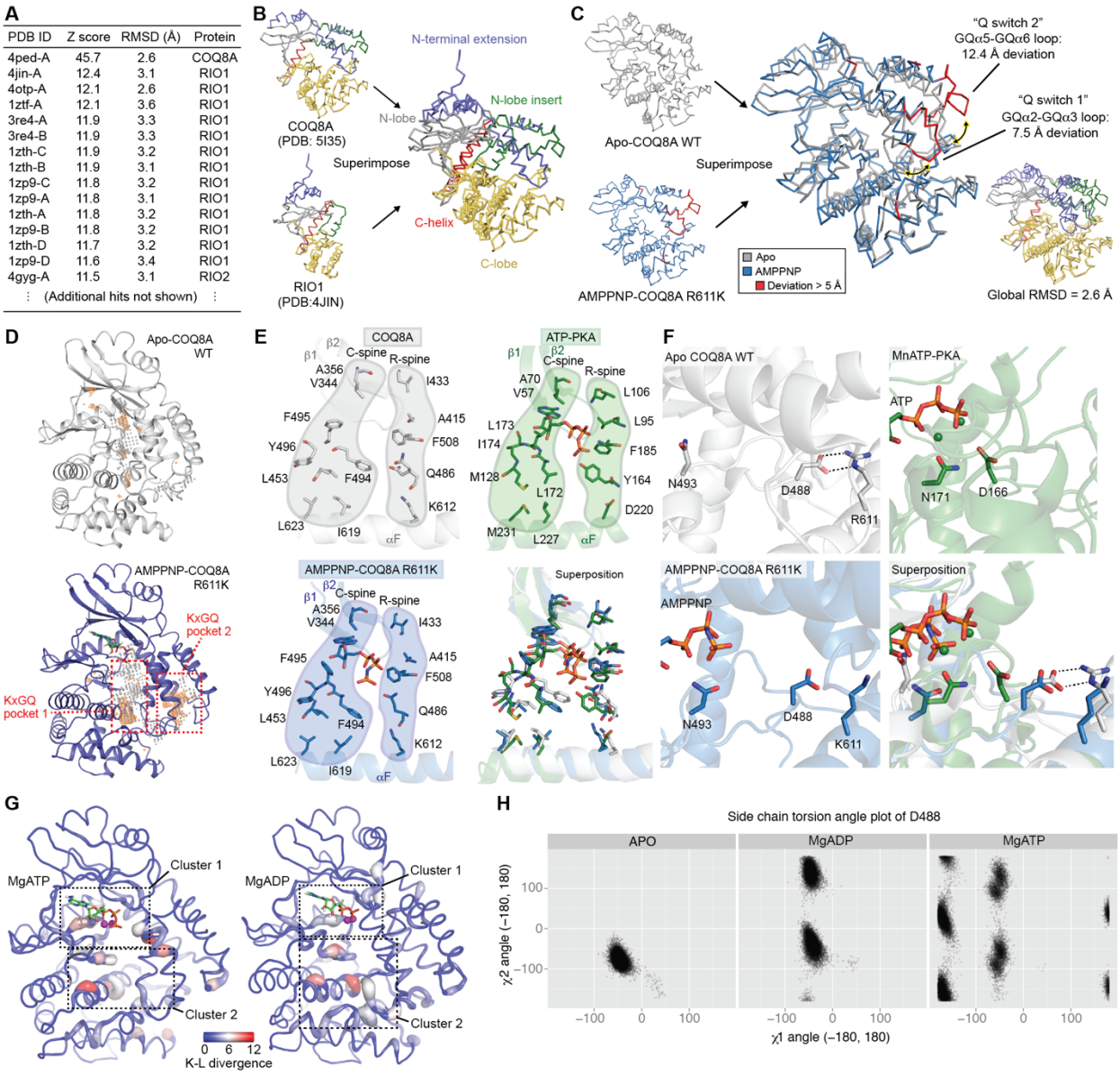

Figure S5, related to Figure 5. Structure and Dynamics of Nucleotide-Bound COQ8A

(A) Structures in the Protein Data Bank (PDB) with the most similarity to AMPPNP-COQ8A$^{N\Delta254}$ R611K (PDB 5I35). The top 15 hits identified with the Dali server (Holm et al., 2008) are shown.

(B) Superposition of AMPPNP-COQ8A$^{N\Delta254}$ R611K (PDB 5I35) and RIO1 (PDB 4JIN).

(C) Superposition of apo-COQ8A WT (PDB 4PED) and AMPPNP-COQ8A R611K (PDB 5I35) indicating in red residues that differ in position by more than 5 Å. The smaller inset superposition (bottom right) is colored by domain as shown in Figures 5A and S3B.

(D) Top-two ranking binding pockets identified by SiteMap on the nucleotide-bound COQ8A structure (PDB 5I35) (blue) and the corresponding pockets on the apo COQ8A structure (PDB 4PED) (gray). The accessible areas of the pockets are shown with white beads, and the hydrophobic regions are shown in orange mesh.

(E) Superposition of "catalytic spine" (C-spine) and "regulatory spine" (R-spine) residues in apo-COQ8A WT (PDB 4PED), AMPPNP-COQ8A R611K (PDB 5I35), and PKA (PDB 1ATP).

(F) Superposition of highly conserved catalytic loop residues in apo-COQ8A WT (PDB 4PED), AMPPNP-COQ8A R611K (PDB 5I35), and PKA (PDB 1ATP).

(G) Kullback–Leibler divergence scores for molecular dynamics (MD) simulations of apo COQ8A compared to MgATP-bound COQ8A (left) or MgADP-bound COQ8A (right). Regions colored red showed highly differential dynamics.
(H) Side chain χ1 and χ2 angle plots of D488 during the MD simulations.

SUPPLEMENTAL TABLE LEGENDS

Table S1. *Coq8a*$^{-/-}$ Mouse Lipidomics, Related to Figure 2B
Table of lipids identified and quantified by LC-MS/MS including lipid name, precursor (MS1) mass, retention time (RT (min)), total signal normalized lipid intensity ([lipid intensity]/[sum of lipid intensities]) for four KO (*Coq8a*$^{-/-}$) mice and four WT mice, average lipid fold change ($\log_2$(*Coq8a*$^{-/-}$/WT)), and $-\log_{10}$(*p*-value). Separate tabs are included for quadriceps, cerebellum, and serum.

Table S2. Δ*coq8* Yeast Lipidomics, Related to Figure S2B
Table of lipids identified and quantified by LC-MS/MS including lipid name, precursor (MS1) mass, retention time (RT (min)), total signal normalized lipid intensity ([lipid intensity]/[sum of lipid intensities]) for four KO (Δ*coq8*) cultures and four WT cultures, average lipid fold change ($\log_2$(Δ*coq8*/WT)), and $-\log_{10}$(*p*-value).

Table S3. *Coq8a*$^{-/-}$ Mouse Proteomics, Related to Figure 2C
Table of proteins identified and quantified by LC-MS/MS including protein description, UniProt ID, gene name, mean normalized log2 fold changes (log2(sample/mean)) for each sample, average protein fold change ($\log_2$(*Coq8a*$^{-/-}$/WT)) (n = 4 WT and 4 KO), and $-\log_{10}$(*p*-value). Separate tabs are included for cerebellum, quadriceps, heart, and kidney.

Table S4. Δ*coq8* Yeast Proteomics, Related to Figure 2F
Table of proteins identified and quantified by LC-MS/MS including protein description, UniProt ID, gene name, mean normalized log2 fold changes (log2(sample/mean)) for each sample, average protein fold changes for each of the three time points (7, 9, and 13 h; before, during, and after the diauxic shift) ($\log_2$(Δ*coq8*/WT)) (n = 3 WT and 3 KO), and $-\log_{10}$(*p*-value) for each time point comparison.

Table S5. *Coq8a*$^{-/-}$ Mouse Phosphoproteomics, Related to Figure S2I
Table of protein phosphosites identified and quantified by LC-MS/MS including protein UniProt ID, protein description, phosphosite(s), average phosphosite fold change ($\log_2$(*Coq8a*$^{-/-}$/WT)) (n = 4 WT and 4 KO), and $-\log_{10}$(*p*-value). Separate tabs are included for quadriceps and cerebellum.

Table S6. Δ*coq8* Yeast Phosphoproteomics, Related to Figures S2J and S2K
Table of protein phosphosites identified and quantified by LC-MS/MS including protein description, phosphosite, UniProt ID, gene name, mean normalized log2 fold changes (log2(sample/mean)) for each sample, average phosphosite fold changes for each of the three time points (7, 9, and 13 h; before, during, and after the diauxic shift) ($\log_2$(Δ*coq8*/WT)) (n = 3 WT and 3 KO), and $-\log_{10}$(*p*-value) for each time point comparison.

SUPPLEMENTAL EXPERIMENTAL PROCEDURES

Coq8a$^{-/-}$ Mice

Generation of Coq8a$^{-/-}$ *Mice*. Mice carrying a conditional allele for *Coq8a*$^{L2+/L2+}$ were established at the MCI/ICS (Mouse Clinical Institute – Institut Clinique de la Souris-Phenomin, Illkirch, France). The conditional allele was generated by inserting two loxP sites into introns 9 and 15 of the *Coq8a (Adck3)* locus (see Figure S1A). The targeting vector was constructed as follows. A 1.9 kb fragment encompassing exons 9, 10, 11, 12, 13 and 14 was amplified by PCR (from 129S2/SvPas ES cells genomic DNA) subcloned in an MCI proprietary vector. This MCI vector contains a LoxP site as well as a floxed and flipped Neomycin resistance cassette. A 4.5 kb fragment (corresponding to the 5' homology arm and 3.5 kb fragment corresponding to the 3' homology arms were amplified by PCR and subcloned in step 1 plasmid to generate the final targeting construct.

The linearized construct was electroporated in 129S2/SvPas mouse embryonic stem (ES) cells. After selection, targeted clones were identified by PCR using external primers and further confirmed by Southern blot with 5' and 3' external probes.

Two positive ES clones were injected into C57BL/6J blastocysts, and male chimaeras derived gave germline transmission. After expression of Cre recombinase under the CMV promoter, a deletion of exons 9–14 was obtained that constitutes the constitutive knockout *Coq8a*$^{-/-}$ (*Adck3*$^{-/-}$) allele. Mice were analyzed in a mixed background (Bl/6J 53.13%, Bl/6N 34.37%, 129svPas 12.5%). Because we did not find any significant difference between WT and *Coq8a*$^{+/-}$ heterozygotes, we considered heterozygotes as controls for some behavioral and histological experiments.

Genotyping. To genotype mice, DNA (mouse tail) was examined by PCR with the following primers:

Wild type (WT) allele: 5'-CTTTCAGTTTTTAGTACTGGCTGCG-3',
5'-GCTCATTAGTGTCCCAGCCATATCC-3';
Coq8a$^{-/-}$ (KO) allele: 5'-CTTTCAGTTTTTAGTACTGGCTGCG-3',
5'-AGAGCACTGGAGGGACAAGGGGC-3'.

General Handling. Mice were maintained in a temperature and humidity controlled animal facility, with a 12 hours light/dark cycle and free access to water and a standard rodent chow (D03, SAFE, Villemoisson-sur-Orge, France). All animal procedures and experiments were approved by the local ethical committee for Animal Care and Use (Com'Eth n° 2012-154) and were performed in accordance with the Guide for the Care and Use of Laboratory Animals (National Institutes of Health).

Blood Analysis. Blood was collected by retro orbital puncture under isoflurane anesthesia after 4 hr fasting at the age of 25 weeks. Blood chemistry was examined using an OLYMPUS AU-400 automated laboratory work station (Olympus France SA, Rungis, France) using commercial reagents (Olympus Diagnostica GmbH, Lismeehan, Ireland).

Mammalian Cell Culture

Primary Myoblasts. Hind limb muscle from 7–9-day-old mice was collected, minced and digested with a mixture of collagenase and dispase (Invitrogen). The digestions were stopped with growth medium containing Iscove's Modified Dulbecco's Medium (IMDM, Gibco), centrifuged (600 *g,* 5 min), filtered, and centrifuged again (1300 *g*, 5 min). The cell pellet was suspended in IMDM supplemented with 10% fetal bovine serum (FBS), 2 mM L-glutamine, and 0.1% gentamycin, and plated into 6-well dishes. Myoblasts were separated from fibroblast contaminants by differential plating for 3–4 hours in an incubator. The cells were subsequently centrifuged (1,500 *g*, 10 min) and plated on matrigel-coated dishes in IMDM supplemented with 20% FBS, 2 mM L-Gln, 1% Chicken Embryo Extract (Seralab), and 0.1% gentamycin. The cells were maintained in an incubator (37 °C, 5% CO_2) and the medium was changed every 2 days.

COS Cells. COS cells were maintained in DMEM supplemented with 5% FBS in a humidified incubator (37 °C, 5% CO_2). Transfections were conducted as described below in the protein interaction method section.

HEK293 Cells. HEK293 cells were maintained in high glucose (25 mM) Dulbecco's modified Eagle's medium (LifeTech) supplemented with 10% (v/v) FBS (LifeTech) and penicillin-streptomycin (1×) (LifeTech) (HGDMEM+FBS+P/S) in a humidified incubator (37 °C, 5% CO_2). Cells were sub-cultured by trypsinization (0.05% Trypsin-EDTA, LifeTech). Transfections were conducted as described below in the protein interaction method section.

Yeast Cultures

Yeast cultures for lipidomics and diauxic shift proteomics and phosphoproteomics. Saccharomyces cerevisae WT strain DS10 was obtained from the laboratory of Elizabeth A. Craig ("WT JH27a DS10", *his3-11,15 leu2-3,112 lys1 lys2 Δtrp1 ura3-52*). Δ*coq8* DS10 yeast were created by replacing the *coq8* gene with a *ura3* selectable marker using

standard methods for PCR amplification and homologous recombination (Baudin et al., 1993). The insertion of the *ura3* marker at the *coq8* locus was confirmed by a PCR assay and DNA sequencing. Single colonies of yeast were used to inoculate starter cultures in YPD media (4 mL), which were incubated (30 °C, 230 rpm, 12 h). Synthetic complete media (500 mL) with glucose (10 g/L) was inoculated with $5x10^6$ yeast cells from a starter culture and incubated (30 °C, 230 rpm). Yeast cell pellets were isolated at three time points during the culture (as shown in Figure S2E) by centrifugation (1,000 *g*, 3 min, 4 °C) and frozen in $N_{2(l)}$. Cell culture density was determined by measuring the optical density at 600 nm (OD_{600}) and converting this value to [cells], as described previously (Hebert et al., 2013). Media glucose concentration was determined with a Glucose (HK) Assay Kit (Sigma), as described previously (Hebert et al., 2013).

Yeast cultures for drop assays. *S. cerevisiae* (W303) Δ*coq8* yeast were transformed as previously described (Gietz and Woods, 2002) with p426 GPD plasmids encoding Coq8p variants and grown on uracil drop-out (Ura^-) synthetic media plates containing glucose (20 g/L). Individual colonies of yeast were used to inoculate Ura^- media (20 g/L glucose) starter cultures, which were incubated (30 °C, ~18 h, 230 rpm). Serial dilutions of yeast (10^4, 10^3, 10^2, or 10 yeast cells) were dropped onto Ura^- agar media plates containing either glucose (20 g/L) or glycerol (30 g/L) and incubated (30 °C, 2 d).

Yeast cultures for LFQ proteomics of coq8 point mutant strains. S. cerevisiae (BY4742) Δ*coq8* yeast were transformed with p426 GPD plasmids encoding Coq8p variants and grown on Ura^- synthetic media plates (20 g/L glucose). Individual colonies of yeast were used to inoculate Ura^- media (20 g/L glucose) starter cultures, which were incubated (30 °C, ~12 h, 230 rpm). 100 mL cultures (Ura^- media with 30 g/L glycerol and 1 g/L glucose) were inoculated with 2.5 million yeast and incubated (30 °C, 230 rpm, 25 h). $1x10^8$ yeast cells were harvested by centrifugation (3,000 *g*, 3 min, 4 °C), the supernatant was removed, and cell pellets were flash frozen in $N_{2(l)}$.

DNA Constructs and Cloning

General Cloning Methods. Standard PIPE cloning methods (Klock et al., 2008) were used where indicated. PIPE reactions were DpnI digested and transformed into DH5α competent *E. coli* cells. Plasmids were isolated from transformants and DNA sequencing was used to identify those containing the correct constructs. pVP68K, a plasmid for expression of recombinant proteins in bacteria [8His-cytoplasmically-targeted maltose-binding protein (MBP) with a linker including a tobacco etch virus (TEV) protease recognition site fused to the protein construct (8His-MBP-[TEV]-Protein)], has been described previously (Blommel et al., 2009). Oligonucleotides were purchased from IDT (Coralville, IA, USA).

Human COQ8A^{NΔ250}-FLAG-3xHA (ADCK3^{NΔ250}-FLAG-3xHA). Cloning of COQ8A^{NΔ250} (ADCK3^{NΔ250}) into pVP68K has been described previously (Stefely et al., 2015). Here, to generate COQ8A^{NΔ250}-Flag-3xHA with PIPE cloning, separate COQ8A^{NΔ250} and FLAG-3xHA amplicons were generated and combined prior to transformation. The 3xHA was amplified from plasmid pJR13019 (Chen et al., 2012), obtained from the laboratory of Jared Rutter. Point mutations were introduced by PCR-based mutagenesis and confirmed by DNA sequencing.

Murine PKA. pET15b PKA Cat (Narayana et al., 1997) was obtained as a gift from Susan Taylor (Addgene plasmid #14921), and PKA was PIPE cloned into pVP68K. Point mutations were introduced by PCR-based mutagenesis and confirmed by DNA sequencing.

Yeast Coq8^{NΔ41}. *S. cerevisiae coq8* was PIPE cloned into pVP68K and the N-terminal 41 amino acid residues were removed by standard PIPE cloning methods. Point mutations were introduced by PCR-based mutagenesis and confirmed by DNA sequencing.

Yeast Coq8. Cloning of *S. cerevisiae coq8* into the yeast expression vector p426 GPD has been described previously (Stefely et al., 2015). Point mutations were introduced by PCR-based mutagenesis and confirmed by DNA sequencing.

Human COQ8A-FLAG (ADCK3-FLAG). Cloning of human COQ8A-FLAG (ADCK3-FLAG) (C-terminal FLAG tag) into pcDNA3.1 has been described (Stefely et al., 2015). Point mutations were introduced by PCR-based mutagenesis and confirmed by DNA sequencing.

Murine Coq8a-FLAG (Adck3-FLAG), Coq3-HA, Coq5-HA, and Coq9-HA. The complete coding sequence of murine *Coq8a* (*Adck3*) was cloned into the pcDNA 3.1/Zeo (Invitrogen) expression vector with a C-terminal FLAG tag. Similarly, full-length murine *Coq3*, *Coq5*, and *Coq9* were cloned into the pcDNA 3.1/Zeo vector with a C-terminal HA tag.

Antibodies and Western Blots (Immunoblots)

Anti-Coq8a Antibody. An anti-Coq8a antibody (targeting the murine COQ8A protein) was generated in-house (IGBMC) against the following peptide: KQMTKTLNSDLGPHWRDKC. The peptide was conjugated to Keyhole limpet hemocyanin (KLH) using Imject Maleimide Activated mcKLH kit (Thermo Scientific, Rockford, USA)

according to the manufacturer's recommendations and then injected with complete Freund's adjuvant into white New Zealand rabbits according to standard procedure. The antibody was purified from serum by affinity chromatography using the SulfoLink Coupling Resin (Thermo Scientific) and PolyPrep Chromatography Columns (Biorad). The antibody was eluted in acidic elution buffer (0.1 M glycine pH 2.8) followed by dialysis of the antibody-containing fractions overnight against PBS (1 L filtered PBS). The reactivity of the antibody with COQ8A in a panel of different cell and tissue lysates was then evaluated by Western blot.

Western blots. Western blots (immunoblots) were performed according to standard protocol, including separation of proteins by SDS Tris-Glycine PAGE. Antibodies were diluted as follows: anti-GAPDH (1/40000, Millipore), anti-COQ7 (1/1000, Abcam), anti-COQ5 (Proteintech 17453-1-AP, 1/1000), anti-Prohibitin (1/1000, Neo Markers), anti-TOM20 (1/250, Santa Cruz Biotechnology), anti-CYC1 (Proteintech), anti-NFU1 (1/5000, a gift from Tracey Rouault, National Institutes of Health), anti-FLAG 1/1000, and anti-HA 1/1000. HRP-coupled secondary antibodies (Horseradish Peroxidase, Jackson Immuno Research) were diluted at 1/5000.

Behavioral Measurements

Accelerating Rotarod. Coordination, balance, and motor skill acquisition were tested using an accelerating rotating rod (Panlab, Barcelona, Spain) test as described previously (Clark et al., 1997). Briefly, mice were placed on the rod in 4 trials every day for a period of 4 days (10 WT and 10 *Coq8a*$^{-/-}$ mutants). The rod accelerated from 4 rpm to 40 rpm in 5 min and remained at maximum speed for the next 5 min. Animals were scored for their latency to fall for each trial and rested a minimum of 10 min between trials to avoid fatigue. Results were analyzed by a repeated-measure ANOVA test considering three factors: days (fixed); genotype (fixed); animals (variable), nested in genotype and crossed with days.

Footprint Analysis (Linear Movement). The test was performed as previously described (Simon et al., 2004). Briefly, after coating of the hind feet with nontoxic ink, mice were allowed to walk through a tunnel (50×9×6 cm) with paper lining the floor. Five parameters were quantified: step length, the average distance of forward movement between alternate steps; σ, describing the regularity of step length; gait width, the average lateral distance between opposite left and right steps; alternation coefficient, describing the uniformity of step alternation; linearity, average change in angle between consecutive right-right steps. A high linearity score is indicative of nonlinear movement.

Beam-Walking (Hindlimb Coordination). Mice were trained to walk along a beam (2 cm wide × 90 cm long) suspended 30 cm above bedding. Three trials were performed for each mouse, and the number of hindfoot missteps was counted while the mouse walked along the length of the beam. The time required to cross the beam from start to end (latency) was also evaluated. Mice were trained to walk the length of the beam 1 day before testing

PTZ-Induced Seizures. Pentylenetetrazole (PTZ) was dissolved in saline (0.9% NaCl) and intraperitoneal (IP) injected at a dose of 30 mg/kg. Immediately after injection, the mouse was placed into a new cage and observed for at least 20 min. The seizure profile (myoclonic, clonic, tonic) and the latency to clonico-tonic seizure were recorded.

Y-Maze Spontaneous Alternation. A Y-maze made of Plexiglas with 3 identical arms (40×9×16 cm) placed 120° from each other was used for this test. Each arm had walls with distinct motifs allowing it to be distinguished from the others. Each mouse was placed at the end of one of the three arms, and allowed to explore freely the apparatus for 5 min, with the experimenter out of the animal's sight. Alternations were operationally defined as successive entries into each of the three arms as overlapping triplet sets (i.e., ABC, BCA...). The percentage of spontaneous alternation was calculated as index of working memory performance. Total arm entries and the latency to exit the starting arm were also scored as indexes of ambulatory activity and emotionality in the Y-maze, respectively.

Object recognition task: The object recognition task was performed in automated open fields (45×45×18 cm). The open fields were placed in a room homogeneously illuminated at 70 Lux at the level of each open field. The objects to be discriminated were a glass marble (2.5 cm diameter) and a plastic dice (2 cm). Animals were first habituated to the open field for 30 min. The next day, they were submitted to a 10 min acquisition trial during which they were placed in the open field in presence of an object A (marble or dice). The time the animal took to explore the object A (when the animal's snout was directed towards the object at a distance ≤ 1 cm) was manually recorded. A 10 min retention trial was performed 3 h later. During this trial, the object A and another object B were placed in the open field, and the times tA and tB the animal took to explore the two objects were recorded. The recognition index (RI) is defined as (tB / (tA + tB))×100.

Morris Water Maze. The water maze consisted of a white circular tank (1.5 m diameter) filled with opaque water. Pool temperature was adjusted to 21±1 °C. For the hidden platform task, the escape platform (10 cm diameter) was positioned 1 cm below water level in the center of one of the pool quadrants. For the cued task, platform position was signaled by the addition of a small flag. The walls surrounding the water maze were hung with posters and flags, which served as visual cues and are visible during all stages of training and testing. Movement of the mice within the pool was tracked and analyzed with a computerized tracking system (ViewPoint, France). Animals were first trained

in the hidden platform protocol (spatial learning). Mice were required to locate a submerged hidden platform by using only extra-maze cues. Each mouse received 5 blocks of training trials over five consecutive days in which they were placed in the pool at one of four randomized start positions, and allowed to locate the hidden platform. Trials lasted for a maximum of 120 s and were separated by 15–20 min intervals. If a mouse failed to find the platform within this period, it is guided to its position by the experimenter. Spatial learning performance was assessed during a probe trial 1 h after training, and for which the target platform was removed from the pool. Mice were then tested for cued training (visible platform), in which they were placed in the pool facing the edge at one of four start positions (NE, SE, SW, NW), and required to locate a flagged platform whose position varies across trials. Each mouse received 4 trials per day for 2 consecutive days. Trials lasted for a maximum of 120 s and were separated by 15–20 min intervals. If a mouse failed to find the platform within this period, it is guided to its position by the experimenter. The latency, distance and the average speed were used to evaluate performance during training trial. For the probe trial, the percentage of time in each quadrant and the number of platform crosses were used as index of spatial learning performance.

Treadmill. Mice were run on a treadmill with a 10° slope. Two protocols were applied: (i) for the V_{max} test, the starting speed of 40 cm/sec was increased 3 cm/sec every 90 seconds up to exhaustion. (ii) For the endurance test, mice were run until exhaustion at 80% of their respective V_{max}. Exhaustion of the mice was verified by blood lactate measurement.

Grip Test. Mice placed on the grid of a dynamometer (BioSeb, Chaville, France) were pulled by their tails in the opposite direction. The maximal strength exerted by the mouse before losing grip was recorded. The mean of 3 measurements allowing 30 sec of recovery time was calculated.

Microscopy

Immunohistochemistry. Animals were intracardiac perfused with 4% paraformaldehyde (PFA) in phosphate buffered saline (PBS), pH 7.3, and the various tissues were dissected, fixed for several days, and embedded in paraffin. Sequential slides (7 µm) of the paraffin blocks were stained with hematoxylin and eosin (H&E), or calbindin (1:1000; rabbit anti-calbindin d-28K; Swant, Bellinzona, Switzerland) to label the cytoplasm of Purkinje cells. For calbindin staining, sections were visualized using the Vectastain ABC Kit (Vector Laboratories, Burlingame, CA) as described in the manufacturer's protocol. Quantification of Purkinje cells was performed in a blinded manner. Images of the Purkinje cell layers were taken with a 20× objective. 3 mice per genotype and 10 images per mouse were included in the analysis.

Electron Microscopy. Animals were intracardiac perfused with 4% PFA. Tissues were fixed in 2.5% glutaraldehyde in PBS. After overnight fixation, the tissues was dissected from the column and fixed for 1 additional day. Tissues were rinsed in PBS, postfixed in 1% osmium tetroxide-PBS (2 hr, 4 °C), dehydrated, and embedded in Epon. Regions of interest were localized on 2 µm sections and stained with toluidine blue. Ultrathin sections from selected areas were stained with uranyl acetate and lead citrate and examined with a Philips 208 electron microscope, operating at 80 kV.

TUNEL Assay. Apoptosis was assessed by the *in situ* DNA end-labeling [terminal deoxynucleotidyl transferase-mediated biotinylated UTP nick end labeling (TUNEL)] method, following the manufacturer's directions (Apoptag, Intergen Co., Purchase, NY). Purkinje cells were blindly counted on H&E sections. 9–11 images were taken per cerebellum and 3 mice per genotype were considered in the analysis.

PCR Assays

Purkinje Cell Markers and Coq8 Expression. Total RNA was extracted from frozen tissues with the Precellys24 homogeniser (Bertin Technologies) and using TRI Reagent (MRC) according to the manufacturer's protocol. cDNA was generated by reverse transcription using the Transcriptor First strand cDNA synthesis kit (Roche). Quantitative RT-PCR was performed using the SYBR Green I Master (Roche) and light Cycler 480 (Roche) with the primers described below. *Gapdh* or *Hprt* was used as internal standard for the quantification.

Pcp2: ACAGTTAATTCCCTGCCTGG and CTCAAGGAGCTTGTGTCTGG
Calb1: GATTGGAGCTATCACCGGAA and TTCCTCGCAGGACTTCAGTT
Gapdh: TTGTGATGGGTGTGAACCAC and TTCAGCTCTGGGATGACCTT
Hprt: GTAATGATCAGTCAACGGGGGAC and CCAGCAAGCTTGCAACCTTAACCA
Coq8a: TCATATCAGGCTTCCCCTTG and TTCTCTAGTTGCGCCGAAGT
Coq8b : ATGGTCCGTGAACTCTGTCC and TGCTTTCAGCTCCTGAGGTT

Quantification of mtDNA copy number. Mitochondrial DNA (mtDNA) copy number was determined as a marker for mitochondrial density using quantitative real time PCR. Total DNA was extracted from frozen tissues that were lysed overnight at 55 °C in NaCl 200 mM, Tris 50 mM pH 8, EDTA 5 mM, SDS 1% in the presence of 100

µg/mL proteinase K. The next day, RNAse treatment (3 mg/mL) was performed at 37 °C for 30 min, before extraction of total DNA using standard phenol/chloroform treatment followed by DNA precipitation. Quantitative PCR was performed using the Light Cycler 480 II (Roche, France) and the Light cycler 480 SYBR Green I Master (Roche, France). 100 ng of total DNA was used for amplification of genomic DNA, while 1 ng of total DNA was used for amplification of mtDNA. The ND1 gene for NADH dehydrogenase subunit 1 was used for quantification of mtDNA. The nuclear gene for lipoprotein lipase (LPL) was used to normalize results. The ratio of ND1 to LPL copy number reflected the tissue concentration of mitochondria per cell.

Nd1 : CCCAGCTACTACCATCATTCAAGT and GATGGTTTGGGAGATTGGTTGATGT
Lpl : CACAGTGGCCGAGAGCGAGAA and GCTGAGTCCTTTCCCTTCTGCA

Purkinje Cell Electrophysiology

Slice preparation and recordings. Slices were prepared as previously described (Chaumont et al., 2013). Briefly, male *Coq8a*$^{-/-}$ mice and WT littermates (3-month-old and 8-month-old) were decapitated under isoflurane anesthesia. 330 µm-thick sagittal slices were prepared (Microm HM 650V, Microm) in potassium-based medium, containing in mM: K-gluconate 130; KCl 14.6; EGTA 2; Hepes 20; Glucose 25; minocyclin 0.00005, and D-AP5 0.05. Slices were soaked in a sucrose- based medium at 34 °C, containing in mM: sucrose 230; KCl 2.5; $NaHCO_3$ 26; NaH_2PO_4 1.25; glucose 25; $CaCl_2$ 0.8; $MgCl_2$ 8; minocyclin 0.00005; and D-APV 0.05 and transferred for recordings in an artificial cerebrospinal medium (ACSF) containing in mM: NaCl 120; KCl 3; $NaHCO_3$ 26; NaH_2PO_4 1.25; $CaCl_2$ 2.5; $MgCl_2$ 2; Glucose 10; Minocyclin 0.00005 (chemicals from Sigma-Aldrich, USA and Abcam, UK). Extracellular recordings of individually identified Purkinje cells were performed at 32–34 °C in the presence of picrotoxin (100 µM) using 15–30 MΩ pipettes filled with 0.5 M NaCl. Data were recorded using an Axopatch 200A (Molecular Devices, USA) and acquired using WinWCP 4.5.4 freeware (John Dempster, University of Strathclyde, UK). Recordings were filtered at 2 kHz and sampled at 50 kHz.

Analyses. Spike detection was performed using OpenElectrophy (Garcia and Fourcaud-Trocme, 2009) and custom based routines written in Python (Antoine Valera). Discharge regularity was assessed by the CV2 of interspike-intervals (ISI): $CV2=2|ISI_{n+1}-ISI_n|/(ISI_{n+1}+ISI_n)$ (Holt et al., 1996). Student's t-test and the Mann–Whitney U test were used for statistics.

Mitochondria Respiration Analysis

Mice were anesthetized with 300 µL of intraperitoneal injection (10 % pentobarbital solution in 10 mM NaCl). Muscles were collected and placed in S solution (see below). Fibers were separated under a binocular microscope in solution S at 4 °C and permeabilized for 30 min in solution S supplemented with 50 µg/mL of saponin. Isolated fibers were subsequently placed for 10 min in solution R (see below) to wash out adenine nucleotides and creatine phosphate. They were then transferred to a 3 mL water-jacketed oxygraphic cell (Strathkelvin Instruments, Glasgow, UK) equipped with a Clark electrode, as previously described (Jeukendrup et al., 1997). Solutions R and S contained 2.77 mM CaK_2EGTA, 7.23 mM K_2EGTA, 6.56 mM $MgCl_2$, 20 mM taurine, 0.5 mM DTT, 50 mM potassium-methane sulfonate (160 mM ionic strength) and 20 mM imidazole (pH 7.1). Solution S also contained 5.7 mM Na_2ATP, 15 mM creatine-phosphate, while solution R also contained 5 mM glutamate, 2 mM malate, 3 mM phosphate, and 2 mg/mL fatty acid free bovine serum. V_{INIT} was measured in the absence of fibers and substrates at 22 °C under continuous stirring. V_0 corresponds to the rate of O_2 consumption after addition of muscle fibers and glutamate-malate as substrate, to which V_{INIT} is subtracted. V_{MAX} (maximal respiration) corresponds to the rate of O_2 consumption after addition of 2 mM of ADP as a phosphate acceptor, to which V_{INIT} is subtracted. The acceptor control ratio, ACR, is defined as the ratio between V_{MAX} and V_0. After measurement, fibers were dried, and respiration rates were expressed as micromoles of O_2 per minute per mg of dry weight.

Metabolomics Analysis of Mouse Quadriceps Muscle by GC-MS

Metabolite extraction. Mouse quadriceps were rapidly isolated from 31-week-old female mice (4 WT and 4 KO) and frozen in $N_{2(l)}$. Samples of frozen mouse quadriceps (~30 mg of tissue) were homogenized under liquid nitrogen using a mortar and pestle, and the resultant powder of frozen tissue was transferred to a tube with ACN/IPA/H_2O (2:2:1, v/v/v, 1.5 mL, pre-cooled to –20 °C and kept on dry ice). After briefly mixing, the tube was flash frozen in $N_{2(l)}$. Once all of the samples were brought to this point, they were thawed in parallel to 4 °C (still ice cold). The samples were mixed by vortexing (4 °C, 1 min) to complete the extraction. The samples were centrifuged (5,000 *g*, 5 min, 4 °C) to pellet insoluble material. The supernatant was transferred to a new tube (pre-cooled to 4 °C), flash-frozen in $N_{2(l)}$, and store at –80 °C.

Tissue extract sample preparation for GC-MS. Tissue extracts were thawed at room temperature for 1 hour, 150 µL of each were aliquoted into glass autosampler vials along with 10 µL of 1 ppm isotopically labeled alanine-

2,3,3,3-d_4 and adipic acid-d_{10}. Samples were then dried to completion using a vacuum concentrator (1 hour). Once dry, the samples were re-suspended in 50 µL of a 1:1 mixture of pyridine and N-methyl-N-trimethylsilyl]trifluoroacetamide (MSTFA) with 1% trimethylchlorosilane (TMCS). The mixture was vortexed for 10 seconds, and then heated to 60 °C for 30 minutes.

Mass spectrometric analysis. Samples were analyzed using a GC/MS instrument comprising a Trace 1310 GC coupled to a Q-Exactive Orbitrap mass spectrometer (Thermo Fisher Scientific). A temperature gradient ranging from 100 °C to 320 °C was employed spanning a total runtime of 25 minutes. Analytes were injected onto a 30 m TraceGOLD TG-5SILMS column (Thermo Fisher Scientific) at 1 µL volume, using a 1:10 split ratio, at an injector temperature of 275 °C, and the GC effluent subjected to electron ionization (EI). The mass spectrometer was operated in full scan mode using a resolution of 30,000 ($m/\Delta m$) relative to 200 *m/z*.

Mass spectral data analysis. The resulting GC-MS data were processed using an in-house developed software suite (*https://github.com/coongroup*). Briefly, all *m/z* peaks are aggregated into distinct chromatographic profiles (i.e., feature) using a 10 ppm mass tolerance. These chromatographic profiles are then grouped according to common elution apex (i.e., feature group). The collection of features (*i.e.*, *m/z* peaks) sharing a common elution apex, therefore, represent an individual EI-MS spectrum of a single eluting compound. The EI-MS spectra were then compared against a matrix run and a background subtraction was performed. Remaining EI-MS spectra are then searched against the NIST 12 MS/EI library and subsequently subjected to a high resolution filtering (HRF) technique as described elsewhere. EI-MS spectra that were not identified were assigned a numeric identifier. Feature intensity, which was normalized using internal standards and total metabolite signal, was used to estimate metabolite abundance.

Targeted HPLC-EC Quantification of CoQ_9 and CoQ_{10}

Homogenates (5%, w/v) of various organs from 5- and 32-week-old *Coq8a*$^{-/-}$ and WT mice were prepared on ice with an Ultra-Turrax in Tris-HCl 50 mM (pH 7.5) containing 50 mM KCl, 10% glycerol, 1 mM EDTA and 0.2% Triton-X 100. Aliquots were adjusted to 0.5 mL with 0.15 M KCl and extracted with 4.5 mL methanol (MeOH) and 3 mL hexane with vigorous shaking after each addition. Following phase separation, the upper hexane phase was collected and evaporated under $Ar_{(g)}$. The lipid residue was dissolved in ethanol (EtOH) and loaded on an Ultimate 3000 HPLC system (Dionex) at a flow rate of 1 mL/min. Separation was achieved on a Thermo Betabasic-18 column (4.6×150 mm, 5 µm particle size) after oxidization of the sample with an ESA 5020 guard cell (E; +700 mV). The linear gradient started at 25% isopropanol (IPA), 20% MeOH, 55% acetonitrile (ACN) and 10% solvent D (200 mM $LiClO_4$ in IPA:H_2O (85:15, v/v) and ended 20 min later at 30% IPA and 15% MeOH with ACN and solvent D unchanged. Detection was performed with a diode array detector and a Coulochem III detector with an ESA 5011A analytical cell (E1; −700mV E2; +700 mV). CoQ_8 was used as internal standard and calibrated at 275 nm in EtOH. Protein was measured with a BCA kit (Sigma).

Mass Spectrometry-Based Lipidomics

Mouse Tissue Homogenization. Mouse cerebellum and quadriceps tissues (4 biological replicates of *Coq8a*$^{-/-}$ mice and 4 biological replicates of WT mice, 8-month-old) were homogenized in Lipidomics Homogenization Buffer [phosphate (11.8 mM), NaCl (137 mM), KCl (2.7 mM), pH 7.2, phosphatase inhibitors (PhosSTOP, Roche), protease inhibitors (cOmplete, Mini, Roche)] at 4 °C (in a cold room) as quickly as possible (< 5 min).

Cerebellum Lipid Extractions. Mouse cerebellum homogenate (0.65 mg protein, 280 µL) was spiked with an internal standard (CoQ_6, 20 µL, 10 µM) and mixed by vortexing (30 s). $CHCl_3$/MeOH (1:1, v/v) (900 µL) was added and vortexed (2 × 30 s). HCl (1 M, 100 µL, 4 °C) was added and vortexed (2 × 30 s). The samples were centrifuged (3,000 *g*, 3 min, 4 °C) to complete phase separation. 500 µL of the lower organic phase was transferred to a clean tube and dried under $Ar_{(g)}$. The organic residue was reconstituted in ACN/IPA/H_2O (65:30:5, v/v/v) (100 µL) by vortexing (2 × 30 s).

Quadriceps Lipid Extractions. Mouse quadriceps homogenate (1 mg protein, 250 µL) was spiked with an internal standard (CoQ_6, 20 µL, 10 µM) and mixed by vortexing (30 s). $CHCl_3$/MeOH (1:1, v/v) (900 µL) was added and vortexed (2 × 30 s). HCl (1 M, 100 µL, 4 °C) was added and vortexed (2 × 30 s). The samples were centrifuged (3,000 *g*, 3 min, 4 °C) to complete phase separation. 500 µL of the lower organic phase was transferred to a clean tube and dried under $Ar_{(g)}$. The organic residue was reconstituted in ACN/IPA/H_2O (65:30:5, v/v/v) (100 µL) by vortexing (2 × 30 s).

Serum Lipid Extractions. Mouse serum (90 µL) was spiked with an internal standard (CoQ_6, 20 µL, 10 µM) and mixed by vortexing (30 s). $CHCl_3$/MeOH (1:1, v/v) (900 µL) was added and vortexed (2 × 30 s). HCl (1 M, 100 µL, 4 °C) was added and vortexed (2 × 30 s). The samples were centrifuged (3,000 *g*, 3 min, 4 °C) to complete phase separation. 700 µL of the lower organic phase was transferred to a clean tube and dried under $Ar_{(g)}$. The organic residue was reconstituted in ACN/IPA/H_2O (65:30:5, v/v/v) (100 µL) by vortexing (2 × 30 s).

LC-MS/MS. LC-MS/MS analysis was performed on an Acquity CSH C18 column held at 50 °C (2.1 × 100 mm × 1.7 µm particle size; Waters) using an Ultimate 3000 RSLC Binary Pump (400 µL/min; Thermo Scientific). Mobile phase A consisted of 10 mM ammonium acetate in ACN/H_2O (70:30, v/v) containing 250 µL/L acetic acid. Mobile phase B consisted of 10 mM ammonium acetate in IPA/ACN (90:10, v/v) with the same additives. Initially, mobile phase B was held at 2% for 2 min and then increased to 30% over 3 min. Mobile phase B was then further increased to 85% over 14 min and then raised to 99% over 1 min and held for 7 min. The column was then re-equilibrated for 5 min before the next injection. Ten microliters of lipid extract were injected by an Ultimate 3000 RSLC autosampler (Thermo Scientific). The LC system was coupled to a Q Exactive Focus mass spectrometer by a HESI II heated ESI source (Thermo). The MS was operated in polarity switching mode acquiring positive and negative mode MS^1 and MS^2 spectra (Top2) during the same separation. MS acquisition parameters were 17,500 resolving power, 1×10^6 automatic gain control (AGC) target for MS^1 and 1×10^5 AGC target for MS^2 scans, 25 units of sheath gas and 10 units of auxiliary gas, 300 °C HESI II and inlet capillary temperature, 100 ms MS1 and 50 ms MS2 ion accumulation time, 200–1,600 Th MS1 scan range, 1 Th isolation width for fragmentation, stepped HCD collision energy (20, 30, 40 units), 1.0% under fill ratio, and 10 s dynamic exclusion.

Data Analysis. Individual lipid species were identified by searching the discovery LC-MS/MS data against the LipidBlast in-silico lipid spectral library (Kind et al., 2013) with a precursor and product ion tolerance of 0.1 Th. Spectral matches with dot products below 500 were not considered. Matching spectra were manually inspected to ensure proper identification. Lipid quantitation was performed by normalizing the apex MS^1 signal for each identified lipid species to the total identified lipid content.

Yeast LC-MS/MS Lipidomics. Yeast lysates (5 mg protein as quantified by BCA assay, 560 µL) (4 biological replicates of Δ*coq8* yeast and 4 biological replicates of WT yeast; post-diauxic shift cultures) were mixed with $CHCl_3$/MeOH (1:1, v/v) (5 mL) and vortexed (2 × 60 s). HCl (1 M, 560 µL, 4 °C) was added and vortexed (30 s). The samples were centrifuged (1,000 *g*, 5 min, 4 °C) to complete phase separation. 2 mL of the lower organic phase was transferred to a clean tube and dried under $N_{2(g)}$. The organic residue was reconstituted in ACN/IPA/H_2O (65:30:5, v/v/v) (100 µL) by vortexing (2×30 s). Yeast LC-MS/MS and data analysis were conducted essentially as described above for the mouse lipidomics analysis.

Mouse Proteomics and Phosphoproteomics

Sample preparation. Mouse tissues (cerebellum, quadriceps, heart, and kidney) (4 biological replicates of *Coq8a*$^{-/-}$ mice and 4 biological replicates of WT mice, 8-month-old) were homogenized in Proteomics Lysis Buffer [urea (8 M), tris, pH 8 (40 mM), NaCl (30 mM), $CaCl_2$ (1 mM), phosphatase inhibitors (PhosSTOP, Roche), protease inhibitors (cOmplete, Mini, Roche)] at 4 °C (in a cold room) as quickly as possible (< 5 min). Homogenates were lysed on ice using probe sonication. Protein content was evaluated using a BCA assay (Thermo). Proteins were reduced with 5 mM dithiothreitol (DTT) (58 °C, 30 min) and alkylated with 15 mM iodoacetamide (incubation in the dark, ~20 °C, 30 min). Alkylation was quenched by adding additional 5 mM DTT (~20 °C, 15 minutes). Proteins were enzymatically digested in a two-step process. First, proteinase LysC (Wako Chemicals, Richmond, VA) was added to each sample at a ratio of 1:100 (enzyme:protein) and the resulting mixtures were incubated (37 °C, 3 h). Next, samples were diluted to a final concentration of 1.5 M urea (pH 8) with a solution of 50 mM Tris and 5 mM $CaCl_2$. Sequencing-grade trypsin (Promega, Madison, WI) was added to each sample at a ratio of 1:50 (enzyme:protein) and the resulting mixtures were incubated (~20 °C, overnight). The following morning each sample was incubated with an additional aliquot of sequencing-grade trypsin at ratio of 1:100 (enzyme:protein) (~1.5 h). Digests were quenched by bringing the pH ~2 with trifluoroacetic acid and immediately desalted using C18 solid-phase extraction columns (SepPak, Waters).

Desalted material was labeled with TMT 8-plex isobaric labels (Thermo). Prior to quenching the TMT reactions, ~5 µg of material from each TMT channel was combined into a test mix and analyzed by LC-MS/MS to evaluate labeling efficiency and obtain optimal ratios for sample recombination. Following quenching, tagged peptides were combined in equal amounts by mass (~1000 µg per channel for phosphorylation analyses, ~500 µg per channel for protein analyses) and desalted. All experiments had ≥ 98% labeling efficiency, calculated by the number N-terminal labeled peptides divided by the total number of peptide identifications.

Sample fractionation. Labeled peptides were fractionated by strong cation exchange (SCX) using a polysulfoethylaspartamide column (9.4×200 mm; PolyLC) on a Surveyor LC quaternary pump (Thermo). Each dried and mixed TMT sample was re-suspended in buffer A, injected onto the column, and subjected to the following gradient for separation: 100% buffer A from 0–2 min, 0–15% buffer from 2–5 min, and 15–100% buffer B from 5–35 min. Buffer B was held at 100% for 10 minutes and then the column was washed extensively with buffer C and water prior to recalibration. Flow rate was held at 3.0 mL/min throughout the separation. Buffer compositions were as follows: buffer A [5 mM KH_2PO_4, 30% ACN (pH 2.65)], buffer B [5 mM KH_2PO_4, 350 mM KCl, 30% ACN (pH

2.65)] buffer C [50 mM KH_2PO_4, 500 mM KCl (pH 7.5)]. Twelve fractions were collected over the first 50 minute elution period and were immediately frozen, lyophilized, and desalted. A small portion of each, 5%, was extracted and used for protein analysis. The remaining material was retained for phosphopeptide enrichment.

Phosphopeptide Enrichment. Phosphopeptides were enriched using immobilized metal affinity chromatography (IMAC) with magnetic beads (Qiagen). Following equilibration with water, the magnetic beads were incubated with 40 mM EDTA (pH 8.0) for 1 hour, with shaking. Next, the beads were washed four times with water and incubated with 30 mM $FeCl_3$ for 1 hour, with shaking. Beads were then washed four times with 80% acetonitrile/0.15% TFA. Each of the 12 fractions were re-suspended in 80% acetonitrile/0.15% TFA and incubated with the magnetic beads for 45 minutes, with shaking. Bound peptides were washed three times with 80% acetonitrile/0.15% TFA and eluted with 50% acetonitrile, 0.7% NH_4OH. Eluted peptides were immediately acidified with 4% FA, frozen, and lyophilized. Each phospho-peptide fraction was re-suspended in 20 µL 0.2% FA for LC-MS/MS analysis.

LC-MS/MS analysis. All experiments were performed using a NanoAcquity UPLC system (Waters) coupled to an Orbitrap Elite mass spectrometer (Thermo). Reverse-phase columns were made in-house by packing a fused silica capillary (75 µm i.d., 360 µm o.d, with a laser-pulled electrospray tip) with 1.7 µm diameter, 130 Å pore size Bridged Ethylene Hybrid C18 particles (Waters) to a final length of 30 cm. The column was heated to 60 °C for all experiments. Samples were loaded onto the column for 12 minutes in 95:5 buffer A [water, 0.2% formic acid, and 5% DMSO]:buffer B [acetonitrile, 0.2% formic acid, and 5% DMSO] at a flow-rate of 0.30 µL/min. Peptides were eluted using the following gradient: an increase to 7% B over 1 min, followed by a 42 min linear gradient from 7% to 18% B, followed by a 28 min linear gradient from 18% to 27% B, followed by a final 1 min ramp to 75% B which was held for 3 min. The column was equilibrated with 5% buffer B for an additional 25 min. Precursor peptide cations were generated from the eluent through the utilization of a nanoESI source.

Mass spectrometry instrument methods consisted of MS^1 survey scans (1e6 target value; 60,000 resolution; 300 Th – 1500 Th) that were used to guide fifteen subsequent data-dependent MS/MS scans (3 Th isolation window, HCD fragmentation, normalized collision energy of 35; 5e4 target value, 30,000 resolution). Dynamic exclusion duration was set to 30 s, with a maximum exclusion list of 500 and an exclusion width of 0.55 Th below and 2.55 Th above the selected average mass. Maximum injection times were set to 50 ms for all MS^1 scans, 150 ms for MS/MS scans in whole protein analyses, and 200 ms for MS/MS scans in phospho enrichment analyses.

Data Analysis. Data was processed using the in-house software suite COMPASS (Wenger et al., 2011). OMSSA (Geer et al., 2004) (version 2.1.8) searches were performed against a target-decoy database (*UniProt (mouse),* www.uniprot.org, August 7th, 2013). Searches were conducted using a 150 ppm precursor mass tolerance and a 0.015 Da product mass tolerance. A maximum of 3 missed tryptic cleavages were allowed. The fixed modifications specified were carbamidomethylation of cysteine residues, TMT 8-plex on peptide N-termini, and TMT 8-plex on lysine residues. The variable modifications specified were oxidation of methionine and TMT 8-plex on tyrosine residues. Additional variable modifications were specified for phospho-peptide analyses (phosphorylation of threonine, serine, and tyrosine residues). TMT quantification of identified peptides was performed within COMPASS as described previously (Phanstiel et al., 2011). Peptides identified within each of 12 fractions were grouped into proteins according to previously reported rules (Nesvizhskii and Aebersold, 2005) using COMPASS. Phosphopeptide localization was performed using *Phosphinator* software within COMPASS, as described previously (Phanstiel et al., 2011). This program both localized phosphorylation sites and combined quantitative data for phospho-isoforms across all 12 fractions. All phosphosites had to be localized for a given phospho-peptide to be included in subsequent quantitative analysis. Protein quantification was performed by summing all of the reporter ion intensities within each channel for all peptides uniquely mapping back to a given protein. All quantitative data was normalized at the protein level, $\log_2$ transformed and mean normalized. Fold-changes were then calculated by averaging protein-normalized values for each condition and calculating the difference of averages. For each comparison, a *p*-value was calculated using Student's t-test (assuming equal variance) and then correcting for multiple hypotheses (Storey method).

Yeast Proteomics and Phosphoproteomics by LC-MS/MS with Isobaric Tags

Yeast cultures and sample harvests were conducted as described above in the yeast culture methods section (diauxic shift cultures). Yeast proteomics and phosphoproteomics were conducted essentially as described above for the mouse proteomics and phosphoproteomics except 6-plex TMT was used instead of 8-plex TMT. Three sets of 6-plex TMT runs were conducted, each with a biological replicate of the 6 conditions (each 6-plex TMT set contained samples from WT and Δ*coq8* yeast across the three time points).

Yeast Proteomics by Label Free Quantitation LC-MS/MS

Sample preparation. Yeast cultures and sample harvests were conducted as described above in the yeast culture methods section (4 biological replicates of each Coq8p point mutant strain, and 4 biological replicates of WT yeast). Yeast pellets were reconstituted in lysis buffer (8 M urea, 100 mM Tris, pH 8). Proteins were extracted with 90% MeOH and centrifuged (14,000 *g*, 5 min). Pellets were reconstituted in lysis buffer containing 40 mM chloroacetamide and 10 mM tris(2-carboxyethyl)phosphine, and incubated (10 min, ~20 °C). Samples were diluted to a final concentration of 1.5 M urea (pH 8) with 50 mM Tris pH 8. Sequencing-grade trypsin (Promega, Madison, WI) was added to each sample at a ratio of 1:50 (enzyme:protein) and the resulting mixtures were incubated (~12 h, ~20 °C). Digests were quenched by bringing the pH to ~2 with trifluoroacetic acid and immediately desalted using Strata-X polymeric reversed phase solid phase extraction (SPE) columns (Phenomenex). SPE eluants were dried down under vacuum and reconstituted in 0.2% formic acid. Peptide content was determined using a colorimetric assay (Thermo).

LC-MS/MS analysis. All experiments were performed using a NanoAcquity UPLC system (Waters) coupled to an Orbitrap Fusion Tribrid mass spectrometer (Thermo). Reverse-phase columns were made in-house as described above in the section on mouse proteomics. The column was heated to 55 °C using a home-built column heater. Mobile phase solvent A was composed of 0.2% formic acid in water. Mobile phase B was composed of 70% ACN, 0.2% formic acid, and 5% DMSO. For each sample, 2 µg of peptides were loaded on-column and separated over a 120 minute gradient, including time for column re-equilibration. Flow rates were set at 350 µL/min. Precursor scans were performed from 300 to 1,500 m/z at 60K resolution (at 400 m/z) using a 5 x 10^5 AGC target. Precursors selected for tandem MS were isolated at 0.7 Th in the quadrupole and fragments were analyzed using turbo scan in the ion trap. Fragmentation method was based on m/z: precursors above 500 m/z were fragmented by HCD with a normalized collision energy of 27.5, and precursors below 500 m/z were fragmented by CAD with a normalized collision energy of 30. The maximum injection time for MS^2 analysis was 25 ms, with an AGC target of 10^4. Precursors with a charge state of 2–8 were sampled for MS^2. Dynamic exclusion time was set at 15 seconds, with a 25 ppm tolerance around the selected precursor and its isotopes. Monoisotopic precursor selection was turned on. Analyses were performed in top speed mode with 3 second cycles.

Database searching and LFQ analysis. The raw data was processed using MaxQuant (Version 1.5.2.8) (Cox and Mann, 2008). Searches were performed against a target-decoy database of reviewed yeast proteins plus isoforms (UniProt, downloaded January 20, 2013) using the Andromeda search algorithm (Cox et al., 2011). Searches were performed using a precursor search tolerance of 4.5 ppm and a product mass tolerance of 0.35 Da. Specified search parameters included fixed modification for carbamidomethylation of cysteine residues, variable modifications for the oxidation of methionine and protein N-terminal acetylation, and a maximum of 2 missed tryptic cleavages. A 1% peptide spectrum match false discovery rate (FDR) and a 1% protein FDR were applied according to the target-decoy method. Proteins were identified using at least one peptide (razor + unique). Proteins were quantified using MaxLFQ with an LFQ minimum ratio count of 2. LFQ intensities were calculated using the match between runs feature, and MS/MS spectra were not required for LFQ comparisons (Cox et al., 2014).

Recombinant Protein Expression and Purification

Yeast Coq8$^{N\Delta41}$. $Coq8^{N\Delta41}$ plasmid constructs were transformed into RIPL competent *E. coli* cells for protein expression. 8His-MBP-[TEV]-$Coq8^{N\Delta41}$ was overexpressed in *E. coli* by autoinduction (Fox and Blommel, 2009). Cells were isolated by centrifugation, frozen in $N_{2(l)}$, and stored at –80 °C until further use. For protein purification, cells were thawed on ice, resuspended in Lysis Buffer (50 mM HEPES (pH 7.5), 150 mM NaCl, 5% glycerol, 1 mM BME, 0.25 mM PMSF, 1 mg/mL lysozyme, pH 7.5) and incubated (1 h, 4 °C). The cells were lysed by sonication (4 °C, 6 V, 60 s × 4). The lysate was clarified by centrifugation (15,000 *g*, 30 min, 4 °C). The cleared lysate was mixed with cobalt IMAC resin (Talon resin) and incubated (4 °C, 1 h). The resin was pelleted by centrifugation (700 *g*, 5 min, 4 °C) and washed four times with Wash Buffer (50 mM HEPES (pH 7.5), 150 mM NaCl, 5% glycerol, 1 mM BME, 0.25 mM PMSF, 10 mM imidazole, pH 7.5) (10 resin bed volumes). His-tagged protein was eluted with Elution Buffer (50 mM HEPES (pH 7.5), 150 mM NaCl, 5% glycerol, 1 mM BME, 100 mM imidazole, pH 7.5). The eluted protein was concentrated with a MW-cutoff spin filter (50 kDa MWCO) and exchanged into storage buffer (50 mM HEPES (pH 7.5), 150 mM NaCl, 5% glycerol, 1 mM BME, pH 7.5). The concentration of 8His-MBP-[TEV]-$Coq8^{N\Delta41}$ was determined by its absorbance at 280 nm (ε = 109,210 $M^{-1}cm^{-1}$) (MW = 96.2 kDa). The fusion protein was incubated with Δ238TEV protease (1:50, TEV/fusion protein, mass/mass) (1 h, 20 °C). The TEV protease reaction mixture was mixed with cobalt IMAC resin (Talon resin) and incubated (4 °C, 1 h). The unbound $Coq8^{N\Delta41}$ was isolated and concentrated with a MW-cutoff spin filter (30 kDa MWCO) and exchanged into storage buffer. The concentration of $Coq8^{N\Delta41}$ was determined by its absorbance at 280 nm (ε = 41,370 $M^{-1}cm^{-1}$) (MW = 52 kDa). The protein was aliquoted, frozen in $N_{2(l)}$, and stored at –80 °C. Fractions from the protein preparation were analyzed by SDS-PAGE.

Mouse PKA. 8-His-MBP-PKA and PKA (mouse PKA, Prkaca) were isolated as described above for $Coq8^{N\Delta41}$. The concentration of 8His-MBP-[TEV]-PKA was determined by its absorbance at 280 nm (ε = 121,700 $M^{-1}cm^{-1}$) (MW = 84.8 kDa). The concentration of PKA was determined by its absorbance at 280 nm (ε = 53,860 $M^{-1}cm^{-1}$) (MW = 40.5 kDa).

Nucleotide Binding

The general differential scanning fluorimetry (DSF) method (thermal shift assay) has been described previously (Niesen et al., 2007). Mixtures (20 µL total volume) of $Coq8^{N\Delta41}$ (2 µM) or PKA (1 µM) were prepared with SYPRO Orange dye (Life Tech.) (2×), NaCl (150 mM), HEPES (100 mM, pH 7.5), and ligands (e.g. MgATP). Otherwise, the general DSF method, ligand screen, and dissociation constant experiments were conducted as described for $COQ8A^{N\Delta250}$ (Stefely et al., 2015).

In Vitro Kinase Activity

In Vitro Autophosphorylation. Unless otherwise indicated, $Coq8^{N\Delta41}$ (4 µM), MBP-$Coq8^{N\Delta41}$ (4 µM), or PKA (4 µM) was mixed with [γ-^{32}P]ATP (0.25 µCi/µL, 100 µM $[ATP]_{total}$) and $MgCl_2$ (20 mM) in an aqueous buffer (100 mM HEPES, 150 mM NaCl, 0.1 mg/mL BSA, 0.5 mM DTT, pH 7.5) and incubated (30 °C, 60 min, 500 rpm) (final concentrations for reaction components). For the divalent cation screen, $MgCl_2$ and $CaCl_2$ were used at 20 mM. Reactions were quenched with 4×LDS buffer (106 mM TrisHCl, 141 mM Tris base, 2% LDS, 10% glycerol, 0.51 mM EDTA, 0.175 mM Phenol Red, 0.22 mM Coomassie Brilliant Blue G-250, pH 8.5). [γ-^{32}P]ATP was separated from $Coq8^{N\Delta41}$ by SDS-PAGE (10% Bis-Tris gel, MES buffer, 150 V, 1.5 h). The gel was stained with Coomassie Brilliant Blue, dried under vacuum, and imaged by digital photography. A storage phosphor screen was exposed to the gel (~5 days) and then imaged with a Typhoon (GE) to generate the phosphorimages. $COQ8A^{N\Delta250}$ autophosphorylation assays were conducted as described previously (Stefely et al., 2015).

LC-MS/MS of Autophosphorylation Sites. $Coq8^{N\Delta41}$ (WT, A197G, D365N, or A197G,K134H) (20 µM) was mixed with nucleotide (ATP, ADP, or none) (1 mM) in an aqueous buffer (100 mM HEPES, 150 mM NaCl, 20 mM $MgCl_2$, 0.1 mg/mL BSA, 0.5 mM DTT, pH 7.5) and incubated (30 °C, 60 min, 500 rpm). All 12 reactions were conducted in parallel. Reactions were flash frozen in $N_{2(l)}$ after completion. A sample of each autophosphorylation reaction (100 µL) was mixed with lysis buffer (300 µL) (8 M urea, 40 mM Tris (pH = 8.0), 30 mM NaCl, 2 mM $MgCl_2$, 1 mM $CaCl_2$, 1 × phosphatase inhibitor cocktail tablet, and 1 × protease inhibitor tablet). DTT was added (to 2 mM) and incubated (37 °C, 30 min) to reduce disulfide bonds. Alkylation of cysteines was achieved by adding iodoacetimide (to 7 mM) and incubating in the dark (~20 °C, 30 min). The alkylation reaction was quenched by adding DTT (to 7 mM) and incubating (~20 °C, 15 min). Protein was digested with lys-C (37 °C, 4 hours) (1:100, enzyme:protein mass ratio). The sample was diluted to 1.5 M urea with 50 mM Tris (pH = 8.0) and 1 mM $CaCl_2$ solution. Trypsin (1:100, enzyme:protein) was added to further digest the proteins. After overnight incubation at 37 °C, another aliquot of trypsin (1:100, enzyme:protein mass ratio) was added and incubated (1 hour). The digestion was quenched by adding 10% trifluoroacetic acid to bring the pH below 2. The peptides were desalted with Sep-Pak Vac 1cc tC18 cartridges (Waters). Immobilized metal affinity chromatography (IMAC) with magnetic agarose beads (Qiagen) was used to enrich for phosphopeptides (Phanstiel et al., 2011). Both non-phospho and phospho fractions were analyzed by reverse phase nano LC coupled to an Orbitrap Elite (Thermo). All MS raw data were analyzed with COMPASS (Wenger et al., 2011). A precursor mass tolerance of 150 ppm and a product ion mass tolerance of 0.01 Da, and up to 3 missed cleavages with trypsin were applied to searching. Carbamidomethylation of cysteines was set as fixed modification, while oxidation of methionines, phosphorylation with neutral loss on serine and threonine residues, and intact phosphorylation on tyrosine residues were set as variable modifications. Peptides were grouped into parsimonious protein groups by Protein Hoarder at 1% FDR at the unique protein group level.

Protein Kinase Activity. PKA (4 µM) or $Coq8^{N\Delta41}$ (4 µM) and protein substrates [myelin basic protein (Millipore 13-104, 6 µM), none, or a mixture of COQ proteins] were mixed with [γ-^{32}P]ATP (0.3 µCi/µL, 100 µM $[ATP]_{total}$) in an aqueous buffer (100 mM HEPES, 150 mM NaCl, 20 mM $MgCl_2$, 0.1 mg/mL BSA, 0.5 mM DTT, pH 7.5) and incubated (30 °C, 40 min, 500 rpm) (final concentrations for reaction components). The mixture of COQ proteins (COQ3–COQ7 and COQ9) was prepared using a cell-free expression system as described (Floyd et al., 2016, *this issue*). Reactions were quenched with 4×LDS buffer (106 mM TrisHCl, 141 mM Tris base, 2% LDS, 10% glycerol, 0.51 mM EDTA, 0.175 mM Phenol Red, 0.22 mM Coomassie Brilliant Blue G-250, pH 8.5). [γ-^{32}P]ATP was separated from phosphorylated proteins by SDS-PAGE (10% Bis-Tris gel, MES buffer, 150 V, 1.5 h). The gel was stained with Coomassie Brilliant Blue, dried under vacuum, and imaged by digital photography. A storage phosphor screen was exposed to the gel (~5 days) and then imaged with a Typhoon (GE) to generate the phosphorimages.

In Vitro ATPase Activity

ELIPA (Cytoskeleton) assays were carried out according to the manufacturer's instructions with the following modifications. 135 µL of ELIPA mix (75 µL ELIPA Reagent 2, 6 mL of reaction buffer (100 mM HEPES [pH 7.5], 150 mM NaCl, 20 mM $MgCl_2$, 0.5 mM DTT, 0.1 mg/mL Bovine Serum Albumin), 1440 µL ELIPA Reagent 1) was mixed with $Coq8^{N\Delta41}$ (2 µM) (final concentrations). 10 µL of ATP (0–2 mM) (final concentrations) was added to start the reactions (final reaction volume 160 µL), and reactions were incubated (~22 °C). The absorbance at 360 nm was read immediately after adding ATP every minute for 20 minutes. A standard curve was constructed using concentration of inorganic phosphate from 0–25 nmol (0, 0.5, 1, 2.5, 5, 12.5, and 25 nmol). The no enzyme reaction was subtracted from each condition prior to calculation of kinetic constants using SigmaPlot v13.0.

Sub-Cellular Fractionation

Mitochondria were purified from the hearts of 11 C57BL/6 female mice (26-week-old) as previously described (Frezza et al., 2007). Sodium carbonate treatment and subsequent centrifugation were used separate soluble (supernatant) and membrane-anchored (pellet) proteins. First, pure mitochondria were exposed to sodium carbonate (0.1 M, pH 11.5) (30 min, on ice), and then ultracentrifuged (100,000 *g*, 1 h, 4 °C). The soluble and peripheral membrane proteins in the supernatant were TCA-precipitated and then solubilized in sample buffer (10 min, ~20 °C). Ultracentrifuged pellets (integral membrane proteins) were resuspended in sample buffer. Mitochondria were subfractionated using mitochondrial swelling. Mitochondria were resuspended in SEM Buffer (250 mM sucrose, 1 mM EDTA, and 10 mM HEPES-KOH, pH 7.4) and treated with nine volumes of 10 mM HEPES-KOH, pH 7.4 for 15 min on ice, or as a control, kept intact in an equivalent volume of SEM Buffer. Accessible proteins were removed by proteinase K treatment (25 µg/mL) or left untreated as control. PMSF was subsequently added at a concentration of 2 mM to inhibit proteinase K activity. The mitochondria or mitoplasts were then pelleted by centrifugation, washed in SEM Buffer and resuspended in sample buffer. Western blot analyses were conducted as described above in the antibody and WB method section.

Liposome-Protein Co-Floatation

Lipids were extracted from Δ*ubiE E. coli* (~1.2 g wet pellet) with $CHCl_3$/MeOH (1:1, v/v), reduced with excess $NaBH_4$, quenched with AcOH, and re-extracted with $CHCl_3$/MeOH (1:1, v/v). The lipids were dried under $Ar_{(g)}$ to afford 12 mg of dry lipid mass. The lipids were reconstituted in $CHCl_3$/MeOH (1:1, v/v, 1 mL) and stored under $Ar_{(g)}$. To form the *E. coli* extract liposomes, 2.2 mg of *E. coli* lipids were mixed with NBD-PC (17.4 µL, 1 mM), dried under $Ar_{(g)}$, and reconstituted in an aqueous buffer (20 mM Tris, 150 mM NaCl, 1 mM DTT). Liposomes were formed by sonication (22 °C, 30 min, bath sonicator). $Coq8^{N\Delta41}$ (1 µM), $COQ8A^{N\Delta250}$ (1 µM), or $COQ9^{N\Delta79}$ (1 µM) (10 µL protein mixture) was mixed with liposomes (135 µL) and incubated (30 °C, 20 min, 230 rpm). After incubation, the reactions were moved onto ice and mixed with 75% (w/v) sucrose buffer (100 µL) (all sucrose buffers in 20 mM Tris, 150 mM NaCl, 1 mM DTT). Onto this mixture, overlaid 25% sucrose (200 µL) and 0% sucrose (50 µL) in a micro ultracentrifuge tube. Centrifuged (240,000 *g*, 4 °C, 1 h), and isolated 150 µL from the top of the gradient and 150 µL from the bottom of the gradient. Both the top and the bottom fractions were analyzed by SDS-PAGE with sliver staining. Flotation of the liposomes was assessed by tracking NBD-PC fluorescence.

LC-MS/MS of Lipids Co-Purifying with Coq8p

His_8-MBP-$Coq8^{N\Delta41}$ and co-purifying lipids were isolated by cobalt IMAC as described above for protein purification of His_8-MBP-$Coq8^{N\Delta41}$. The elution from the first IMAC was isolated directly without further concentration and snap frozen in $N_{2(l)}$. A sample of His_8-MBP-tagged protein (40 nmol, 310 µL, 129 µM) in "Elution Buffer" (50 mM HEPES, 150 mM NaCl, 5% glycerol, 1 mM BME, 100 mM imidazole, pH 7.5) was mixed with CoQ_6 (internal standard, 0.1 nmol, 10 µL, 10 µM) by vortexing (30 s, 4 °C). $CHCl_3$/MeOH (1:1, v/v) (5 mL) was added and vortexed (2 × 30 s). HCl (1 M, 400 µL) was added and vortexed (30 s). $NaCl_{(aq)}$ (saturated, 1 mL) was added and vortexed (30 s). The samples were centrifuged (1,800 *g*, 4 min, 4 °C) to complete phase separation. The lower organic phase was transferred to a clean tube and dried under $Ar_{(g)}$. The organic residue was reconstituted in ACN/IPA/H_2O (65:30:5, v/v/v) (200 µL) by vortexing (60 s) and transferred to a glass autosampler vial.

Lipids from 10 µL of extract were separated by LC on an Ascentis Express C18 column (150 mm × 2.1 mm × 2.7 µm particle size, Supelco, Bellefonte, PA) using an Accela HPLC pump (Thermo Scientific, San Jose, CA) at a flow-rate of 0.4 mL/min. Mobile phase A was 70/30 acetonitrile/water containing 10 mM ammonium acetate and 0.025% acetic acid and B was 90/10 isopropanol/acetonitrile containing the same additives. At the beginning of the gradient, the flow was maintained at 20% B for 1 min, then ramped to 30% at 4 min, to 50% at 5 min, to 85% at 20 min, to 99% at 21 min, held there until 25 min, returned to 20% B at 25.5 min, and finally the column was re-

equilibrated to 30 min before beginning the next injection sequence. The auto sampler (HTC PAL, Thermo Scientific) vigorously mixed each sample before injection to ensure homogeneity.

The MS conditions were as follows: a Q Exactive mass spectrometer (Thermo Scientific, Build 2.5) was operated in fast polarity switching mode, acquiring both positive and negative mode MS and MS/MS spectra. The mass ranges were 300–1600 Th in positive mode and 200–1600 Th in negative ion mode. Tandem MS acquisition was data dependent, fragmenting the two most abundant precursors from each MS scan with a 10 s exclusion duration. The MS was equipped with a HESI II spray source kept at 350 °C and ± 4 kV. The inlet capillary was kept at 350 °C and sheath and auxiliary gases were set to 35 and 15 units. Resolving power was 17,500 for all scans, AGC target was $1x10^6$ for MS scans and $1x10^5$ for MS/MS scans, the isolation width was 1 Th for MS/MS scans, normalized collision energy was stepped at 20, 30, and 40 units, and maximum injection time was set to 100 ms for MS scans and 50 ms for MS/MS scans. Quantitation was performed by integrating MS^1 elution profiles of lipids using the Xcalibur software suite (Thermo Scientific, Version 3.0).

Protein Co-Expression-Co-Purification

COS cells were transiently transfected with pcDNA3.1 constructs encoding murine COQ8A-FLAG (C-terminal FLAG tag) and COQ3-HA (C-terminal HA tag) or COQ5-HA or COQ9-HA using FuGene 6 according to the manufacturer's instructions. Cells were harvested 24 h after transfection, lysed in a digitonin buffer (50 mM Tris, pH 7.4, 10% glycerol, 100 mM KCl, 0.014% digitonin and 1× Complete Protease Inhibitor Cocktail (Roche)), and a mitochondria-enriched pellet was isolated by centrifugation (10,000 *g,* 10 min, 4 °C). Proteins were extracted from the mitochondria-enriched pellet in a Triton X-100 buffer (10 mM Tris, pH 7.4, 10% glycerol, 100 mM NaCl, 50 mM KCl, 0.2% Triton X-100 and 1× Protease Inhibitors). The protein extract was incubated with anti-FLAG M2 affinity beads (Sigma) (2 h, 4 °C) and eluted with 0.2 M Glycine, pH 2.8.

COQ8A-FLAG Co-Immunoprecipitation-Mass Spectrometry

COQ8A-FLAG Expression in HEK293 Cells. 5 million HEK293 cells were plated into a 15 cm dish with HGDMEM+FBS+P/S (37 °C, 25 mL) and incubated (37 °C, 5% CO_2) until the cultures were ~65–75% confluent (~12–24 h). Cells were transfected by dropwise addition of an OptiMEM+DNA+PEI mixture [900 µL OptiMEM (Thermo) warmed to 37 °C, 20 µg plasmid DNA (pcDNA3.1 COQ8A-FLAG plasmid), 72 µg PEI (72 µL, 1 µg/µL, linear polyethylenimine MW 25,000)] and incubated (37 °C, 5% CO_2, 1 day). After the 1 day of transfection had passed, the media was gently aspirated and replaced with glucose-free DMEM+FBS+P/S with 10 mM galactose (37 °C, 25 mL) and incubated (37 °C, 5% CO_2, 24 h). Immediately prior to cell harvest, the media was aspirated and the cells were gently washed with PBS (~7 mL, ~20 °C). The PBS wash was aspirated, PBS with 1× protease inhibitor cocktail (700 µL, 4 °C) was added, and the cells were harvested by gently scraping and transferring the resuspended cells into a 1.5 mL tube on ice. The cells were isolated by centrifugation (2000 *g*, 1 min, 4 °C). The supernatant was aspirated, and the cell pellets were snap frozen in $N_{2(l)}$ and stored at –80 °C.

Co-Immunoprecipitation. The transfected HEK293 cells were resuspended in Lysis Buffer (200 µL, 4 °C) [20 mM HEPES, pH 7.4, 100 mM NaCl, 10% (w/v) glycerol, 3% (w/v) digitonin (Sigma), 1 mM DTT, protease inhibitors (10 µM benzamidine, 1 µg/mL 1,10-phenanthroline and 0.5 µg/mL each of pepstatin A, chymostatin, antipain, leupeptin, aprotinin; Sigma), phosphatase inhibitors (500 µM imidazole, 250 µM NaF, 300 µM sodium molybdate, 250 µM sodium orthovanadate, 1 mM sodium tartrate; Sigma)]. The cells were vortexed (~15 s) and incubated (10 min, on ice) to lyse the cells. Soluble proteins were isolated by centrifuging (16,000 *g*, 10 min, 4 °C) the lysate to pellet insoluble materials and transferring the supernatant to a clean tube on ice. Anti-FLAG M2 magnetic beads were pre-equilibrated with Final Wash Buffer (20 mM HEPES, pH 7.4, 100 mM NaCl). The soluble protein mixture (equal total masses of protein, 200 µL) was loaded onto the anti-FLAG beads and incubated (60 min, 4 °C, end-over-end agitation). The beads were washed four times with Wash Buffer (170 µL, 4 °C) [20 mM HEPES, pH 7.4, 100 mM NaCl, 0.05% (w/v) digitonin, 10% (w/v) glycerol] and once with Final Wash Buffer (170 µL, 4 °C). Proteins were eluted with Elution Buffer (80 µL, ~21 °C) (20 mM HEPES, pH 7.4, 100 mM NaCl, 0.2 mg/mL 1×FLAG-peptide) (30 min incubation, ~21 °C, 500 rpm shaking) for LC-MS/MS analysis.

Protein digestion. coIP elutions were mixed 1:2 (v/v) with 3 M Urea, 100 mM Tris (pH 8). Protein was reduced with DTT (5 mM, 37 °C, 45 min), alkylated with iodoacetamide (15 mM, in the dark, ~20 °C, 45 min), and alkylation was quenched with an additional 5 mM DTT (~20 °C, 15 min). Protein was enzymatically digested with 0.01 µg/µL of sequencing-grade trypsin (Promega, Madison, WI) (agitation with rocker, ~20 °C, overnight). An additional 0.005 µg/µL of trypsin was added to each sample the next morning and incubated (~20 °C, 1 h). Digests were quenched by bringing the pH below 2 with 10% trifluoroacetic acid and immediately desalted using C18 solid-phase extraction columns (SepPak, Waters, Milford, MA). Peptides were washed with 1 mL of 5% acetonitrile/0.1%

TFA solution on the C18 columns to reduce the abundance of the 1×FLAG peptide from each mixture prior to washing the peptides with 3 mL of 0.1% TFA.

LC-MS/MS analysis. Samples were analyzed on a Dionex UPLC system (Thermo Fisher Scientific, San Jose, CA) coupled to an Orbitrap Elite mass spectrometer (Thermo Fisher Scientific, San Jose, CA). A reverse-phase column was made in-house by packing a fused silica capillary (75 µm i.d., 360 µm o.d., with a laser-pulled electrospray tip) with 3.5 µm diameter, 130 Å pore size Bridged Ethylene Hybrid C18 particles (Waters) to a final length of 30 cm. The column was heated to 55 °C. Samples were re-suspended in 0.2% formic acid and loaded onto the column in 92:8 buffer A [water, 0.2% formic acid, and 5% DMSO] : buffer B [acetonitrile, 0.2% formic acid, and 5% DMSO] at a flow-rate of 0.45 µL/min. Peptides were eluted using the following gradient: an increase to 22% B over 36 min, followed by a 5 min linear gradient from 22% to 28% B, followed by a 3 min linear gradient from 28% to 70% B which was held for 3 minutes. The column was equilibrated with 5% buffer B for an additional 15 min. Precursor peptide cations were generated from the eluent through the utilization of a nanoESI source. To minimize carryover, a 3 run wash sequence was used between samples sets. The first and second washes injected 4.5 µL acetonitrile. The first wash was a short run to trap acetonitrile and the second consisted of a 45 min high organic gradient. A pre-blank wash was run by injecting 4.5 µL 0.2% formic acid using the 60 min gradient described above to allow the identification of carryover proteins. Mass spectrometry instrument methods consisted of MS^1 survey scans ($1x10^6$ target value; 60,000 resolution; 300–1500 Th) that were used to guide fifteen subsequent data-dependent MS/MS scans (2 Th isolation window, HCD fragmentation, normalized collision energy of 30; $5x10^4$ target value, 15,000 resolution). Dynamic exclusion duration was set to 45 s, with a maximum exclusion list of 500 and an exclusion width of ±10 ppm around the selected average mass. Maximum injection times were set to 50 ms for all MS^1 scans and 200 ms for MS/MS scans.

Data analysis. Data was processed using the MaxQuant software suite, version 1.5.2.8 (Cox and Mann, 2008). Searches were performed against a target-decoy database (UniProt (human) database, www.uniprot.org, April 4, 2014, canonical). A maximum of 2 missed tryptic cleavages were allowed. The FTMS MS/MS tolerance was set to 0.015 with the rest of the settings set to the default. Modifications were specified as carbamidomethylation of cysteine residues for fixed and oxidation of methionine for variable. Results grouped into proteins within MaxQuant were filtered to 1% FDR. Proteins were quantified across all samples using MaxLFQ (Cox et al., 2014) with matching between runs within a retention time window of 1 min.

Fluorescence Microscopy

100,000 HEK293 cells were plated onto a poly-D-lysine-coated coverslip in a 6-well dish with HGDMEM+FBS+P/S (37 °C, 2.5 mL) and incubated (37 °C, 5% CO_2) until the culture was ~50% confluent (~24 h). Cells were transfected by dropwise addition of an OptiMEM+DNA+PEI mixture [200 µL OptiMEM (Thermo) warmed to 37 °C, 1 µg pcDNA3.1 COQ8A-FLAG, 0.5 µg plasmid encoding green fluorescent protein with an N-terminal mitochondrial localization sequence (MLS-GFP) (Hanson et al., 2004), and 4.5 µg PEI (4.5 µL, 1 µg/µL, linear polyethylenimine MW 25,000)] and incubated (37 °C, 5% CO_2, 1 day). After 24 hours, the cells were fixed (4% formaldehyde in PBS), permeabilized (0.2% Triton X-100 in PBS), blocked (1% BSA in PBS), and probed with mouse anti-FLAG M2 1° antibody (F1804, Sigma, 1:2000 (v/v) in 0.1% BSA in PBS) and Alexa Fluor 594-conjugated goat anti-mouse 2° antibody (Thermo A-11005, 1:2000 (v/v) in 0.1% BSA in PBS). Cells were stained with Hoechst 33342 dye (1 µg/mL) to label nuclear DNA and placed in mounting medium (1:1, v/v, glycerol/PBS). Microscopy was performed on a Keyence BZ-9000 microscope using 100X oil immersion optics at room temp.

Protein Crystallization and X-Ray Structure

Crystals of selenomethionine-labeled $COQ8A^{N\Delta254}$ R611K were obtained by applying the high throughput screening and optimization platform developed at the Center for Eukaryotic Structural Genomics (Markley et al., 2009). Crystallization screens were set with a TTP Labtech Mosquito robot, and a Tecan Genesis was used for optimization solutions. The best crystals were obtained by hanging drop vapor diffusion using 2 µL of 0.2 mM COQ8A, 2 mM AMPPNP, 4 mM $MgCl_2$ mixed with 2 µL of reservoir solution, 26% sodium acrylate 5100, 20 mM $MgCl_2$, and 100 mM NaHEPES pH 7.5. Crystals were cryopreserved by increasing the sodium acrylate 5100 concentration to 30%. All operations were tracked using SESAME LIMS (Zolnai et al., 2003). Samples were screened for diffraction quality at the LS-CAT and GM/CA beamlines at the Advanced Photon Source. Molecular replacement with the apoprotein structure of wild type COQ8A (ADCK3) 4PED proved difficult, so single-wavelength anomalous diffraction data at 0.9786Ā was collected on a MAR300 CCD detector at GM/CA beamline 23-ID-B. Diffraction data was collected at 100 K, and was reduced with XDS (Kabsch, 2010). The selenium substructure was determined with HySS (Grosse-Kunstleve and Adams, 2003) and phased using Phenix Autosolve (Terwilliger et al., 2009). The model was iteratively improved using ARP/wARP (Langer et al., 2008)-Refmac (Murshudov et al., 1997), Phenix (Afonine et al., 2012)

refinement and Coot (Emsley et al., 2010) with 5% of reflections consistently held in a crossvalidation set. Traditional 2mFo–DFc, mFo–DFc and composite simulated annealing omit maps were calculated throughout the refinement procedure. The final model was continuous from residues 261–644. Electron density for AMPPNP unambiguously places the ADP portion of the ligand, with some ambiguity and potential partial hydrolysis of the terminal imidophosphate group. Electron density for residues 281–298 is relatively poor, probably indicating multiple unresolvable conformations for this portion of the protein. 94% of the residues are in favored backbone conformations and four residues are in disallowed space (Chen et al., 2010).

Identification of Hydrophobic Binding Pockets

The X-ray structures of apo COQ8A (PDB 4PED) and nucleotide-bound COQ8A were subjected to the standard protein preparation procedure implemented in Maestro (Maestro version 9.8, Schrödinger, LLC). The SiteMap module (Halgren, 2007) was used with its default settings to identify the top 5 ranked binding sites on the two structures. Briefly, SiteMap first locates binding sites by grouping site points that are in spatial proximity to the protein and have favorable interaction energies with the protein. For each site identified, it constructs hydrophilic (further divided into donor and acceptor) and hydrophobic maps, and evaluates pockets through their physicochemical properties. The top two ranking pockets found on nucleotide-bound COQ8A are associated with the signature KxGQ domain of COQ8A, and were thus named KxGQ Pocket 1 and KxGQ Pocket 2. The corresponding pockets on apo COQ8A ranked as the first and the fourth, respectively. Overall, due to its different conformation, apo COQ8A encompasses pockets that are less favorable (based on the key evaluation criteria of SiteMap) and less hydrophobic in nature.

Molecular Dynamics (MD) Analysis of COQ8A Structure

PDB structure 4PED was used to model the apo state of COQ8A (residues 261–644) (Stefely et al., 2015). The ADP and ATP bound forms were modeled by replacing AMPPNP in the AMPPNP-COQ8A R611K structure reported here (PDB 5I35) using the homology modeling routine of MODELLER version 9.12 (Fiser et al., 2000). MSE residues in the crystal structure were substituted to MET in our MD simulations. For these MD simulations, we also replaced K611 with R611, as observed in WT COQ8A sequence. Mg^{2+} ions were placed based on the crystal structure of protein kinase A (PDB 1ATP) (Knighton et al., 1991; Zheng et al., 1993). The modeled structures were manually checked for steric clashes before simulation.

MD simulations were performed using GROMACS 5.0.4 (Pronk et al., 2013). AMBER ff99SB-ildn force field (Lindorff-Larsen et al., 2010) was used with parameters for ATP/ADP adopted from previous quantum mechanics calculations (Meagher et al., 2003). The protein was solvated with TIP3P water in a dodecahedron periodic box that was at least 1 nm larger than the protein on all sides. Energy minimization was carried out by coupling steepest descent and conjugate gradient algorithms so that Fmax was less than 50 kcal/mol. Temperature equilibrium was achieved by NVP ensemble in 200 ps at 310 K with a berendsen thermostat. NPT ensemble was done for 200 ps using berendsen thermostat and berendsenbarostat. The positions of the ligand and magnesium ions were restrained in the NVT and NPT equilibration step. The unrestrained MD productions were run for 200 ns using a time step of 2 fs after NPT ensemble for apo/ADP•Mg2+-bound/ATP•Mg2+-bound forms. Root mean square deviation (RMSD) of each simulation was checked to be stable before additional analysis. Torsion angle dynamics were calculated by g_chi programs in the GROMACS package. Kullback–Leibler divergence analysis was performed using mutinf package (McClendon et al., 2009; McClendon et al., 2012). All protein visualization was done using PyMOL.

SUPPLEMENTAL REFERENCES

Afonine, P.V., Grosse-Kunstleve, R.W., Echols, N., Headd, J.J., Moriarty, N.W., Mustyakimov, M., Terwilliger, T.C., Urzhumtsev, A., Zwart, P.H., and Adams, P.D. (2012). Towards automated crystallographic structure refinement with phenix.refine. Acta Crystallogr. D Biol. Crystallogr. *68*, 352–367.

Baudin, A., Ozier-Kalogeropoulos, O., Denouel, A., Lacroute, F., and Cullin, C. (1993). A simple and efficient method for direct gene deletion in Saccharomyces cerevisiae. Nucleic Acids Res. *21*, 3329–3330.

Blommel, P.G., Martin, P.A., Seder, K.D., Wrobel, R.L., and Fox, B.G. (2009). Flexi vector cloning. Methods Mol. Biol. *498*, 55–73.

Chaumont, J., Guyon, N., Valera, A.M., Dugue, G.P., Popa, D., Marcaggi, P., Gautheron, V., Reibel-Foisset, S., Dieudonne, S., Stephan, A.*, et al.* (2013). Clusters of cerebellar Purkinje cells control their afferent climbing fiber discharge. Proc. Natl. Acad. Sci. USA *110*, 16223–16228.

Chen, V.B., Arendall, W.B., Headd, J.J., Keedy, D.A., Immormino, R.M., Kapral, G.J., Murray, L.W., Richardson, J.S., and Richardson, D.C. (2010). MolProbity: all-atom structure validation for macromolecular crystallography. Acta Crystallogr. D Biol. Crystallogr. *66*, 12–21.

Chen, Y.C., Taylor, E.B., Dephoure, N., Heo, J.M., Tonhato, A., Papandreou, I., Nath, N., Denko, N.C., Gygi, S.P., and Rutter, J. (2012). Identification of a protein mediating respiratory supercomplex stability. Cell Metab. *15*, 348–360.

Clark, H.B., Burright, E.N., Yunis, W.S., Larson, S., Wilcox, C., Hartman, B., Matilla, A., Zoghbi, H.Y., and Orr, H.T. (1997). Purkinje cell expression of a mutant allele of SCA1 in transgenic mice leads to disparate effects on motor behaviors, followed by a progressive cerebellar dysfunction and histological alterations. J. Neurosci. *17*, 7385–7395.

Consortium, G.T. (2015). Human genomics. The Genotype-Tissue Expression (GTEx) pilot analysis: multitissue gene regulation in humans. Science *348*, 648–660.

Cox, J., Hein, M.Y., Luber, C.A., Paron, I., Nagaraj, N., and Mann, M. (2014). Accurate proteome-wide label-free quantification by delayed normalization and maximal peptide ratio extraction, termed MaxLFQ. Mol. Cell. Proteomics *13*, 2513–2526.

Cox, J., and Mann, M. (2008). MaxQuant enables high peptide identification rates, individualized p.p.b.-range mass accuracies and proteome-wide protein quantification. Nat. Biotechnol. *26*, 1367–1372.

Cox, J., Neuhauser, N., Michalski, A., Scheltema, R.A., Olsen, J.V., and Mann, M. (2011). Andromeda: a peptide search engine integrated into the MaxQuant environment. J. Proteome Res. *10*, 1794–1805.

Emsley, P., Lohkamp, B., Scott, W.G., and Cowtan, K. (2010). Features and development of Coot. Acta Crystallogr. D Biol. Crystallogr. *66*, 486–501.

Fiser, A., Do, R.K., and Sali, A. (2000). Modeling of loops in protein structures. Protein Sci. *9*, 1753–1773.

Fox, B.G., and Blommel, P.G. (2009). Autoinduction of protein expression. Curr. Protoc. Protein Sci. *Chapter 5*, Unit 5.23.

Frezza, C., Cipolat, S., and Scorrano, L. (2007). Organelle isolation: functional mitochondria from mouse liver, muscle and cultured fibroblasts. Nat. Protoc. *2*, 287–295.

Garcia, S., and Fourcaud-Trocme, N. (2009). OpenElectrophy: An Electrophysiological Data- and Analysis-Sharing Framework. Front. Neuroinform. *3*, 14.

Geer, L.Y., Markey, S.P., Kowalak, J.A., Wagner, L., Xu, M., Maynard, D.M., Yang, X., Shi, W., and Bryant, S.H. (2004). Open mass spectrometry search algorithm. J. Proteome Res. *3*, 958–964.

Gietz, R.D., and Woods, R.A. (2002). Transformation of yeast by lithium acetate/single-stranded carrier DNA/polyethylene glycol method. Methods Enzymol. *350*, 87–96.

Grosse-Kunstleve, R.W., and Adams, P.D. (2003). Substructure search procedures for macromolecular structures. Acta Crystallogr. D Biol. Crystallogr. *59*, 1966–1973.

Halgren, T. (2007). New method for fast and accurate binding-site identification and analysis. Chem. Biol. Drug. Des. *69*, 146–148.

Hebert, A.S., Merrill, A.E., Stefely, J.A., Bailey, D.J., Wenger, C.D., Westphall, M.S., Pagliarini, D.J., and Coon, J.J. (2013). Amine-reactive neutron-encoded labels for highly plexed proteomic quantitation. Mol. Cell. Proteomics *12*, 3360–3369.

Holm, L., Kaariainen, S., Rosenstrom, P., and Schenkel, A. (2008). Searching protein structure databases with DaliLite v.3. Bioinformatics *24*, 2780–2781.

Holt, G.R., Softky, W.R., Koch, C., and Douglas, R.J. (1996). Comparison of discharge variability in vitro and in vivo in cat visual cortex neurons. J. Neurophysiol. *75*, 1806–1814.

Kabsch, W. (2010). Xds. Acta Crystallogr. D Biol. Crystallogr. *66*, 125–132.

Kind, T., Liu, K.H., Lee do, Y., DeFelice, B., Meissen, J.K., and Fiehn, O. (2013). LipidBlast in silico tandem mass spectrometry database for lipid identification. Nat. Methods *10*, 755–758.

Klock, H.E., Koesema, E.J., Knuth, M.W., and Lesley, S.A. (2008). Combining the polymerase incomplete primer extension method for cloning and mutagenesis with microscreening to accelerate structural genomics efforts. Proteins *71*, 982–994.

Knighton, D.R., Zheng, J.H., Ten Eyck, L.F., Ashford, V.A., Xuong, N.H., Taylor, S.S., and Sowadski, J.M. (1991). Crystal structure of the catalytic subunit of cyclic adenosine monophosphate-dependent protein kinase. Science *253*, 407–414.

Langer, G., Cohen, S.X., Lamzin, V.S., and Perrakis, A. (2008). Automated macromolecular model building for X-ray crystallography using ARP/wARP version 7. Nat. Protoc. *3*, 1171–1179.

Lein, E.S., Hawrylycz, M.J., Ao, N., Ayres, M., Bensinger, A., Bernard, A., Boe, A.F., Boguski, M.S., Brockway, K.S., Byrnes, E.J.*, et al.* (2007). Genome-wide atlas of gene expression in the adult mouse brain. Nature *445*, 168–176.

Lindorff-Larsen, K., Piana, S., Palmo, K., Maragakis, P., Klepeis, J.L., Dror, R.O., and Shaw, D.E. (2010). Improved side-chain torsion potentials for the Amber ff99SB protein force field. Proteins *78*, 1950–1958.

Markley, J.L., Aceti, D.J., Bingman, C.A., Fox, B.G., Frederick, R.O., Makino, S., Nichols, K.W., Phillips, G.N., Jr., Primm, J.G., Sahu, S.C.*, et al.* (2009). The Center for Eukaryotic Structural Genomics. J. Struct. Funct. Genomics *10*, 165–179.

McClendon, C.L., Friedland, G., Mobley, D.L., Amirkhani, H., and Jacobson, M.P. (2009). Quantifying Correlations Between Allosteric Sites in Thermodynamic Ensembles. J. Chem. Theory Comput. *5*, 2486–2502.

McClendon, C.L., Hua, L., Barreiro, A., and Jacobson, M.P. (2012). Comparing Conformational Ensembles Using the Kullback-Leibler Divergence Expansion. J. Chem. Theory Comput. *8*, 2115–2126.

Meagher, K.L., Redman, L.T., and Carlson, H.A. (2003). Development of polyphosphate parameters for use with the AMBER force field. J. Comput. Chem. *24*, 1016–1025.

Murshudov, G.N., Vagin, A.A., and Dodson, E.J. (1997). Refinement of macromolecular structures by the maximum-likelihood method. Acta Crystallogr. D Biol. Crystallogr. *53*, 240–255.

Narayana, N., Cox, S., Shaltiel, S., Taylor, S.S., and Xuong, N. (1997). Crystal structure of a polyhistidine-tagged recombinant catalytic subunit of cAMP-dependent protein kinase complexed with the peptide inhibitor PKI(5-24) and adenosine. Biochemistry *36*, 4438–4448.

Nesvizhskii, A.I., and Aebersold, R. (2005). Interpretation of shotgun proteomic data: the protein inference problem. Mol. Cell. Proteomics *4*, 1419–1440.

Niesen, F.H., Berglund, H., and Vedadi, M. (2007). The use of differential scanning fluorimetry to detect ligand interactions that promote protein stability. Nat. Protoc. *2*, 2212–2221.

Phanstiel, D.H., Brumbaugh, J., Wenger, C.D., Tian, S., Probasco, M.D., Bailey, D.J., Swaney, D.L., Tervo, M.A., Bolin, J.M., Ruotti, V.*, et al.* (2011). Proteomic and phosphoproteomic comparison of human ES and iPS cells. Nat. Methods *8*, 821–827.

Pronk, S., Pall, S., Schulz, R., Larsson, P., Bjelkmar, P., Apostolov, R., Shirts, M.R., Smith, J.C., Kasson, P.M., van der Spoel, D.*, et al.* (2013). GROMACS 4.5: a high-throughput and highly parallel open source molecular simulation toolkit. Bioinformatics *29*, 845–854.

Simon, D., Seznec, H., Gansmuller, A., Carelle, N., Weber, P., Metzger, D., Rustin, P., Koenig, M., and Puccio, H. (2004). Friedreich ataxia mouse models with progressive cerebellar and sensory ataxia reveal autophagic neurodegeneration in dorsal root ganglia. J. Neurosci. *24*, 1987–1995.

Stefely, J.A., Reidenbach, A.G., Ulbrich, A., Oruganty, K., Floyd, B.J., Jochem, A., Saunders, J.M., Johnson, I.E., Minogue, C.E., Wrobel, R.L.*, et al.* (2015). Mitochondrial ADCK3 employs an atypical protein kinase-like fold to enable coenzyme Q biosynthesis. Mol. Cell *57*, 83–94.

Terwilliger, T.C., Adams, P.D., Read, R.J., Mccoy, A.J., Moriarty, N.W., Grosse-Kunstleve, R.W., Afonine, P.V., Zwart, P.H., and Hung, L.W. (2009). Decision-making in structure solution using Bayesian estimates of map quality: the PHENIX AutoSol wizard. Acta Crystallogr. D Biol. Crystallogr. *65*, 582–601.

Wenger, C.D., Phanstiel, D.H., Lee, M.V., Bailey, D.J., and Coon, J.J. (2011). COMPASS: a suite of pre- and post-search proteomics software tools for OMSSA. Proteomics *11*, 1064–1074.

Zheng, J., Trafny, E.A., Knighton, D.R., Xuong, N.H., Taylor, S.S., Ten Eyck, L.F., and Sowadski, J.M. (1993). 2.2 A refined crystal structure of the catalytic subunit of cAMP-dependent protein kinase complexed with MnATP and a peptide inhibitor. Acta Crystallogr. D Biol. Crystallogr. *49*, 362–365.

Zolnai, Z., Lee, P.T., Li, J., Chapman, M.R., Newman, C.S., Phillips, G.N., Jr., Rayment, I., Ulrich, E.L., Volkman, B.F., and Markley, J.L. (2003). Project management system for structural and functional proteomics: Sesame. J. Struct. Funct. Genomics *4*, 11–23.

III. Interactions

COQ8A was suggested, in the literature, as regulating the CoQ biosynthesis, notably in regards to its homology with the yeast protein Coq8p and bacterial protein UbiB (Lagier-Tourenne et al., 2008; Mollet et al., 2008). Moreover, published data showed that COQ8A (ADCK3) was partially able to restore yeast Coq3p, Coq5p and Coq7p phosphorylation state, although it is not clear yet whether this is a direct or indirect mechanism (Xie et al., 2011). Furthermore, in yeast, most COQ proteins act in a multi-subunit complex, called the CoQ biosynthesis complex and Coq8p stabilizes this complex (He et al., 2014).

Proteomic analysis of 30 weeks old Coq8a$^{-/-}$ mice tissues (cerebellum, heart, kidney and muscle), showed decreased levels of some COQ proteins (Table 5 and Stefely et al., 2016 Figure 2C). In the kidney of 30 weeks old mutant's mice, COQ3-7 and COQ9 were found to be under expressed, and the same proteins, except for COQ4, were also down in the heart. Lower levels of COQ3, 5, 7 and 9 were measured in quadriceps muscle, and COQ 5, 7 and 9 in cerebellum, of Coq8a$^{-/-}$ mice. These data show that there might be some tissue specificity, even though downregulations of COQ5, 7 and 9 were observed in all tissues for which proteomic analysis was done. These downregulations suggest that COQ8A interact with the CoQ biosynthesis complex.

	Cerebellum		Heart		Kidney		Muscle	
Protein	**Fold-change (KO / WT)**	**p-value**	**Fold-change (KO / WT)**	**p-value**	**Fold-change (KO / WT)**	**p-value**	**Fold-change (KO / WT)**	**p-value**
COQ3	0,73	2,96E-01	0,30	2,03E-05	0,86	8,33E-03	0,31	6,79E-06
COQ4	-	-	0,88	1,63E-01	0,81	5,10E-04	-	-
COQ5	0,40	2,24E-05	0,44	1,07E-04	0,84	8,89E-04	0,29	1,96E-05
COQ6	-	-	0,30	2,05E-06	0,88	2,79E-02	0,88	2,26E-01
COQ7	0,53	2,07E-05	0,39	4,20E-06	0,82	1,37E-02	0,49	2,62E-04
COQ9	0,66	4,59E-04	0,62	7,55E-04	0,78	1,33E-03	0,59	3,22E-04
COQ8A	-	-	0,25	4,19E-08	0,49	1,63E-06	0,30	5,22E-05
ADCK5	-	-	-	-	1,17	2,80E-01	-	-
DPS1	-	-	-	-	-	-	-	-
DPL1	-	-	-	-	-	-	-	-
COQ10B	0,94	5,79E-01	1,17	3,30E-01	1,00	9,99E-01	-	-
ADCK1	0,86	4,60E-01	1,06	5,42E-01	-	-	-	-
ADCK2	-	-	-	-	-	-	-	-
COQ8B	0,95	7,12E-01	-	-	-	-	-	-

Table 5 : Results of proteomic analysis of using 30 weeks old Coq8a$^{-/-}$ and WT mice.

Data obtained by proteomic analysis in Dr. David Pagliarini's laboratory using 30 weeks old Coq8a$^{-/-}$ and WT mice. Fold change: Coq8a$^{-/-}$ protein expression divided by WT expression obtained. n=3.

- : not identified : COQ proteins downregulated in all assessed tissues

By proteomic analysis, peptides of COQ8A were detected in Coq8a$^{-/-}$ mice tissues (heat, kidney and muscle, Table 5). These peptides were significantly decreased in mutant mice and only represented non-deleted parts of the protein (the knock-out mice model was generated by an in-frame deletion of exons 9 to 14). These results provide evidence that the remaining part of COQ8A in Coq8a$^{-/-}$ mice is transcribed and translated, and might not be completely degraded in heart, kidney and muscle of Coq8a$^{-/-}$ mice.

In regards to the proteomic data and the knowledge on the CoQ biosynthesis complex, the goals were to determine how early the COQ proteins downregulations occur and to see if COQ8A directly interacts with some of the COQ proteins.

1. COQ proteins downregulations

If COQ8A loss destabilizes the CoQ biosynthesis complex, the downregulations of certain COQ proteins should arise as early as the complex formation, so early during development. To test this hypothesis, COQ7 levels were assessed by Western blot. Downregulation, observed by proteomic studies, had first been confirmed in 10 weeks old KO mice (Stefely et al., 2016, Figure 2D). COQ7 deregulation was then assessed in cerebellum and quadriceps of 2,5 weeks old mice, as well as in myoblasts, where it was also found to be decreased (Stefely et al., 2016, Figure S2C and 2E). Finally, to see if this downregulation indeed happened as early as during development, proteins were extracted from whole embryos between embryonic day 17,5 and 18,5. Already at that stage COQ8A is expressed and COQ7 was found to be decreased (Figure 12). Actually, COQ7 downregulation appears early on, demonstrating that it is a very early phenotype, starting during embryogenesis.

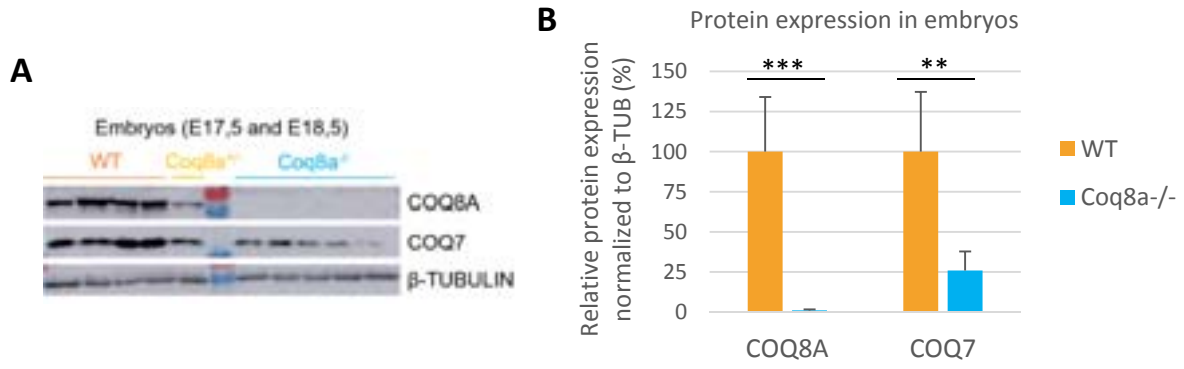

Figure 12 : Loss of COQ8A induces a deficiency in COQ7 in embryos.

A) Western blots showing COQ8A and COQ7 in protein extracts of whole embryos between embryonic day 17,5 and 18,5 (E17,5 and E18,5). B) Quantification of protein levels using Fiji. Protein levels are normalized over β-TUBULIN expression and plotted as a percentage compared to WT. **p<0.01, ***p<0.001.

2. COQ8A interactors

We were then interested in further uncovering the interacting partners of COQ8A. This was particularly interesting in regards to the reduced levels of CoQ and COQ proteins in certain organs of the Coq8a$^{-/-}$ mice (Stefely et al., 2016). Previous immunoprecipitation studies, performed by Leïla Laredj, pointed towards direct interactions between COQ8A and other proteins of the CoQ biosynthetic complex (Stefely et al., 2016, Figure 3A). Moreover, our collaborators had found, by mass spectrometry, an increased interactions of COQ8A with other COQ proteins when HEK293 cells were grown in galactose (Floyd et al., 2016), and they showed that COQ8A preferentially binds ADP (Stefely et al., 2015). To confirm these results and get a better understanding of COQ8A interactors, and the influence of sugar (glucose/galactose) or substrate (ADP/ATP) on these interactions, immunoprecipitations assays were performed in different conditions. These experiments were performed by overexpressing FLAG and HA tagged proteins (COQ8A-FLAG and COQ3, 4, 5, 6, 7 or 9-HA) in COS cells. Shortly, COS cells were transfected with the COQ8A-FLAG and one of the COQ-HA plasmids, and the cells were grown either in medium containing glucose or medium with galactose. Expression of COQ8A-FLAG or COQ-HA alone, in the same conditions, were used as controls. The next day, cells were harvested and pellets snap frozen before processing further with an immunoprecipitation assay. Overexpressed COQ8A-FLAG proteins were then isolated using FLAG beads and interaction was assessed by Western blot using anti-FLAG and -HA antibodies.

First, immunoprecipitations were carried out with extracts of COS cells, grown in glucose conditions, and transfected with COQ8A-FLAG and COQ3-HA or COQ4-HA or COQ5-HA or COQ6-HA or COQ7-HA or COQ9-HA, to check interaction. For all immunoprecipitations experiments, the expected proteins came up at elevated molecular weight in the immuno-precipitated (IP) fractions by Western blot. Despite optimizations (sample dilution, change of elution buffer) proteins remained shifted in the IP fractions (Figure 13). Nevertheless, these experiments enabled to confirm that COQ8A interacts with COQ5 (Figure 13A) but not with COQ9 (Figure 13B) when cells are grown in glucose conditions. In these glucose conditions, COQ4 also precipitated with COQ8A (Figure 13B) in COS cells, as previously observed in HEK293 cells (Stefely et al., 2016). Concerning interactions with other COQ proteins, expression was either too low to detect an interaction by western blot (COQ3-HA and COQ6-HA) or, like for COQ7-HA, the tagged protein could not be expressed.

Then, COS cells were grown in galactose conditions and transfected with COQ8A-FLAG and COQ5-HA. In these conditions, when cells are grown in a medium with galactose instead of glucose, no conclusion can be drawn yet regarding the interactions, as the expression of COQ8A-FLAG with COQ5-HA were too low (data not shown). Further optimizations, such as changing the quantities or ratios of the plasmids, or transfecting the cells longer before harvesting them, would be needed to obtain higher expression and be able to proceed to the immunoprecipitation.

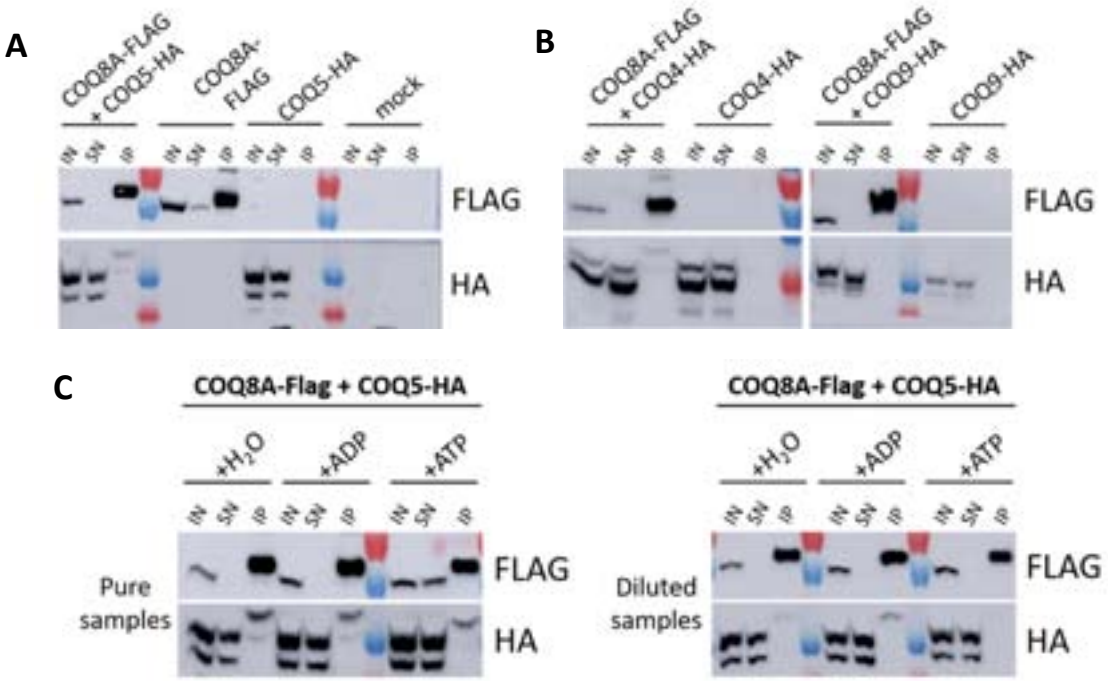

Figure 13 : COQ8A interacts with COQ5 and COQ4, and the interaction with COQ5 increases in presence of ADP.

Western blots showing immunoprecipitation of COQ8A-FLAG with COQ-HA transfected in COS cells and immunoprecipitated using anti-FLAG beads. Detection was performed using antibodies against the FLAG and HA tags. IN: input, SN: supernatant, IP: immunoprecipitation. A) COQ8A-FLAG and COQ5-HA transfected in COS cells grown in medium with glucose. COQ8A-FLAG alone, as well as COQ5-HA and mock (only addition of Fugene) serve as controls for the immunoprecipitation. B) COQ8A-FLAG and COQ4 or COQ9-HA transfected in COS cells grown in medium with glucose. C) COQ8A-FLAG and COQ5-HA transfected in COS cells grow in medium with glucose. ADP or ATP were added to the lysates before and during immunoprecipitation (H2O taken as a control), left: pure samples, right: samples diluted before loaded on the gel.

COQ8A was shown to be stabilized by adenine nucleotides and preferentially bind ADP (Stefely et al., 2015). So finally, to assess if COQ8A selectivity for ADP could influence its interactions with COQ proteins, ATP, ADP or water (as a control) were added as soon as proteins were extracted from cell pellets and during all the steps of the immunoprecipitations. For this assay, COS cells were grown in medium with glucose and transfected with COQ8A-FLAG and COQ5-HA plasmids. COQ5 was previously shown to interact with COQ8A without addition of any nucleotides (Figure 13A), accordingly, COQ8A interacts with COQ5 in presence of ADP, ATP or in their absence (Figure 13C). Still, when the different fractions are diluted before being loaded on a gel, the interaction, between COQ8A and COQ5, seems to be stronger in presence of ADP compared to the conditions without nucleotides or with ATP (Figure 13C right panel).

These data therefore enabled to confirm that COQ4 and COQ5 interact with COQ8A (Stefely et al., 2016), and that ADP seems to stabilize these interactions.

Nevertheless, it has to be noted that all the immunoprecipitation assays were performed with overexpressed tagged proteins. Most, or all of the COQ8A-FLAG proteins were precipitated during immunoprecipitation assays but this is not the case for the other COQ proteins. Even though COQ4-HA and COQ5-HA precipitated with COQ8A-FLAG, part of these proteins were also found in the supernatant fractions (SN), as seen in Figure 13. This shows that part of the overexpressed COQ4-HA and COQ5-HA do not interact with COQ8A-FLAG. Whether this is due to overexpression, overflowing COQ8A interacting capacity or reflects the need of interaction within the entire CoQ complex for part of these proteins remains to be elucidated. Furthermore, the experiments were performed with exogeneous proteins carrying a tag, which could have slightly different behaviors as the endogenous proteins.

IV. Mitochondrial respiration

COQ8A deficiency downregulates the level of certain COQ proteins (Table 5) and induces a slight CoQ decrease in certain tissues like kidney, liver and muscle (Licitra, 2013; Stefely et al., 2016 Figure 2A and B). Furthermore, abnormal mitochondria were observed, by electron microscopy in quadriceps of Coq8a$^{-/-}$ mice, at late stages (Licitra, 2013; Stefely et al., 2016). As CoQ is required for electron transport from complex I and II to complex III in the respiratory chain (Green and Tzagoloff, 1966), we hypothesized that the mitochondrial respiration might be affected in Coq8a$^{-/-}$ mice, in particular in cells with a high energy demand, like neurons and muscle cells. If mitochondrial respiration is altered, we speculate that this phenotype should arise early on, since low levels of COQ7 were observed in embryos and in 2,5 weeks old Coq8a$^{-/-}$ mice. To test this hypothesis, primary myoblasts were derived from control and mutant mice hind limbs muscles (around postnatal day 8).

1. Establishment of myoblast primary cultures

First, in order to confirm that the downregulation of certain COQ proteins, observed in embryos and 2,5 weeks old mutant's quadriceps, also occur in COQ8a$^{-/-}$ primary myoblasts, the levels of some COQ proteins were assessed in this cell type. In mutant primary myoblasts COQ5 and COQ7 levels were decreased (Figure 14).

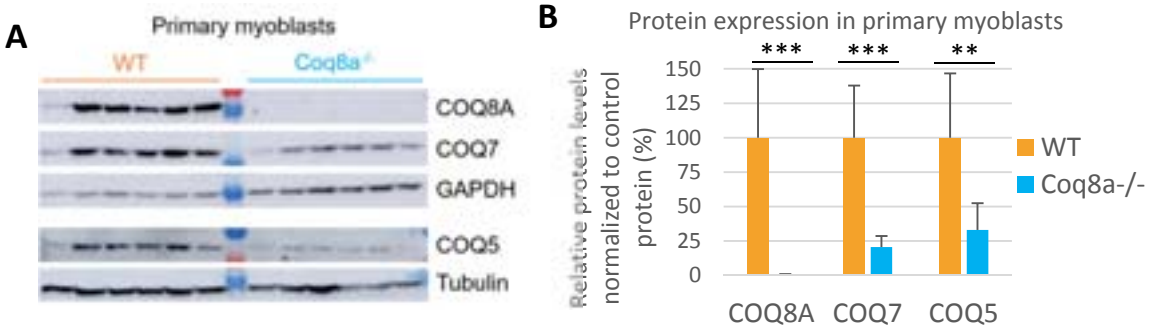

Figure 14 : Loss of COQ8A induces a deficiency in COQ7 and COQ5 in myoblasts.

A) Western blots showing COQ8A, COQ7 and COQ5 expression in myoblasts primary cultures (cells from P8 pups grown 11 days in culture), GAPDH and Tubulin are taken as controls. B) Quantification of protein levels using Fiji. Protein levels are normalized over GAPDH expression (for COQ8A and COQ7) or Tubulin (COQ5) and plotted as a percentage compared to WT. Error bars: SD, ** = p<0.01, *** = p<0.001.

While the primary muscle cells were in culture, it appeared that Coq8a$^{-/-}$ myoblasts divided faster and appeared to fuse more rapidly or to form bigger myotubes networks when differentiated (Figure 15). Therefore, further characterization was performed, with a proliferation and a differentiation assay. In the proliferation test, no significant difference between KO and WT myoblasts doubling time could be observed (Figure 16). Coq8a$^{-/-}$ myoblasts divide at the same rate as the WT.

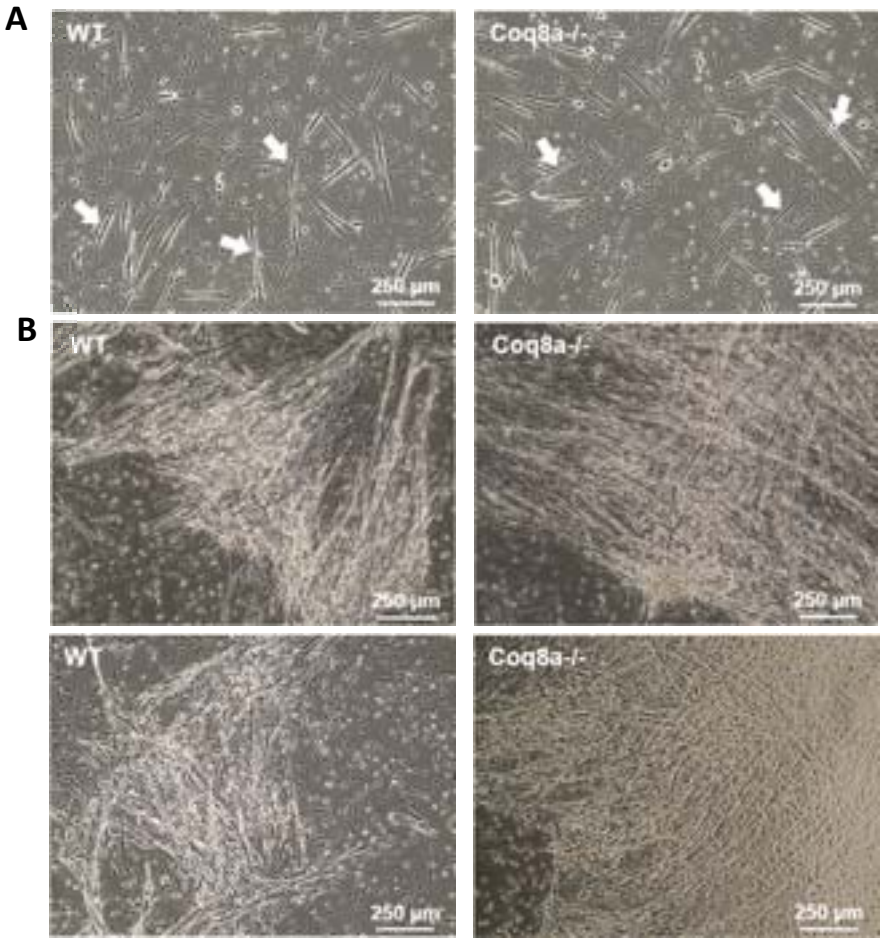

Figure 15 : Coq8a$^{-/-}$ myotubes seem to form bigger networks.

Microscopy of myoblasts and myotubes, 10x magnification. A) Myoblasts and a few myotubes spontaneously forming (arrows). B) Myotubes forming contracting fibers after a few days of differentiation, Coq8a$^{-/-}$ myotubes seem to be denser. Left panels: WT and right panels Coq8a$^{-/-}$ myoblasts.

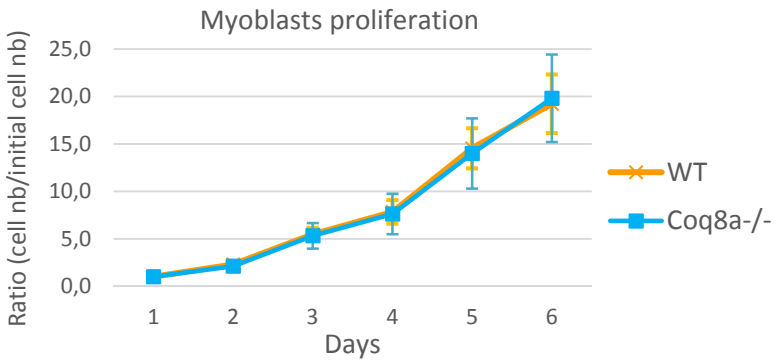

Figure 16 : Coq8a$^{-/-}$ myoblasts do not proliferate more rapidly.

Proliferation assay performed by counting cells each day for 6 days, expressed as a ratio of the counted cells over to number of cells counted at day 1. Error bars: SD. n=6.

Next, differentiation was assessed. During myogenic differentiation, specific genes are expressed (Figure 17A) (Douillard-Guilloux et al., 2009). *Pax7* is majorly expressed in myoblasts and its transcript levels diminish during differentiation (Zammit, 2006). *MyoD* expression is transient during

differentiation, whereas *Des*, *Myf5* and *MyoG* start to be expressed when myoblasts fuse to form myotubes and their transcript levels increase while going towards muscle fibers (Li and Capetanaki, 1993; Montarras et al., 1991; Trouche et al., 1993). Hence primary myoblasts (D0) were differentiated during 9 days and cells were harvested every 2 days for this analysis. The transcripts levels, of the 5 genes differentially expressed during differentiation, were assessed by RT-qPCR. Results for *Pax7* expression are only showed until day 7 (D7) as the expression levels were too low to be assessed at day 9 (D9).

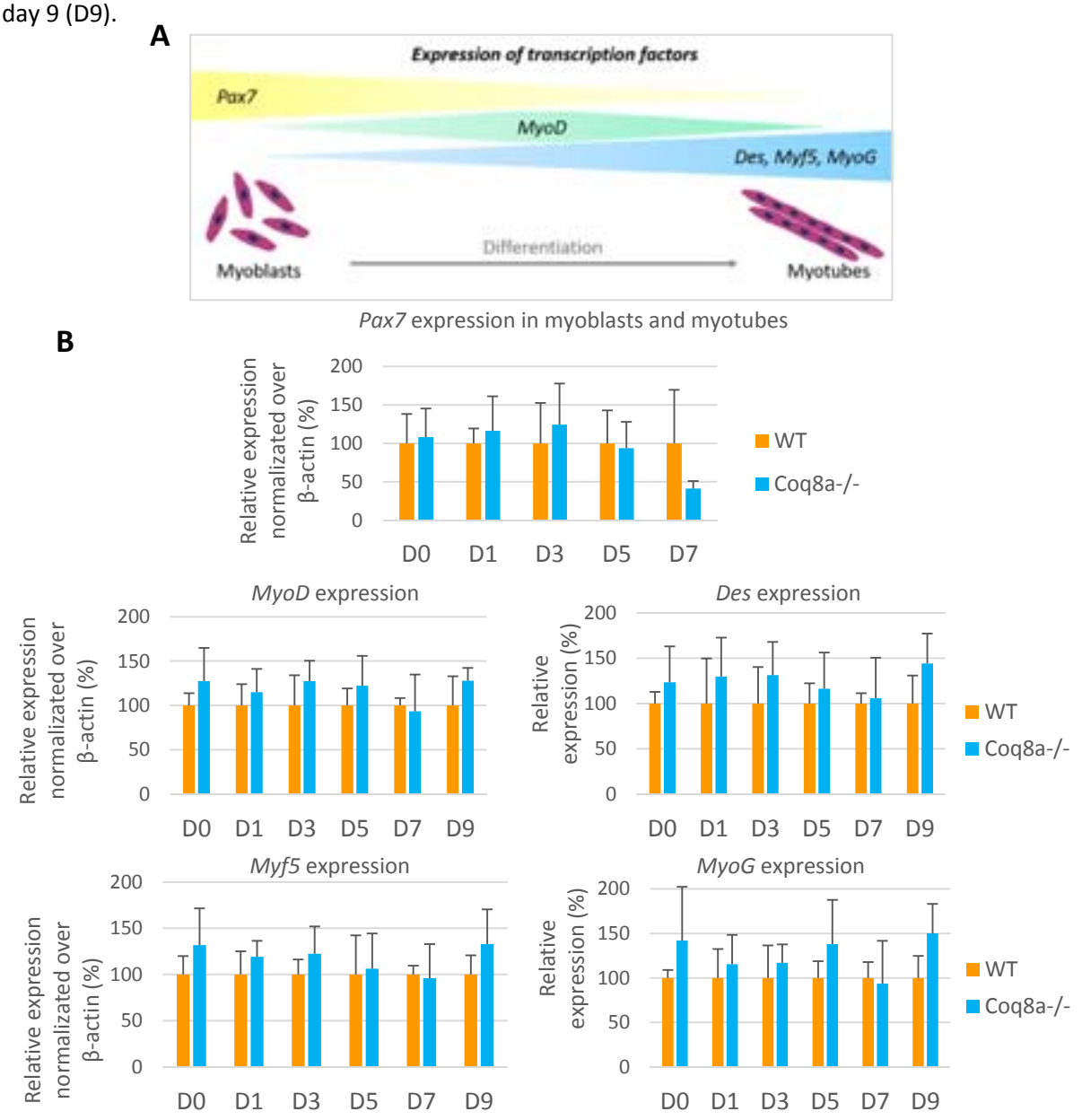

Figure 17 : Myogenic transcription factors expression are unchanged in Coq8a$^{-/-}$ primary muscle cells.

For all these experiments the transcripts levels of each gene was normalized over the transcripts levels of β-actin (control gene) and expressed as a percentage compared to WT. Coq8a$^{-/-}$ cells in orange, WT in blue. A) Scheme of the transcription factors expressed in myoblasts, myotubes and during differentiation. B) Relative expression of Pax7, MyoD, Myf5, Desmin and Myogenin in Coq8a$^{-/-}$ and WT myoblasts (D0) and during differentiation (D1-D9) (n=3). Error bars: SD.

β-actin was taken as a control gene, as previously done by other teams (Douillard-Guilloux et al., 2009). It would have been interesting to assess the decreased expression of *Pax7* and the increase expression of *MyoD*, *Des*, *Myf5* and *MyoG*, to confirm that differentiation occurred. Unfortunately, *β-actin* was not a good control gene to normalize the data of such an experiment, as its expression varied during myoblast to myotube differentiation. If these results were to be repeated, another control gene should be used, which has ubiquitous and constant expression at the different steps of differentiation. Genes expressions were therefore expressed as percentage compared to WT for each time point. No significant transcriptional difference could be observed in Coq8a$^{-/-}$ primary cells compared to WT for all of the tested genes, that is to say for *Pax7*, *MyoD*, *Des*, *Myf5* and *MyoG*, and at all time points, from D0 to D9 (Figure 17B). These results indicate that Coq8a$^{-/-}$ myoblasts differentiate at the same rate than WT. This suggests that the phenotype observed by microscopy in Figure 15 is most likely due to disparate cells densities at the beginning of the differentiation experiment.

Since Coq8a$^{-/-}$ primary myoblasts morphologies were similar to WT, as well as the proliferation and differentiation rate, these cells could be used for further experiments.

2. Measurements of mitochondrial respiration

In consideration of reduced CoQ levels in muscles and decreased COQ5 and COQ7 levels in Coq8a$^{-/-}$ primary myoblasts, mitochondrial respiration was evaluated in these myoblasts. For this purpose, oxygen consumption rates were measured with a Seahorse apparatus, which contains an oxygen biosensor (Agilent Seahorse XF Technology). At the beginning of the assay, basal respiration is measured. Then oligomycin is added to inhibit ATP synthase (complex V), which enables to assess ATP production. Afterwards, addition of FCCP (Carbonyl cyanide-p-trifluoromethoxyphenylhydrazone), a mitochondrial oxidative phosphorylation uncoupling agent, leads to proton leak and allow measurement of mitochondrial maximum respiration. At last, rotenone (an inhibitor of electron transport from complex I to CoQ) and antimycin A (an inhibitor of CoQ oxidation in complex III) completely shuts down mitochondrial respiration and make it possible to measure non-mitochondrial oxygen consumption (Figure 18, Seahorse Agilent).

First, optimization was necessary in order to define the proper seeding density as well as the best concentration of the drugs to add (Table 6). The cell seeding density influences the basal respiration, which has to be within a fixed threshold for a proper measurement with the Seahorse XF apparatus. If the basal oxygen consumption rate is lower than 20 pmol/min or higher than 160 pmol/min, the

measured values might be aberrant, and this phenomenon will be amplified after addition of FCCP. Furthermore, proper oligomycin and FCCP concentrations must be defined to be able to measure the ATP production, the maximal respiration and the spare respiratory capacity.

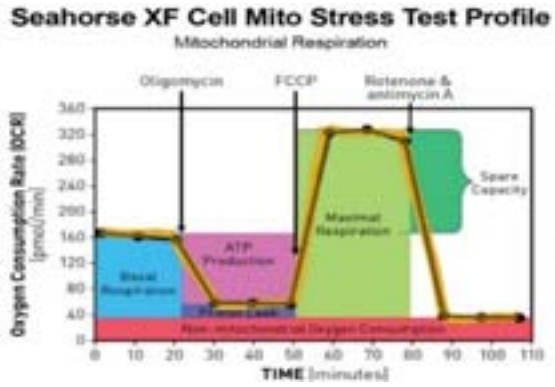

Figure 18 : Scheme of the measurements performed with a Seahorse apparatus.

Agilent Seahorse scheme of the different parameters assessed. Blue: basal respiration, pink: ATP production, light green: maximal respiration, dark green: spare respiratory capacity, purple: proton leak, red: non-mitochondrial oxygen consumption.

Optimization

Cell density (cells per well)	12 000	15 000	18 750	20 000		
Oligomycin concentration (µM)	1,5	2,0				
FCCP concentration (µM)	0,125	0,25	0,50	0,75	1,00	1,50

Table 6 : Optimizations for Seahorse assays on primary myoblasts

In basal conditions, when myoblasts are grown in medium with glucose, Coq8a$^{-/-}$ cells respired as well as the WT cells in all replicates performed, even after addition of oligomycin or FCCP (Figure 19A). To challenge the cells, and force them to use their oxidative phosphorylation, glucose was removed and replaced by galactose, since galactose was shown to enhance oxidative metabolism in human primary muscle cells (Aguer et al., 2011). Even under these galactose conditions, mutant myoblasts had a similar basal respiration, ATP production and maximal respiration as WT (Figure 19B). When assessing basal respiration or the spare respiratory capacity of the mitochondria, both in glucose and in galactose medium, no significant change could be measured (Figure 19C), in accordance with the observations on the oxygen consumption graphs (Figure 19 A and B). A trend towards lower basal respiration when cells are cultured in galactose can be observed for some Coq8a$^{-/-}$ myoblasts cell lines (each point corresponding to the mean value of the replicates of a specific cell line) but this is not significant considering the variability between the different cell lines (Figure 19C). This variability can be explained by the fact that each myoblast cell line is being extracted from a single pup.

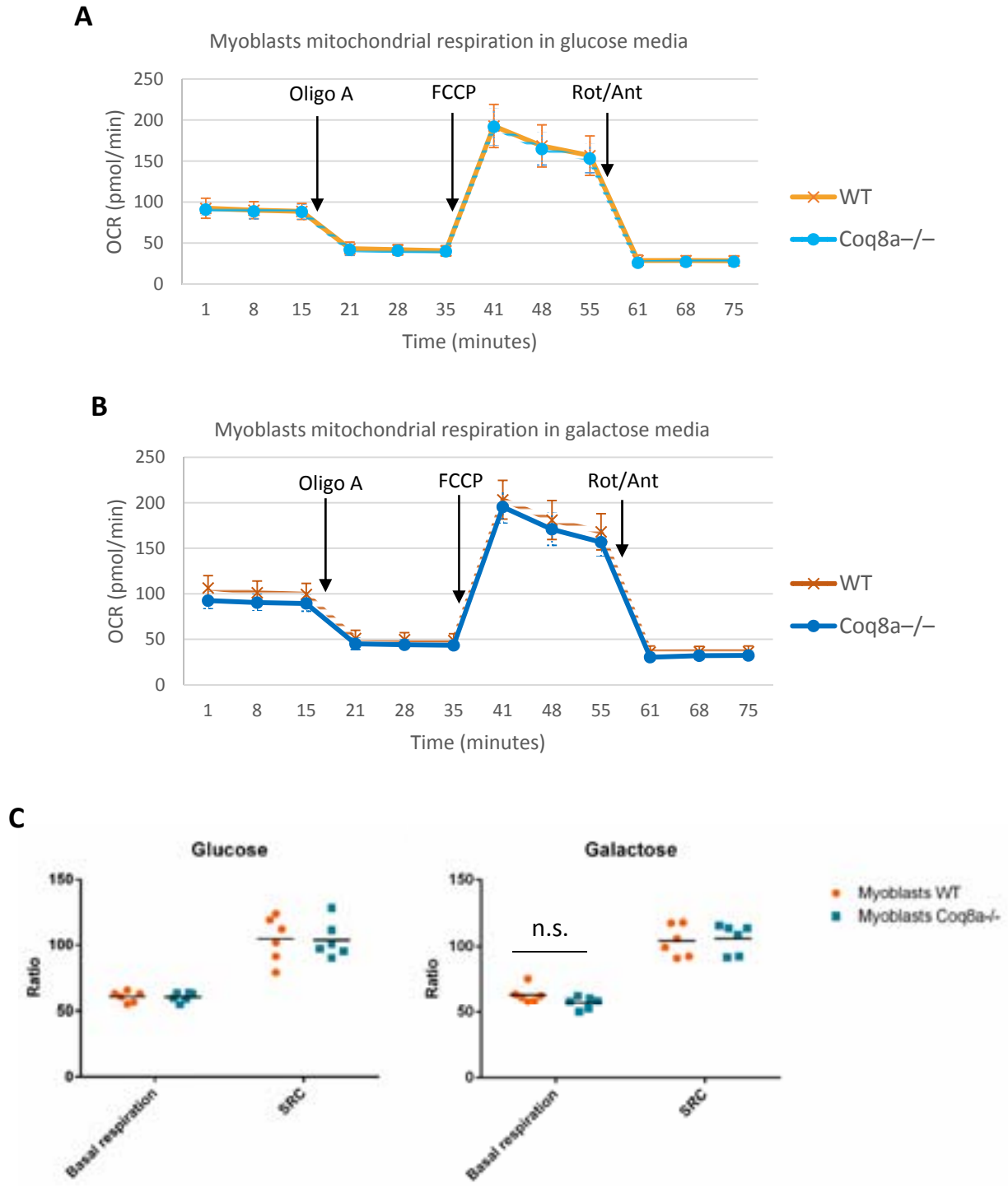

Figure 19 : Mitochondrial respiration is not affected in Coq8a$^{-/-}$ myoblasts.

Oxygen consumption rate (OCR) measured with a Seahorse apparatus, in pmol O_2/min. Data normalized with cell number. Errors bars: SD, n=6. A) in glucose conditions (with Oligomycin (OligoA) injection to a final concentration of 1,5 µM, FCCP 1 µM and Rotenone/Antimycin A (Rot/Ant) 0,5 µM). B) in galactose conditions (with oligomycin injection to a final concentration of 2 µM, FCCP 1 µM and Rotenone/Antimycin A 0,5 µM). C) Basal respiration and spare respiratory capacity measured for the two experiments (A and B): in glucose and in galactose conditions. Each point represents the mean value for the replicates of a specific cell line. The mean was calculated from at least 6 replicates for each of the 6 cell lines of each cohort. n.s.= not significant. Glucose condition: 10 mM glucose, galactose condition: 10 mM galactose.

When primary myoblasts were grown in galactose conditions, respiration was indeed increased compared to glucose conditions, but only slightly. Considering data published on C2C12 murine myoblasts, showing that low glucose and not galactose would improve usage of mitochondrial respiration (Elkalaf et al., 2013), this new parameter was tested. Primary myoblasts were cultured in medium with 5 mM glucose instead of 25 mM. This lowering of glucose did not exacerbate any phenotype as Coq8a$^{-/-}$ myoblasts still respired as WT (Figure 20). Albeit lower glucose was shown to increase mitochondrial respiration in immortalized myoblasts, this did not seem to be the case for WT and Coq8a$^{-/-}$ mouse primary myoblasts. While comparing the data for 5 mM glucose with previous experiments with 25 mM glucose and the same number of cells, basal oxygen consumption rates appeared similar, however these were two distinct experiments.

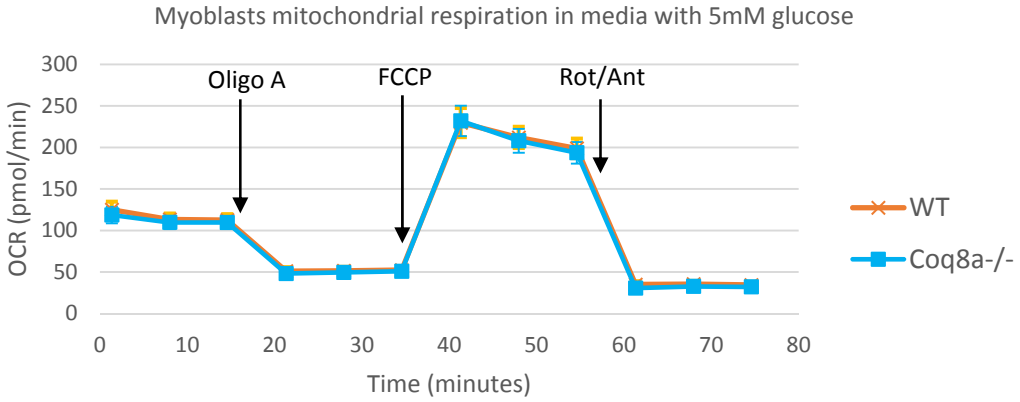

Figure 20 : Mitochondrial respiration is not affected in Coq8a$^{-/-}$ myoblasts under low glucose conditions.

Oxygen consumption rate (OCR) measured with a Seahorse apparatus, in pmol/min. Data normalized with cell number. Errors bars: SD, n=6. Cells grown in 5 mM glucose media (with oligomycin (OligoA) injection to a final concentration of 2 µM, FCCP 1 µM and Rotenone/Antimycin A (Rot/Ant) 0,5 µM.

Myotubes might have a different metabolism than myoblasts, and being closer to the one of muscle fibers. Consequently, a last assay was performed in differentiated primary cultures. As previously, mutant myotubes have a similar oxidative phosphorylation as WT, even after addition of inhibitors (Figure 21).

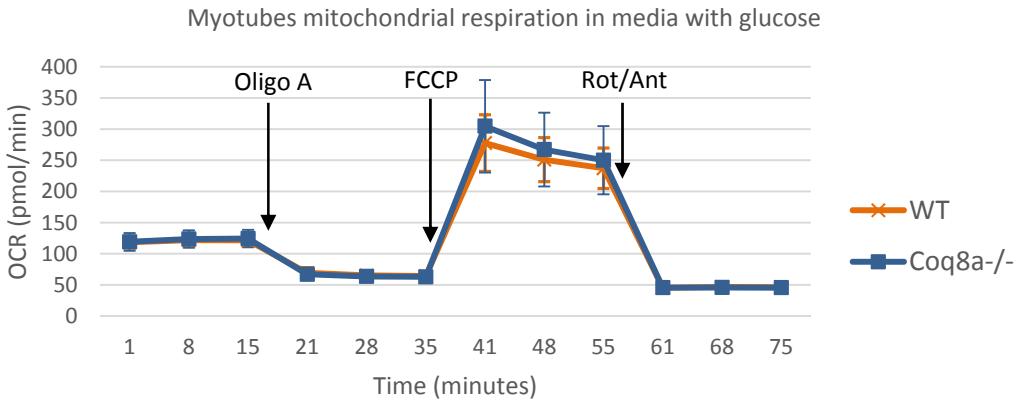

Figure 21 : Mitochondrial respiration is not affected in Coq8a$^{-/-}$ myotubes.

Oxygen consumption rate (OCR) measured with a Seahorse apparatus, in pmol/min. Data normalized over the cell number. Errors bars: SD, n=6. Cells grown in 10 mM glucose media (with oligomycin (OligoA) injection to a final concentration of 2 µM, FCCP 1 µM and Rotenone/Antimycin A (Rot/Ant) 0,5 µM).

Finally, it is known that Coq8a$^{-/-}$ mice have a higher basal circulating blood glucose level compared to WT (Licitra, 2013). Moreover, some patients show elevated levels of lactate (Lagier-Tourenne et al., 2008), which can be a sign of glycolysis usage to produce energy. It could be that the mutant cells favor glycolysis to produce energy and compensate for a mitochondrial defect. Accordingly, glycolysis was measured by assessing the extracellular acidification rates (ECAR, in mpH/min), with to a pH biosensor, in the Agilent Seahorse XF Technology. The principle is the following: glucose addition at first, enables to evaluate glycolysis. Oligomycin A, then blocks ATPase, forcing the cells to produce energy only through glycolysis. At last, 2-DG (2-Deoxy-D-glucose), a glucose analog, restrains glycolysis, to evaluate the non-glycolytic acidification (Figure 22A). Mutant and WT myoblasts were therefore seeded in medium without glucose prior to the assay, and the proton levels were measured at the different steps. The acidification of the medium occurred as much for Coq8$^{-/-}$ myoblasts as for WT, even after addition of glucose and oligomycin (Figure 22B). Glycolysis and the other glycolytic parameters: glycolytic capacity and reserve, were unaffected (Figure 22 B and C). Results for glycolysis were consistent, whereas for glycolytic capacity and glycolytic reserve, the different cells lines behaved differently, inducing large variability in between samples (Figure 22C). These variabilities were found both for WT and mutant's myoblasts cell lines.

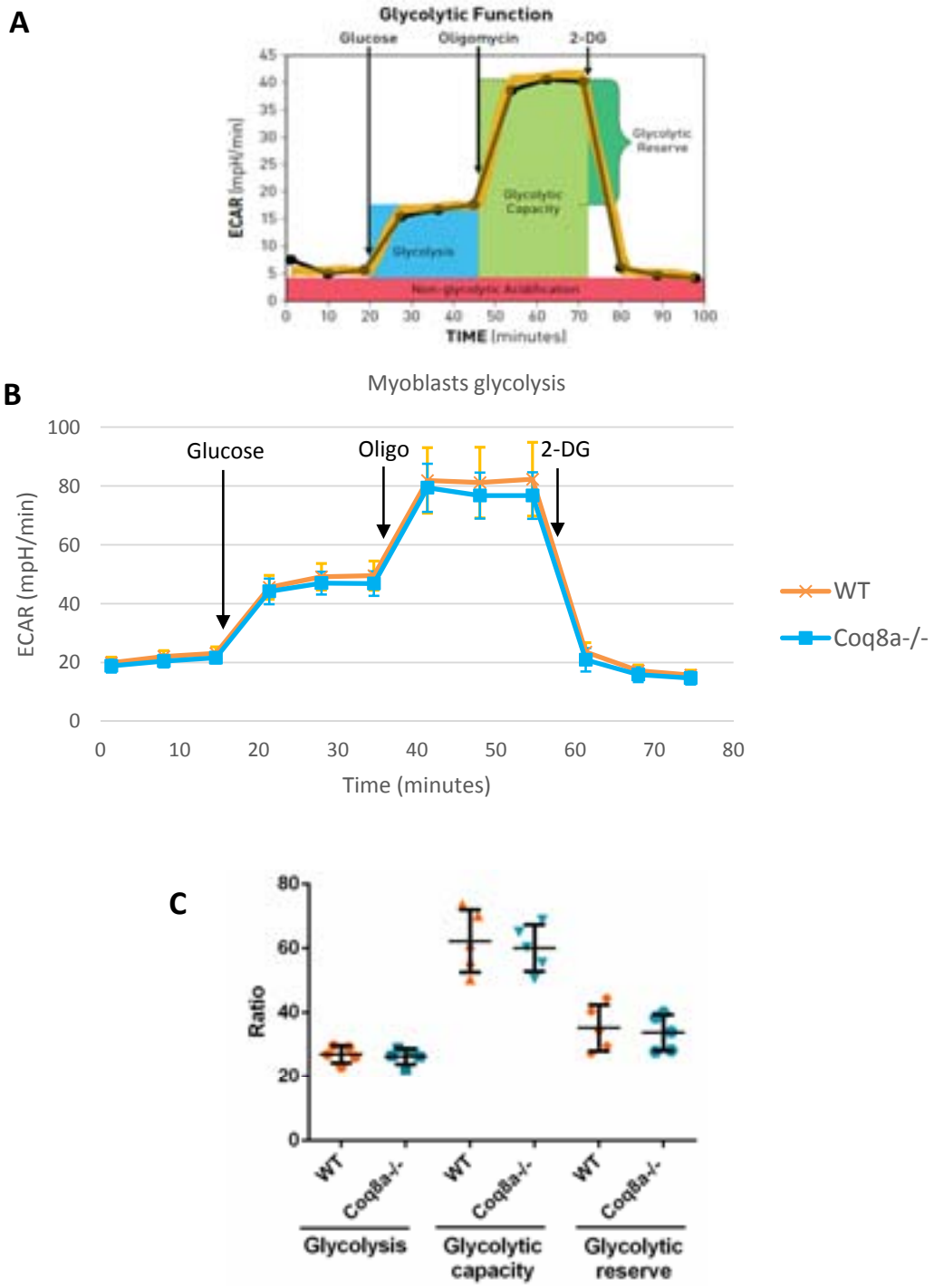

Figure 22 : Glycolysis is not affected in Coq8a$^{-/-}$ myoblast.

A) Agilent Seahorse scheme of the different parameters assessed. B) Extracellular acidification rate (ECAR) measured with a Seahorse apparatus, in mpH/min. Data normalized over the cell number. Errors bars: SD, n=5. Measurement after successively, glucose injection to a final concentration of 10 mM, oligomycin at 1 µM (Oligo) and 2-Deoxy-D-glucose (2-DG) at 50 mM. C) Glycolysis, glycolytic capacity and glycolytic reserve measurements. Each point represents the mean value for the replicates of a specific cell line. The mean was calculated from at least 6 replicates for each of the 5 cell lines of each cohort.

Muscles cells have a high-energy demand, but this is also the case for neurons. Since Coq8a$^{-/-}$ cerebellar primary cultures were healthy and no phenotype could be observed, different parameters were optimized to assess mitochondrial respiration in cerebellar cells. Attempts to measure oxidative phosphorylation with the Seahorse technology in these cultures were so far not conclusive. Basal respiration could be measured but hitherto spare respiratory capacity could not be determined. Although proper seeding density was found, the other parameters, and notably FCCP concentration, are not optimal yet. Indeed, the concentrations of FCCP assessed so far do not allow the measurement of the maximal respiration and the spare respiratory capacity. Regarding basal respiration, it is unchanged in Coq8a$^{-/-}$ cerebellar cultures compared to WT (Figure 23). Additional optimizations might be performed, in particular regarding initial glucose and pyruvate levels added in the media prior to the assay, in order to uncover a phenotype. In view of unchanged mitochondrial respiration in myoblasts and the unaltered cerebellar basal respiration, this aspect was left aside for the time being.

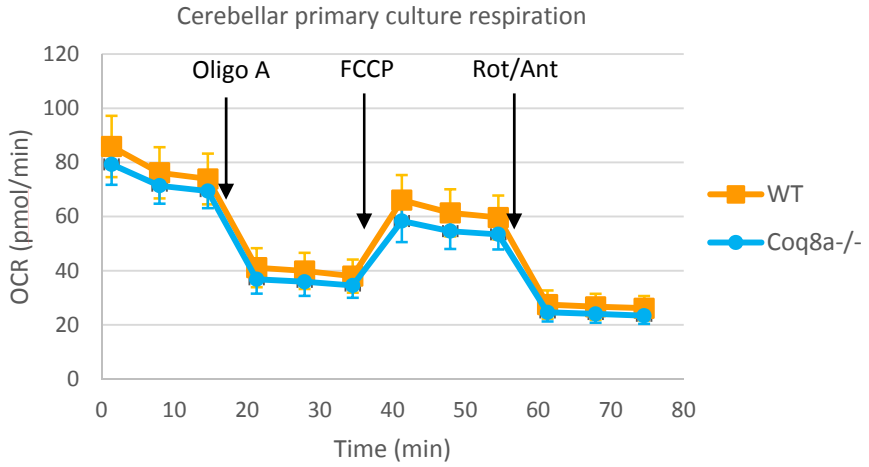

Figure 23 : Mitochondrial basal respiration is not affected in Coq8a$^{-/-}$ cerebellar cultures.

Oxygen consumption rate (OCR) measured with a Seahorse apparatus, in pmol O_2/min. Data normalized with cell number. Mean ± SD, n=6. Assay performed in glucose conditions (10mM glucose, 2mM sodium pyruvate, 2mM L-glutamine) with Oligomycin (OligoA) injection to a final concentration of 1,5 µM, FCCP 0,45 µM and Rotenone/Antimycin A (Rot/Ant) 0,5 µM). Orange: WT, blue: Coq8a$^{-/-}$ cerebellar primary cultures.

In conclusions, Coq8a$^{-/-}$ myoblasts do not show any oxidative phosphorylation nor glycolysis defect, although COQ5 and COQ7 levels are decreased. Measurement of CoQ in myoblasts and myotubes would therefore be needed to get a clearer picture. Interestingly, similar results were obtained by measurement of mitochondrial respiration, in muscles fibers extracted from 10 months old mice, using Clark electrodes (Stefely et al., 2016). Despite lower levels of CoQ and stress by exhaustion, mitochondrial respiration was similar in WT and Coq8a$^{-/-}$ mice muscles fibers. Putting cells in culture should induce a stress, and could have exacerbated a phenotype. This was not the case but confirms that mitochondrial respiration is not affected in the Coq8a$^{-/-}$ mouse model generated. Furthermore, a strong reduction of CoQ, was shown to induce only a mild reduction of respiratory capacity, in liver conditional *Mclk1* KO mouse (COQ7 deficient mice in the liver) (Wang and Hekimi, 2013b). Low levels of CoQ might therefore be enough to sustain mitochondrial respiration, and CoQ deficiency pathogenesis would then arise as the defect of another role of CoQ.

COQ8A might have a role at another level and not necessarily affecting mitochondria, even if it is majorly located in this compartment (Stefely et al., 2016). CoQ also acts as an antioxidant, and a CoQ deficiency can induce increased levels of reactive oxygen species (ROS). Floriana Licitra had previously shown that ROS were not increased in Coq8a$^{-/-}$ mice, and that these ROS were even reduced in quadriceps of mutant mice (Licitra, 2013). Additional experiments are needed, first to assess if CoQ levels are decreased early on or if this reduction only happens later, and if it happens early, which functions of CoQ are affected.

V. Epilepsy

Two different neuronal phenotypes have been observed in Coq8a$^{-/-}$mice: epilepsy and ataxia (Stefely et al., 2016). In addition to cerebellar ataxia, some ARCA2 patients present epileptic seizures and mild mental retardation (Horvath et al., 2012; Lagier-Tourenne et al., 2008; Mignot et al., 2013; Mollet et al., 2008). Coq8a$^{-/-}$ mice mimic these phenotypes with an increased susceptibility to epilepsy (at 6 months of age when treated with PTZ) and a mild spatial learning memory defect (Stefely et al., 2016). As hippocampus is necessary for spatial memory and is implicated in certain types of epilepsy, we wanted to address if this brain structure was affected in Coq8a$^{-/-}$ mice.

1. Morphometric analysis

To address the question whether hippocampus was affected, histology and primary cultures were performed. Initially a morphometric analysis was launched to determine if any of the hippocampal cell layer was affected more specifically. This assay was performed thanks to a standard operating procedure available in Dr. Binnaz Yalcin laboratory (IGBMC). Different parameters, on the whole brain section, were assessed. This included different areas and length of the hippocampus, but also of other surrounding regions like the cortex, the corpus callosum or the ventricles (Figure 24). The overall morphology of mutant brains was similar to WT (Figure 25), which could be confirmed by the measurement of the total brain area (Figure 26A). Neither the areas, nor the length of any of the measured parameters were significantly different between WT and Coq8a$^{-/-}$ brains (Figure 26B and C). The areas, height, length and width of the different part of the cortex (retrosplenial granular: RSGc, piriform: Pir, motor: M1, and secondary somatosensory: S2 cortex) were similar for both genotypes. The same was true for the corpus callosum (cc), the internal capsule (ic), the habenular nucleus (Hb), the amygdala nuclei (AM), the mammillothalamic tract (mt) and the optic tract (opt). Regarding the ventricles, the Coq8a$^{-/-}$ dorsal third ventricle (D3V) surface was comparable to WT, whereas for lateral ventricles (LV), the surface was found to be reduced in KO compared to WT, although there is variability in between WT. The tendency of reduced areas of the mutant lateral ventricles are most probably due to different cutting angles when performing brain slices, or slices not taken at the exact same position. Finally, none of the areas, height and length of the different parts of the hippocampus were either affected in Coq8a$^{-/-}$ mice. These parameters included the areas of the dorsal hippocampal commissure (dhc), the fimbria hippocampus (fi), and the total area of the hippocampus (HP) but also the length of the hippocampal stratum radiatum layer (Rad), of the hippocampal oriens layer (Or), of the dentate

gyrus (DG), and of the total internal hippocampal pyramidal cell layer (TILpy), as well as the height of the molecular layer of the hippocampus (Mol).

To conclude, in this region of the brain, all structures appeared normal, meaning that no morphological changes could be observed, in particular in the hippocampus, our region of interest. The limit of the morphometric analysis was, at that time, that only overall structures were measured, enabling to decipher only major cell loss or agenesis. No affection of a particular cell layer of the hippocampus was observed in Coq8a$^{-/-}$ mice. The questions remains whether seizures come from an affection of the hippocampus, due to specific cell death or cellular abnormalities or if it is rather another brain region such as the cortex which is implicated (Biagini et al., 2013a).

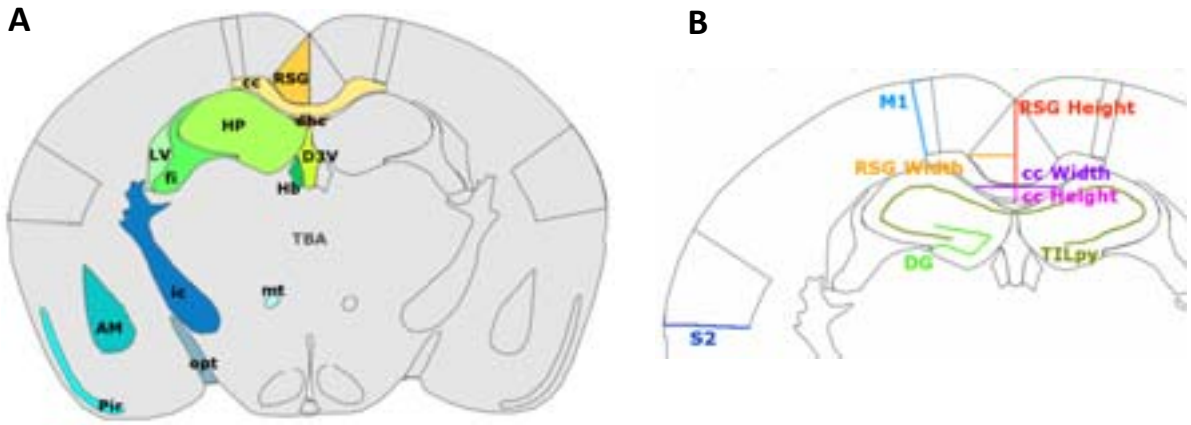

Figure 24 : Areas (A) and lengths (B) of brain structures measured for morphometric analysis.

A) Areas measured. RSG: retrosplenial granular cortex, cc: corpus callosum, dhc: dorsal hippocampal commissure, HP: hippocampus, LV: lateral ventricle, D3V: dorsal 3rd ventricle, fi: fimbria hippocampus, Hb: habenular nucleus, TBA: total brain area, AM: amygdala nuclei, ic: internal capsule, mt: mammillothalamic tract, Pir: piriform cortex, opt: optic tract. B) Length measured: RSG width (orange), RSG height (red), cc width (violet), cc height (pink), DG (length of the dentate gyrus: light green), M1 (height of the primary motor cortex, light blue), S2 (length of the secondary somatosensory cortex, navy blue), TILpy: total internal length of the hippocampal pyramidal cell layer (dark green).

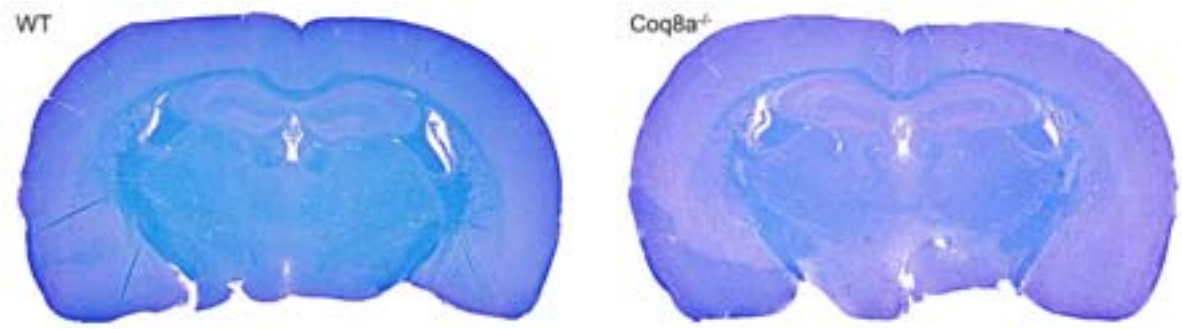

Figure 25 : Coq8a$^{-/-}$ brain morphology is similar to WT.

Brain sections of 25 weeks old mice stained with cresyl violet and luxol blue, at the level of the hippocampus (in a critical section).

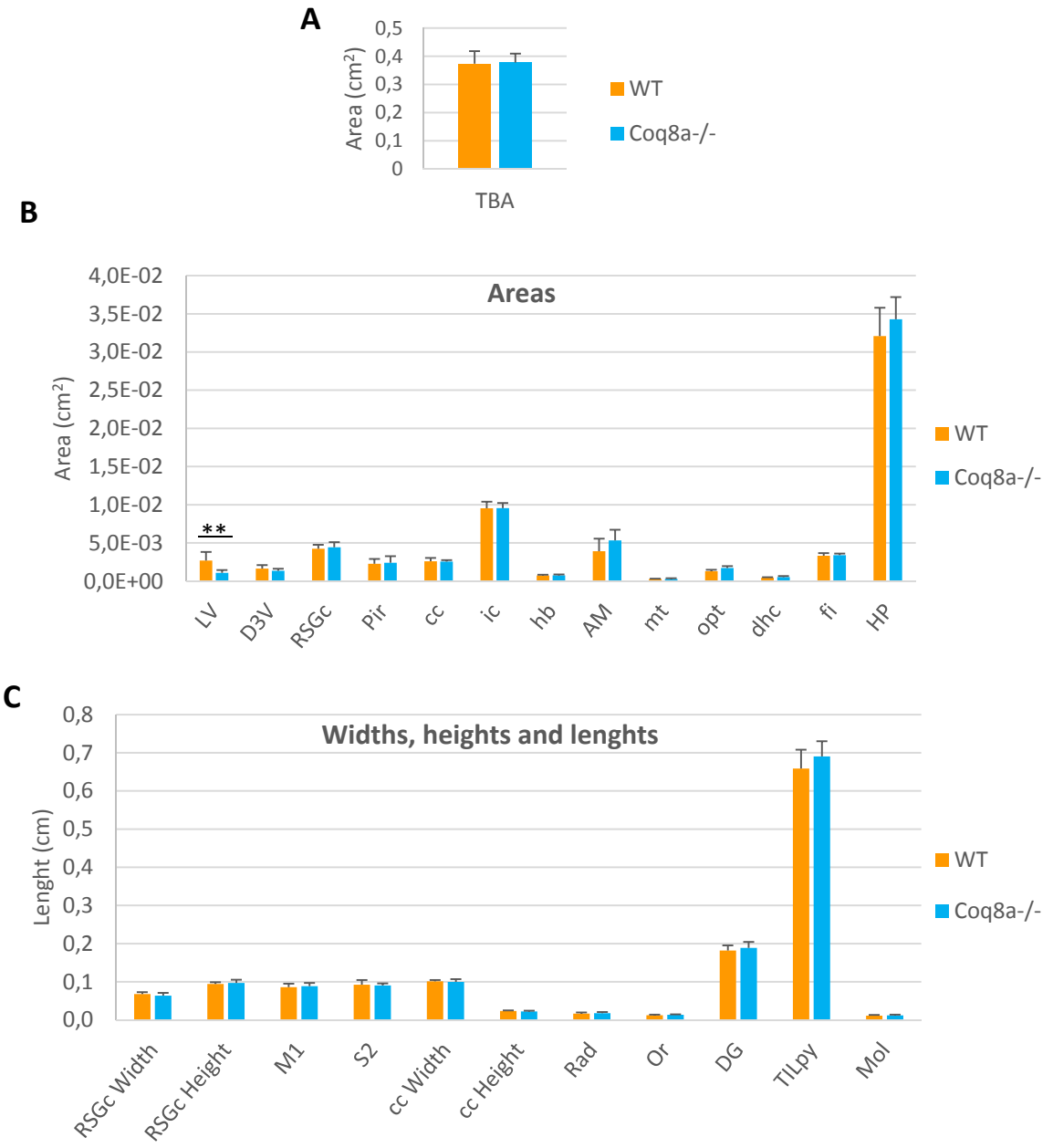

Figure 26 : Similar brain morphologies of Coq8a$^{-/-}$ mice compared to WT, observed by morphometric analysis of brain critical sections at the level of the hippocampus.

Measurement performed with Fiji on 30 weeks old mice brain sections stained with cresyl violet and luxol blue. Mean ± SD, n=4. A) Total brain area (TBA), in cm^2 B) Areas measured in cm^2: LV (lateral ventricles), D3V (dorsal 3rd ventricle), RSGc (retrosplenial granular cortex), Pir (piriform cortex), cc (corpus callosum), ic (internal capsule), hb (habenular nucleus), AM (amygdala nuclei), mt (mammillothalamic tract), opt (optic tract), dhc (dorsal hippocampal commissure), fi (fimbria hippocampus), HP (hippocampus area). C) Length measured in cm: RSGc Width (retrosplenial granular cortex width), RSGc Height (retrosplenial granular cortex height), M1 (height of the primary motor cortex), S2 (length of the secondary somatosensory cortex), cc Width (corpus callosum width), cc Height (corpus callosum height), Rad (length of the stratum radiatum layer of the hippocampus), Or (length of the oriens layer of the hippocampus), DG (length of the dentate gyrus), TILpy (total internal length of the hippocampal pyramidal cell layer), Mol (height of the molecular layer of the hippocampus). ** = p<0.005

2. Ultrastructural analysis

Since no gross morphological abnormality was observed in the hippocampus, we were interested in knowing if ultrastructural defects could be seen upon Coq8a$^{-/-}$ deficiency. So, to further this study, the ultrastructure of 30 weeks old hippocampal neurons was explored by transmission electron microscopy, as at this age spontaneous epilepsy is supposed to have occurred. Some neurons had signs of degeneration both in WT and mutant hippocampus (Figure 27A). These results are not surprising in regards to published data, showing that, in the hippocampus, programmed cell death appear to regulate the total number of neuronal cells, as new neurons are constantly being generated (Biebl et al., 2000; Sun et al., 2004). Mitochondria, Golgi and endoplasmic reticulum appeared normal, in both WT and Coq8a$^{-/-}$ sections. Axons were preserved and myelin sheets correctly formed (Figure 28 A and B). The only striking phenotype in this region was the increased length and number of nuclear invagination in Coq8a$^{-/-}$ neurons, observed in two different mutant animals (Figure 27B). Whether these invaginations are physiological, reflecting a zone with more transcriptionally active neurons (Malhas et al., 2011), or whether these invaginations are part of the pathology remains to be determined. It might be that the sections of WT and KO were not cut at the exact same place of the hippocampus. Two mutant and two WT were used for the experiment and a section of each was observed. Sections from other mice or different sections of the same hippocampus should be looked at to be able to judge if this is significant or not, and quantify the number of invaginations and their length. Considering that no hypothesis could be found at that time to explain these invaginations, these results were left aside. Since then, further bibliographic search lead us to a new hypothesis that these invaginations might be due to an affected calcium signaling (Mauger, 2012; Wittmann et al., 2009). Calcium imaging would help elucidating if calcium signaling is indeed affected in the hippocampus upon COQ8A loss.

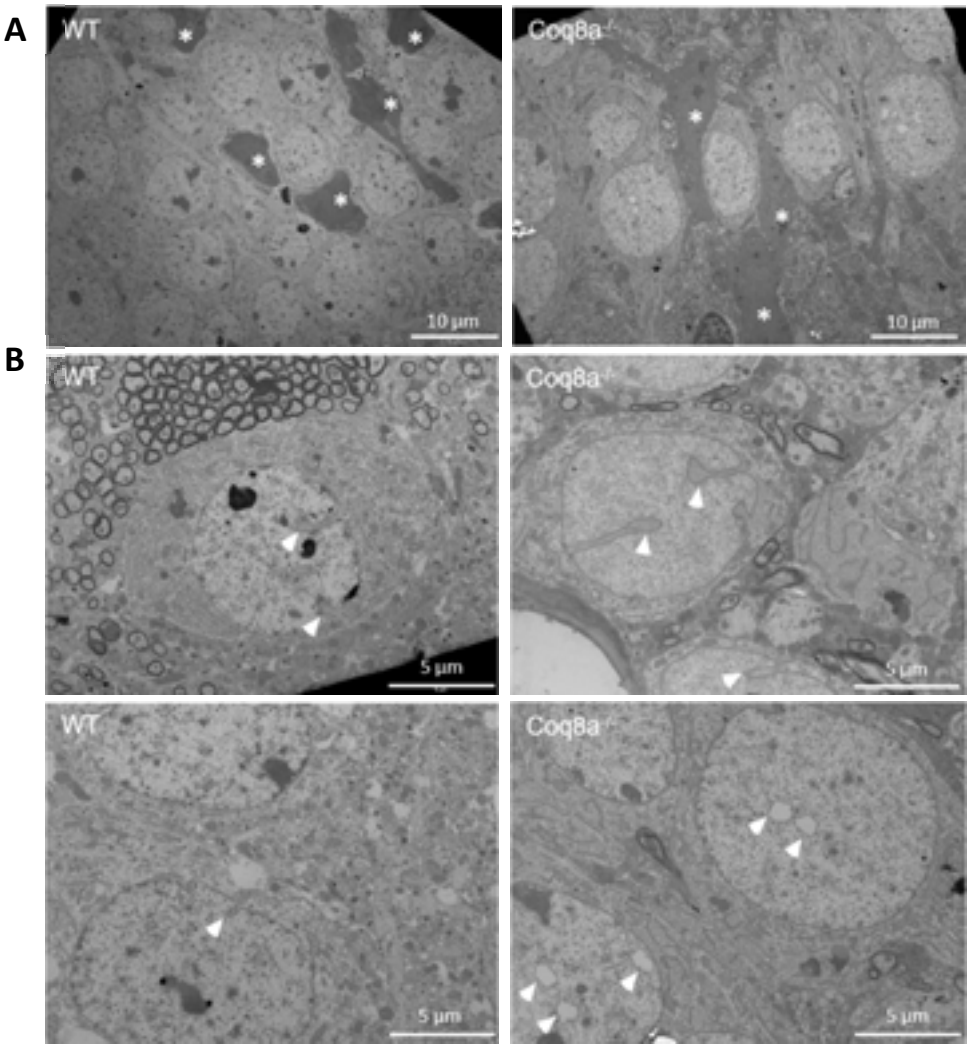

Figure 27 : Invagination of neuronal nuclei in hippocampus observed by electron microscopy in 30 weeks old Coq8a$^{-/-}$ mice.

Electron microscopy of 30 weeks old mice hippocampus. A) Shrunken neurons (*). Scale bars represent 10 µm. B) Nuclear invaginations (arrows). Scale bars represent 5 µm. Left panels: WT and right panels Coq8a$^{-/-}$ 30 weeks old hippocampus. n=2.

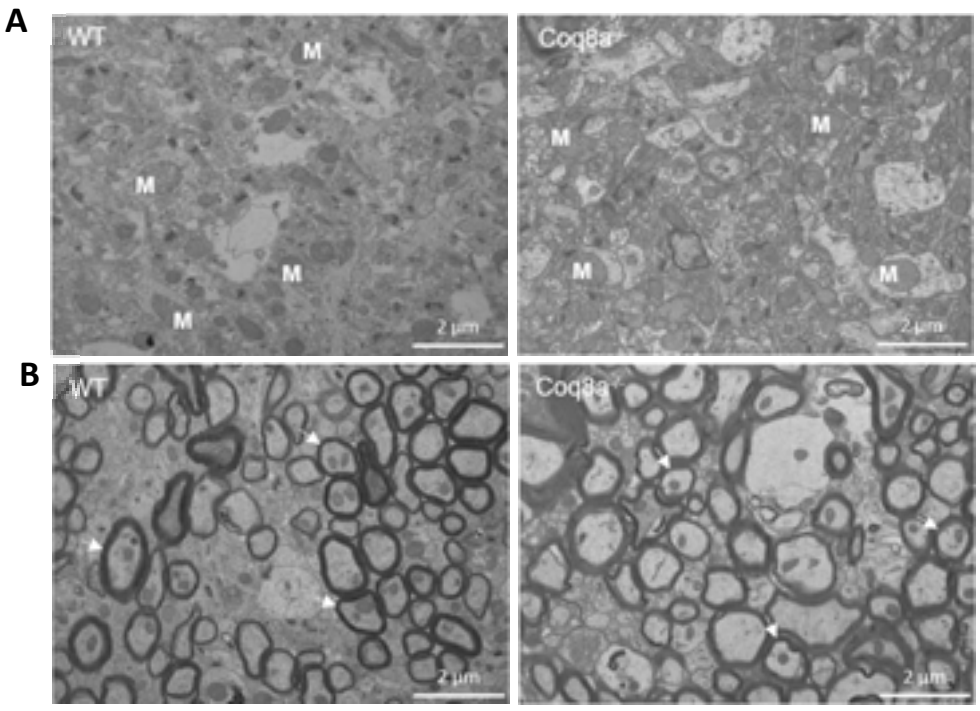

Figure 28 : Normal axons observed by electron microscopy in hippocampus of 30 weeks old Coq8a$^{-/-}$ mice.

Electron microscopy of 30 weeks old mice hippocampus. A and B) Normal axons and nerve fibers with mitochondria (M) having a normal structure. Axons with myelin sheet and a mitochondria (arrows). Scale bars represent 2 µm. Left panels: WT and right panels Coq8a$^{-/-}$ 30 weeks old cerebellum. n=2.

3. Hippocampal primary cultures

In parallel, hippocampal primary cultures were set up to be able to test hypothesis like a potential affected vesicular trafficking. The cultures are derived from littermate's embryos at embryonic day 18,5. It has been determined, that already at that age, in whole embryos extract, COQ7 levels are down (Figure 12). None of the data showed that heterozygous mice had a phenotype, so cultures derived from heterozygous embryos were taken as control. The cultures are healthy when derived either from mutant or from heterozygous embryos. The neurons developed well and no gross defect could be observed when staining for βIII-tubulin (a neuronal marker) and GFAP (a protein expressed in glial cells) (Figure 29).

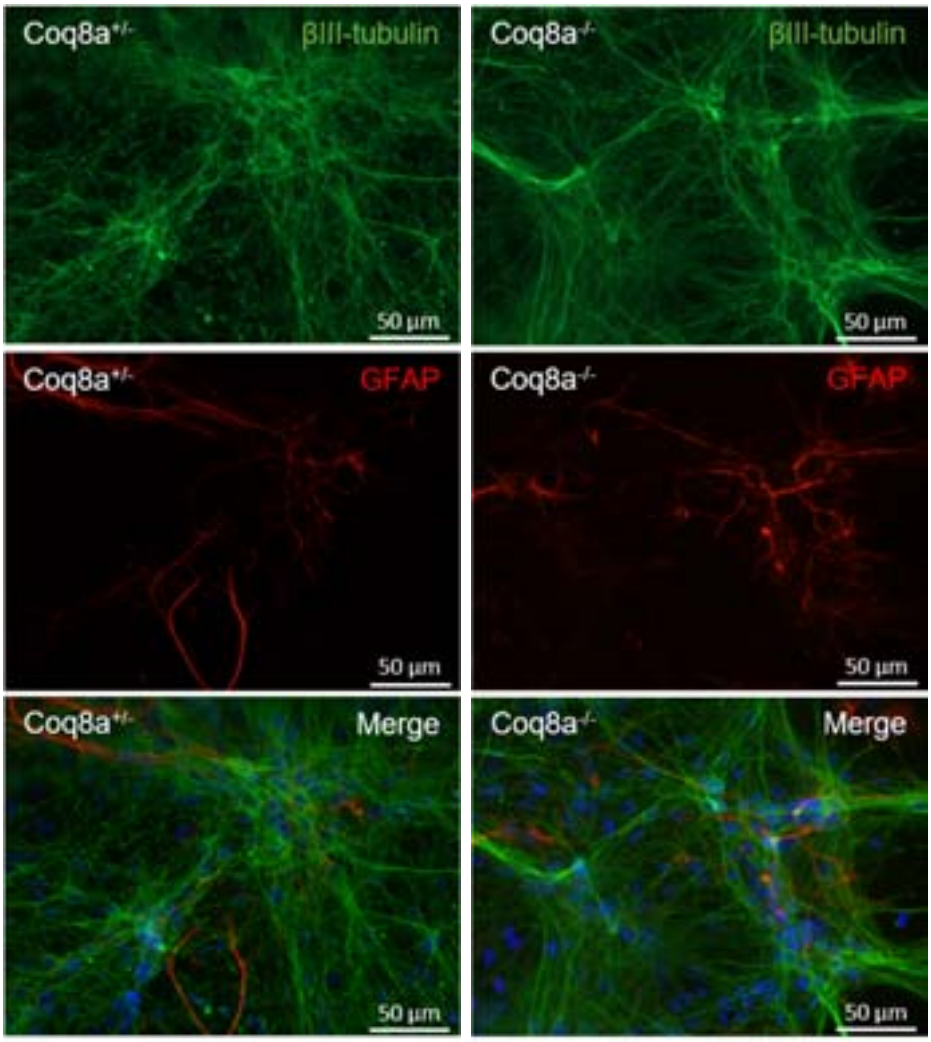

Figure 29 : Coq8a$^{-/-}$ hippocampal primary cultures are as healthy as heterozygous.

Immunostaining of βIII-tubulin: staining neurons (in green), and GFAP: staining glial cells (in red). In the merge image: DAPI (in blue, staining nuclei). Left panels: heterozygous (Coq8a$^{+/-}$) and right panels: mutant (Coq8a$^{-/-}$) hippocampal cells. Scale bars represent 50 µm.

4. Excitotoxicity

Epilepsy is often induced by excitotoxicity, and some proteins are known to be deregulated in these cases. NR2B, a NMDA (N-methyl-D-aspartate) glutamate receptor, was described as upregulated upon seizures (Di Maio et al., 2011). Deregulation of GAD65 and 67 also occurs in epilepsy. GAD65 and 67 are two isoforms of the glutamic acid decarboxylase, involved in the production of the GABA neurotransmitter (Esclapez and Houser, 1999). Finally, in some cases of epilepsy, vGLUT2, a transporter mediating the uptake of glutamate in synaptic vesicles, was found to be decreased (Van Liefferinge et al., 2015). Hence, the level of these proteins was assessed in Coq8a$^{-/-}$ mice hippocampus, to determine if seizures and epilepsy are due to excitotoxicity, in this mouse model.

Beforehand, the level of some COQ proteins was checked in the hippocampus. We wanted to ensure that deregulations previously observed also occur in this tissue. Hippocampi of 30 weeks old mice were taken, as epilepsy induced by PTZ was tested in 6 month old mice (Stefely et al., 2016). As in other tissues, COQ5 and COQ7 decrease was confirmed in Coq8a$^{-/-}$ adult hippocampus (Figure 30). COQ9 levels diverge between the mice and no significant downregulation could be seen (Figure 30).

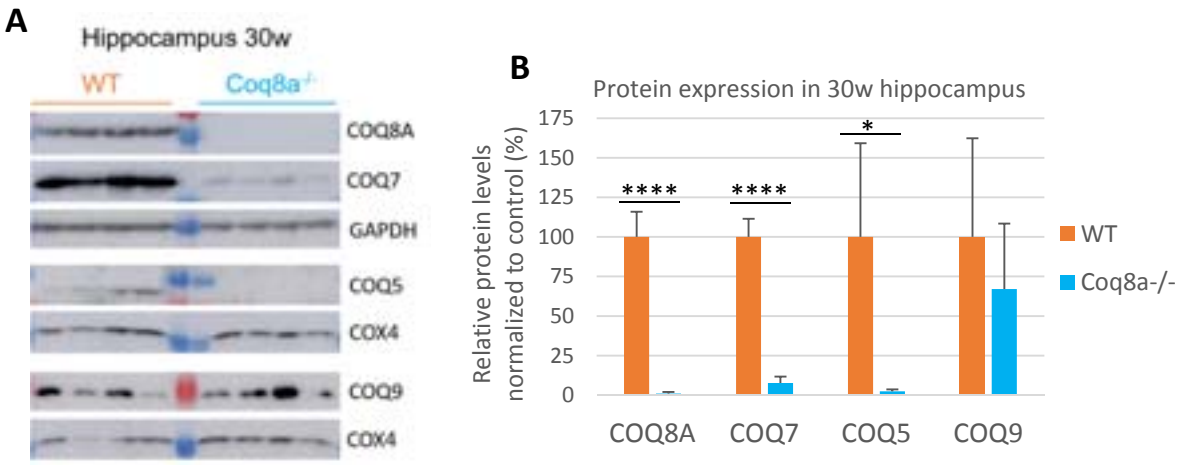

Figure 30 : Loss of COQ8A induces a deficiency in COQ7 and COQ5 in hippocampus.

A) Western blots showing COQ8A, COQ7, COQ5 and COQ9 expression in hippocampus of 30 weeks old mice, GAPDH and COX4 taken as controls. B) Quantification of protein levels using Fiji. Protein levels are normalized over GAPDH expression (for COQ8A and COQ7) or COX4 (COQ5 and COQ9) and plotted as a percentage compared to WT. Error bars: SD, * = p<0.05, **** = p<0.00005.

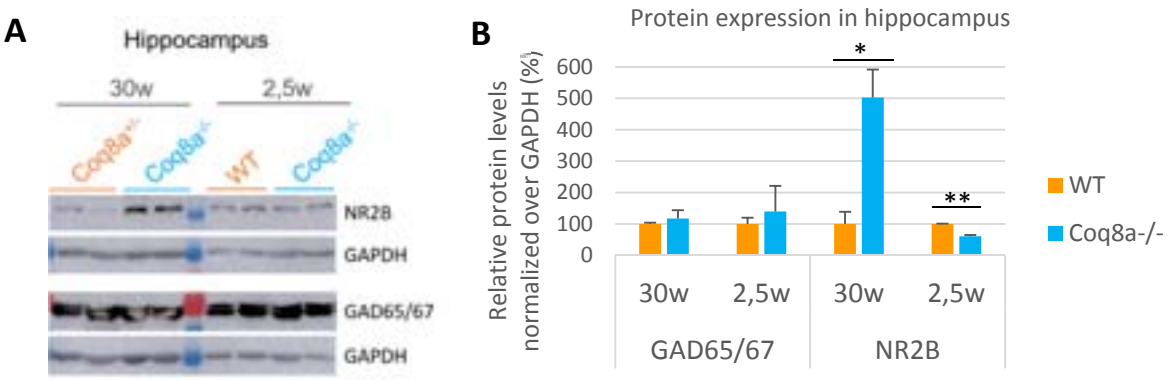

Figure 31 : Loss of COQ8A deregulates NR2B in the hippocampus

A) Western blots showing NR2B and GAD65/67 expression in hippocampus of 30 and 2,5 weeks old mice, GAPDH taken as controls. B) Quantification of protein levels using Fiji. Protein levels are normalized over GAPDH expression and plotted as a percentage compared to WT. Error bars: SD, * = p<0.05, ** = p<0.01

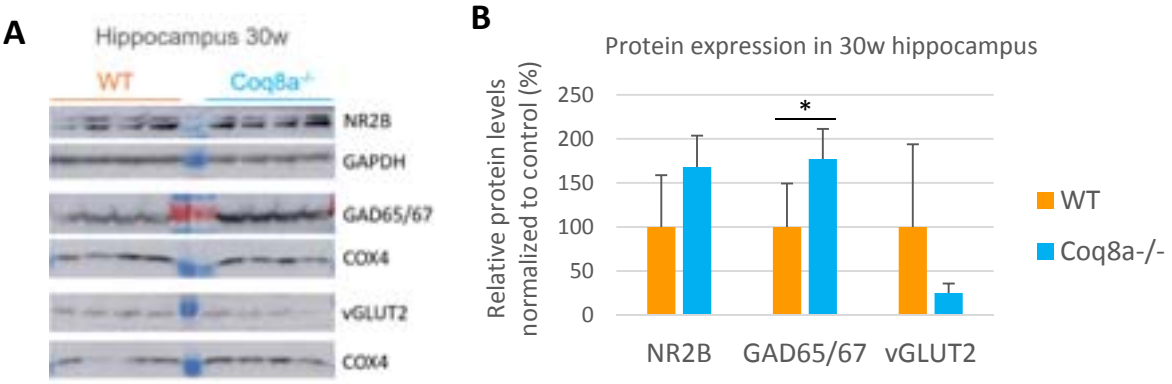

Figure 32 : Loss of COQ8A deregulates GAD65/67 in the hippocampus.

A) Western blots showing NR2B, GAD65/67 and vGLUT2 expression in hippocampus of 30 weeks old mice, GAPDH and Cox4 taken as controls. B) Quantification of protein levels using Fiji. Protein levels are normalized over GAPDH (NR2B) and COX4 (GAD65/67, vGLUT2) expression and plotted as a percentage compared to WT. Error bars: SD, *= p<0.05.

In a first attempt to determine NR2B and GAD65/67 levels in 2,5 weeks (pre-symptomatic) and 30 weeks old (post-symptomatic) mice hippocampi, NR2B was found to be decreased in mutants at 2,5 weeks but increased at 30 weeks, whereas GAD65/67 levels were similar to WT, in hippocampus at both ages (Figure 31A). As a trend towards elevated levels of NR2B at 30 weeks and decreased levels at 2,5 weeks were observed, the blots were quantified to get a clearer answer, and indeed NR2B levels are significantly up at 30 weeks and down at 2,5 weeks in mutant's hippocampus (Figure 31B). The elevated levels of NR2B at 30 weeks are in accordance with an excitotoxicity mechanism (Yang et al., 2014), indicating that epilepsy might indeed arise from deregulations in the hippocampus. An experiment with a new cohort of 30 weeks old mice revealed different results, with NR2B levels being similar to WT, while GAD65/67 was increased in Coq8a$^{-/-}$ mice hippocampus (Figure 32). NR2B levels

appear similar and are not significantly elevated in mutant mice hippocampus, but this could be due to the expression variability in between WT. The elevated levels of GAD65/67 are in agreement with the hypothesis of seizures emanating from the hippocampus, according to previous published data where, in case of seizures, GAD65 synthesis was increased (Patel et al., 2006). Regarding vGLUT2, no difference could be seen, although there is a trend towards decreased levels in mutant mice hippocampus, but this is not significant (Figure 32). These results can be explained by the weak signal in Western blot. Furthermore, COX4 might not be the best loading control to quantify vGLUT2, as COX4 is a mitochondrial protein and vGLUT2 a plasma membrane protein. Nevertheless, if vGLUT2 protein levels are indeed lower in mutant mice compared to WT, this could reflect excitotoxicity in Coq8a$^{-/-}$ mice hippocampus (Lobo et al., 2011). New cohorts would be needed to confirm these different results and another loading control, like vinculin, a membrane-cytoskeletal protein, should be used.

So far, no conclusion can be drawn in regards to glutamatergic receptors, nor the production of GABA, as different results were obtained in two independent experiments. Regarding elevated levels of NR2B and GAD65/67, and decreased levels of vGLUT2, epilepsy might still be due to excitotoxicity in the hippocampus, but it remains to be confirmed. Moreover, no spontaneous seizures were observed in Coq8a$^{-/-}$ mice during the last four years. An analysis after induction of epilepsy by PTZ could give a more consistent answer, although WT mice might also have deregulated levels of certain proteins. By electron microscopy degenerating neurons were observed both in Coq8a$^{-/-}$ and WT hippocampus further refraining a clearer picture of possible excitotoxicity. The only consistent phenotype was increase in the number and size of nuclear invaginations in mutant hippocampal neurons at 30 weeks, although this feature was not quantified. This last observation, of nuclear invaginations, could point towards a deregulated calcium signaling (Mauger, 2012). Finally, hippocampal neuronal cultures were healthy with glial cells and branched neurons which made us think that this cellular model is not appropriate to study what happens in older mice. For this cellular model, cells are taken from embryos, so too early in regards to the phenotype.

All in all, further experiments are needed to get a clearer idea of the implication, or not, of the hippocampus, in seizures observed in Coq8a$^{-/-}$ mice but also in some patients. A hint, dropped during a discussion with clinicians, indicated that epilepsy in ARCA2 patients is most probably emanating from cortex. Lastly some studies also show that affection of the cerebellum could lead to seizures (Lascano et al., 2013). Precise epilepsy foci should therefore be determined to be able to dig further into the mechanisms inducing the seizures.

VI. Ataxia

The ARCA2 disease is characterized by the ataxic phenotype, which is due to an atrophy of the cerebellum in humans. The cerebellar affection, is also found in Coq8a$^{-/-}$ mice especially with degenerating Purkinje neurons, as well as ultrastructural and electrophysiological defects (Stefely et al., 2016) but without cerebellar atrophy.

1. Deregulated ions channels?

As part of my thesis project, I decided to try and identify the causes for the ataxia and see if it can be explained by the misregulation of specific molecular pathways, or of certain ion channels, like in other types of ataxias. Initially, regarding the Purkinje cells abnormal firing, observed in Coq8a$^{-/-}$ mice cerebellum, by electrophysiology (Stefely et al., 2016), it was thought that a specific transporter could be defective. By a candidate approach, ion channels already know to be responsible for ataxia and inducing a similar pattern in electrophysiology were studied. The list included: a calcium channel (CACNA1A, $Ca_v2.1$ calcium channel voltage-dependent, P/Q type, implicated in EA2), a receptor for glutamate (GRM1, mGluR1α metabotropic receptor of glutamate, implicated in SCAR13), a receptor for inositol phosphate (ITPR1, inositol 1,4,5-triphosphate receptor, implicated in SCA16 and 29), a potassium channel (KCNC3, Kv3.3 voltage-gated potassium channel, implicated in SCA13) and an amino-acid transmembrane transporter (SLC7A5, under-expressed in RNA-sequencing and proteomic analysis of Coq8a$^{-/-}$ mice). The assays were performed on 25 to 30 weeks old mice cerebellum, when it is known that Purkinje neurons degenerate (Stefely et al., 2016).

Immuno-staining was performed but did not yield any exploitable results. Even calbindin staining, successfully performed in other teams, and done with a broadly used anti-calbindin antibody (Sadakata et al., 2007; Shakkottai et al., 2011), did not work. A lot of optimization (with different blocking solutions and antibodies dilutions) and various attempts of demasking (basic, acidic and with heat) were tested but none were conclusive. These results remain puzzling and the only hypothesis so far is that there was an issue with the paraffin embedding or formaldehyde fixation which prevented antibodies binding onto the brain sections. Cryo-sections and perhaps EM-grade paraformaldehyde should alleviate these issues.

Nonetheless, the protein levels were assessed and none were found to be significantly deregulated at any tested age. The levels of CACNA1A, GRM1, ITPR1 and KCNC3 were similar in Coq8a$^{-/-}$ cerebellum compared to WT, in 10, 20 and 30 weeks old mice (Figure 33). The antibody for SLC7A5 did not show a band at the proper molecular weight (data not shown).

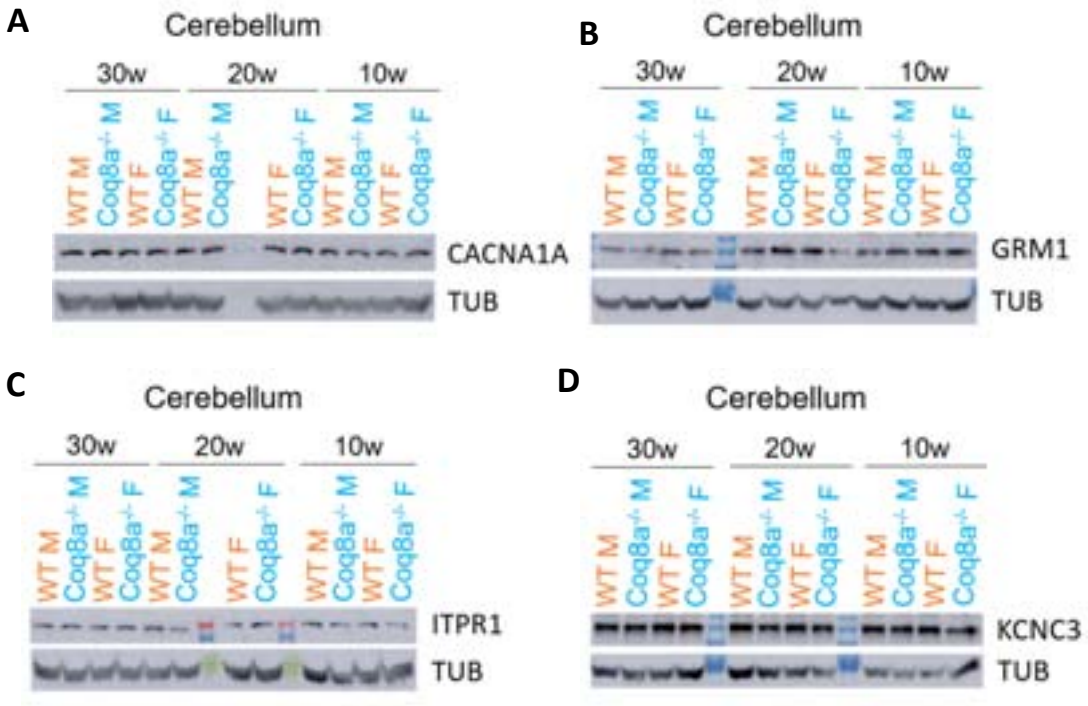

Figure 33 : Loss of COQ8A does not deregulate ion channels tested in the cerebellum.

Western blots showing A) CACNA1A, B) GRM1, C) ITPR1, D) KCNC3 expression in cerebellum of 10, 20 and 30 weeks old mice, TUB (tubulin) taken as controls.

Yet it was not known if the Purkinje neurons degeneration phenomenon could be observed in the entire cerebellum or was restricted to certain zones (lobules, vermis, hemispheres…). Furthermore, it was shown that in certain cerebellar pathologies, degeneration follows defined motifs, corresponding to zebrin-II positive or negative bands (Sarna et al., 2003). The goal was to elucidate if Purkinje neurons degenerate in a specific patterned manner. Unfortunately, like for the ion channels, a big effort was put to try and optimize immunohistochemistry in the slices but was unfruitful (as discussed above), so this part was abandoned at that time, to focus on more promising perspectives.

2. Cellular models of cerebellum

To assess cerebellum early on and have *in vitro* models, organotypic and cerebellar primary cultures were derived from WT and KO mice. Organotypic cultures were derived from post-natal day 7 to 12 (P7-P12) pups whereas primary cultures needed to be derived at birth (P0 pups).

a. Cerebellar organotypic cultures

Characterization

The goal, when setting up the cerebellar organotypic cultures, was to be able to assess specific deregulated mechanisms. In particular, this *in vitro* system would have allowed to assess the affection of a specific ion channel, by blocking it and recoding Purkinje neurons firing by electrophysiology. Unfortunately, no affected ion channel was found at that time. Organotypic slices of cerebellum have the advantage to retain the lobulated structures and are more physiological as the layers, so the environment around neurons, are preserved. Organotypic cultures are not suited for all experiments. It is hard to have cultures of the same sections of the cerebellum, and with similar Purkinje neurons orientation, for all the different pups (depending on the sections that detached well and were preserved during slicing). Nevertheless, these cultures are adapted for immunofluorescence staining and enabled the assessment of the ion channels for which histology, on 25 weeks old cerebellar sections, did not work.

In the cerebellum, Calbindin (CALB) is specifically expressed in Purkinje neurons. Thus, calbindin staining allowed us to determine that Purkinje neurons are present with a nice arborization. Purkinje cells appeared healthy and branched properly both in wild-type and Coq8a$^{-/-}$ slices and the lobules were preserved (Figure 34). These cultures could be maintained for at least six weeks.

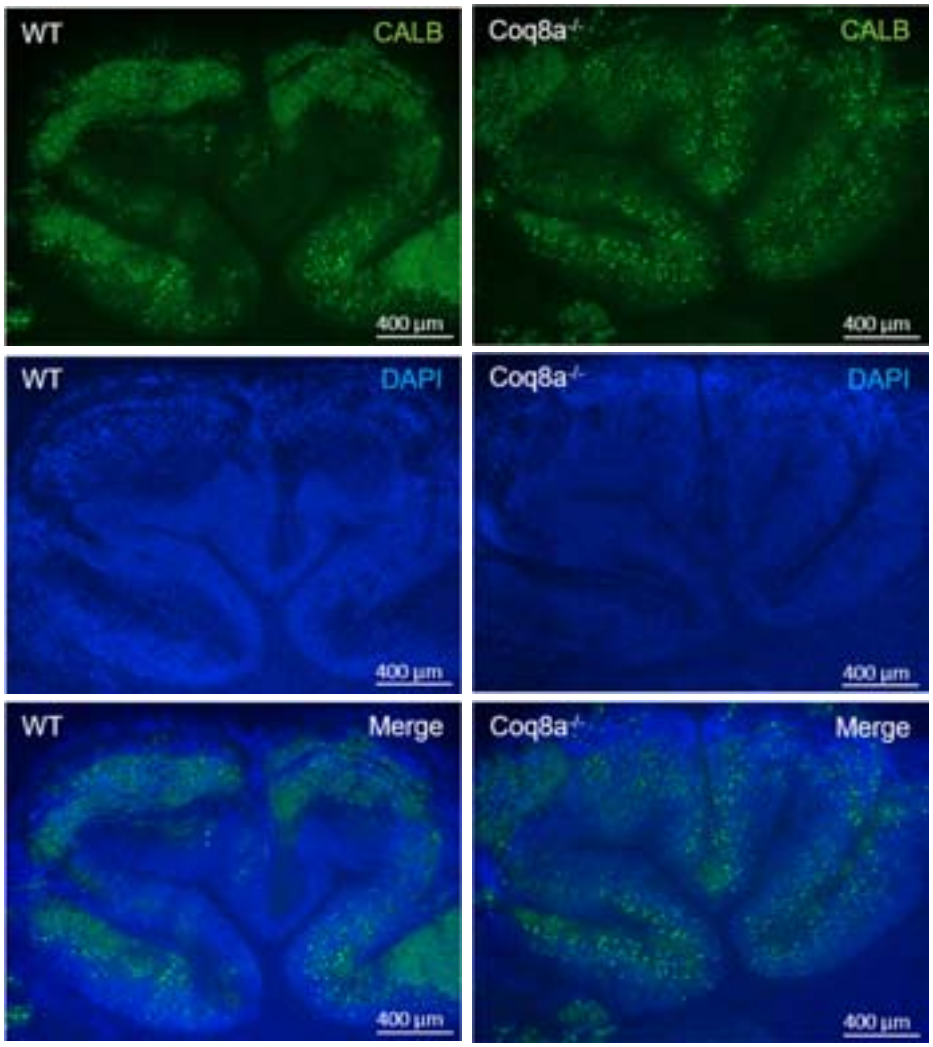

Figure 34 : Coq8a$^{-/-}$ and WT cerebellar organotypic cultures have preserved lobules.

Immunostaining of organotypic cultures derived from P10 pups and kept 6 weeks in culture. Calbindin: staining Purkinje neurons (in green), and DAPI (staining nuclei, in blue). Left panels: WT and right panels: mutant (Coq8a$^{-/-}$) organotypic cultures. Scale bars represent 400 µm.

The dendrites of Purkinje neurons developed well in organotypic cultures, or were at least maintained (Figure 35 and Figure 36). Interestingly, the Golgi apparatus seemed to form a bigger network in these neurons. Golgi staining was more pronounced in Purkinje cells bodies then in other cells, but this is probably due to the bigger cell soma of these neurons (Figure 35 and Figure 36). Purkinje neurons

arborization was not measured as it varied depending on the slices, and dendrites of different Purkinje neurons overlapped. Golgi apparatus staining (with GM130) worked well on organotypic slices and enabled to observe that it was well organized in cultures, and in mutant slices (Figure 36).

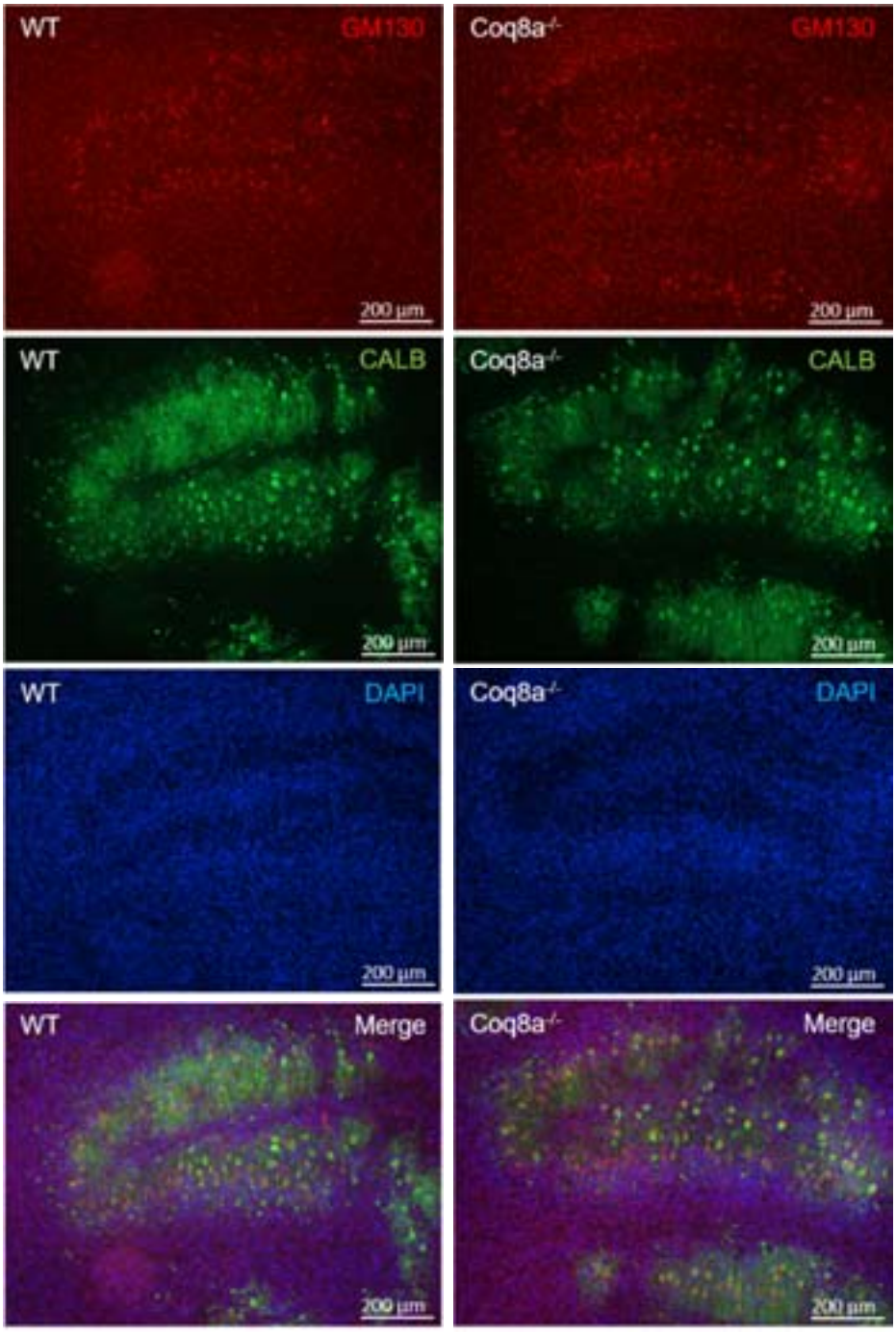

Figure 35 : Coq8a$^{-/-}$ cerebellar organotypic cultures have preserved Purkinje neurons.

Immunostaining of organotypic cultures derived from P7 pups and kept 6 weeks in culture. GM130 (staining Golgi apparatus, red), calbindin (staining Purkinje neurons, green) and DAPI (blue). Left panels: WT and right panels Coq8a$^{-/-}$ organotypic cultures. Scale bars represent 200 µm.

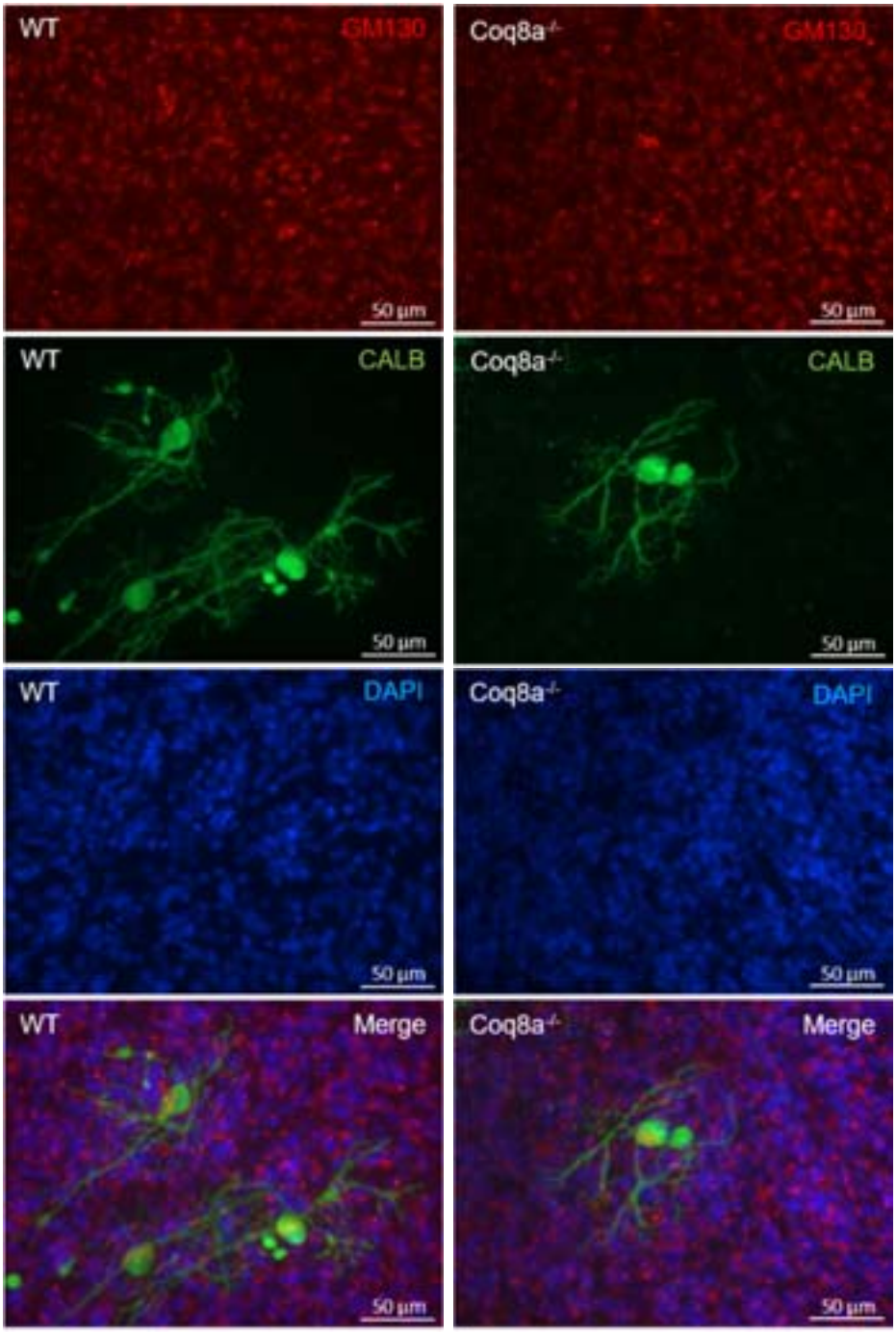

Figure 36 : Coq8a$^{-/-}$ cerebellar organotypic cultures have preserved Purkinje neurons and Golgi organization.

Immunostaining of organotypic cultures derived from P10 pups and kept 6 weeks in culture. GM130 (staining Golgi apparatus, red), calbindin (staining Purkinje neurons, green) and DAPI (blue). Left panels: WT and right panels: Coq8a$^{-/-}$ organotypic cultures. Scale bars represent 50 µm.

To further characterize these organotypic cultures, electron microscopy was then performed. It enabled to assess a potential ultrastructural defect, such as Golgi dilatation, which would have been difficult to assess by immunostaining. It appeared that some Purkinje neurons degenerate, both in Coq8a$^{-/-}$ and WT cultures, whereas some others have a normal shape (Figure 37A). Granules cells had classical structures in mutant and WT organotypic cultures (Figure 37A). Regarding the Golgi apparatus, it was observed as swollen in some Purkinje neurons, in particular in the ones degenerating, in mutant and WT organotypic cultures (Figure 37B). The other structures, such as mitochondria or endoplasmic reticulum were well preserved and vesicles could be observed in axons, next to synapses (Figure 38A and B), indicating healthy cultures and active neurons. No defects in myelin sheets could be seen (Figure 38B). Some empty axons could be found in Coq8a$^{-/-}$ and WT cultures but result, most probably, from the sectioning of slices. Finally, abnormal structures, which could be lipids, were found in neuronal bodies, in cultures of both genotypes (Figure 38A). All in all, no ultrastructural defect, different from the ones also observed in WT, could be seen for Coq8a$^{-/-}$ cultures. Whether cerebellar organotypic cultures are a good model to study ARCA2 is not sure yet. It might be too early to have the appearance of a phenotype. Further characterization, like with electrophysiology to assess Purkinje neuronal firing, would be needed.

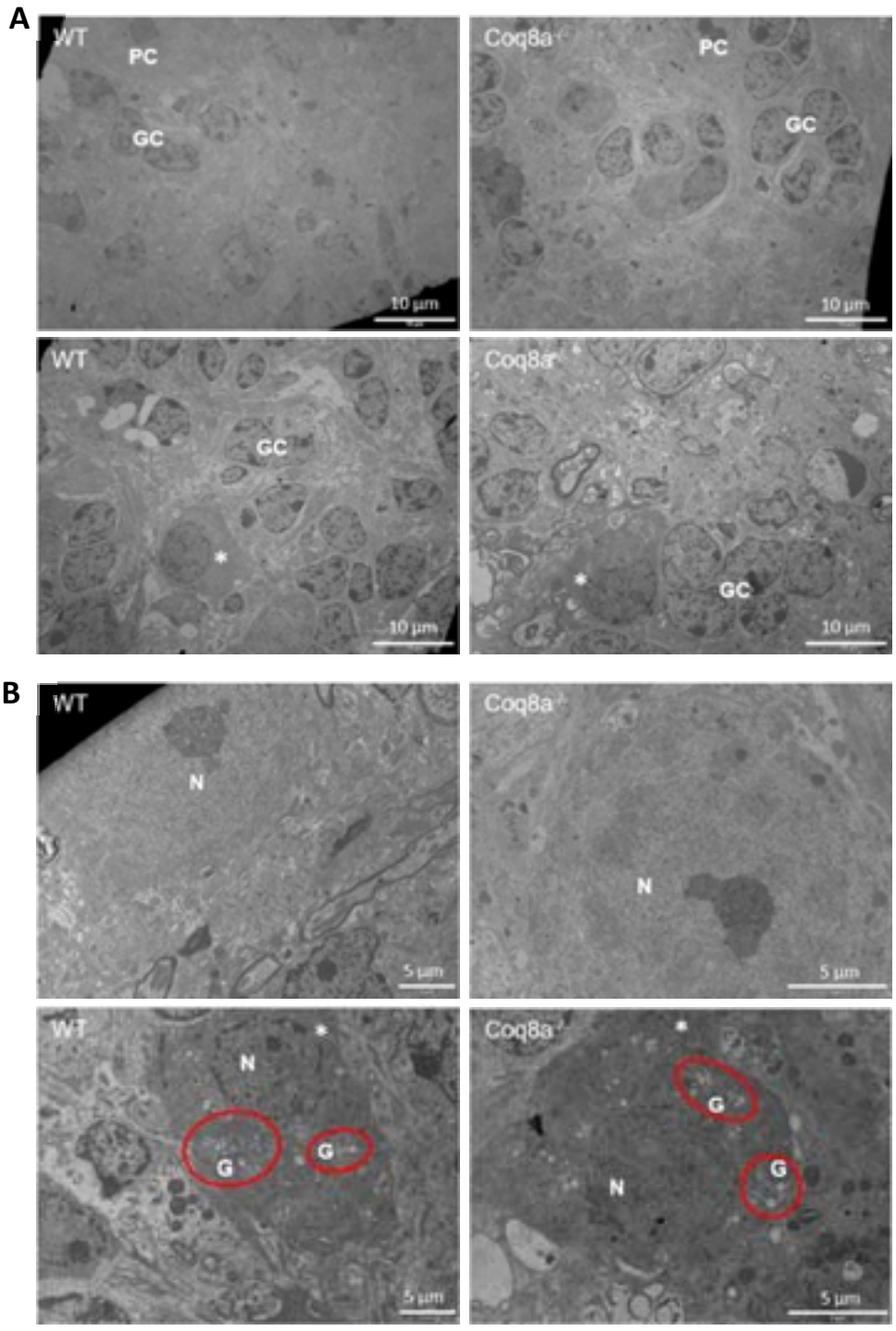

Figure 37 : Swollen Golgi and degenerating Purkinje neurons are observed in Coq8a$^{-/-}$ and WT cerebellar organotypic cultures.

Electron microscopy of organotypic cultures. A) PC: healthy Purkinje neuron, GC: granule cell and shrunken Purkinje neurons (*). Scale bars represent 10 µm. B) Normal cytoplasm with classical structures (upper panels) or cytoplasm with swollen Golgi (red circle) in shrunken neurons (*). Scale bars represent 5 µm. Left panels: WT and right panels Coq8a$^{-/-}$ organotypic cultures.

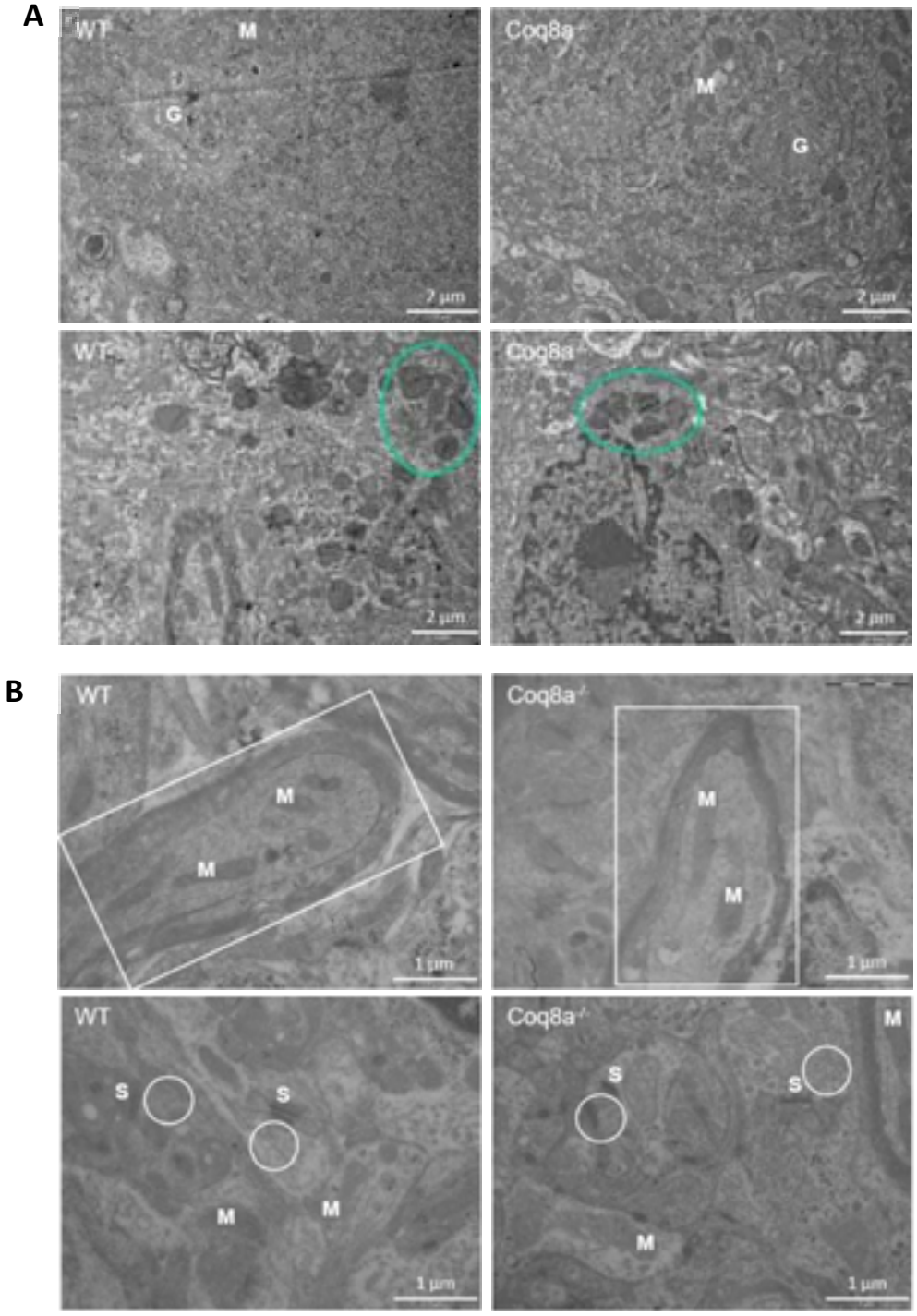

Figure 38 : Abnormal lipid structures and healthy axons and synapses are observed in Coq8a$^{-/-}$ and WT cerebellar organotypic cultures.

Electron microscopy of organotypic cultures. A) Golgi (G) and mitochondria (M) with classical structures, or abnormal structures/lipids (blue circle). Scale bars represent 2 µm. B) Axons and nerve fibers with mitochondria (M) having a normal structure. Axons with myelin sheet and mitochondria (white rectangle), vesicles next to synapses (white circle). Scale bars represent 1 µm. N: nucleus, G: Golgi apparatus, M: mitochondria, S: synapses. Left panels: WT and right panels Coq8a$^{-/-}$ organotypic cultures.

Ion channels

As immunohistochemistry on 30 weeks old cerebellum did not work, the selected ions channels were assessed in organotypic cultures. The quantity of CACNA1A, ITPR1 and KCNC3, as seen by western blot, and the localization of these proteins and SLC7A5 appeared equivalent in Coq8a$^{-/-}$ and WT organotypic cultures. As expected, all proteins seemed to have a membranous localization (Figure 39, Figure 40, Figure 41, Figure 42). Calbindin was used for counterstaining to check the localization in Purkinje neurons of each of these ion channels. ITPR1 and KCNC3 appeared to be localized specifically in Purkinje neurons, whereas SLC7A5 was also present in other neighboring cells (Figure 40, Figure 41 and Figure 42). CACNA1A seemed majorly present in Purkinje neurons, with a punctuated pattern but might also be expressed in surrounding cells (Figure 39). KCNC3 is known to be expressed on the plasma membrane surface (McMahon et al., 2004), which is coherent with the observed localization, at the periphery of Purkinje neuronal bodies (Figure 41).

Ion channels localization could have been evaluated more in details, to look for subtle changes between Coq8a$^{-/-}$ and WT mice, but it was unsure if cerebellar organotypic cultures were a good model for this assessment. No obvious phenotype had been observed in this *in vitro* model. Electrophysiology assessment of spontaneous Purkinje cells firing would be needed in order to decipher if organotypic cultures reproduce the phenotype observed in 3 months old mice (Stefely et al., 2016). Nor the quantity, observed by Western blot for CACNA1A, GRM1, ITPR1 and KCNC3 on 10, 20 and 30 weeks old mice cerebellar extracts, nor the overall localization, observed for CACNA1A, ITPR1, KCNC3 and SLC7A5 on cerebellar organotypic cultures were affected.

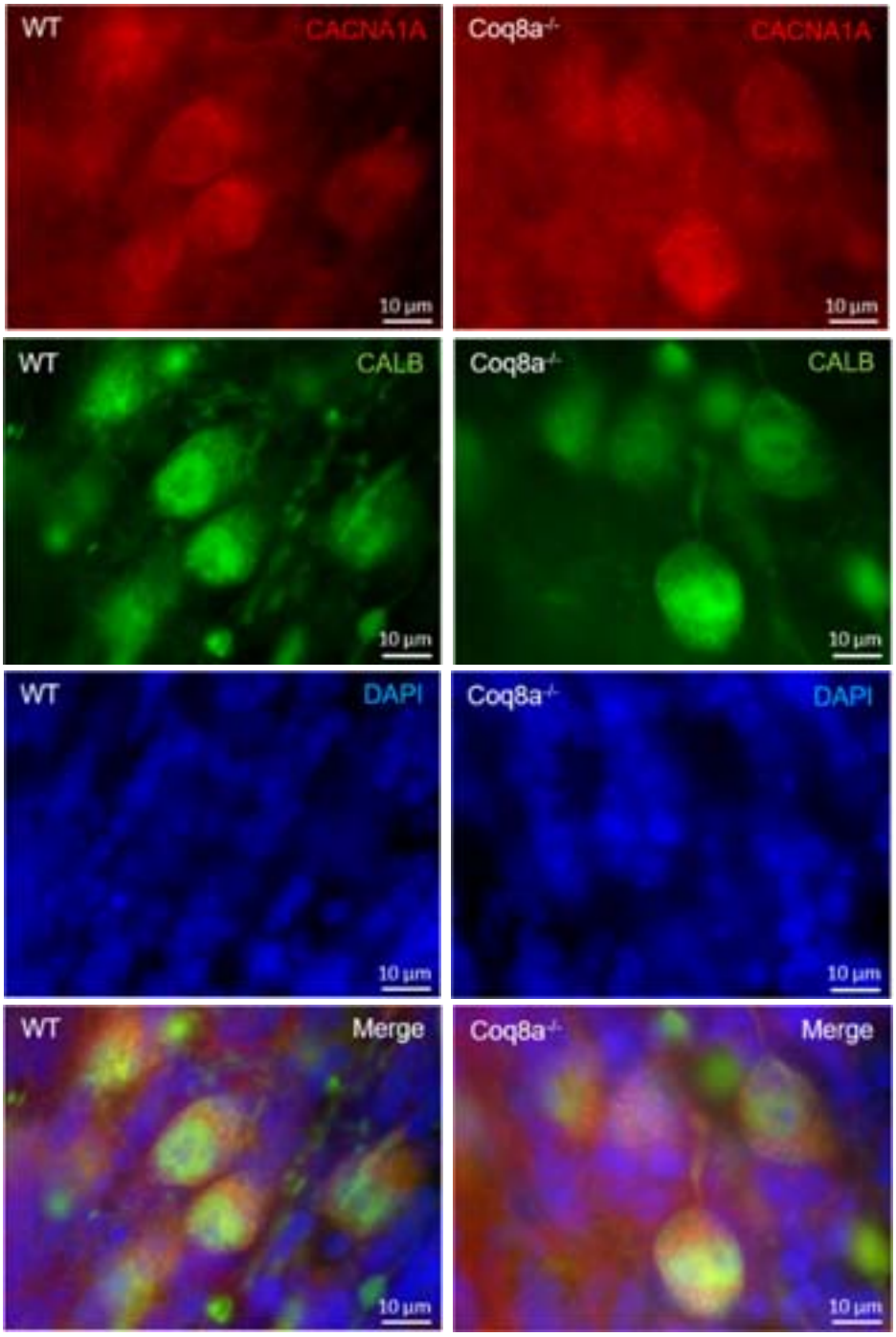

Figure 39 : Similar pattern for CACNA1A in Coq8a$^{-/-}$ and WT cerebellar organotypic cultures.

Immunostaining of organotypic cultures derived from P12 pups and kept 24 days in culture. CACNA1A (red), calbindin (green), DAPI (blue). Left panels: WT and right panels Coq8a$^{-/-}$ organotypic cultures. Scale bars represent 10 µm.

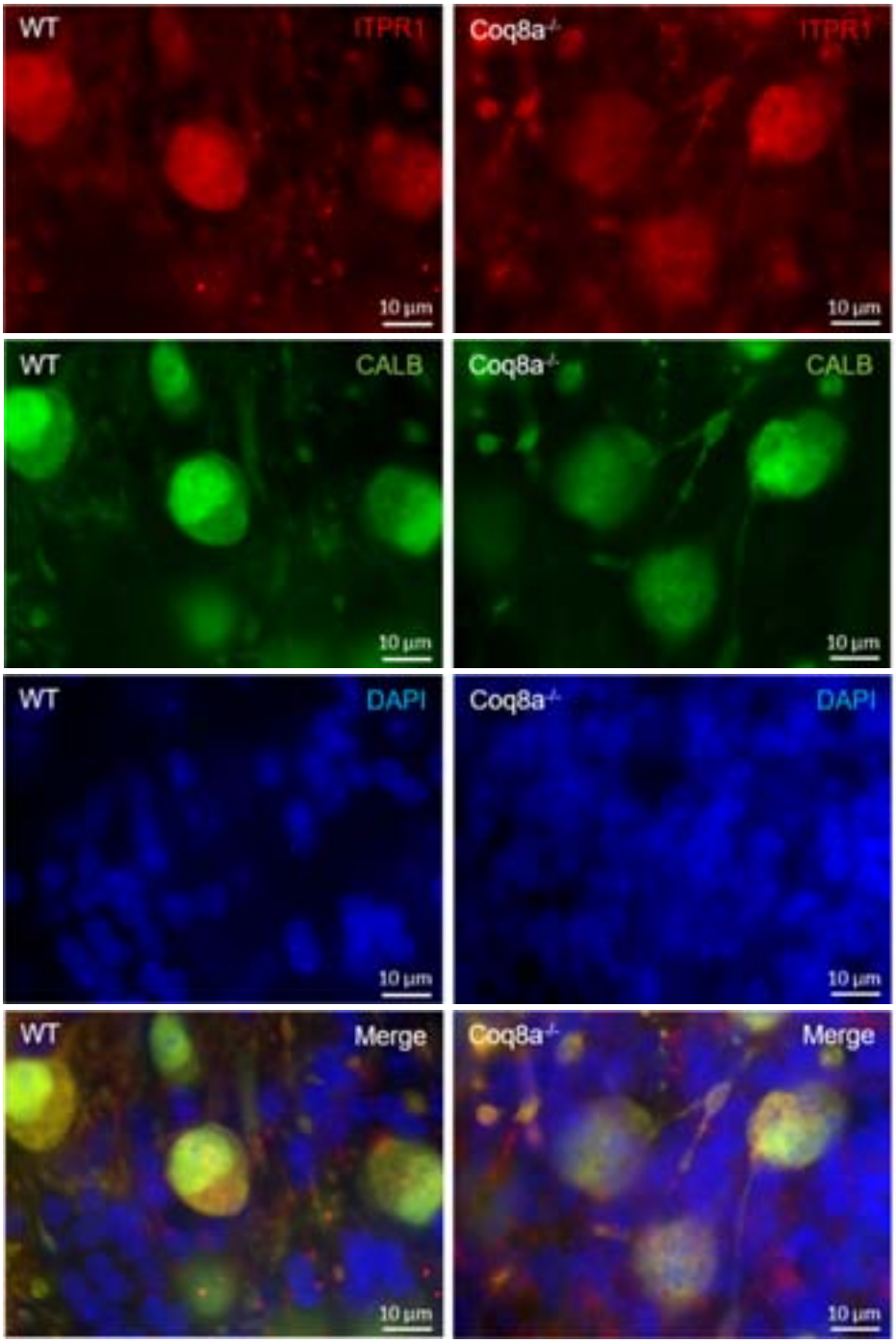

Figure 40 : Similar pattern for ITPR1 in Coq8a$^{-/-}$ and WT cerebellar organotypic cultures.

Immunostaining of organotypic cultures derived from P12 pups and kept 24 days in culture. ITPR1 (red), calbindin (green), DAPI (blue). Left panels: WT and right panels Coq8a$^{-/-}$ organotypic cultures. Scale bars represent 10 µm.

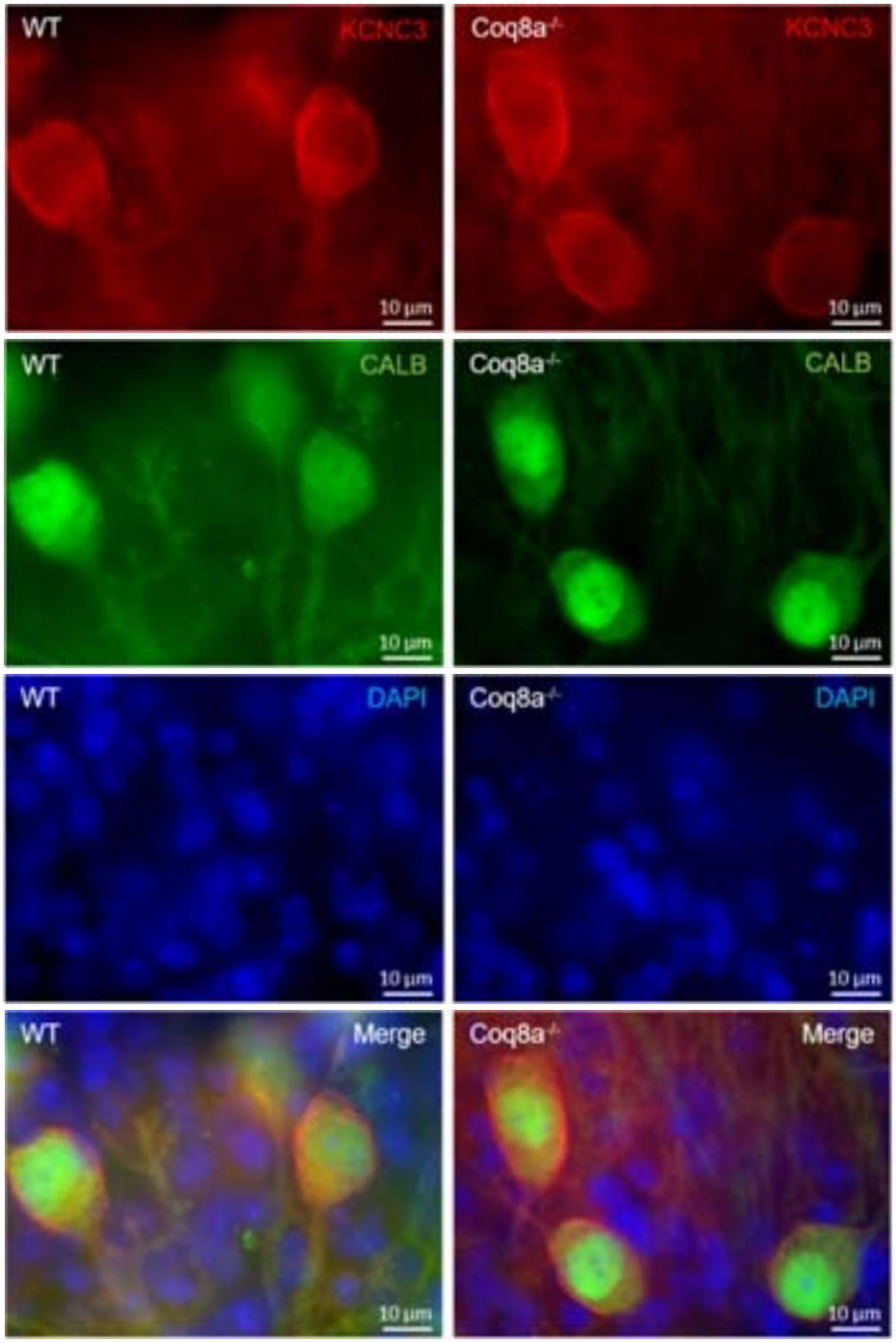

Figure 41 : Similar pattern for KCNC3 in Coq8a$^{-/-}$ and WT cerebellar organotypic cultures.

Immunostaining of organotypic cultures derived from P12 pups and kept 24 days in culture. KCNC3 (red), calbindin (green), DAPI (blue). Left panels: WT and right panels Coq8a$^{-/-}$ organotypic cultures. Scale bars represent 10 µm.

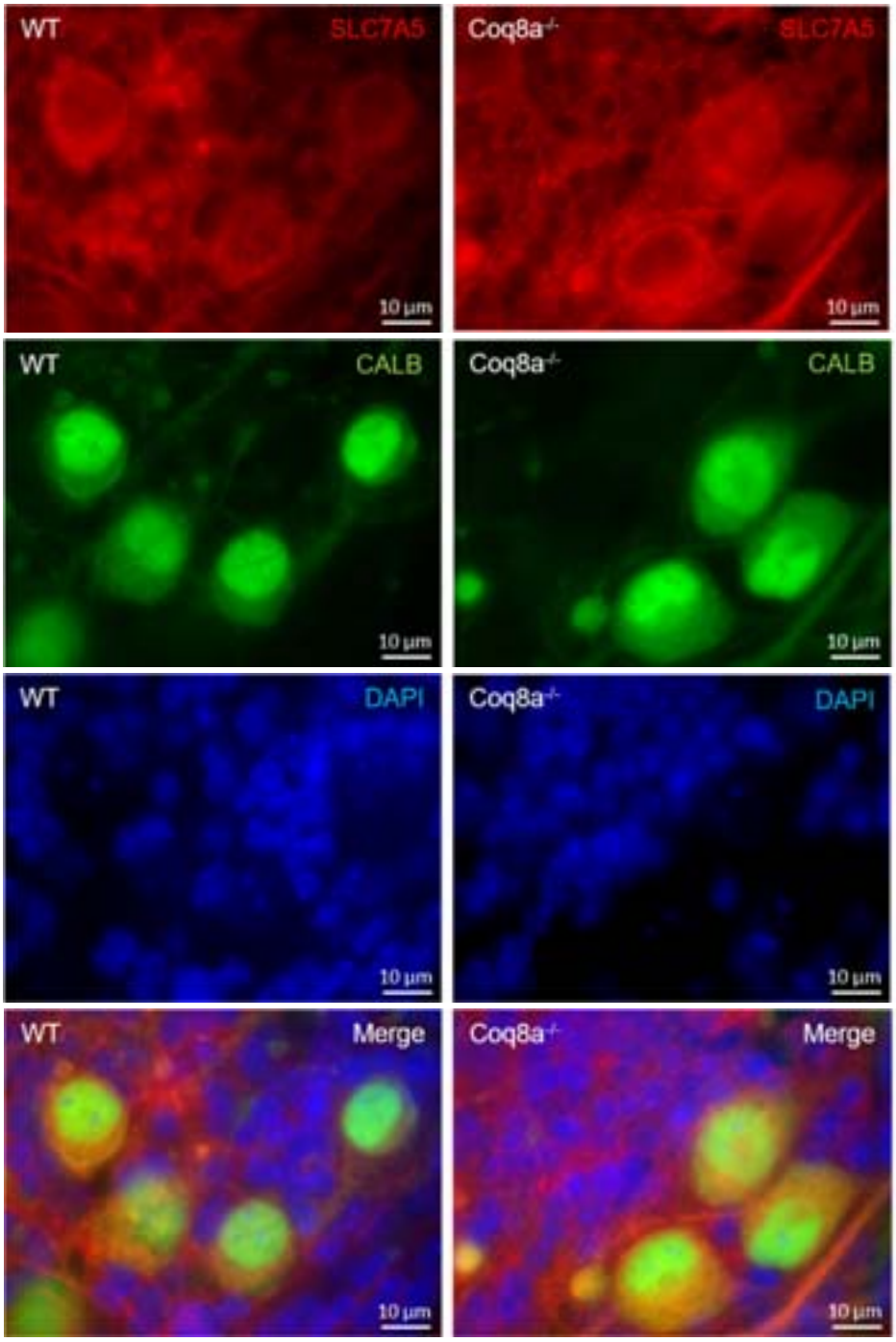

Figure 42 : Similar pattern for SLC7A5 in Coq8a$^{-/-}$ and WT cerebellar organotypic cultures.

Immunostaining of organotypic cultures derived from P12 pups and kept 24 days in culture. SLC7A5 (red), calbindin (green), DAPI (blue). Left panels: WT and right panels Coq8a$^{-/-}$ organotypic cultures. Scale bars represent 10 µm.

b. Cerebellar primary cultures

Characterization

To further our study of cerebellum, dissociated cultures were set up. These cerebellar primary cultures were established especially in order to measure mitochondrial respiration and try to understand if altered oxidative phosphorylation could be a cause for the degeneration of Purkinje neurons. As for the organotypic cultures, Coq8a$^{-/-}$ Purkinje neurons developed well and the dendrites and axons extended normally (Figure 44). The number and branching of cerebellar neurons (stained with β-III tubulin) in theses cultures was similar for both genotypes (Figure 43). A precise quantification could not be performed as neurons formed a network and overlapped. Regarding the neurons, they were mostly forming networks with cells bodies concentrated at specific places and with dendrites and axons joining the different places where the neuronal bodies were (Figure 43). Purkinje neurons tended to be close or in these dense neuronal bodies zones (Figure 43). For glial cells (stained with GFAP), as for neurons, the amount was similar between Coq8a$^{-/-}$ and WT cerebellar primary cultures (Figure 45). Glial cells were spread on the whole coverslips but the amount was more important around Purkinje neurons (Figure 45), so probably where neurons gather in a dense network. Purkinje neurons appeared with different shape so measuring the arborization would have given variable results (Figure 43, Figure 44, Figure 45 and Figure 46). Next, the network of the Golgi apparatus was looked at in these primary cultures, and like in organotypic cultures, it had a similar organization in mutant and WT cultures (Figure 46). It therefore seems that loss of COQ8A does not alter the development of these neurons in mouse, and that the degeneration phenotype appears later. Still it remains unknow if Coq8a$^{-/-}$ neurons, and Purkinje cells especially, are functional or not and if some deregulations can already be observed.

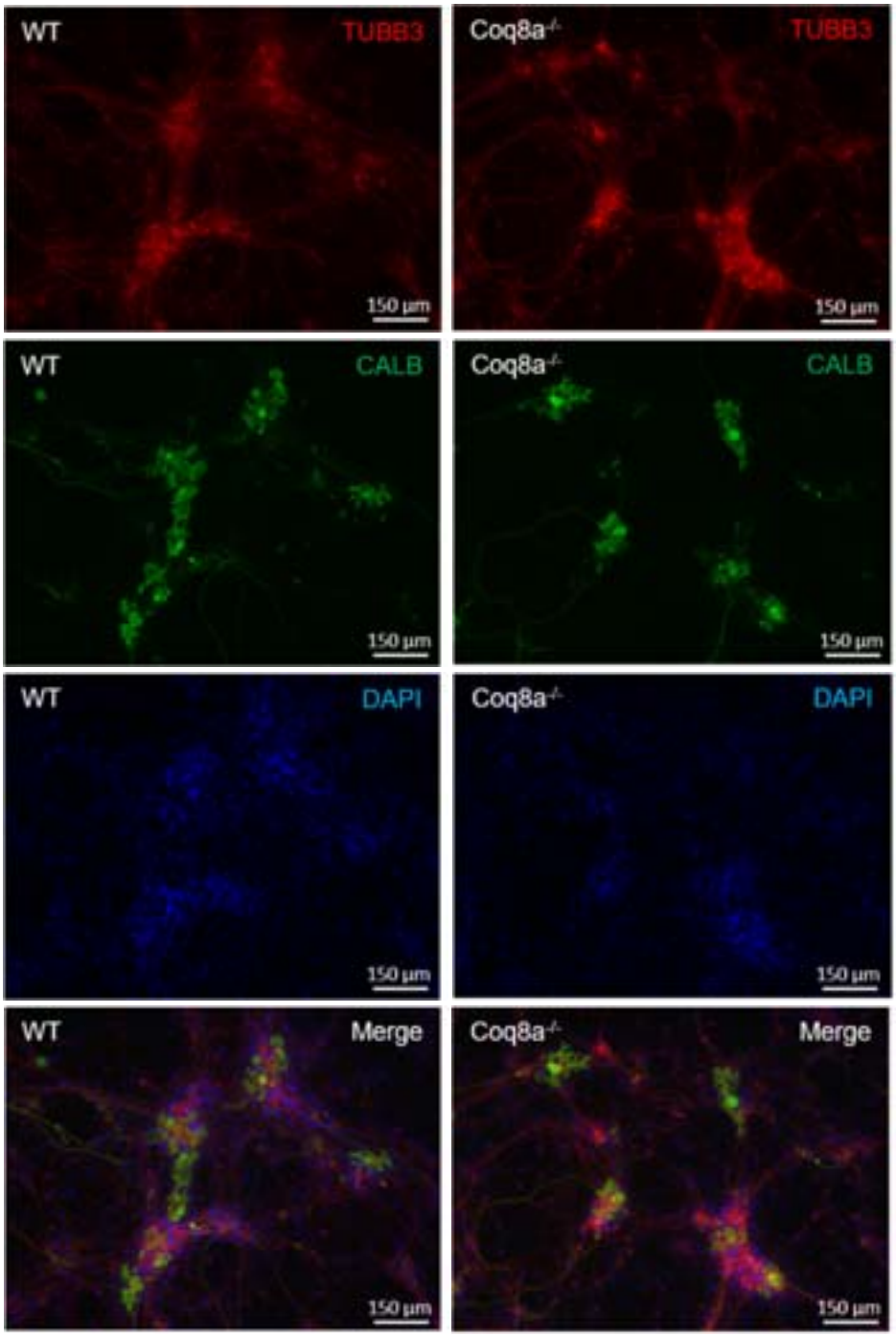

Figure 43 : Coq8a$^{-/-}$ cerebellar primary cultures have preserved neurons which form networks.

Immunostaining of cerebellar primary cultures derived from P0 pups and kept 14 days in culture. TUBB3 (staining neurons, red), calbindin (staining Purkinje neurons, green) and DAPI (blue). Left panels: WT and right panels Coq8a$^{-/-}$ cultures. Scale bars represent 150 µm.

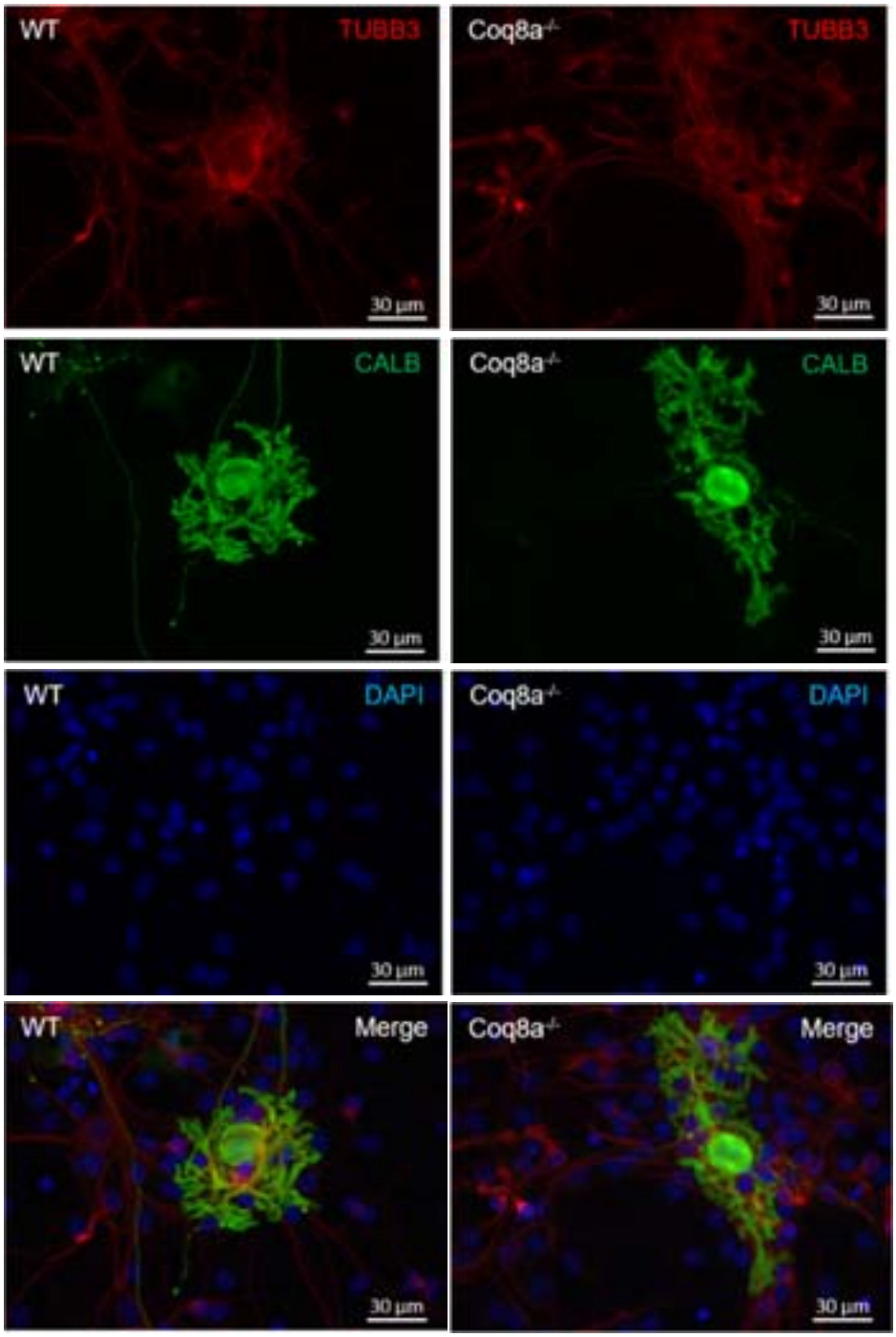

Figure 44 : Coq8a$^{-/-}$ cerebellar primary cultures have preserved neural arborization.

Immunostaining of cerebellar primary cultures derived from P0 pups and kept 14 days in culture. TUBB3 (staining neurons, red), calbindin (staining Purkinje neurons, green) and DAPI (blue). Left panels: WT and right panels Coq8a$^{-/-}$ cultures. Scale bars represent 30 µm.

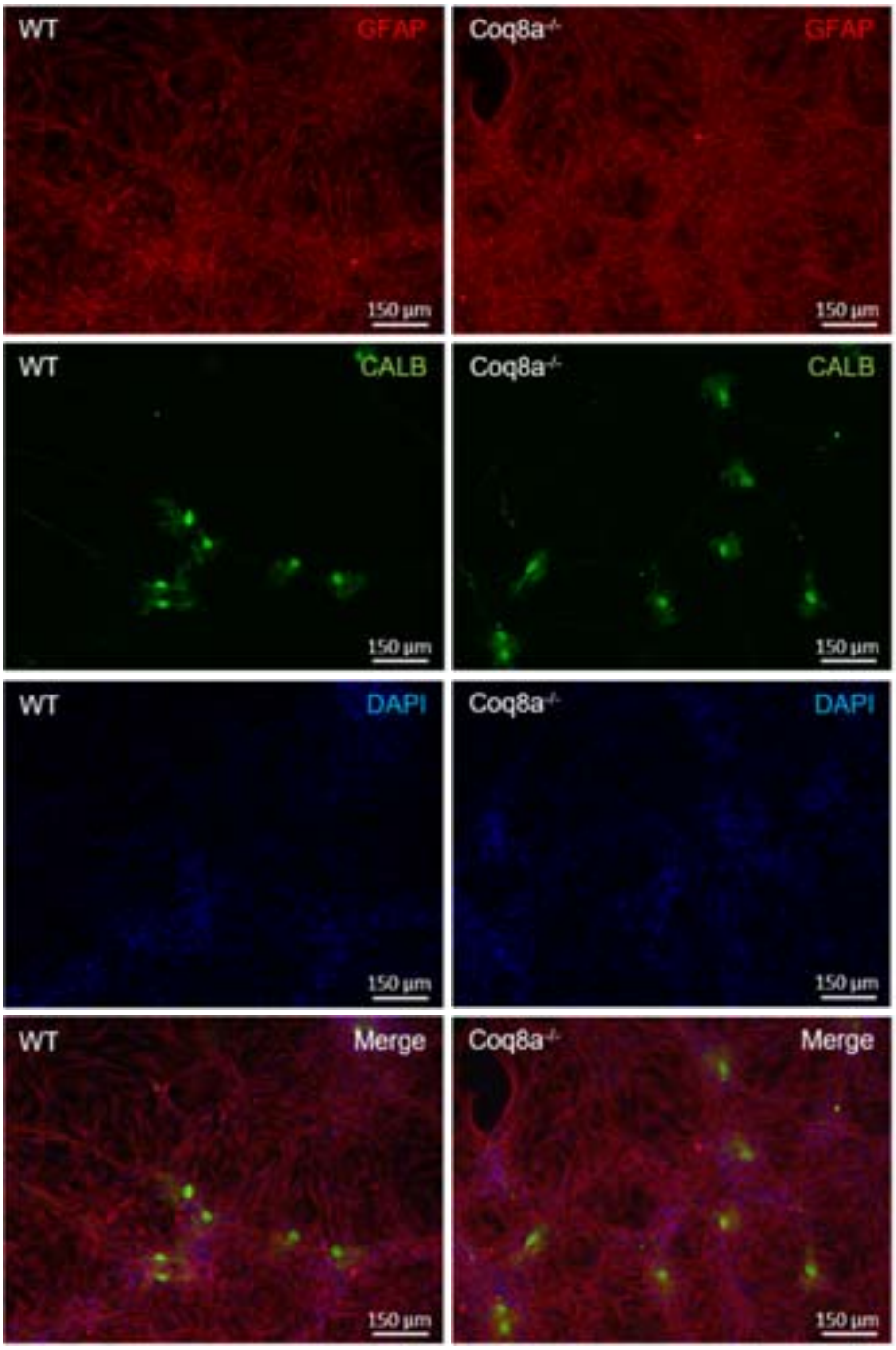

Figure 45 : Coq8a$^{-/-}$ cerebellar primary cultures have preserved Purkinje neurons and glial cells.

Immunostaining of cerebellar primary cultures derived from P0 pups and kept 14 days in culture. GFAP (staining glial cells, red), calbindin (staining Purkinje neurons, green) and DAPI (blue). Left panels: WT and right panels Coq8a$^{-/-}$ cultures. Scale bars represent 150 µm.

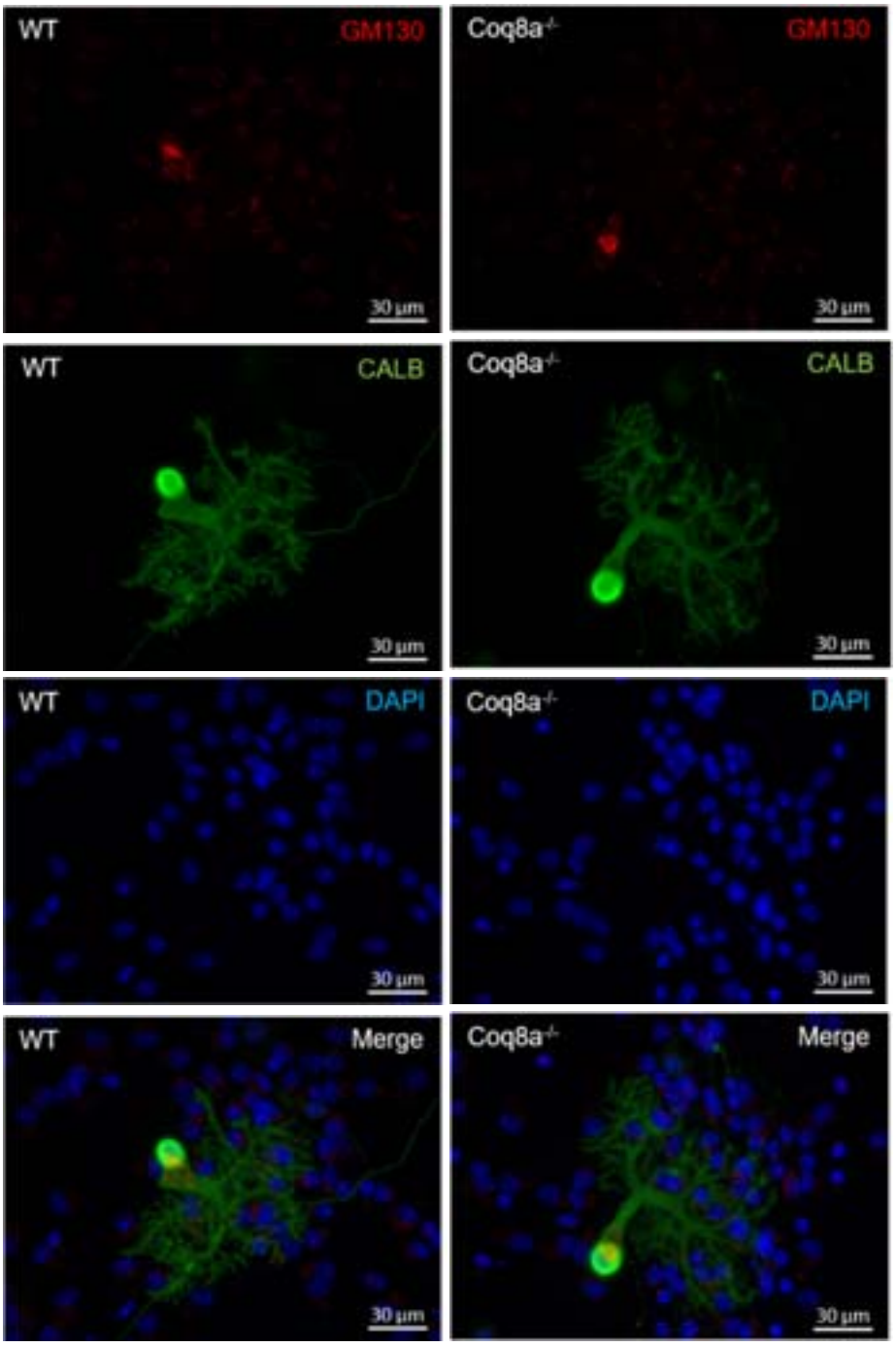

Figure 46 : Golgi apparatus is similar in Coq8a$^{-/-}$ and WT cerebellar primary cultures.

Immunostaining of cerebellar primary cultures derived from P1 pups and kept 14 days in culture. GM130 (staining Golgi apparatus, red), calbindin (staining Purkinje neurons, green) and DAPI (blue). Left panels: WT and right panels Coq8a$^{-/-}$ cultures. Scale bars represent 30 µm.

3. CoQ levels in cerebellum

COQ7 was diminished in all previously tested tissues, thus a similar pattern was awaited in the cerebellum. This could be confirmed in cerebellar extracts of 5 and 10 weeks old mice, with COQ7 levels in Coq8a$^{-/-}$ mice cerebellum being less than half of the amount observed in WT in 10 weeks old mice and less than one tenth in 5 weeks old mice (Figure 47). The variability of COQ7 expression between 5 and 10 weeks old mice is probably due to a problem with the Western blot or reflect a non-homogeneous expression between mice. Furthermore, for 10 weeks old mice levels were only assessed in three mice compared to the six mice at 5 weeks. Although this difference does not seem to be biologically relevant, if it was confirmed it would indicate a regulatory mechanism, to compensate and increase COQ7 expression over time.

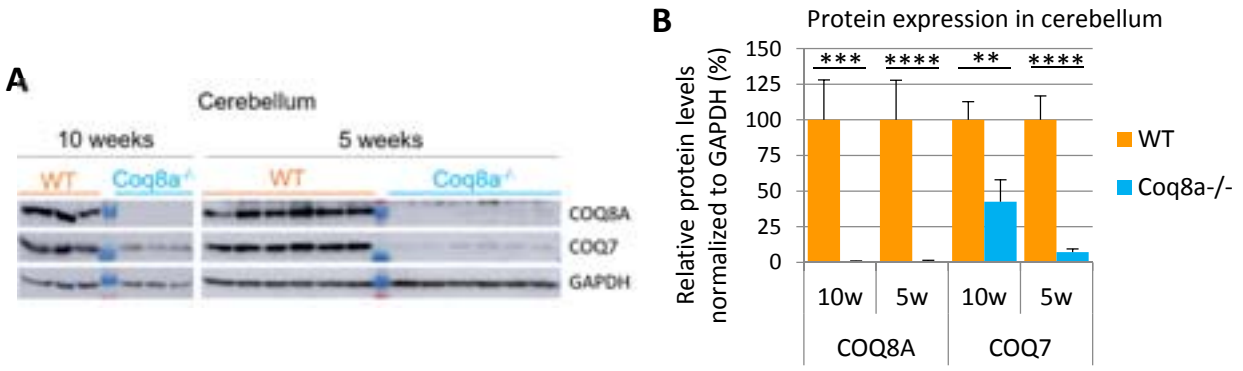

Figure 47 : Loss of COQ8A induces a deficiency of COQ7 in cerebellum.

A) Western blots showing COQ8A and COQ7 expression in cerebellum of 10 and 5 weeks old mice, GAPDH taken as controls. B) Quantification of protein levels using Fiji. Protein levels are normalized over GAPDH expression and plotted as a percentage compared to WT. Error bars: SD, **=p<0.01, *** = p<0.005, ****=p<0.00005.

Organotypic and primary cerebellar cultures are derived from young pups. It was known that COQ7 levels were already deregulated in embryos, but on whole embryos extract. To make sure this was also the case in cerebellum at the time when the cultures are performed, the experiment was repeated with 6 to 8 days' cerebellar extracts. Surprisingly, COQ7 levels are similar to WT in Coq8a$^{-/-}$ cerebellum of 1 week old mice (Figure 48). Further experiments are needed to assess the levels of this protein when cerebellum is in culture. This will enable to determine if organotypic and primary cerebellar cultures are good models to study ARCA2 or not.

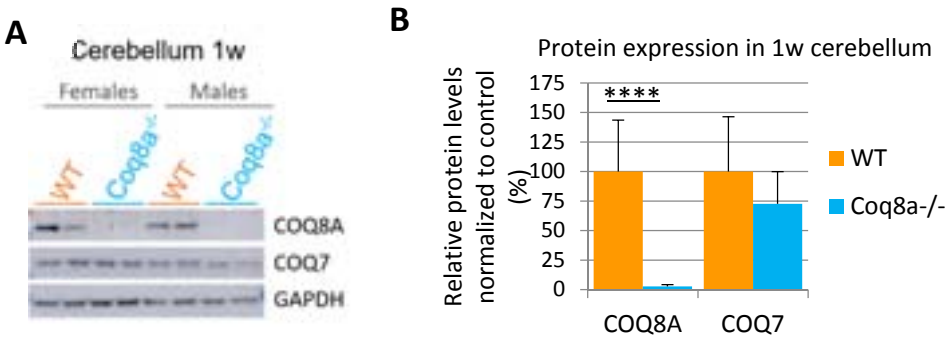

Figure 48 : Loss of COQ8A does not induce a deficiency in COQ7 in cerebellum of 1 week old mice.

A) Western blots showing COQ8A and COQ7 expression in cerebellum of 1 week old mice, GAPDH taken as control. B) Quantification of protein levels using Fiji. Protein levels are normalized over GAPDH expression and plotted as a percentage compared to WT. Error bars: SD, ****=p<0.0005.

4. Pure genetic background

A question that arose during my thesis was whether the genetic background of the animals could influence the phenotype. Indeed, it was previously shown that some phenotypes are more pronounced in some strains, and varies depending on the genetic background (Crawley et al., 1997; Doetschman, 2009; Lalouette et al., 2001). Initially, the Coq8a$^{-/-}$ mice generated had a mixed background (C57/BL6J 53.13%, C57/BL6N 34.37%, 129S2/svPas 12.5%). The mouse line was progressively backcrossed to generate pure C57/BL6J Coq8a$^{-/-}$ mice and their WT littermates. Coq8a$^{-/-}$ mice were characterized while in a mixed background. To determine if the ataxic phenotype was retained in the pure background, to which we got to, behavioral analyses were repeated. On the one hand, results of the beam test were not clear as WT mice also did a lot of mistakes, misplacing their hindlimbs on the beam (Figure 49A). Previously, when Floriana Licitra had performed the beam test in 20 weeks old mice, Coq8a$^{-/-}$ mice did approximately 4 mistakes and WT 1 (Licitra, 2013; Stefely et al., 2016), whereas in this recent trial, around 5 mistakes were counted for 25 weeks old mice of both genotypes (Figure 49A). A new cohort with more mice is needed to get a clearer answer (the recent study was performed with 4 mice per sex and genotype whereas it had previously been done with 8 to 12 mice). On the other hand, retention time on the accelerating rotarod yielded similar results as previously described (Stefely et al., 2016). Knock-out mouse were less able to remain on the accelerating rod compared to WT (Figure 49B). This rotarod test evaluates the general coordination of the mice, and cerebellum is implicated in this task, so a cerebellar affection can be depicted by a diminished retention time. The ataxic phenotype seems to be preserved even in the pure background, but further analysis would be needed for confirmation. Validation could be performed by analyzing the mouse gait with footprint for example.

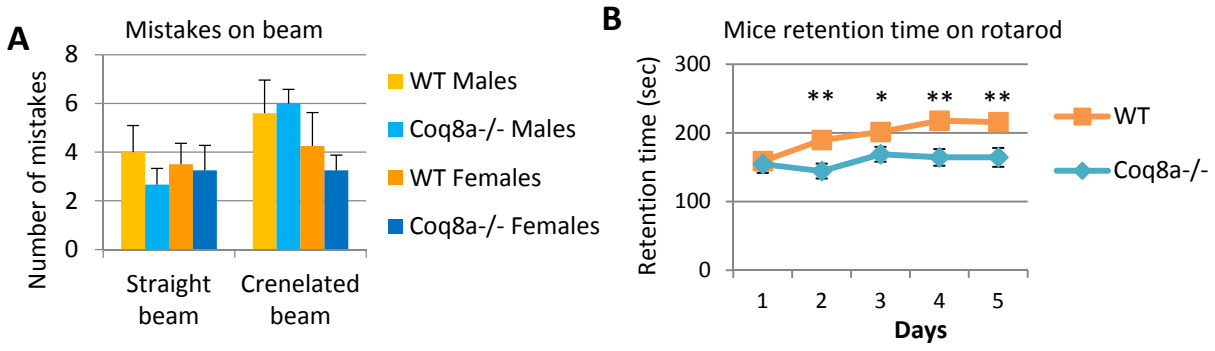

Figure 49 : Coq8a$^{-/-}$ mice still present motor coordination deficiency on accelerating rotarod.

A) Number of hindlimb coordination errors on beam test, of 25 weeks old Coq8a$^{-/-}$ and WT mice, mean ± SEM, n=4. B) Retention time on an accelerating rotarod (in seconds) of 20 weeks old Coq8a$^{-/-}$ and WT mice. Mean ± SEM, *=p<0.05, **=p<0.01, n=7.

As behavioral analyses were repeated, we also repeated electron microscopy in 30 weeks old mice cerebellum. As previously (Stefely et al., 2016), shrunken Purkinje neurons were observed only in mutant cerebellum (Figure 50 and Figure 51). Granule cells had a normal structure (Figure 50) and some Purkinje neurons had lobulated nuclei (Figure 51A) in both Coq8a$^{-/-}$ and WT cerebellum. Dilated Golgi apparatus appeared in Coq8a$^{-/-}$ Purkinje neurons, and was also detected in WT Purkinje neurons but to a lesser extent (Figure 51 B and D). Still, this dilatation seemed more pronounced in degenerating, shrunken neurons. It is not known whether this dilation is induced by the degeneration of cells, being a consequence, or if it is more the cause for degeneration. In conclusion, the ARCA2 phenotype characterized by the degeneration of Purkinje neurons in adult mice, with Golgi dilatation, could be observed and confirmed the preserved phenotype in the Coq8a$^{-/-}$ mice with a pure C57/BL6J background.

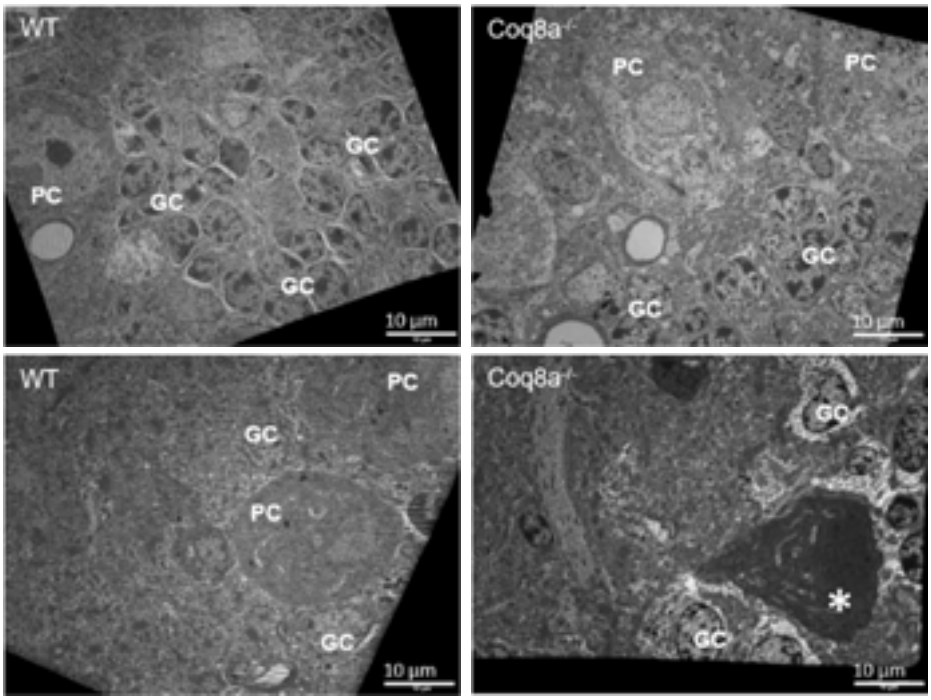

Figure 50 : Degenerating Purkinje neurons observed in Coq8a$^{-/-}$ cerebellum of 30 weeks.

Electron microscopy of 30 weeks old cerebellum. Healthy neurons, PC: healthy Purkinje neuron, GC: granule cell, *: shrunken neuron. Scale bars represent 10 µm. Left panels: WT and right panels Coq8a$^{-/-}$ cultures.

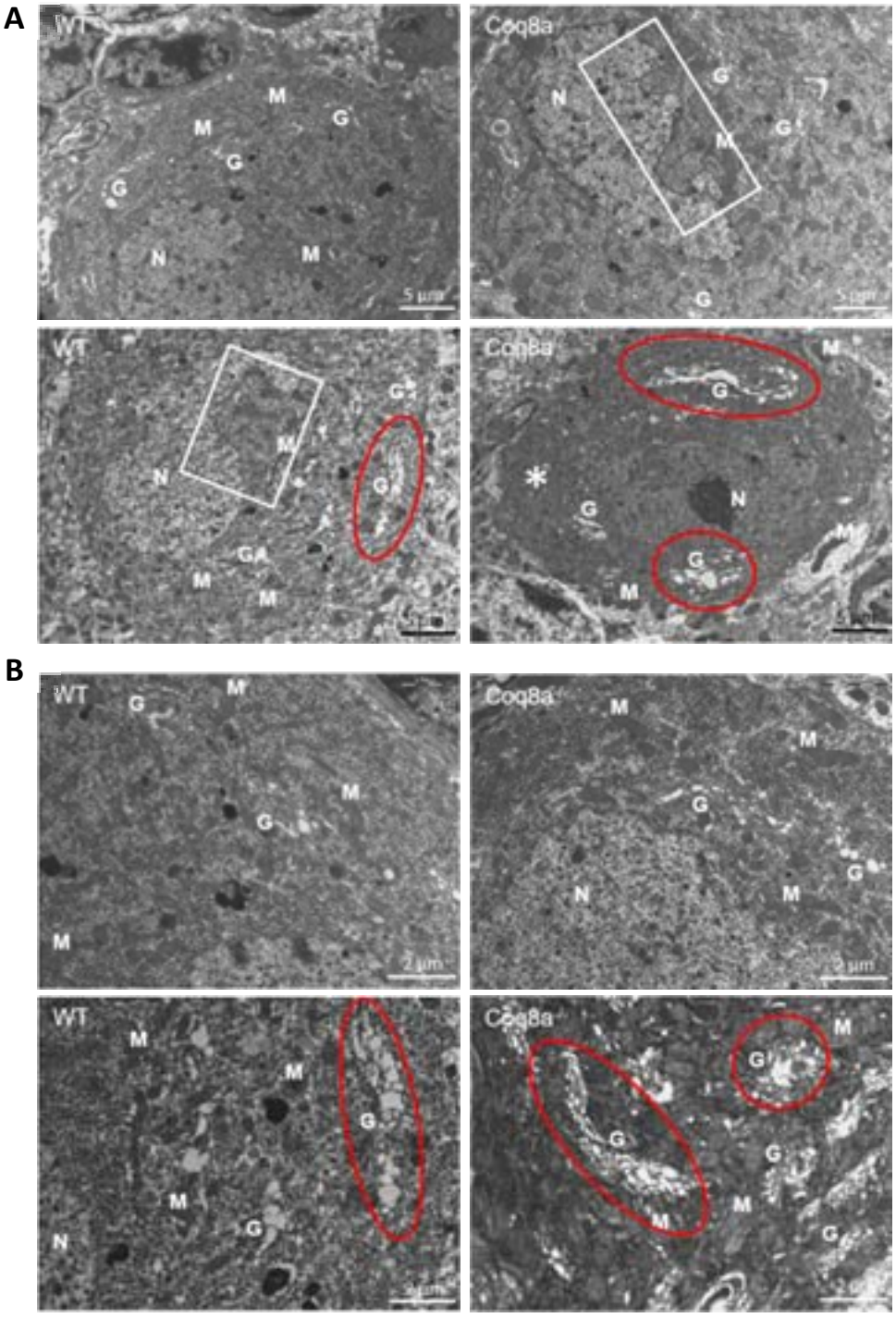

Figure 51 : Swollen Golgi observed in Coq8a$^{-/-}$ and WT cerebellum of 30 weeks.

Electron microscopy of 30 weeks old cerebellum. A) Normal cytoplasm with classical structures, lobulated nuclei (white rectangle), cytoplasm with swollen Golgi (red circle). Degenerating, shrunken neurons (*) Scale bars represent 5 µm. B) Classical Golgi, and swollen Golgi (red circle). Scale bars represent 2 µm. N: nucleus, G: Golgi apparatus, M: mitochondria. Left panels: WT and right panels Coq8a$^{-/-}$ cultures.

5. Deregulated pathways

a. Transcriptional level

Previously, in order to uncover molecular pathways implicated in the pathology, RNA-sequencing was performed by Floriana Licitra, in muscle and cerebellum of 30 weeks old Coq8a$^{-/-}$ and WT mice (Licitra, 2013). A few hundred genes appeared as significantly deregulated. We were hence interested in knowing which deregulated molecular pathways, in the cerebellum, can lead to ataxia, and how early these deregulations arise. The analysis was thus pursued with an Ingenuity Pathway Analysis (IPA, Quiagen) of cerebellum RNA-sequencing data. No clear pathways came out of in this IPA analysis, due to the low number of transcripts deregulated. Indeed, in 30 weeks old Coq8a$^{-/-}$ mice cerebellum, 38 transcripts were found to be significantly down-regulated and 36 upregulated (considering the adjusted p-value), by RNA-sequencing. Still, when the diseases and functions predicted to be affected by the IPA software were examined, glucose metabolism and neuronal functions came out (Table 7). When studying the RNA-sequencing list of genes, in light of the IPA results, it appeared that a number of genes were implicated in ion transport or lipid metabolism. In regards to COQ8A function, and the phenotypes observed in mutant mice (Stefely et al., 2016), these functions were interesting to explore. Validation of selected genes was first performed by qRT-PCR in cerebellum of 30 weeks old mice. If transcriptional deregulation could be confirmed at 30 weeks, the transcriptional levels were progressively assessed in younger mice up to 1 week (30, 20, 10, 5 and 1 week).

Categories	Diseases or functions annotation	Predicted activation state and activation z-score	Genes	Nb of genes
Cancer, organismal injury and abnormalities	tumorigenesis of tissue	Increased 2,508	Ache, Apoa2, Atf4, Atp1a3, B3galt2, Cars, Copa, Dusp12, Grin2d, Hsd17b7, Kcnab3, Kcnh2, Kcnj10, Kcnk2, Lrp1b, Mthfd2, Myoc, Pcp4, Plch1, Plcl2, Ppargc1a, Ret, Sccpdh, Sesn2, Slc24a3, Slc6a7, Slc7a3, Slc7a5, Syt17, Tmem25, Trpm2	477
Metabolic disease	glucose metabolism disorder	-1,829	Ache, Apoa2, Atf4, Cars, Ifi202b, Kcnab3, Kcnh2, Lrp1b, Plin2, Ppargc1a, Rsad2	97
Neurological or muscular disorders	neuromuscular disease	-1,387	Ache, Atf4, Gas5, Grin2d, Hpca, Kcnh2, Kcnk2, Ppargc1a, Ret, Slc24a3, Vamp1	73
Endocrine system	insulin-dependent diabetes		Ifi202b, Kcnab3, Lrp1b	43
Neurological disease	Movement Disorders	-1,660	Ache, Atf4, Atp1a3, Coq8a, Cplx1, Gas5, Grin2d, Hpca, Kcnh2, Kcnj10, Kcnk2, mt-nd5, Ppargc1a, Vamp1	78
Neurological Disease	progressive motor neuropathy	-0,555	Ache, Atf4, Grin2d, Kcnh2, mt-nd5, Mthfd2, Nrxn1, Ret, Rsad2, Slc24a3, Vamp1	46
Cell death and survival	neuronal cell death	Decreased -2,538	Ache, Atf4, Kcnj10, Nos1ap, Pcp4, Ret	48
Nervous system development and function	development of neurons	Increased 3,325	Ache, Faim2, Kcnj10, Myoc, Nrxn1, Ret	56
Molecular transport	transport of monovalent inorganic cation	3,325	Atp1a3, Kcnab3, Kcnh2, Kcnj10, Kcnk2, Slc7a5, Slc8a3	21

Table 7 : Ingenuity Pathway Analysis, diseases and functions probably affected in cerebellum according to RNA-sequencing data.

For a clear picture, redundant functions or diseases were omitted and only genes deregulated by RNA-sequencing were kept in the gene column. The predicted activation score and the activation z-score correspond to the probability of the specified pathway to be up or down-regulated. The number of genes corresponds to all the genes described as being implicated in this pathway.

Out of the fifty genes already tested (see ANNEX Table 10), twenty-seven are deregulated as early as 5 weeks in the cerebellum of knock-out mouse. Furthermore, two genes even have reduced expression at 1 week. *ApoAII* (encoding an apolipoprotein found in high density lipoprotein lipoparticles), and *Copa* (a gene coding for a protein mediating the retrograde transport of dilysine motifs from Golgi to ER) are two genes for which expression is consistently deregulated in Coq8a$^{-/-}$ cerebellum from 1 to 30 weeks (Figure 52, Figure 53). These deregulations are maintained over time, but it is still unknown how early they appear. These two transcripts levels must yet be assessed in the *in vitro* models and will

enable to judge if the cultures are useful for further experiment and reproduce these phenotypes or not.

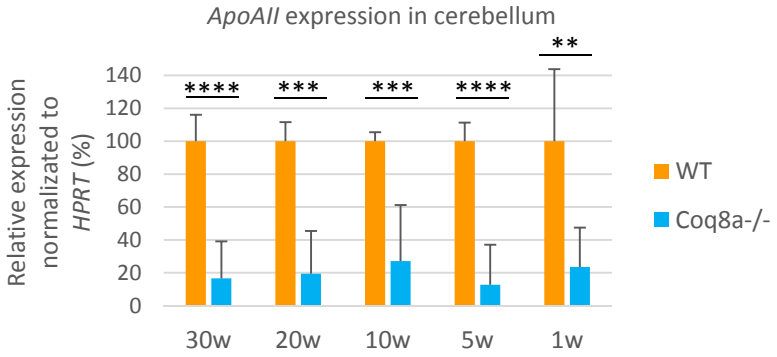

Figure 52 : Coq8a$^{-/-}$ mice have reduced levels of ApoAII from 1 to 30 weeks in cerebellum.

Relative expression of ApoAII in cerebellum of 30, 20, 10, 5 and 1 week old Coq8a$^{-/-}$ and WT mice (n=6). For all the experiments the transcripts levels were normalized over the transcripts levels of Hprt (control gene). Error bars : SD, ** = p<0.005, ***=p<0.0005 ****=p<0.00005.

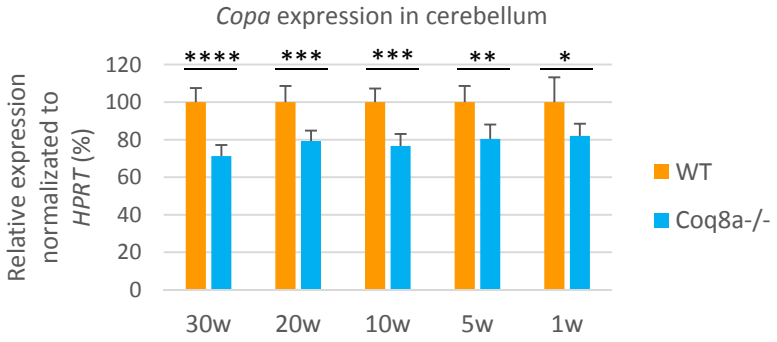

Figure 53 : Coq8a$^{-/-}$ mice have reduced levels of COPA from 1 to 30 weeks in cerebellum.

Relative expression of Copa in cerebellum of 30, 20, 10, 5 and 1 week old Coq8a$^{-/-}$ and WT mice (n=6). For all the experiments the transcripts levels were normalized over the transcripts levels of Hprt (control gene). Error bars: SD, *=p<0.05, ** = p<0.005, ***=p<0.0005 ****=p<0.00005.

The decrease in *ApoAII* transcription in Coq8a$^{-/-}$ mice cerebellum is striking, with around 80% reduction (Figure 52), although it is a gene which is not well expressed in the cerebellum. This low expression might be due to an expression restricted to a specific cell type. So far ApoAII was only reported as being present in high density lipoproteins and in liver (Maïga et al., 2014). It will be seen (in section VII on Dyslipidemia, in Figure 63C) that *ApoAII* levels are not altered in Coq8a$^{-/-}$ liver. It therefore seems that this deregulation is specific to cerebellum.

Deregulation of some potassium channels were revealed to induce ataxia, and in some cases led to abnormal firing of Purkinje neurons (Bockenhauer et al., 2009; Duarri et al., 2012; Irie et al., 2014). Regarding the altered pacemaker activity in the ARCA2 mouse model (Stefely et al., 2016), potassium channels found to be significantly deregulated by RNA-sequencing were tested. Two, out of the four were deregulated in cerebellum of 5 weeks old mice, namely *Kcnab3* and *Kcnj10*, being upregulated (Figure 54). *Kcnab3* encodes a regulatory subunit of a potassium channel: it modulates the activity of Kv1.5 which is a voltage gated channel implicated during action potential, by inducing a faster inactivation of this pore (Leicher et al., 1998). *Kcnj10* is described to be mainly expressed in glial cells (Kir4.1 channel) where it has a role in buffering extracellular potassium, and in cerebellum it is expressed in the deep cerebellar nuclei as well as in the Purkinje cell layer in Bergmann glia (Poopalasundaram et al., 2000; Takumi et al., 1995).

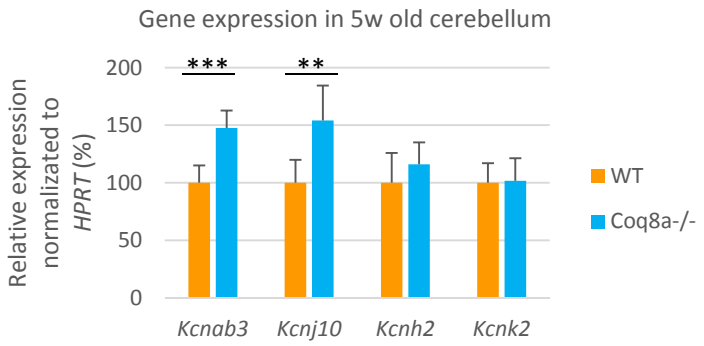

Figure 54 : Kcnab3 and Kcnj10 are upregulated in cerebellum of 5 weeks old Coq8a$^{-/-}$ mice.

Relative expression of Kcnab3, Kcnj10, Kcnh2 and Kcnk2 in cerebellum of 5 weeks old Coq8a$^{-/-}$ and WT mice (n=6). For all the experiments the transcripts levels were normalized over the transcripts levels of Hprt (control gene). Error bars: SD, ** = p<0.005, ***=p<0.0005.

Transporters and channels also contribute to neuronal functions. Thus, the ones found to be deregulated by RNA-sequencing were assessed. The transcript levels of three solute carriers were found to be significantly deregulated (Figure 55). These three gene are: *Slc6a7*, encoding a synaptic protein, implicated in L-proline (a GABA-mimetic) uptake, most probably having a regulatory role in presynaptic excitatory transmission (Crabtree et al., 2016; Velaz-Faircloth et al., 1995); *Slc7a3*, encoding a cationic L-amino acid transporter expressed in the granular and Purkinje cell layer neurons, which has high affinity for L-arginine, an amino acid that could have a regulatory role in nitric oxide synthesis (Hosokawa et al., 1999; Ito and Groudine, 1997); and *Slc24a3*, encoding a sodium/calcium exchanger, useful for calcium homeostasis, and expressed in cerebellar granule cells (Kiedrowski et al., 2002; Kraev et al., 2001).

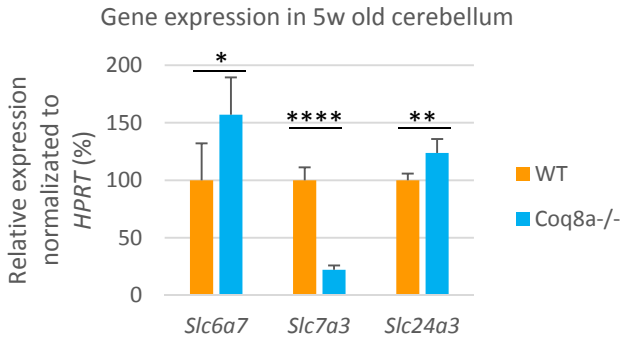

Figure 55 : Some ionic transporters are upregulated in cerebellum of 5 weeks old Coq8a$^{-/-}$ mice.

Relative expression of Slc6a7, Slc7a3 and Slc24a3 in cerebellum of 5 weeks old Coq8a$^{-/-}$ and WT mice (n=6). For all the experiments the transcripts levels were normalized over the transcripts levels of Hprt (control gene). Error bars: SD, *=p<0.05, ** = p<0.005, ****=p<0.00005.

Furthermore, other gene implicated in neuronal function or neurotransmitter modulation were also found to be upregulated as early as 5 weeks in cerebellum of Coq8a$^{-/-}$ mice (Figure 56). *Ache* inactivates acetylcholine esterase neurotransmitter to terminate signal transmission and is mostly expressed in mossy fibers during adulthood in mouse (Olschowka and Vijayan, 1980). *Cplx1*, is mainly expressed in deep cerebellar nuclei, and in Purkinje cells, where it acts as a regulator of neurotransmitter release depending on calcium concentration (Freeman and Morton, 2004; Xue et al., 2007). *Grin2d* codes for a subunit of a NMDA glutamatergic receptor (NMDAR2D) involved in neuronal excitation, and is expressed in Purkinje as well as in granule, Golgi, basket and stellate cells (Hess et al., 1998; Scherzer et al., 1997). *Hpca* product is a neuronal calcium sensor implicated in neuronal plasticity and is expressed in Purkinje neurons (Kobayashi et al., 2005; Saitoh et al., 1993). Expression in Purkinje neurons was also found for *Nrsn1*, which is necessary for neurite outgrowth and axonal regeneration

(Kiyonaga-Endou et al., 2016; Suzuki et al., 2007). *Syt17* encodes a synaptotagmin: a protein that should regulate membrane fusion or trafficking in axons (Dean et al., 2012). Lastly, Trpm2 is widely expressed (in neurons and glial cells) and functions as a non-selective calcium channel which was described to be activated by multiple pathways such as oxidative stress or adenine second messengers (Xie et al., 2010).

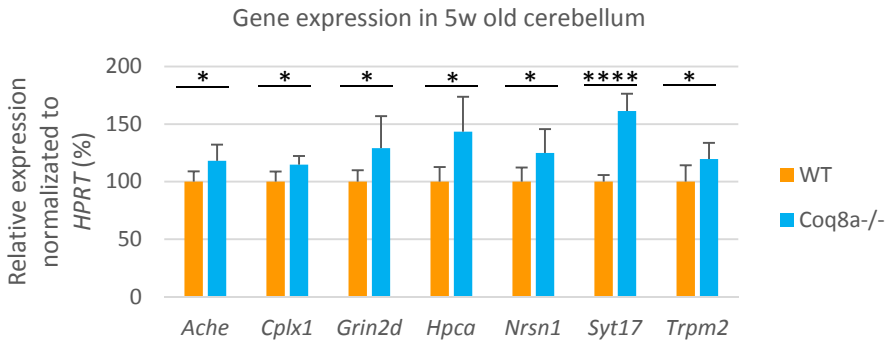

Figure 56 : Genes implicated in neuronal functions are upregulated in cerebellum of 5 weeks old Coq8a$^{-/-}$ mice.

Relative expression of Ache, Cplx1, Grin2d, Hpca, Nrsn1, Syt17 and Trpm2 in cerebellum of 5 weeks old Coq8a$^{-/-}$ and WT mice (n=6). For all the experiments the transcripts levels were normalized over the transcripts levels of Hprt (control gene). Error bars: SD, *=p<0.05, ****=p<0.00005.

COQ8A link with neuronal functions remains puzzling, whereas its implication in metabolism, in particular lipid metabolism, seems more obvious in regards to its functions described so far, as an unorthodox protein kinase like (Stefely et al., 2016). Therefore, some gene were selected for validation of transcriptional deregulation. Eleven were found to be deregulated as early as 5 weeks in Coq8a$^{-/-}$ mouse cerebellum (Figure 57). This list includes *Asns*, *Atf4*, *βIII-GalT2*, *Cars*, *Faim2*, *Nudt3*, *Plch1*, *Ret*, *Sccpdh*, *Sesn2* and *Snhg11*.

Gene	*Functions*
Atf4	Transcriptional regulator implicated in a variety of stress responses, including amino acid deprivation, unfolded protein response, ER and oxidative stress (Ameri and Harris, 2008). Mostly shown to be upregulated in metabolic stress conditions (Siu et al., 2002)
Asns	Enzyme converting glutamine, ATP and aspartate to asparagine (Richards and Schuster, 1998). Its mRNA levels were described to be increased in case of amino acid starvation and ER stress, under the control of *Atf4*, as upregulation of its transcripts levels follow Atf4 transcriptional upregulation (Chen et al., 2004; Hutson and Kilberg, 1994).
Sesn2	Expressed under the control of *Atf4* (Brüning et al., 2013), in particular in the context of amino acid starvation when eIF2α upregulates *Atf4* which in turns upregulates *Sesn2*

	transcript levels (Ye et al., 2015). SESN2 also regulates various other stress responses such as responses to hypoxia, low glucose, excessive fatty acid or oxidative stress, each time under the control of a specific transcription factor (Garaeva et al., 2016).
β3-Gal-T2	Galactosyltransferases, which specifically catalyzes glycosylation of saccharide with a beta-N-acetylglucosamine (βGlcNAc) terminal residue (Amado et al., 1998; Kolbinger et al.).
Cars	Involved in protein synthesis by its gene product cysteinyl-tRNA synthetase, and was shown to inhibit certain lipid oxidation and induce transcription of some serine biosynthesis and transsulfuration genes when knocked-down (Davidson et al., 2001; Hayano et al., 2016).
Faim2	Also named *Lfg*, is expressed in the neurons of the Purkinje and granule cell layers in cerebellum (Schweitzer et al., 2002). It encodes a protein specifically protecting cells from Fas-induced apoptosis, localized in plasma lipid rafts (Fernández et al., 2007; Somia et al., 1999). Transcriptional regulation of this gene seems to be regulated by phosphatidylinositol-3-kinase/Akt/protein kinase B, and its upregulation was shown to protect neurons from apoptosis (Beier, 2005).
Nudt3	High transcripts levels found in mouse brain, including in the cerebellum (Williams et al., 2015). NUDT3, also named DIPP, is a RNA decapping enzyme, involved in regulation of mRNA decay, which controls cell migration and it hydrolyzes diphosphoinositol polyphosphates (Grudzien-Nogalska et al., 2016).
Plch1	Phospholipase, hydrolyzing phosphatidylinositol 4,5-bisphosphate (PtdIns(4,5)P2) to convert it to the secondary messenger inositol (1,4,5)-trisphosphate (Ins(1,4,5)P3) (Kim et al., 2011). This enzyme has a role in calcium signaling mediated by G-protein-coupled receptor and is activated by ER calcium release (Kim et al., 2011). Its transcripts are expressed throughout the brain including in the cerebellar Purkinje cell layer (Hwang et al., 2005).
Ret	Found in the Purkinje cell layer and to a lesser extend in the granule cell layer of the cerebellum (Burazin and Gundlach, 1999). RET is recruited to lipid rafts (Tansey et al., 2000). This protein acts as a receptor tyrosine kinase, activated by glial cell line derived neurotrophic factor (GDNF), and is implicated in dopaminergic neurons maintenance and regeneration, as well as dendrites development (Kowsky et al., 2007; Luca Colucci-D 'amato et al., 1996; Soba et al., 2015). *Ret* overexpression was found to rescue mitochondrial impairment and bioenergetics, in case of PINK1 knock-down (Klein et al., 2014). When *Ret* was conditionally deleted, increase apoptosis could be observed in the cerebellar molecular layer interneurons, which led to Purkinje neurons increased firing frequencies but no motor or coordination defective activity (Sergaki et al., 2017)
Sccpdh	Putative saccharopine dehydrogenase-like oxidoreductase which is supposed to act in lysine catabolism by converting L-lysine to L-saccharopine or further to L-glutamate or α-ketoglutarate in presence of NAD^+ or $NADP^+$ as oxidant (de Mello Serrano et al., 2012; Pink et al., 2011). These ascribed functions are based on homology, and it seems that in mammals the saccharopine pathway occurs only in mitochondria (Hallen et al., 2013).
Snhg11	Non-protein-coding small nucleolar RNA (C20orf198), which might cause obesity (Naukkarinen et al., 2010).

According to the gene regulations described in the table above, it could be that the decrease in *Atf4* expression leads to the decrease of *Asns* expression (Chen et al., 2004; Hutson and Kilberg, 1994). The same could be true for *Sesn2*, which was shown to be expressed under the control of *Atf4* (Brüning et al., 2013).

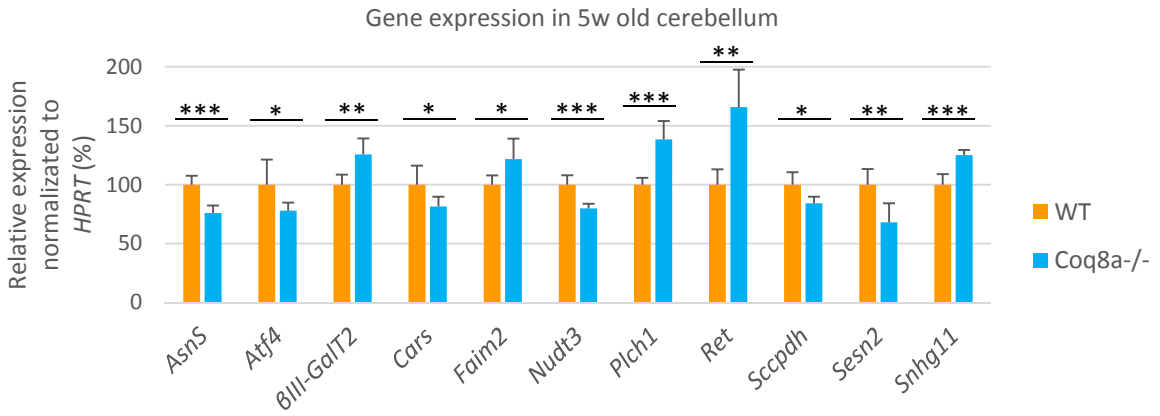

Figure 57 : Genes implicated in metabolism are deregulated in cerebellum of 5 weeks old Coq8a$^{-/-}$ mice.

Relative expression of Asns, Atf4, βIII-GalT2, Cars, Faim2, Nudt3, Plch1, Ret, Sccpdh, Sesn2 and Snhg11 in cerebellum of 5 weeks old Coq8a$^{-/-}$ and WT mice (n=6). For all the experiments the transcripts levels were normalized over the transcripts levels of Hprt (control gene). Error bars: SD, *=p<0.05, **=p<0.005, ***=p<0.0005.

Finally regarding the transcriptional deregulations, sixteen genes, not deregulated in RNA-sequencing data of 30 weeks old mice, were assessed to gain insight in the possibly deregulated mechanisms. *ApoAII* was found to be significantly deregulated, so we were wondering if this was specific to this apolipoprotein or if others would also have decreased expression. APOE and APOJ are known to be well expressed in the brain and were described to be misregulated notably in Alzheimer's disease (Stukas et al., 2014). Moreover, APOAII was mostly described as a component of HDL, and so was APOAI (Alexander and Phillips, 2013). Out of these genes only *ApoAII* (as previously described) and ApoAI were significantly downregulated in Coq8a$^{-/-}$ mice cerebellum at 5 weeks (Figure 58 A). *ApoE* and *ApoJ* levels remained unchanged (Figure 58 A). SREBP, sterol regulatory element-binding proteins, are transcription factors which regulate cholesterol and fatty acid biosynthesis. SREBP1C primarily induces fatty acid genes synthesis, SREBP2: cholesterol genes, whereas SREBP1a activates both cholesterol, fatty acids and triglycerides genes (Horton et al., 2002). As APOA1 in implicated in cholesterol efflux in HDL particles, we were wondering if one of these transcription factor was deregulated. Indeed, in Coq8a$^{-/-}$ cerebellum of 5 weeks old mice, *Srebp1c* was deregulated but not

Srebp1a, nor Srebp2 (Figure 58 B). *ApoAI* and *Srebp1c* levels were also assessed in cerebellum of 1 week old mice but unlike *ApoAII*, their transcript levels were similar to WT at this age. It therefore seems that *ApoAII* decreased expression is a specific event which appears early, during cerebellum development, and that it is followed by ApoAI deregulation. These results are still intriguing because the only ApoA levels found in the brain so far were assigned as coming from the peripheral circulation (Karten et al., 2006).

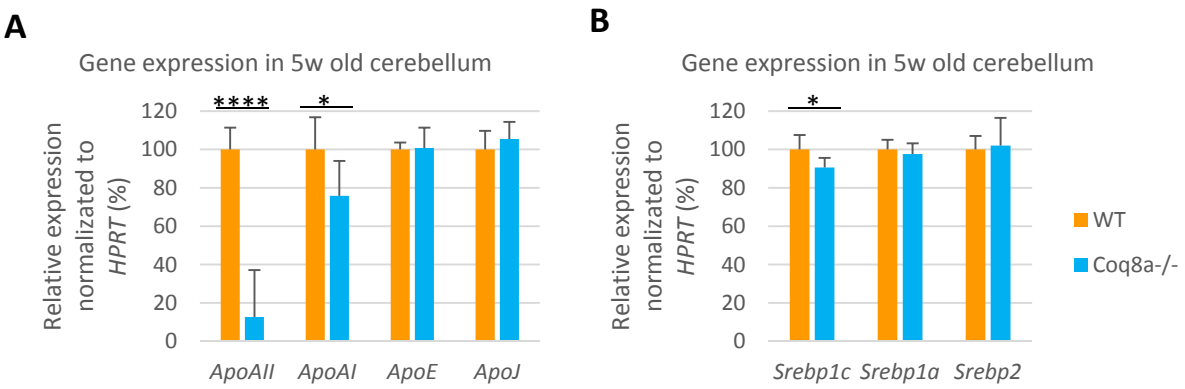

Figure 58 : Genes implicated in lipid metabolism are deregulated in cerebellum of 5 weeks old Coq8a$^{-/-}$ mice.

A) Relative expression of ApoAII, ApoAI, ApoE and ApoJ in cerebellum of 5 weeks old Coq8a$^{-/-}$ and WT mice (n=6). B) Relative expression of Srebp1c, Srebp1a and Srebp2 in cerebellum of 5 weeks old Coq8a$^{-/-}$ and WT mice (n=6). For all the experiments the transcripts levels were normalized over the transcripts levels of Hprt (control gene). Error bars: SD, *=p<0.05, ****=p<0.00005.

b. Translational level

Different mechanisms might influence the deregulation of these transcripts. It might be that some common transcriptional regulators are implicated, but they were not found yet, except for *Atf4* which might account for the deregulation of two genes: *Asns* and *Sesn2*. Moreover *Kcnj10* transcription was described to be correlated with the DNA methylation status (Nwaobi et al., 2014), which could also be the case for other genes. We started by assessing protein levels of the first transcripts found to be deregulated. For these, antibodies were ordered to be able to determine if the proteins levels were also affected or if it was restricted to transcripts levels. APOAII, COPA, KCNAB3, PLCH1 and SYT17 expression were therefore assessed. Unfortunately, antibodies for APOAII and KCNAB3 did not work in western blot or need further optimization. Nevertheless, only SYT17 was found to be significantly upregulated in the cerebellum of 5 weeks old Coq8a$^{-/-}$ mice (Figure 59). PLCH1 was found to be

significantly decreased but only in Coq8a$^{-/-}$ females, which is surprising regarding the elevated levels of transcripts measured but might reflect further regulatory mechanisms (Figure 59C). COPA had similar expression in mutant and WT mice, even when males and females were assessed separately, due to high variability in between samples. For confirmation, these results should be repeated and performed in a new cohort of mice. To further this study, the histological analysis is ongoing. KCNAB3 was already found to localize mostly in Purkinje cells soma and its levels and localization seemed similar in Coq8a$^{-/-}$ cerebellum compared to WT at 5 weeks (Figure 60). Additional experiments are now needed to explore deregulated metabolic pathways that might be of interest and linked to the ARCA2 phenotypes.

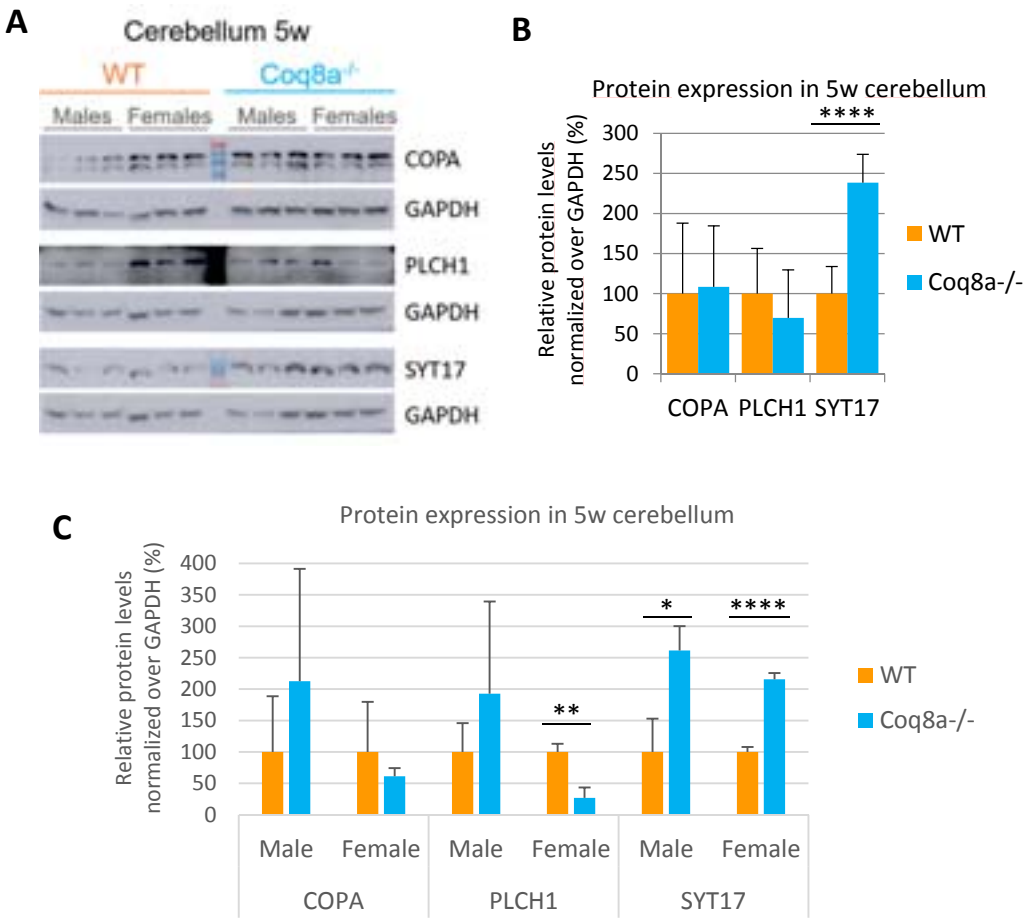

Figure 59 : SYT17 was the only deregulated transcript also found to be deregulated at the protein level in Coq8a$^{-/-}$ cerebellum at 5 weeks.

A) Western blots showing COPA, PLCH1 and SYT17 expression in cerebellum of 5 weeks old mice, GAPDH taken as control. B) Quantification of protein levels using Fiji. Protein levels are normalized over GAPDH expression and plotted as a percentage compared to WT. Error bars: SD, ****=p<0.0005. C) Quantification of protein levels using Fiji. Protein levels are normalized over GAPDH expression and plotted as a percentage compared to WT. Error bars: SD, *=p<0.05, **=p<0.005, ****=p<0.00005.

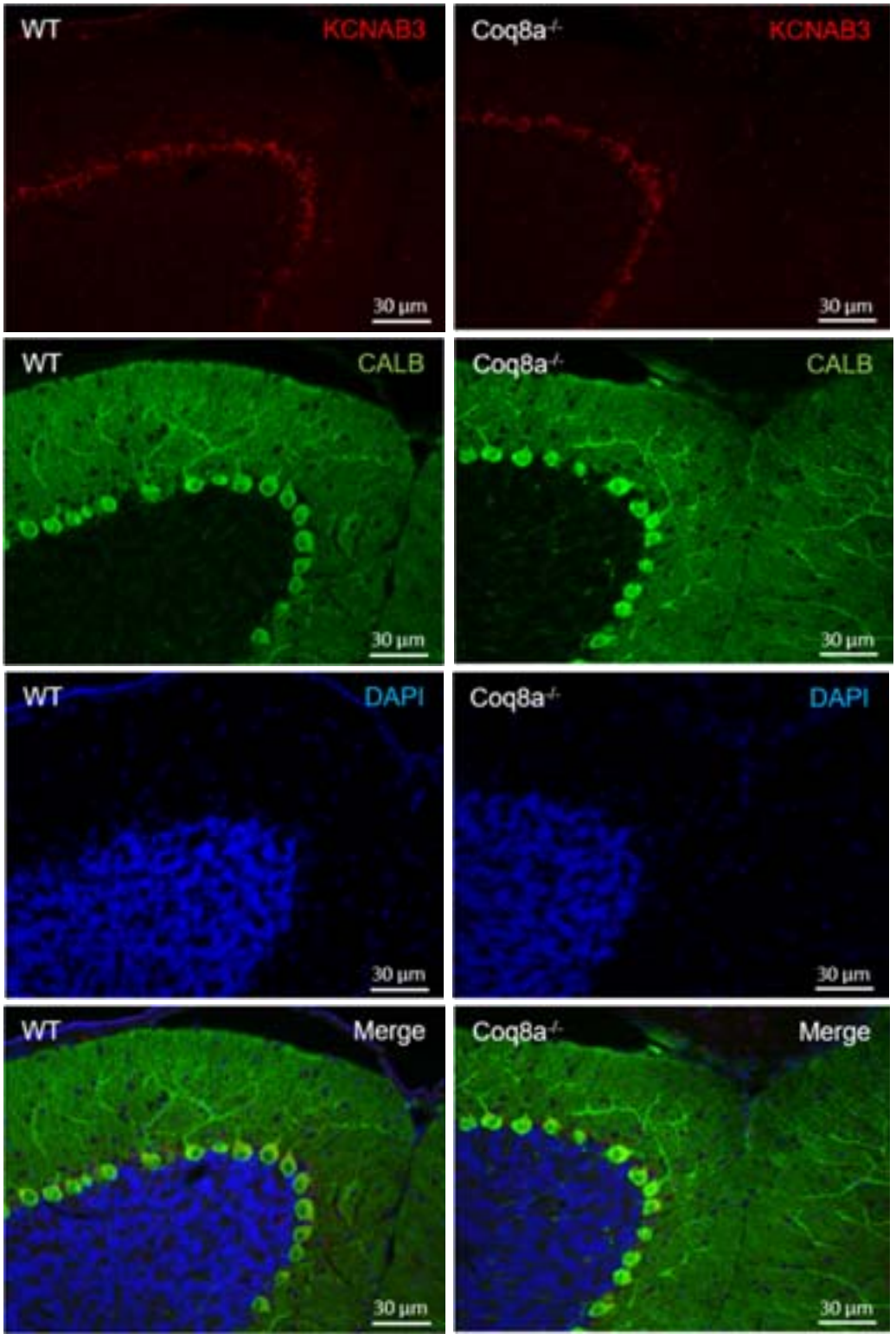

Figure 60 : KCNAB3 levels and localization look similar in Coq8a$^{-/-}$ and WT 5 weeks old cerebellum.

Immunostaining of 10µm thick sagittal cerebellar frozen sections of 5 weeks old mice. KCNAB3 (red), calbindin (green) and DAPI (blue). Left panels: WT and right panels: Coq8a$^{-/-}$ cultures. Scale bars represent 30 µm.

c. Hydrogen sulfide metabolism

At last, in view of two papers recently published, on CoQ deficient models reporting alteration of the sulfide oxidation pathway (Luna-Sánchez et al., 2017; Ziosi et al., 2017), the question was raised if this was also the case in the Coq8a$^{-/-}$ mouse model. Unfortunately, antibodies against SUOX and SQRDL need further optimization to get nice signal at the right molecular weight. Nevertheless, TST could be assessed and its expression was increased but only in 5 weeks old Coq8a$^{-/-}$ female's cerebellum (Figure 61). This protein is a thiosulfate sulfur-transferase, also named rhodanese, localized in the mitochondria, which is implicated in cyanide conversion to thiocyanate, sulfide detoxification, as well as in 5 S rRNA mitochondrial import (Aminlari et al., 2007; Ogata and Volini, 1990; Smirnov et al., 2010). An increased expression was shown to decrease cells sensitivity to H_2S toxicity (Ramasamy et al., 2006).

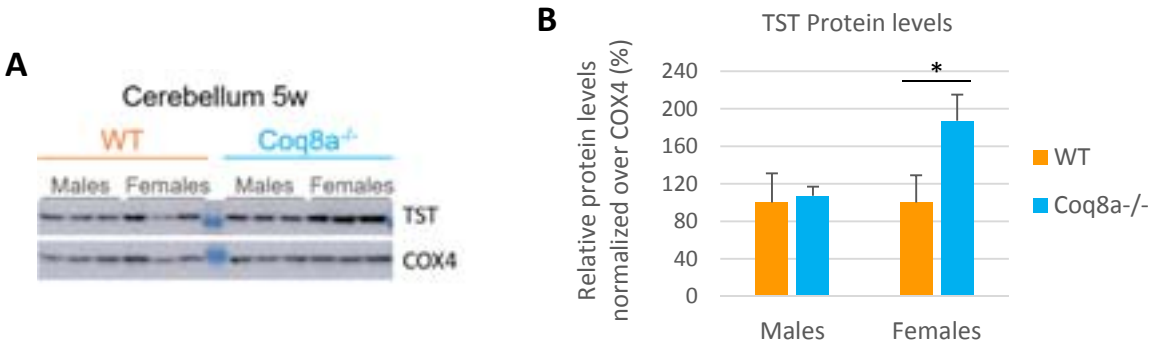

Figure 61 : Loss of COQ8A induces an increase in TST levels specifically in female's cerebellum at 5 weeks.

A) Western blots showing TST expression in cerebellum of 5 weeks old mice, COX4 taken as control. B) Quantification of protein levels using Fiji. Protein levels are normalized over COX4 expression and plotted as a percentage compared to WT. Error bars: SD, *=p<0.05.

The link between theses deregulations, both at transcripts and proteins levels, and COQ8A loss, still need to be uncovered. It could be that effects are not direct but mediated by cell signaling molecules such as hydrogen sulfide or linked to the oxidoreduction status in the cells. Further experiments are needed in order to get a clearer picture of what is going on in absence of COQ8A.

VII. Dyslipidemia

At 25 weeks, Coq8a$^{-/-}$ mice show deregulated levels of lipids in the blood (such as cholesterol, HDL, LDL, and free fatty acids) as well as CoQ deficiency in the liver (Stefely et al., 2016: Figure S1C and Figure 2A). Liver is one of the major organ involved in lipid metabolism, therefore it was decided to concentrate on this tissue, to assess the molecular dysregulation leading to dyslipidemia. First, the focus was put on the mevalonate pathway, as this biosynthesis route is common for both the synthesis of cholesterol and CoQ. This raised the question whether these two parameters could be linked, explaining the high blood cholesterol levels. Indeed, an upregulation of the overall mevalonate pathway, to compensate for the lower levels of CoQ, could lead to a higher production of cholesterol. The reverse mechanisms was already described, with the blockage of the mevalonate pathway with statins (drugs to treat hypercholesterolemia) resulting in lower cholesterol but also lower CoQ levels in the blood (De Pinieux et al., 1996). Key enzymes of different pathways, which are implicated in lipid regulation and synthesis in the liver, and known to be deregulated at the transcriptional level in case of dyslipidemia, were also assessed. As the phenotype was more pronounced in males, hence males were primarily used for this experiment.

To assess the potential deregulation of the mevalonate pathway, *Hmgcr* (3-Hydroxy-3-Méthyl-Glutaryl-CoA reductase) and *Fdft1* (Farnesyl-Diphosphate Farnesyltransferase) were tested. Hmgcr is the rate controlling enzyme of the mevalonate pathway, therefore it is highly regulated at the transcriptional level. Its transcript levels are inhibited notably by cholesterol itself when the levels are high, and HMGCR is the target of drugs like statins used against hypercholesterolemia (Goldstein and Brown, 1990). Fdft1 acts downstream by catalyzing the first reaction of the sterol metabolic pathway branch, when synthesis of cholesterol and ubiquinone diverge (Figure 62). This enzyme is also regulated by cholesterol levels (Tansey and Shechter, 2000).

In parallel, enzymes implicated in the synthesis of fatty acid and β-oxidation were also assessed as it is known that there is a common regulation of fatty acid and cholesterol synthesis. Furthermore, free fatty acids levels in the blood are also elevated. Acc1 (acetyl-coenzyme A carboxylase, encoded by the *Acaca* gene) is a regulator of the fatty acid metabolism and catalyzes the rate limiting reaction in long chain fatty acids biogenesis. Its gene expression is regulated by two transcription factors, in response to the nutritional status: SREBP (sterol regulatory element binding proteins, which also regulates *Hmgcr*, as it is a master regulator at the transcriptional level of both fatty acid and cholesterol synthesis) and ChREBP (carbo-hydrate response element binding protein) (Ishii et al., 2004; Tong,

2005). Fasn (fatty acid synthase) acts downstream of Acc1 and is also regulated by SREBP (Latasa et al., 2003). It catalyzes the formation of long chain fatty acids from Acetyl-CoA, malonyl-CoA and NADPH. A mitochondrial enzyme was also assessed: Cpt1 (carnitine palmitoyl transferase I), the fatty acid oxidation rate-limiting enzyme, which has an important role in triglycerides metabolism and is regulated by the transcription factor PGC1α (Louet et al., 2002). PGC1α, a transcriptional coactivator, regulates genes involved in lipid metabolism and may regulate cholesterol homeostasis. Mcad (medium-chain acyl coenzyme A dehydrogenase) encoded by *Acadm* is also transcriptionally regulated by PGC1 α (Vega et al., 2000). This enzyme catalyzes the initial step in mitochondrial fatty acid beta-oxidation of medium chain fatty acids (C4 to C12-acylCoA) whereas Lcad (long-chain acyl coenzyme A dehydrogenase, encoded by *Acadl*) does it for long chains (C12 and C16-acylCoA). The mRNA levels of both enzymes appeared to change in case of certain lipid deficiency (Tucci et al., 2012), therefore a deregulation might also arise in case of lipids elevation.

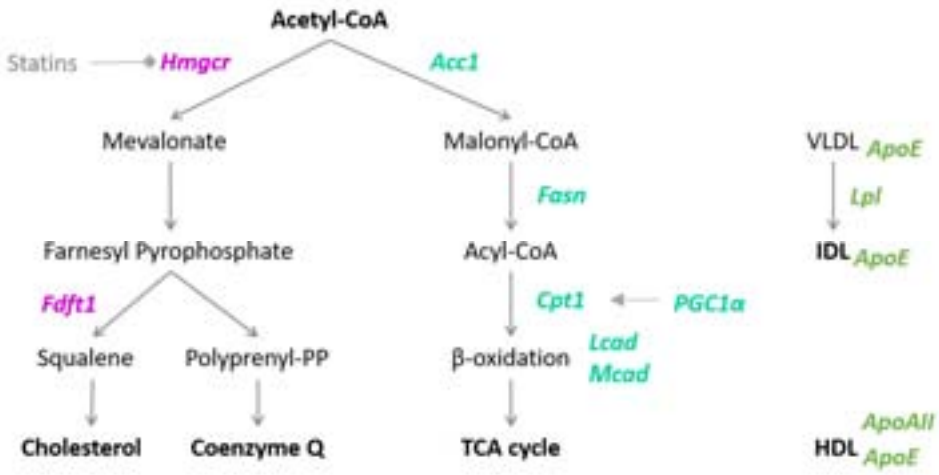

Figure 62 : Scheme of the mevalonate pathway as well as the fatty acid synthesis and oxidation pathway.

Hmgcr: 3-Hydroxy-3-Méthyl-Glutaryl-CoA reductase, Fdft1: Farnesyl-Diphosphate Farnesyltransferase, Acc1: Acetyl-Coenzyme A Carboxylase, Fasn: Fatty acid synthase, Cpt1: Carnitine palmitoyltransferase I, PGC1α: Peroxisome Proliferator-Activated Receptor Gamma Coactivator 1, Lcad= ACADL: Acyl-CoA Dehydrogenase Long chain, Mcad=ACADM: Acyl-CoA Dehydrogenase C-4 to C-12 Straight Chain, Lpl: Lipoprotein lipase, ApoE: Apolipoprotein E, ApoAII: Apolipoprotein AII, CoA: coenzyme A; PP: Pyrophosphate; TCA cycle: tricarboxylic acid cycle, VLDL: very low density lipoproteins, IDL: intermediate density lipoproteins, HDL: high density lipoproteins.

Finally, the levels of *Lpl*, *ApoAII* and *ApoE* were assessed as *ApoAII* was found to be deregulated in the cerebellum of 30 weeks old Coq8a$^{-/-}$ mice compared to WT, by an RNA-sequencing approach. APOAII and APOE are two apolipoproteins that are required for sterol efflux in high density lipoprotein (HDL) particles (Chang et al., 2017). A dysregulation of these enzymes could therefore also lead to changes in the blood cholesterol level. In the blood stream, cholesterol is also transported in VLDL and IDL (Very Low Density Lipoprotein and Intermediate Density Lipoprotein respectively), and Lpl (lipoprotein lipase) enables to convert VLDL into IDL. Additionally this enzyme hydrolyzes triglycerides in free fatty acids and is involved in lipid transport in different organs (Mead et al., 2002).

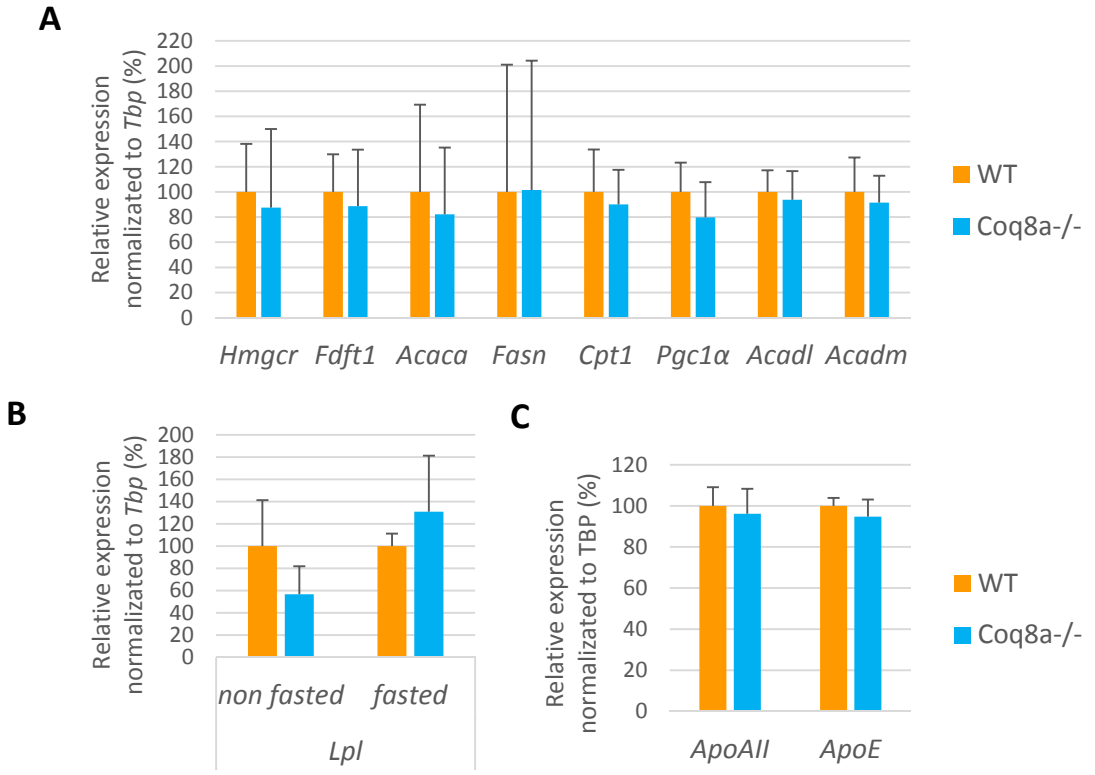

Figure 63 : Coq8a$^{-/-}$ mice do not show any difference in the expression of genes implicated in lipid biosynthesis in the liver.

For all the experiments the transcripts levels of each gene was normalized over the transcripts levels of Tpb (control gene). A) Relative expression of genes involved in lipid biosynthesis, in liver of 27 weeks old Coq8a$^{-/-}$ mice compared to WT (n=6). B) Relative expression of Lpl, in liver of 27 weeks old Coq8a$^{-/-}$ non-fasted and 25 weeks old fasted mice compared to WT (n=6). C) Relative expression of ApoAII and ApoE, in liver of 25 weeks old Coq8a$^{-/-}$ fasted mice compared to WT (n=6). Error bars: SD.

The levels of expression of each gene were measured by qRT-PCR in liver samples and normalized over the expression levels of *Tbp* (Tata binding protein). None of the eight genes tested (*Hmgcr*, *Fdft1*, *Acaca*, *Fasn*, *Pgc1α*, *Cpt1*, *Acadl*, *Acadm*) showed a significant dysregulation of their transcript levels in liver of 27 weeks old mice (Figure 63A). For most of the assessed genes, and in particular for *Hmgcr*, *Acaca* and *Fasn*, the variability between the transcript levels in between mice of each cohort was high, giving insignificant results. Thus, clear conclusion cannot be drawn, at least for the genes with a high variability of expression. For *Lpl*, the gene expression was first assessed in mice under a normal diet, and a trend towards decreased levels in Coq8a$^{-/-}$ mice liver was observed, although again these results were not significant due to the high variability of expression within the two cohorts (Figure 63B). In fed conditions, variability might arise between the mice due to unequal food absorption before the dissection (difference in quantities of food ingested and duration between absorption and dissection time). Therefore, the assessment was repeated in fasted mice, to ensure a similar feeding state of all the mice. Under fasted conditions, the opposite results were obtained with a trend towards elevated *Lpl* transcripts levels in Coq8a$^{-/-}$ mice liver, but still not significant, with a high variability between the different mutant mice only (Figure 63B). As before, no clear conclusion can be settled although *Lpl* levels do not seem to be affected. Regarding the apolipoproteins tested, neither *ApoAII*, nor *ApoE* showed any dysregulation in liver of mutant mice (Figure 63C). These last results, for the apolipoproteins, are more convincing, as the expression levels in between mice of the same cohort are within the same range. Testing proteins levels would probably not have been better as most of these enzymes are also regulated by phosphorylation which would increase the number of assays to perform. Consequently, the candidate approach did not seem to be adapted to get insight into a potential alteration in the liver. RNA sequencing, proteomic or phosphoproteomic analysis might be more suited, although it is not sure that liver is really the organ inducing dyslipidemia.

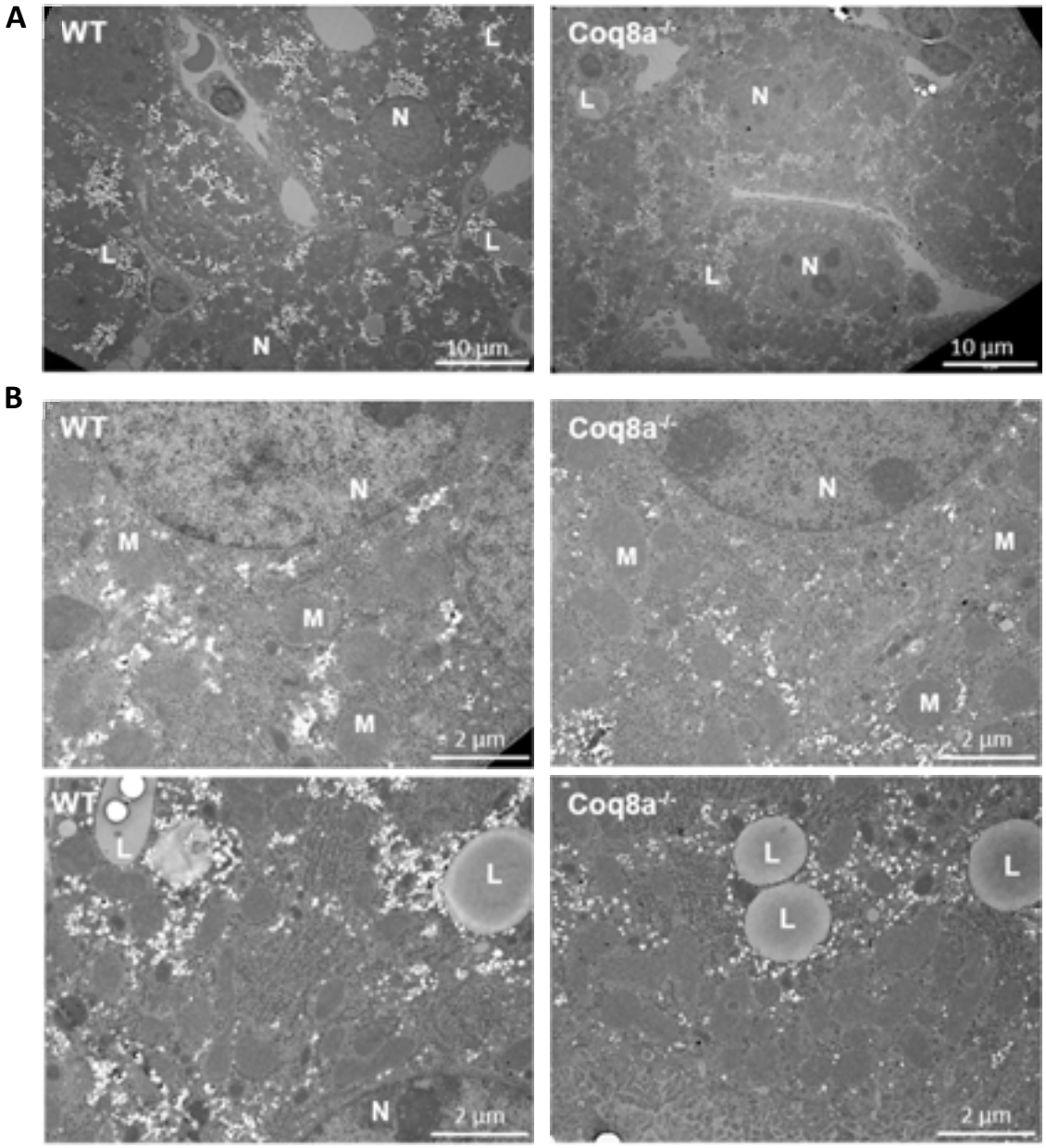

Figure 64 : Coq8a$^{-/-}$ mice show similar structures in the liver at 25 weeks.

Electron microscopy N: nucleus, L: lipid droplet, M: mitochondria, white dots: lipids A) Scale bars represent 10 µm. B) Scale bars represent 2 µm. Left panels: WT and right panels: Coq8a$^{-/-}$ liver.

To further determine the effect of COQ8A deficiency in liver , other than the decreased level of CoQ (Stefely et al., 2016), electron microscopy was performed. No structural or ultra-structural defects could be observed in mutant mice. Both in WT and Coq8a$^{-/-}$ liver, the shape of mitochondria and other cell compartments seemed normal (Figure 64). This project was therefore left aside. However, since then, a post-doctoral fellow has been working on the project, and seems to have uncovered a general lipid dysregulation, not only in the blood, but also in different tissues.

DISCUSSION AND PERSPECTIVES

Discussion and perspectives

During this thesis, I was able to show: that the mevalonate pathway does not seem to be deregulated, and therefore would not explain the Coq8a$^{-/-}$ mice dyslipidemia; that COQ8A interacts with COQ4 and COQ5, reinforcing the hypothesis that COQ8A is part of the CoQ biosynthesis pathway; that neither mitochondrial respiration, nor glycolysis are affected early in skeletal muscles despite COQ5 and COQ7 downregulation; and finally, that molecular deregulations appear early on in mutant mice cerebellum.

I. Dyslipidemia

As Coq8a$^{-/-}$ mice, and particularly males, presented with reduced levels of CoQ in their liver and elevated levels of blood lipids, including cholesterol, a hypothesis was that the mevalonate pathway, synthetizing both cholesterol and CoQ, might be upregulated to compensate for the reduced levels of CoQ (Stefely et al., 2016). The assessed transcripts levels of genes involved in the mevalonate pathway or β-oxidation were not found to be deregulated in the liver of Coq8a$^{-/-}$ mice. The mevalonate pathway does not seem to be majorly affected in the liver, at least through transcriptional regulation of two key regulatory enzymes, Hmgcr and Fdft1. As neither the levels nor the potential phosphorylation status of proteins were checked, a deregulation of the mevalonate pathway cannot be totally excluded. Cholesterol levels were only measured in the blood and not in organs. It could therefore be that the hypercholesterolemia arose from the excretion of cholesterol from another organ than liver or by a combination of excretion by different tissues. For further assessment, levels of lipids in different organs needed to be measured.

No blood dyslipidemia was reported so far in any of the ARCA2 patients described in the literature (Horvath et al., 2012; Lagier-Tourenne et al., 2008; Mignot et al., 2013; Mollet et al., 2008). Still, in certain patients, lipid accumulation was revealed by muscle histology (Horvath et al., 2012; Mollet et al., 2008), pointing towards a potential role of lipids in the pathophysiology of ARCA2.

Currently, Pankaj Kumar Singh, is trying to uncover a lipid deregulation in Coq8a$^{-/-}$ mice. He was able to show that total cholesterol as well as free cholesterol levels are unchanged in liver, muscle, white adipose tissue and brown adipose tissue, whereas cholesteryl ester is increased in liver and brown

adipose tissue but not in muscle, nor in white adipose tissue of Coq8a$^{-/-}$ mice. In high density lipoproteins in plasma of the mutant mice, the three forms of cholesterol were found to be elevated (total and free cholesterol, and cholesteryl ester). Regarding triacylglycerol, higher levels were measured in white and brown adipose tissues of the Coq8a$^{-/-}$ mice. The link between the increase of these lipid species and COQ8A deficiency needs to be uncovered, but might point toward an implication of COQ8A in lipid metabolism.

COQ8A has been found to be highly expressed in brown adipose tissue (Figure 65A). Furthermore, upon cold exposure (mice put at 4°C during 4 hours), COQ8A expression in brown adipocytes was increased compared to room temperature conditions (Figure 65B). Under cold conditions, animals need to increase their heat production to maintain their body temperatures. This heat production is performed through thermogenesis by mitochondrial uncoupling (Klingenberg and Huang, 1999; Nedergaard et al., 2001). CoQ is a cofactor, enabling the transport of protons from the intermembrane space to the matrix of the mitochondria by uncoupling proteins, for the generation of heat (Echtay et al., 2000). The increase in COQ8A content could therefore reflect the need for higher CoQ levels during thermogenesis. Exploration of BAT in Coq8a$^{-/-}$ mice seems of interest to better understand COQ8A function.

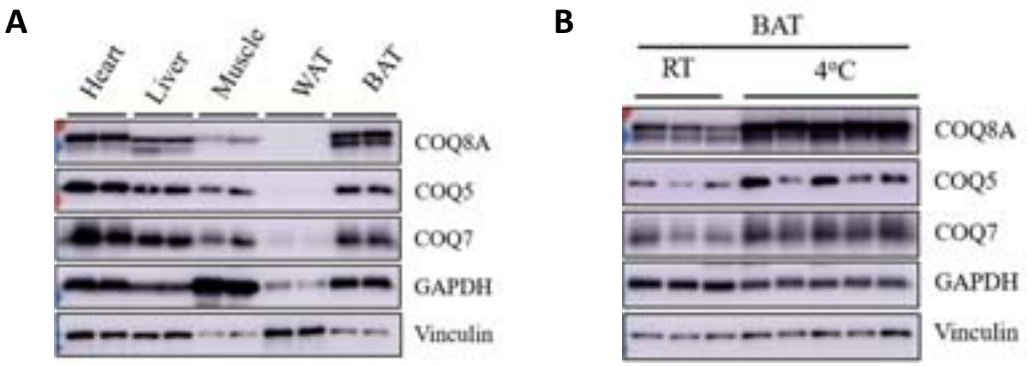

Figure 65 : COQ8A is expressed in brown adipose tissue and its expression increases upon cold exposure in mice.

A) Western blots showing COQ8A, COQ5 and COQ7 expression in different tissues (WAT: white adipose tissue, BAT: brown adipose tissue) of WT mice, GAPDH and vinculin taken as controls. B) Western blots showing COQ8A, COQ5 and COQ7 expression in WT mice's brown adipose tissue (BAT) when mice are keep at room temperature (RT) or under cold conditions (4h at 4°C), GAPDH and vinculin taken as controls.

II. Epilepsy

The causes of epilepsy can be diverse ranging from genetic mutations to trauma, or infections to hypoxia, furthermore different brain regions can be involved. The only consistent feature is the electrical hyperactivity (Biagini et al., 2013b; Koeleman, 2016; Mazarati et al., 2017; Pitkänen et al., 2016; Sarnat and Flores-Sarnat, 2013).

Coq8a$^{-/-}$ mice presented with spontaneous seizures, were found to be more susceptible to epileptic crisis (after PTZ injection) and had a delayed spatial memory (Stefely et al., 2016). In an attempt to determine if the hippocampus was the affected brain region, responsible for the delayed spatial memory and the focus of epilepsy in Coq8a$^{-/-}$ mice, histology and electron microscopy were performed, and levels of three neurotransmitter's receptors were assessed, in 30 weeks old mice. The overall structure of the brain and of specific regions, in a defined critical section, were unaltered in Coq8a$^{-/-}$ mice compared to WT. When the ultrastructure of the hippocampus was analyzed, the only striking phenotype, which appeared in mutant sections, was an increased number and size of nuclear invaginations in Coq8a$^{-/-}$ hippocampal neurons.

A study on isolated hippocampal neurons and on organotypic hippocampal slices, revealed that the geometry of hippocampal neuron's nuclei was controlled by synaptic activity and NMDA receptor activation. Upon synaptic activity (burst of action potential) and calcium entry, the researchers observed an increase in the formation of nuclear invaginations (Wittmann et al., 2009). Furthermore, nuclear invaginations increase the surface of exchange with the cytoplasm and the endoplasmic reticulum, and could affect calcium signaling and in turn transcriptional activity (Mauger, 2012). The increase of nuclear invaginations in Coq8a$^{-/-}$ hippocampal neurons could therefore be due to activation by glutamate or glycine neurotransmitters and in turn be more transcriptionally active. The increased expression of NR2B (an NMDA receptor) and GAD65/67 (an enzyme converting glutamate to GABA) could be in line with this hypothesis. More excitation might be found in mutant hippocampus, but this hypothesis remains to be tested. Nuclear invaginations were found to be a reversible process, it is therefore unsure whether this phenomenon was part of the phenotype or simply reflects a region of more excited neurons (Wittmann et al., 2009). Quantification of invaginations on different mutant and WT hippocampal slices would enable to answer this question. Finally, epilepsy seems to arise from cortex in patients (Dr. Anheim personal communication), leading us to think that hippocampus might not be the best brain structure to look at. Two common features, found in patients, are the ataxia and the cerebellar atrophy. Moreover studies have shown that affection of the cerebellum could also

induce seizures (Lascano et al., 2013). The focus should therefore be put on cerebellar affection to try and better understand ARCA pathophysiology.

Nevertheless, morphometric analysis should be repeated on a new cohort of mice, as the standard operating procedure in the laboratory of Binnaz Yalcin as evolved. This method is used in routine in her laboratory, measurement would therefore be more accurate. One defined brain section was analysed, whereas if ARCA2 mice enter their pipeline, three brain sections, including one at the level of the cerebellum, would be assessed. The new standard operating procedure also enables the measurement of additional parameters, including cell densities in precise regions, which should help us refining our knowledge on Coq8a$^{-/-}$ mice.

III. Ataxia

Coq8a$^{-/-}$ mice were shown to develop ataxia and have abnormal firing and degeneration of Purkinje neurons (Stefely et al., 2016). To assess the causes of these phenotypes, two approaches were undertaken: a candidate approach, with ions channels known to be involved in other ataxias, and an analysis of deregulated transcript levels.

No deregulation of the levels of four ions channels, mutated in the case of other ataxias, was observed by the candidate approach. Histology did not yield results at the time it was performed, but recent trials on cerebellum fixed with electron microscopy grade paraformaldehyde and embedded in cryopreservation medium enabled immunohistochemistry staining. Further analysis can therefore be done.

In cerebellum, certain proteins, like zebrin II (also called aldolase C), PLCβ3 (phospholipase Cβ3), or GABABR2 (GABA B receptor subtype 2), were found to be expressed in Purkinje neurons, but only in a subset of them. Their expression is restricted to certain zones of the cerebellum, forming bands or stripes, and the pattern is conserved in between individuals of a species. Purkinje neurons in which zebrin II is expressed are called zebrin II positive cells and the others zebrin II negative (Cerminara et al., 2015; Gravel and Hawkes, 1990; Scott, 1964). Different mouse models in which Purkinje neurons degenerate, show a pattern of degeneration with either zebrin II positive Purkinje neurons degenerating or zebrin II negative neurons degenerating (Cerminara et al., 2015). This pattern can, for example, be seen in a mouse model for Niemann Pick type C disease, in which only zebrin II negative

neurons degenerate (Sarna et al., 2003). Hence, zebrin II (aldolase C) staining should be optimized, in order to decipher if the degeneration of Purkinje neurons in the Coq8a$^{-/-}$ mouse model occurs in a patterned way or not. This information could help us gain more insight in the pathomechanism, as zebrin II positive and zebrin II negative neurons express specific subsets of genes.

Hitherto the two cerebellar *in vitro* model generated, organotypic and primary cultures, do not show any phenotype. It might be that cultures are performed too early, and that a phenotype would only appear later on. Electrophysiology could be performed to assess if the spontaneous firing activity of Purkinje neurons is maintained or if in cultures an increased interspike interval can also be measured, as in 13 weeks old mice (Stefely et al., 2016). To try and exacerbate a phenotype, we could consider to stress cerebellar cultures, with H_2O_2 for example, and monitor cellular and mitochondrial ROS production with fluorescent dyes (CM-H2-DCFDA and mitoSOX respectively).

Degeneration of Purkinje neurons is observed upon loss or mutations of different genes, implying that Purkinje neurons might be sensitive to deregulations (Cerminara et al., 2015). We were wondering if degeneration of Purkinje neurons in Coq8a$^{-/-}$ mice, observed at 30 weeks, is due to an intrinsic molecular deregulation in this type of cell, or extrinsic, due to deregulated spiking of other neurons which synapses onto Purkinje cells or perturbed signaling by another type of cell, like Bergmann glia. To answer this question, a Purkinje specific conditional knock-out mouse model was generated. Coq8a conditional mice were crossed with transgenic mice expressing Cre-recombinase driven by the Purkinje cell-specific Pcp2 promoter (Todorov et al., 2012). Unfortunately, the expression of the cre-recombinase was not only expressed in cerebellum, but also broadly in the mice tissues. Generation of a new mouse line should be achieved if a mouse with specific expression of Pcp2-Cre is found. Therefore, the question remains whether some Purkinje neurons degenerate due to the loss of COQ8A in their cell bodies (in a cell autonomous way) or if this phenotype is due to a specific affection, for example of the inferior olivary nucleus if the deregulation would occur through firing by the climbing fibers.

Laser capture microdissection of Purkinje neurons and of the three layers of the cerebellar cortex could be performed in order to assess the deregulated molecular mechanisms in each of these regions and in Purkinje neurons. Regarding Purkinje neurons, only the neuronal body can be microdissected, and not the axons or the dendritic tree if one wants to separate Purkinje neurons from the other cerebellar cell types. Still, the analysis of RNA and proteins specifically misregulated in Purkinje neurons soma will help to better understand the mechanism possibly implicated in the degeneration of this type of

neuron. A comparative analysis of the molecular, granular and Purkinje cell layer might also give new clues about the pathophysiology. Regarding the unchanged CoQ levels measured in the cerebellum of Coq8a$^{-/-}$ mice, but the appearance of the ataxic phenotype, it could be that COQ8A is expressed specifically in a cell types or in a restrained number of cells in this tissue. Microdissection, followed by protein analysis, should give an answer to this question. If COQ8A expression is not restricted to certain cells, compensatory mechanism might come into action to produce CoQ or COQ8A would have another function in this type of cells.

RNA-sequencing of 30 weeks old mice's cerebellum had been performed in an attempt to better understand the deregulated mechanisms inducing ataxia. The transcript level of part of the genes found to be deregulated by RNA sequencing, have been assessed by qRT-PCR in 5 weeks old mice. Twenty-seven genes were found to be differentially transcribed in Coq8a$^{-/-}$ mice compared to WT. Whether these deregulations are inducing ataxia or ensue from compensatory mechanism remains to be elucidated.

ApoAII transcripts were found to be highly decreased (80% decrease) already in 1 week old Coq8a$^{-/-}$ mice cerebellum and the decrease was stable over time. As the expression level is low in this tissue, the question remained whether this could be a false positive. Hints that this deregulation is most probably relevant came from the proteomic analysis which revealed that APOAII protein levels were significantly decreased in the cerebellum of 30 weeks old Coq8a$^{-/-}$ mice (65% decrease, ANNEX Table 11). ApoAII is an apolipoprotein described as a major constituent of the high-density lipoproteins (HDL) particles which are found in the plasma. The expression and excretion of ApoAII are well recognized in hepatic cells (Maïga et al., 2014). Nonetheless, ApoAII transcripts levels were not found to be deregulated in the liver of 30 weeks old Coq8a$^{-/-}$ mice, arguing towards a specific deregulation in the cerebellum. ApoAII knock-out mouse were only reported has having lower levels of total cholesterol, HDL-cholesterol, free fatty acid and insulin in their plasma (Weng and Breslow, 1996). ApoAII seems to be implicated in cholesterol and free fatty acid metabolism, but it remains to be determined to which extend (Blanco-Vaca et al., 2001). *ApoAII* transcription was described as being controlled by different regulatory elements, most regulated by lipids (Chan et al., 2012), it could therefore be that a lipid dysregulation occurs in cerebellum. Interestingly, in Niemann-Pick type C, a disease due to impaired lipid trafficking, including cholesterol trafficking, Purkinje neurons were shown to degenerate in a cell autonomous manner (Elrick et al., 2010). It would therefore be interesting to assess if the content in cholesterol or other lipids is altered in the cerebellum, and in particular in Purkinje neurons. For this assessment, immunohistochemistry using filipin to stain cholesterol could be performed for example.

If *ApoAII* transcriptional downregulation is also observed in cerebellar cultures, the use of dyes to stain lipids, like the BODIPY® 542/563 cholesteryl ester (Invitrogen), would enable to visualize lipids and their transport (cholesterol transport in the case of the BODIPY® 542/563 cholesteryl ester). However, the limitation of these techniques is that specific lipids have to be assessed one by one.

Copa was also found to have deregulated transcription early, in 1 week old Coq8a$^{-/-}$ mice, with constant deregulation over time, with a decrease of around 20%. So far, the protein levels were not found to be deregulated but these results should be confirmed, although proteomic data of 30 weeks old Coq8a$^{-/-}$ mice also showed no significant deregulation (ANNEX Table 10). *Copa* encodes the α-subunit of the coatomer complex, which is the main component of the coat protein I (COPI). This complex is implicated in retrograde transport of vesicles from the Golgi to the ER but probably also within the Golgi (Eugster et al., 2000; Popoff et al., 2011). COPI was also shown to facilitate localization of mRNA encoding mitochondrial proteins which are nuclear-encoded (Zabezhinsky et al., 2016). Moreover, COPA was shown to move within the axons in murine motor neurons and to co-immunoprecipitate with certain RNA in neuronal cells (Peter et al., 2011; Todd et al., 2013). The deregulation of *Copa* could therefore be linked to the neuronal phenotype. *Copa* might also lead to the generation of xenin-25, a hormone, by post-translational modification (xenin corresponds to the 25 N-terminal amino acids of COPA) (Chow and Quek, 1997). This hormone was shown to act in the gut but also in the hypothalamus and white adipose tissue and to be involved in the feeding behavior and lipid metabolism (Bhavya et al., 2016; Kim et al., 2016). Whereas xenin-25 is produced in the cerebellum and is relevant in the case of COQ8A deficiency remains unknown but if xenin is indeed produced in the cerebellum there might be a link with Coq8a$^{-/-}$ mice dyslipidemia. This last hypothesis remains highly questionable and a deregulation of *Copa*, as a result of another mechanism, seems much more probable.

Potassium channels are important channels known to be implicated in action potentials for the repolarization of neurons, but also serve in intercellular signaling. In the cerebellum of 5 weeks old Coq8a$^{-/-}$ mice, genes encoding for a potassium channel and a regulatory subunit of a voltage gated potassium channel, namely *Kcnj10* and *Kcnab3* respectively, were found to be transcriptionally deregulated. *Kcnab3* was found to induce a faster inactivation of the Kv1.5 voltage gated channel during action potential (Leicher et al., 1998), whereas *Kcnj10* was described as buffering the extracellular potassium (Poopalasundaram et al., 2000; Takumi et al., 1995). Interestingly, in humans, mutations in the *KCNJ10* gene were found to induce a syndrome with ataxia and epilepsy, the “SeSAME syndrome” (for seizures, sensorineural deafness, ataxia, mental retardation, and electrolyte imbalance) (Bockenhauer et al., 2009; Sala-Rabanal et al., 2010). Regarding the functions of potassium

channels, it is not surprising that deregulation leads to defects. KCNJ10 was found to be localized in Bergmann glia, so surrounding Purkinje neurons (Poopalasundaram et al., 2000; Takumi et al., 1995). It is of interest to explore if the protein level is also affected or if only transcripts levels are elevated in cerebellum of 5 weeks old Coq8a$^{-/-}$ mice. Nevertheless, KCNJ10 was not found to have significant higher levels in 30 weeks old Coq8a$^{-/-}$ mice cerebellum compared to WT by proteomic analysis, and KCNAB3 was not reported (ANNEX Table 11). KCNAB3 is expressed in the brain, predominantly in the cerebellum, and we could detect it in Purkinje neurons by immunofluorescence (Leicher et al., 1998). Deeper analysis of KCNAB3 immunofluorescence staining is needed to gain insight in a potential altered protein level which might be slight. The protein deregulation of one or both of these potassium channels could be the cause for the abnormal firing of the Coq8a$^{-/-}$ Purkinje neurons measured by electrophysiology (Stefely et al., 2016). If none of these two proteins have deregulated levels, it remains to be determined why the transcripts levels show a significant increase of around 50%. In regards to the importance of the potassium channels, it could be that a control at the translational level occur to prevent overexpression of the proteins. These deregulations should therefore be assessed more in details.

Another gene, which seems of interest regarding the highly significant deregulation measured is *Slc7a3*. A decreased of more than 75% of the transcripts levels of *Slc7a3* were observed in Coq8a$^{-/-}$ mice cerebellum compared to WT. This gene encodes the cationic amino acid transporters 3 (CAT-3), which is a transporter mediating L-type cationic amino acid entry in the cells, and which has high affinity for L-arginine (Ito and Groudine, 1997). *Slc7a3* was shown to be expressed in neurons, and particularly in the granular and Purkinje cell layer in the cerebellum in mouse (Braissant et al., 1999), and the protein CAT-3 was found to be internalized upon NMDA neurotransmission (Huang et al., 2007). CAT-3 might therefore contribute to the ataxic phenotype and the pathophysiology of Purkinje neurons. Accordingly, protein levels should be assessed, and immunohistochemistry performed to see if a protein deregulation follows the transcriptional deregulation. If the protein is mislocalized or the levels decreased, it would imply that a reduced level of arginine is probably internalized in cerebellar neurons and therefore the production of molecules requiring arginine for their synthesis might be affected. As arginine serves as a precursor for a number of molecules and proteins, including the neurotransmitter glutamate and the signaling molecule nitric oxide (Wu and Morris Jr., 1998), decrease levels of CAT-3 could induce a decrease synthesis of glutamate and nitric oxide, for example, leading to altered neurotransmission and cell signaling. In humans, missense variants of *SCLC7A3* were identified in five patients with autism spectrum disorders (Nava et al., 2015), reinforcing the idea that

a deficiency in the CAT-3 protein is deleterious and that this gene appears to be of interest in the pathophysiology of the Coq8a$^{-/-}$ mice.

Syt17 transcript levels, as well as the protein levels, were found to be highly increased in 5 weeks old Coq8a$^{-/-}$ mice cerebellum. *Syt17* encodes a synaptotagmin. Synaptotagmins are proteins suggested as regulating membrane fusion or trafficking, as half of the 17 synaptotagmins act in calcium induced exocytosis. The function of SYT17 remains unknown but it was found to be predominantly localized in vesicles in axons and might undergo exocytosis, in rat primary hippocampal cultures (Dean et al., 2012). Immunohistochemistry should now be performed to see where SYT17 localizes in the cerebellum and if a differential localization can be seen in between WT and mutants. If an increase in SYT17 is also present in cerebellar neuronal cultures, exocytosis could be assessed with neurotransmitter fluorescence probes. As calcium signaling is involved in exocytosis, in addition to other signaling, calcium imaging with dyes like Fura-2 could also be performed (Grienberger and Konnerth, 2012).

Twenty other genes were found to have deregulated transcripts levels but for most of them this deregulation was slight and can probably not be detected at the protein level, by Western blot, if indeed it leads to a change in protein levels. The question also remains if these deregulations have a real biological significance. The data should be reproduced in a new cohort of mice to clarify the importance of these deregulations. Nevertheless, *Atf4* is a transcriptional regulator so small changes might be sufficient to produce specific responses. The slight decrease of *Atf4* transcripts levels might explain the decrease in *AsnS* and *Sesn2*, which are both in part regulated by this gene (Chen et al., 2004; Ye et al., 2015). Regarding *Faim2*, *Nudt3 and Snhg11*, all three genes were found to be associated with human obesity, so they might have a link with lipid metabolism and the dyslipidemia observed in mice (Naukkarinen et al., 2010; Williams et al., 2012). FAIM2 and RET were described as being recruited to lipid rafts (Tansey et al., 2000) and CoQ is present in all membranes. By proteomic analysis in 30 weeks old Coq8a$^{-/-}$ mice cerebellum, CARS, NUDT3, SCCPDH CPLX1, ASNS, FAIM2 had unaffected levels (when considering the adjusted p-value: Q-value) and the other proteins were not reported (ANNEX Table 11). For Plch1, a phospholipase, the results are puzzling, with an increase of the transcripts levels in males and female's animals but a decrease of the protein levels restricted to females in 5 weeks old Coq8a$^{-/-}$ mice. The Western blot should be repeated to confirm these results. A gender specificity is yet possible, for example high LDL cholesterol and free fatty acids contents were only measured in the blood of male Coq8a$^{-/-}$ mice whereas increase of total cholesterol and HDL cholesterol was reported for both sex (Stefely et al., 2016).

CoQ is implicated in diverse mechanisms, including mitochondrial respiration, as described previously, but also in hydrogen sulfide (H_2S) oxidation. Indeed, the first step of hydrogen sulfide oxidation metabolism in mammals is performed by a sulfide-quinone oxidoreductase. H_2S although present in low amount to not be toxic for the cells, exerts cell signaling, like nitric oxide. H_2S is synthetized and catabolized by the cells, and this last mechanism was described as occurring in the mitochondria (Ziosi et al., 2017). The levels of SQR and other enzyme of the H_2S catabolism pathway were found to be decreased in certain CoQ deficiencies both in patient's fibroblasts and in a mouse model (Luna-Sánchez et al., 2017; Ziosi et al., 2017). SQR levels could not be determined so far in the Coq8a$^{-/-}$ mice and optimization is needed to get a specific signal. However, levels of TST, were found to be specifically increased in the cerebellum of Coq8a$^{-/-}$ female mice. TST is an enzyme acting downstream in the degradation of H_2S into sulfate. By proteomic analysis of 30 weeks old Coq8a$^{-/-}$ mice, SQR levels were found to be increased in muscle, heart and kidney, and TST was increased only in muscle, of mutant mice, but none were found to be deregulated in cerebellum (ANNEX Table 12). The deregulation of other enzymes in this pathway remains to be explored, as well as the amount of CBS, one of the enzymes responsible for H_2S synthesis, which is expressed in the cerebellum including in Purkinje neurons (Robert et al., 2003). By proteomic analysis, TST levels in the cerebellum probably do not show a significant difference due to the low number of animals (n=3) and a mix of males and females. The divergence of TST expression between males and females raises the question of gender specificity. If a deregulation of the hydrogen sulfide metabolism can be observed, in particular in the cell models in which mitochondrial respiration was not shown to be affected it could imply that different pools of CoQ are used to perform different functions. At least the levels of TST and SQR should be assessed in the cerebellum, muscle and primary cultures to assess if defective hydrogen sulfide could play a role in ARCA2 pathophysiology. Quantification of the hydrogen sulfide would also be of interest to see if its signaling might be affected, which could contribute notably to degeneration of Purkinje neurons.

RNA sequencing or at least proteomic analysis of 5 weeks old Coq8a$^{-/-}$ mice cerebellum would be of interest in order to gain insight in the deregulated mechanisms occurring early on, as primary events, and limit the number of compensatory mechanisms observed.

The deregulated metabolic pathways remain to be explored to better understand what happens during the establishment of the phenotypes and clarify COQ8A role in the different tissues.

IV. Mitochondrial respiration

Although COQ8A precise functions have not been determined yet, this protein has, at least, a role in stabilizing the complex Q in CoQ biosynthesis (Stefely et al., 2016). Indeed COQ8A interacts with COQ4, COQ5, COQ6 and COQ7 (Stefely et al., 2016, Figure 3 A, B and C). Furthermore, COQ8A deficiency induces a decrease of different COQ proteins levels in Coq8a$^{-/-}$ mice, probably in all tissues, and starting early on, in embryos.

As COQ8A interacts with COQ7 within the Complex Q, a deficiency of COQ8A can explain the decrease of COQ7 observed in Coq8a$^{-/-}$ mice. In cerebellum of Coq8a$^{-/-}$ mice, lower COQ7 levels were found but the content in CoQ remained similar to WT. These results are puzzling regarding COQ7 catalytic role in the biosynthesis of CoQ (hydroxylation of demethoxyubiquinone) (García-Corzo et al., 2013; Herebian et al., 2017).

Regarding the decrease in CoQ and abnormal mitochondria observed in muscles of 30 weeks old Coq8a$^{-/-}$ mice, it was of interest to assess mitochondrial function in this tissue. An *in vitro* model was generated and Coq8a$^{-/-}$ primary myoblasts were found to have reduced protein levels of COQ5 and COQ7, similarly to the reduction observed in adult muscles. As COQ5 and COQ7 are two catalytic enzymes required for CoQ biosynthesis, it was assumed that CoQ levels were decreased. These primary cultures therefore seemed adapted to assess a potential deregulation of mitochondrial respiration. Nonetheless, oxidative phosphorylation (measured with an Agilent Seahorse XFe96 Analyzer) was not altered in Coq8a$^{-/-}$ myoblasts, which raises the question of an effective CoQ decrease. To answer this question and get a better insight in this muscular cell model, CoQ levels should be assessed.

Usage of the glycolysis pathway was evaluated to determine if cells would compensate for a less efficient energy production even though mitochondrial respiration was not affected. Coq8a$^{-/-}$ myoblasts were found to have a similar glycolysis and glycolytic capacity as WT. Results of mitochondrial respiration and glycolysis point towards an efficient energy supply in myoblasts, at least through glucose and the citric acid cycle.

To better characterize the muscle primary cultures, some experiments could be added, such as the measurement of the differentiation index (number of nuclei per myotubes at a fixed time point after differentiation). Furthermore, the differentiation of myoblasts in myotubes could be assessed by qRT-PCR with an appropriate control gene to be able to monitor the increase and decrease of the gene expressed, or by assessing the protein amounts by Western blot.

Similarly to the unaltered myoblast's oxidative phosphorylation, mitochondrial respiration of 42 weeks old Coq8a$^{-/-}$ mice's muscles fibers was unaffected when measured with Clark electrodes (Stefely et al., 2016), albeit that at 30 weeks, CoQ levels were found to be decreased by 30% in quadriceps of mutant mice, compared to WT. Mitochondrial respiration is therefore functional in Coq8a$^{-/-}$ mice's muscles.

A bias that could occur, both during Seahorse or Clark electrodes measurements, is that the initial substrate provision is different in Coq8a$^{-/-}$ and WT muscle cells, leading to a compensation which could explain unaltered basal respiration. To get rid of this possibility, cells could be permeabilized prior to the assay to have an equivalent media surrounding WT and mutant mitochondria (Divakaruni et al., 2014). This permeabilization was performed for the measurement in adult muscles fibers with the Clark electrodes but not for the measurement in myoblasts with the Seahorse apparatus. Considering the similar results obtained with both methods, permeabilization of myoblasts prior to the Seahorse experiment should not yield different results.

While unequal substrate storage could explain an unaltered basal respiration despite low levels of CoQ, this hypothesis is also dismissed by recent data showing that strong CoQ reduction in mice only mildly reduced mitochondrial respiratory capacities. Indeed, in a Mclk1 liver conditional knock-out mouse (COQ7 KO in liver), a mild mitochondrial respiratory defect was observed although there was a strong (85%) CoQ reduction (Wang and Hekimi, 2013b). CoQ levels might therefore be preferentially used by mitochondrial respiration to sustain this function. The pathogenicity of CoQ deficiency would then arise as the defect of another role of CoQ.

With Clark electrodes on Coq8a$^{-/-}$ adult mouse fibers, only the respiration rate with complex I substrates (glutamate + malate) and respiration after addition of ADP, to increase complex V activity, were measured. Regarding the significant but mild CoQ deficiency in muscle of 30 weeks old Coq8a$^{-/-}$ mice (29% decrease in CoQ_9 and CoQ_{10} content), it might be that measurement of oxygen consumption is not sensitive enough to detect a decreased activity of complex I, II or III, alone or in combination, if it is subtle, or simply reflects the non-affection of respiratory complexes activity. Assessment of enzymatic activities might not give a different result.

Regarding data obtained in muscles of ARCA patients, the data from Coq8a$^{-/-}$ mice remain surprising. In muscles biopsies, CoQ levels were found to be reduced for all patients except one, with highly variable results ranging from 10 to 90% reduction compared to controls. Furthermore, in all patients in which a decrease in CoQ content was measured and for which mitochondrial respiratory chain activities were assessed, reduced activities were measured (with values and complexes activity varying

from one patient to the other). The variability might be due to the type of mutation or the residues affected. Coq8a$^{-/-}$ mice display an ataxic phenotype, susceptibility to epilepsy and weaken endurance, similarly to ARCA patients, but without mitochondrial respiratory defects. Therefore, the question remains if the phenotype observed in patients are due to an affection of the mitochondrial respiratory chain, or the affection of another function of CoQ or COQ8A.

At 30 weeks, Coq8a$^{-/-}$ mice had unchanged levels of ROS in quadriceps muscles compared to WT, which is in line with the unaltered mitochondrial respiration (Licitra, 2013; McLennan and Esposti, 2000). These results reinforce the question about the affection of mitochondria and the role of COQ8A.

Concerning assessment of mitochondrial respiration in cerebellar primary cultures, unfortunately no clear answer, at least regarding respiration due to complex I and III activities, could be obtained so far. Optimizations would be need, but would possibly lead to the same results as for myoblasts, with unaltered mitochondrial respiration in Coq8a$^{-/-}$ cultures. Unchanged levels of CoQ in the cerebellum of 30 weeks old mice, as well as the absence of phenotype in these cultures, strengthen this hypothesis.

V. Long term perspectives

1. Redundancy

Deletion of *Coq8* in *Saccharomyces cerevisiae* induces the loss of production of CoQ_6 and the impossibility to grow on non-fermentable carbon source, reflecting an altered mitochondrial respiratory chain, that is reversed upon supplementation with CoQ_6 (Do et al., 2001). A decrease of more than 90% of the CoQ content was found In *Caenorhabditis elegans Coq8* knock-out animals compared to WT, and mutant animals had developmental arrest (Asencio et al., 2009). On the opposite, the CoQ reduction is slight in Coq8a$^{-/-}$ mice and is only present in certain tissues. Furthermore, the phenotype is mild (Stefely et al., 2016). These results raise the question of a possible redundant role of other proteins in mammals in the biosynthesis of CoQ which would compensate for the loss of COQ8A. A good candidate would be COQ8B. Indeed, COQ8B is the closest homolog of COQ8A and is also an ortholog of Coq8 in yeast. Moreover, COQ8B was shown to interact with some of the COQ proteins forming the CoQ biosynthesis complex (Ashraf et al., 2013; Floyd et al., 2016). COQ8A and COQ8B share 61% amino acid identity, some of their functions might therefore be redundant, although COQ8B lacks the N-terminal part found in COQ8A which is probably the

membrane binding domain. So far mRNA levels of COQ8B were found to be lower than the ones of COQ8A in all mice tissues tested, and in some human tissues except in the kidney (Stefely et al., 2016). COQ8B transcript levels were also found to be mildly decreased upon reduction of CoQ levels in ARCA2 patient's fibroblasts (Lagier-Tourenne et al., 2008). By proteomic analysis, COQ8B levels were unchanged in the cerebellum of 30 weeks old Coq8a$^{-/-}$ mice but could not be detected in heart, kidney and muscles of WT and mutant mice. These results are puzzling regarding the known expression of COQ8B in the kidney. The presence of COQ8B in cerebellum in which CoQ deficiency was not observed, and the absence of COQ8B in kidney and muscle in which a reduced level of CoQ was measured would be in accordance with this possible redundancy, although COQ8B protein levels should be verified as proteomic data from kidney are surprising. Furthermore, in heart COQ8B could not be detected and CoQ content was unaltered (Stefely et al., 2016). The questions remain whether a compensation occurs and if ADCK1, 2 and 5 could also play a role and display functional redundancy, at least in certain tissues. This hypothesis could be assessed by knocking-down the other *Adck* genes in Coq8a$^{-/-}$ mice by shRNA and looking if a phenotype would be exacerbated. Muscle would be an interesting tissue for this experiment, however, at least in 30 weeks old mice, none of the other ADCK proteins could be detected by proteomic analysis. The protein levels should first be assessed before taking this approach and would enable to target first the ADCK proteins which are more highly expressed in this tissue.

2. Tissue specificity

In cerebellum of Coq8a$^{-/-}$ mice, COQ7 levels are reduced but the content in CoQ remains unchanged compared to WT. Either the cells are able to produce the same amount of CoQ even though less enzymes are present or it could be that CoQ is synthetized through another route. Two enzyme have so far been described in the Golgi and in the peroxisome (Kalen et al., 1990; Tekle et al., 2002).

It was shown that all tissues do not contain the same amount of CoQ when normalized on the amount of proteins (Parrado-Fernández et al., 2011; Stefely et al., 2016). Intriguingly, CoQ levels were found to be high in rat and human's heart, while in CoQ deficiencies only very few cases of heart affection were described (Åberg et al., 1992; Quinzii et al., 2014). It could therefore be, that not all tissues require the same amount of CoQ and are therefore differentially affected by a loss of CoQ.

Patients with COQ8B mutations only present with nephrotic symptoms, whereas patient with COQ8A mutations were described as having cerebellar, brain and in some, muscle affection but not a kidney

defect (Ashraf et al., 2013; Mignot et al., 2013). It therefore seems that COQ8A and COQ8B have tissue specific functions. This idea is reinforced by the fact that Coq8a$^{-/-}$ mice do not have altered levels of CoQ in the cerebellum but have cerebellar affection with shrunken neurons (Stefely et al., 2016).

By proteomic analysis of 30 weeks old Coq8a$^{-/-}$ mice tissues, only the proteins levels of COQ5, 7 and 9 were found to be decreased in all four tested tissues of Coq8a$^{-/-}$ mice (cerebellum, heart, kidney and muscle), levels of COQ3, COQ4 and COQ6 were either not altered in all tissues or could not be detected some of them, such as COQ4 not detected in cerebellum and muscle (Stefely et al., 2016). Hence it seems that there is a tissue specificity.

3. Localization

A study showed localization of COQ6 and COQ7 in the Golgi apparatus of rat podocytes and in another study COQ8B protein was found in a cytosolic and in a mitochondrial fraction extracted from rat podocytes (Ashraf et al., 2013; Heeringa et al., 2011). We know that COQ8A localizes to the mitochondria from different studies, both by exogenous expression of tagged protein and subfractionation of the endogenous protein in mouse heart (Licitra, 2013; Stefely et al., 2016). Still, the question remains if COQ8A only localizes to the mitochondria or if it is also present in other cells compartments. Indeed COQ6 was only found to localize in the mitochondria when exogenously expressed but the endogenous protein was also detected in Golgi (Heeringa et al., 2011). So far immunofluorescence staining did not give an answer, due to the lack of an antibody specific for COQ8A, working for this technique. The development of an antibody suited for immunofluorescence or subfractionation of different cell compartments should be considered. An alternative would be to use the CRISPR/Cas9 technology to generate an endogenously tagged protein that would enable immunofluorescence studies, but the method remains time consuming. Thus, to gain insight in COQ8A localization subfractionation should first be performed.

4. Function

The function of COQ8A in the stabilization of, at least, part of the CoQ biosynthesis complex is now established with COQ8A direct interaction with other COQ proteins and the decrease of COQ5, 7 and 9 proteins levels upon loss of COQ8A in the knockout mouse model (Stefely et al., 2016).

COQ7 was found to have a mitochondrial and a nuclear targeting sequence and to localize in both cell compartments (in HeLa cells and in *C. elegans*), but with distinct functions in each. In the mitochondria COQ7 is required for CoQ biosynthesis, whereas in the nucleus, it modulates gene expression of certain mitochondrial stress responses (Monaghan et al., 2015). Moreover, in plants, two members of the ABC1 family, the homologs of the ADCK family, were found to be present in plastoglobules, which are lipid droplets and to play a role in the lipid metabolism (Lundquist et al., 2013; Martinis et al., 2014). Furthermore, COQ8A has recently been suggested has having an alternate splice form and therefore lead to a novel isoform which should also be targeted to the mitochondria. COQ8A bares an unconventional cleavage site, as the peptides identified so far in the mitochondria are cleaved at the level of the 160th amino acid (Calvo et al., 2017). Together these data raise the question of a possible additional function of COQ8A either in the mitochondria or in other cell compartments.

COQ8A localization and substrates should be determined to further understand its functions and in turn better explain the phenotypes observed in Coq8a$^{-/-}$ mice and ARCA2 patients.

5. Final conclusion

As lines of inquiries, I think the deregulated mechanisms in the cerebellum should be investigated deeper, in particular ApoAII, Syt17, Kcnj10, Kcnab3 and Slc7a3, at the transcript and protein level, as well as their localization. For ApoAII in particular, the potential restricted expression should be explored. In parallel morphometric analysis and staining with zebrin should be performed to assess if all Purkinje neurons are affected or only a subset. COQ8A subcellular localization should then be explored and COQ8A substrates determined in order to gain insight in the link between COQ8A functions and the deregulated mechanisms.

ANNEX

Annex

I. Material and Methods

Mice

Coq8a$^{-/-}$ (Adck3$^{-/-}$) mice were generated by homologous recombination with deletion of exons 9-14, as reported in (Stefely et al., 2016).

Behavioural analysis

Accelerating rotarod: 7 Coq8a$^{-/-}$ and 9 WT mice were placed on an accelerating rotating rod (Panlab, Barcelona, Spain) as described previously to assess their coordination, balance and motor skill acquisition (Stefely et al., 2016). Four trials per day were performed per mice, with at least 15 minutes resting time in between trials. Mice performed the test during five days.

Beam-walking test: 7 Coq8a$^{-/-}$ and 9 WT mice were left to walk along a beam (2 cm wide × 90 cm long, and 30 cm above the bedding) and the number of misplacement of the paws when walking were counted. The latency to cross the beam was also evaluated.

Morphometric analysis

The evaluation was carried out using 30 weeks-old Coq8a$^{-/-}$ and WT mice, for which brain were dissected and fixed in 4% formaldehyde. Brains were then embedded in paraffin and 7 µm histological coronal sections were collected in a precise region of the brain. Sections were stained with cresyl violet and luxol blue for the measurement of the twenty-five parameters (areas and length) with Fiji (Schindelin et al., 2012). Measurements were performed blind for the genotypes. The staining and analysis were performed as described (Mikhaleva et al., 2016).

Microscopy

Electron microscopy

Mice were intracardiacally perfused with 4% paraformaldehyde (PFA) diluted in PBS1x (phosphate buffered saline), tissues were subsequently dissected out and post-fixed in 2.5% glutaraldehyde-2.5% PFA in cacodylate buffer. Following steps were performed as described (Stefely et al., 2016). For cerebellar organotypic cultures, fixation was immediately performed with 2.5% glutaraldehyde-2.5% PFA in cacodylate buffer and processed further as the other samples dehydration and embedding in Epon.

Immunohistochemistry

Mice were perfused with 4% paraformaldehyde (in PBS 1X), and tissues post-fixed in the same solution overnight at 4°C. Tissues were then transferred in sucrose solutions up to 30% before being embedded in OCT. 10 µm thick sections were cut with a cryostat. Sections were blocked with 3% normal goat serum in PBS 1x and permeabilized with 0.25% Triton X-100. Samples were then incubated with primary antibodies at 4°C overnight. Secondary antibodies (goat anti-mouse or goat anti-rabbit) were then applied for 1h at RT. Staining with DAPI was performed at RT for 20 min. Slides were mounted with ProlongGold.

Immunofluorescence

Cultures were fixed in a solution of 4% formaldehyde in PBS 1x, and subsequently blocked and permeabilized with 10% NGS (Normal goat serum), 0.1% BSA (Bovine serum albumin) and 0.1% Triton X-100 in PBS. Primary antibodies were incubated overnight at 4°C in the permeabilization solution and secondary antibodies coupled to Alexa fluorophores were incubated on the cultures in the same solution but with DAPI. Slides were mounted with ProlongGold. For organotypic slices, permeabilization and incubation with the antibodies were performed for 24h at 4°C. In this case, blocking and permeabilization was performed with a solution of 10% NGS, 1% BSA and 0.1% Triton X-100 in PBS, and incubation of the antibodies was done in 5% NGS, 1% BSA and 0.1% Triton X-100 in PBS.

Microscopic analysis were performed either with a classical light microscope, a DMRXA2 Leica microscope or by confocal microscopy.

Antibodies and dilution were as following:

Antibody against	Dilution	Produced in	Reference, supplier
Calbindin	1/1 500	mouse	C9848, Sigma-Aldrich
Calbindin	1/1000	rabbit	CB38, Swant
GM130	1/500	mouse	610822
CACNA1A	1/100	rabbit	ACC-001, Alomone labs
ITPR1	1/100	goat	Sc-6093, Santa Cruz biotechnology
KCNC3	1/100	rabbit	APC-102, Alomone labs
KCNAB3	1/100	rabbit	PA5-36970, Invitrogen
SLC7A5	1/300	rabbit	Ab111106, Abcam
TUBB3	1/400	mouse	MAB1637, Millipore
GFAP	1/100	rabbit	04-1062, Milipore

Secondary antibodies: goat anti-rabbit, goat anti-mouse or donkey anti-goat coupled to Alexa Fluor 488 or 594 (Life technologies) were used depending on the combination of primary antibodies.

Primary cell culture

Primary myoblasts

Hind limb muscles of P7 to P10 newborn mice were dissected, and kept in PBS on ice until minced. Minced tissues were then transferred in a digestion mix (0.5 mg/mL collagenase (Sigma, C9263) and 3.5 mg/mL dispase (Invitrogen, 17105041) in IMDM) containing collagenase and dispase) and incubated for 1h30 at 37°C under agitation. Digestion was stopped by addition of dissection medium (IMDM with Glutamax (Invitrogen, 31980022), 0.1% gentamycin, 10% FBS). Suspensions were centrifuged (600rpm, 5min) and supernatant was kept for further centrifugation (1300rpm, 5 min). Pelleted cells were then resuspended in 2-3mL dissection medium (for each cell suspension from a pup). Cell suspensions were filtered (through a 40mm cell strainer) and pre-plated for 3h at 37°C (cell culture incubator) in 6 well-plates (1 well per cells extracted from a pup). This pre-plating enables to eliminate contamination with fibroblasts. At the end of the pre-plating, supernatant was collected and centrifuged (1500rpm, 10min). Pelleted cells were then resuspended in proliferation medium (IMDM with Glutamax (Invitrogen, 31980022), 0.1% gentamycin, 20% FBS and 1% CEE (MP Biomedical, 2850145)) and plated in Matrigel (BD Bioscience) coated wells. Cells were incubated as classically: at

37°C in a humidified chamber containing 5% CO_2. Medium was changed every 2 days and myoblasts were trypsinized and splitted when almost at confluence. For myoblasts differentiation in myotubes, when myoblasts reached confluence, medium was switched to differentiation medium (IMDM with Glutamax (Invitrogen, 31980022) and 2% horse serum) and the day after the switch, Matrigel was added on top of the cells.

Proliferation assay: myoblasts were initially seeded at a density of 5 000 cells per well in 6 well-plates coated with Matrigel. Six myoblasts lines were used per genotype with each line derived from a different animal. One well for each cell line was trypsinized per day and the cell number was counted with an automated Scepter™ 2.0 Cell Counter (Merck Millipore). Trypsination and counting were reapeated for 6 days. Medium was replaced every two days. Population doubling was counted as a ratio over the number of cell counted on day 1 for each cell line.

Diffentiation assay: myoblasts were seeded to $3.0*10^4$ cells per well in 6-well plates coated with Matrigel and left to grow until they reached around 80% confluence (six wells were seeded per cell line). At that point, proliferation medium was replaced by differentiation medium. The day after the switch of medium, Matrigel was added on top of the cells and Agrin incorporated into the medium. Differentiation medium with Agrin was replaced every two days. Cells were harvested just before the switch of medium (D0), then on the next day (D1) before addition of Matrigel on top of the cells, and then every two days (D3-D9). Cells pellets were snap frozen and RNA extracted as mentioned for quantitative real time PCR.

Primary hippocampal cultures

Cultures were derived from E17.5 and E18.5 embryos. The pregnant mouse was sacrificed and embryos sampled within the uterus and kept in S1 solution (2.56 mg/ml D-glucose, 3 mg/ml BSA and 1.16 mM $MgSO_4$ in PBS 1x). Embryos were then taken out from the embryonic sac and dissected in S1 solution. Hippocampus were detached and cut in small pieces before being centrifuged in S1 solution 1 min at 1000 rpm at RT. S2 solution (S1 solution with 0.25 mg/ml trypsin and 0.08 mg/ml DNase) was added on the pellet and incubated 20 min at 37°C. To stop the reaction S4 (84% S1 solution and 16% S3 solution) was added and samples centrifuged 5 min at 1000 rpm. The pellet was mechanically resuspended in S3 solution (S1 solution with 0.52 mg/ml soybean trypsin inhibitor SBTI, 0.08 mg/ml DNase and 1.5 mM $MgSO_4$) and centrifuged 5 min at 1000 rpm. Seeding medium (DMEM with 10 mM

Hepes, 10% horse serum, 50 µg/ml gentamycin and 1 µg/ml insulin) was added to the pelleted cells and cells seeded on poly-L-lysine coated coverslips. Cultures were incubated at 37°C with 5% CO_2. The next day, medium was replaced by neurobasal medium (Neurobasal medium with 0.5 mM glutamine, 2% B27 supplements and penicillin/streptomycin) which was changed every 3-4 days.

Primary cerebellar cultures

Cerebellum of P0 pups were dissected out in HBSS and stored on ice. Papain was added (10 units of papain latex in 1ml of a solution with 0.45 mg/ml L-cysteine, 1.982 mg/ml kynurenate, 74 mM Na_2SO_4, 27 mM K_2SO_4, 15 mM $MgCl_2$, 0.2 mM $CaCl_2$, 1.4 mM Hepes, and 18 mM glucose) on the cerebellum and incubated 30 min at 30°C. Cerebellum were than washed with pre-warmed HBSS and slowly triturated in a solution containing DNase (0.05% DNase in HBSS and 12 mM $MgSO_4$). Samples were than centrifuged 5 min at 800 rpm and cells were resuspended in supplemented medium with 10% FBS before being plated on poly-L-lysine coated coverslips in a small volume and being incubated at 37°C with 5% CO_2. After 3h, supplemented medium (DMEM/F12 with 100 µM putrescine, 30 nM sodium selenite, 1.4 mM glutamine, 40 nM progesterone, 20 µg/ml insulin, 200 µg/ml transferrin, 0.5 ng/ml T_3 supplement, 100 µg/ml BSA) with 5% FBS was added. The supplemented medium without serum was changed every 3-4 days and fluorodeoxyuridine was added.

Organotypic cerebellar cultures

Cerebella of P8 to P12 mice were dissected out and transferred to dissection medium (MEM with 25 mM Hepes (ThermoFischer scientific, 11544456) + 5g/L of D-glucose (Sigma, G8769), sterile filtered). Cerebella were then cut sagittally with a tissue chopper (McIlwain Tissue chopper) in 350 µm thick slices. These slices were separated from one another with spatulas in dissection medium, and transferred on a Millicell membrane (Millipore, PICM03050). The Millicell insert with 8-10 isolated cerebellar slices was then put in a 6 well-plate with incubation medium (50 % MEM with 25 mM Hepes + 25% inactivated horse serum + 25% BME (ThermoFischer scientific, 41010) + 5g/L of D-glucose + 2µM L-glutamine + 1x penicillin/streptomycin, sterile filtered). Medium was changed every 2-3 days.

Mitochondrial respiration

Myoblasts from *Coq8a*$^{-/-}$ and WT mice were seeded in Seahorse XFe-96 assay plates and cultured for 12 to 24 hours. Cellular respiration was quantified using the Seahorse Extracellular Flux Analyzer XF-96 (Seahorse Biosciences, USA). Prior to each experiment, 96-well Seahorse culture plates were pre-coated with Matrigel (BD Biosciences, Erembodegem, Belgium). Cells were incubated for 1 h in bicarbonate-free (unbuffered) XF Base Medium supplemented with 2 mM L-Glutamine, 1 mM pyruvate and 10 or 5 mM glucose or 10 mM galactose, prior to the experiment. The XF^{e} Analyzer was then calibrated according to the manufacturer's instructions, and respiration of cells was quantified as the oxygen consumption rate (OCR) at baseline and following treatment with different mitochondrial modulators. In glucose conditions, 1.5 µM oligomycin, 1 µM of FCCP (carbonyl cyanide-p-trifluoromethoxyphenylhydrazone), and 0.5 µM rotenone with 0.5 µM antimycin A were progressively added. In galactose conditions, 5 mM glucose conditions and for myotubes, the concentrations remained the same except for oligomycin for which 2 µM were added. The OCR results shown are representative of 2 independent experiments with each time 6 biological replicates. Assays were performed prior to experiments to determine the optimal concentration of each compound. After measurements were completed, data was normalized to the total number of cells per well (cell nuclei stained with DAPI, counted by microscopy with an automated counting system). An ANOVA test was performed for statistical analysis, using GraphPad Prism. For cerebellar primary cultures, the settings remained the same except that the cultures were seeded in the Seahorse 96 well-plate on the day of the experiment and left to grow for at least one week prior to the assay.

Glycolysis

The glycolysis assay was similar to the mitochondrial respiration assay. Myoblasts were seeded in a Seahorse 96 well-plate coated with Matrigel, 12 to 24 h prior to the assay. 1 h before the experiment the media was changed and bicarbonate-free (unbuffered) XF Base Medium supplemented with 1 mM glutamine was added. The XF^{e} Analyzer was then calibrated according to the manufacturer's instructions, and glycolysis of cells was quantified as the extracellular acidification rate (ECAR) at baseline and following treatment with different modulators. Progressive addition of modulators: 10 mM glucose, followed by 1 µM oligomycin and finally 50 mM 2-DG. After measurements were completed, data was normalized to the total number of cells per well (cell nuclei stained with DAPI,

counted by microscopy with an automated counting system). The ECAR results shown are representative of 3 independent experiments with each time 6 biological replicates. An ANOVA test was performed for statistical analysis, using GraphPad Prism

Quantitative real-time PCR

RNA was extracted using TRI Reagent® (Molecular Research Center) according to the manufacturer protocol. Tissues were homogenized in TRI Reagent® using Precellys® tubes with ceramic beads and a Precellys24 homogenizer apparatus (Bertin instruments). Cells or grinded tissues were directly lysed in TRI Reagent®. Reverse transcription was achieved using the Transcriptor Reverse Transcriptase kit (Roche Biosciences). Quantitative real-time PCR was performed using SYBR Green I Master (Roche Biosciences) and Light Cycler 480 (Roche Biosciences). Quantification was performed with *Hprt* as internal standard, and statistical analysis were performed with an unpaired t-test. Primers were as following:

	Sequence 5' to 3'	
Gene name	Forward #1	Reverse #1
Abca1	GGTTTGGAGATGGTTATACAATAGTTGT	TTCCCGGAAACGCAAGTC
Abcg1	AGGTCTCAGCCTTCTAAAGTTCCTC	TCTCTCGAAGTGAATGAAATTTATCG
Acaca - ACC1	AAGGCTATGTGAAGGATG	CTGTCTGAAGAGGTTAGG
Ache	GCCCCATGGCTATGAAATCGAGTT	ATTTGGAGTCTCGAGGGTCATTGG
Acox	ATCATGTGGTTTAAAAACTCTGTGC	GGAACATGCCCAAGTGAAGG
AdipoQ	CAGTCATGCCGAAGATGACG	TAGGACCAAGAAGACCTGCATC
ApoA1	CCAACAGCTGAACCTGAATCTCCT	GCTGCACCTTCTGTTTCACTTCC
ApoAII	ATGCAGAGCCTGTTCACTCA	CTGACCTGACAAGGGGTGTC
ApoE	GACTTGTTTCGGAAGGAGC	CCACTCGAGCTGATCTGTCA
ApoJ	AAGCCGTGCGGAATGAGATAGAAG	GCAAGTGCAGGCATTAGTGTACAG
AsnS	ATTACGACAGTTCGGGCATC	TCTCAGTTCGAGACCGTGTG
Atf4	GGCCAAGCACTTGAAACCTC	TCCTCCTTGCCGGTGTCTGA
Atp1a3	CTTTGCTTTGTGGGTCTCATGTCC	GCGATGTCTTCGACAGTCTCGTTA
B3galt2	GATGGCGTGCCAAAAGTATT	TCATCGTCTTCTGGTTCAGGT
Cars	ATAGCAGGCTGCAAGATGTCCAAG	GCAGACTCCATAGTGTTGCTGGAA
Cebpa	AGACCTAGGTTTCTGGGCTTTGTG	TCTGGGATGGATCGATTGTGCTTC
Ckmt1	ACAGGCAGCGTCTTTGACATCT	GGGGATGGGGAGTTAATGTTTGCT
Copa	GCCCAAGCCTGAAGTAGCTC	TCTCCACTGGTTTTCCACGG
Cox8a	TCGGGGTCCTGGATATCACCATT	ATGATCAAGGTGGGCTGGCAAA
Cplx1	CCATGGAGTTCGTGATGAAA	CCTCCTTCTTAGCAGCATCG

Cpt1a	ACCAACGGGCTCATCTTCT	CAAAATGACCTAGCCTTCT
Des	CGACACCAGATCCAGTCCTAC	GCAATGTTGTCCTGATAGCCAT
Dgat2	GAACGCAGTCACCCTGAAGA	GGGAACCAGATCAGCTCCAT
Dusp10	ACAAACAGAACCTGCGGCAGTA	CATCAAGTAGGCGATGACGATGGT
Dusp10	ACAAACAGAACCTGCGGCAGTA	CATCAAGTAGGCGATGACGATGGT
Enah	AACGGCAGTAAGTCACCTGTCATC	AGCCTGTCATAGTCAAGGCCTTCT
Faim2	GGGCAAGCCCTCAGCCATAAATAA	CAGGGGTCAACATCAAGGCTTTCT
Fasn	CCCTGACCAAGGTGCTGTTA	GGATCTCAGGGTTGGGGTTG
Fdft1	ATCAGACCAGTCGCAGCTTT	CGGAGAACCAGGTAGAACACA
Fos	AGATACACTCCAAGCGGAGACAGA	GTCGGTGGGCTGCCAAAATAAAC
Gas5	ACCTCAAGTGAAGGCACTGCAA	CCATCCAGGCACCTCAGAAACAAA
Grin2d	ATGGTGCGATACAACCAGCCAA	ATCCTTTCGGGCCATGTAGTTGAG
Hmgcr	TGATTGGAGTTGGCACCAT	TGGCCAACACTGACATGC
Hpca	ATGTATGACCTGGATGGCAATGGC	TCGACTCATCCTCGGGCATTTTC
Hprt	GTAATGATCAGTCAACGGGGGAC	CCAGCAAGCTTGCAACCTTAACCA
Hsd17b7	ATCTGGACGTTGCTCCTACCCATA	GCCCGTGACGTAATTAGTCCCAAA
Irf17	CAGGTTCTGCAGTACAGCCACATA	GCTGCATAGGGTTCCTCGTAAACA
Kcnab3	ATCTTCTCCCAACTGCTCGC	ACAATCACTCCGCATTGGGT
Kcnh2	TTTGGTCTAGCCTGGAGATCACCT	TACGCCTGCGGAATGACAGTTT
Kcnj10	CCCCGGACAAACCCTTATCTGATT	ATAGACCTTAGCGACCGACGTCAT
Kcnk2	GTGGCAGGTGGATCAGACATTGAA	CAGTCCCCAATCATGCTCAGAACA
Ldlr	CTGTGGGCTCCATAGGCTATCT	GCGGTCCAGGGTCATCTTC
Lpl	TTTTCTGGGACTGAGGATGG	GTCAGGCCAGCTGAAGTAG
Lrp1	TGGGTCTCCCGAAATCTGTT	ACCACCGCATTCTTGAAGGA
Lrp8	CTGGGGTTTCCAGGCAAAGATTGA	AGTACAAACGCTGGCTCAGCAA
LXRalpha	AGGAGTGTCGACTTCGCAAA	CTCTTCTTGCCGCTTCAGTTT
LXRbeta	AAGCAGGTGCCAGGGTTCT	TGCATTCTGTCTCGTGGTTGT
Lyplal1	GAGAGTGGATCAAGCACGTGCTAA	AGGTGTTCTGGGCAGTCCATAGAT
Mcad	GAACCAGACCTACAGTCGCA	AGGGCATACTTCGTGGCTTC
Mt1	TCACTTACTCCGTAGCTCCAGCTT	GGTGCACTTGCAGTTCTTGCAG
Myf5	GGAGATCCTCAGGAATGCCAT	TCGTGTTCTTTCGGGACCAGA
Myoc	ACGTTGGCCTTCCAGGAATTGA	ACTTGCCAGCGATTGTTTCAGC
MyoD	GCTGCCTTCTACGCACCTG	GCCGCTGTAATCCATCATGC
MyoG	GACTCCCCACTCCCCATTCACATA	GGCAGCTTTACAAACAACACA
Ncs1	GCTCGACATAGTGGACGCCATTTA	ACTCCTGAAGAGTCAGCTTCCCAT
Nnat	CGGCCCTTCACTGATCTTGCTTAT	TCCCTGTCTCCAGGAGCTTACAAT
Nos1ap	AGAATGCAGATGGCCAGGAAGATG	ACACCTCGGCTGAATTCCAGAATG
Nrsn1	ACAGGTGGAGCTCAGTATTCTGGA	CAGCTTCGCCAAAAGCTTCGAT
Nrxn1	AGTGTCCCAGTGACGATGAGG	ATGGTTCACGGCCACCTACTC
Nudt3	ACTCGGTGAACATCGGAAGGAAGA	GCCTTGCCTCAACGTCTCAAAGTA
Pax7	GGCACAGAGGACCAAGCTC	GCACGCCGGTTACTGAAC
Pcp4	CATTGCCTTCTGAGCTGTTCTGTG	TGACGTCTTGTCTTTTCCGTTGGT

Pgc1α	GCAGGTCGAACGAAACTGAC	CTTGCTCTTGGTGGAAGCAG
Plch1	CTACCGGCATGTCTACCTGG	TTCTGAAGAAGCGTGCCTGG
Plcl2	CAGAAGGCAGTGGAGAGCTT	TTCTGGGCCTCGGAGTTTTC
Pltp	ACGTGGCCTTTTCCGAGTTCTT	TCACTGTCGGACTCAGGAGAACAA
Pltp	ACGTGGCCTTTTCCGAGTT	TCACTGTCGGACTCAGGAG
Plxna4	CTCATCGCCTACAAACGCAAATCC	GATATCTGTCTGCAGCTCGGCAAA
Ppargc1a	GGTGTAGCGACCAATCGGAAATCA	AGAACCGCTAGCAAGTTTGCCT
Ret	GGGACGGAAGATGAAGATTTCCGA	GACTCAATTGCCATCCACTTGACG
Sccpdh	CATTGGAAGCAGTGGCTTTGACTC	ATTGCCGACTTCCAGGTTCCAT
Scd1	TCACTTCACCACGTTCTTC	CTCCCGTCTCCAGTTCTCTT
Sesn2	TGCAGCCTCACCTATAACACCATC	ACCTCGCCGTAATCATAGTCATCG
Slc24a3	AAGCCAATTTCCACCGCAAAGC	TTAACATGCGACTGGCCATGGA
Slc6a7	TGGACCTGGATGTAGACTTCGCA	ATTCCACAGATGGCCAGCATGA
Slc7a3	AGCCCTCTGCCTGAAGCATTTT	GTGAACCTTAGCAAGGACACGGAA
Slc7a5	TCTTCGCCACCTACTTGCTC	GCCTTTACGCTGTAGCAGTT
Slc8a3	CCTCTGTGCCAGATACATTTGCCA	GCCAAACCAATACCCAGGAAGACA
Sncg	CCAAGCAGGGAGTAACGGA	GGTTCCAAGTCCTCCTTGCG
Snhg11	TTTCCCAAGGGCTGTTTCCCA	TGATAAACGGCAGCGACTCCAA
Srebp1a	GCCGGCGCCATGGACGAG	ATGTCGTTCAAAACCGCTGTGTC
Srebp1c	CGCGGAAGCTGTCGGGGTAG	AAATGTGCAATCCATGGCTCCGTGGTC
Srebp2	CACAATATCATTGAAAAGCGCTACCGGTCC	TTTTTCTGATTGGCCAGCTTCAGCACCATG
Synj1	TCACCACAGCTGCAGGTAA	TTTGCGATGCAGAAGGCAAC
Syt17	CTGGAAAACGCCAGCCTAGT	CGGAGGAATACTGGCCGATG
Tmem25	GCCAATGCCTCTGTCATCCTCAAT	AGGGCAAACAGGACAACCAGAA
Trpm2	CTTGCTGATGCAAGGTACAGAGGT	CACGGGTCAACTCCTTTGGATCAT
Tuba1a	ACGGTCATCGATGAAGTTCGCA	GTGTAGTGGCCACGAGCATAGTTA
β-actin	GGCATAGAGGTCTTTACGG	GTGGCATCCATGAAACTACAT

Transfection

COS1 cells were grown in DMEM media with glucose or galactose (Dulbecco's modified Eagle's medium: DMEM with 1g/L of glucose or of galactose + 5% fetal calf serum: FCS 202+ gentamycin), at 37°C in a humidified chamber containing 5% CO_2. These cells were transfected with pc DNA3.1 plasmids encoding murine COQ proteins. Transfection was performed either with only the plasmid encoding COQ8A-FLAG, or COQ5-HA, or COQ4-HA, or COQ3-HA or COQ7-HA or COQ9-HA, or a combination of the COQ8A-FLAG and a COQ-HA encoding plasmid. Shortly, COS cells were plated a few days before the experiment and transfected when approximately 80% confluence was reached. Transfection was performed with FuGENE®6 Transfection Reagent (Promega) according to the manufacturer protocol. On the day of the transfection, cells were washed with PBS and new media was added. Then FuGENE®6

was mixed with serum free medium: Opti-MEM (1,5ml Opti-MEM with 80µl FuGENE®6 Transfection Reagent per 20cm dishes). This solution was vortexed and left at RT for 5 minutes. After this incubation time, DNA was added in a 1:4 ratio (4µl of FuGENE®6 per µg of plasmid added). This final mix was vortexed and incubated 20 minutes at RT, before being added dropwise into the cells and gently mixed. Cells were incubated for 24h before being washed and harvested, then the pellets were snap frozen (in NH_2) for immunoprecipitation assays.

Immunoprecipitation

Immunoprecipitation was performed as described for COS cells (Stefely et al., 2016). For elution, 2 solutions were assessed: 0.2M Glycine solution at pH 2.8 and 0.2mg/ml FLAG peptide in TBS (10 mM Tris HCl, 150 mM NaCl, pH 7.4). Both solutions yielded the same results. For the assays with nucleotides: 4 mM $MgCl_2$ and 1 mM nucleotide (ATP or ADP) were added to all immunoprecipitation solutions except to the elution buffer (so in the lysing solution with digitonin, the mitochondrial resuspension buffer with Triton X-100 and the wash buffer which is the same as the mitochondrial resuspension buffer).

Western blots

Protein were extracted with RIPA buffer (50 mM Tris pH 8, 150 mM NaCl, 0.5% Na-deoxycholate, 0.1% SDS, 1x cOmplete™ Protease Inhibitor Cocktail (Roche), 1% Triton X-100) or PEB buffer (10 mM Tris pH 7.4, 10% glycerol, 100 mM NaCl, 50 mM KCl, 1x cOmplete™ Protease Inhibitor Cocktail (Roche), 0.2% Triton X-100, and for immunoprecipitation assays or phospho-protein immunoblot: 1x PhosSTOP™ (Roche) was also added). For Western blot, proteins were separated by SDS-Tris-Glycine PAGE, run in a Tris-glycine solution (14.4 g/l glycine, 3.02 g/l Tris base, 0.1% SDS) and transferred onto nitrocellulose membranes (200 mA, 1h20). Aspecific antigens were then blocked in PBS-T (Phosphate Buffer Saline 1x with 0.05% Tween 20) with 5% dried milk and proteins were probed with primary antibodies in PBS-T with 1% dried milk. Proteins of interest were detected with HRP-conjugated secondary antibodies: goat anti-mouse or goat anti-rabbit IgG antibody (1: 5 000, Jackson Immuno Research and ab 97051, Abcam) and visualized with the Amersham™ Imager 600 (GE Healthcare, Little Chalfont, UK), according to the provided protocol.

Antibody against	Dilution	Produced in	Reference, supplier
COQ5	1/500	rabbit	17453-1-AP, Proteintech
COQ7	1/800	rabbit	15083-1-AP, Proteintech
COQ9	1/200	rabbit	Ab104189, Abcam
COQ8A	1/3 000	rabbit	pL52 n°3388 AE2.4, IGBMC in-house production (Stefely et al., 2016)
GAPDH	1/70 000	mouse	MAB374, Merck Millipore
Tubulin	1/40 000	mouse	2A2, IGBMC in-house production
FLAG	1/5 000	mouse	F3165, Sigma Aldrich
HA	1/ 800	rabbit	Ab9110, Abcam
NR2B	1/1 000	rabbit	06-600, Millipore
GAD65/67	1/10 000	goat	SC-7513, Santa Cruz
vGLUT2	1/5 000	Guinea pig	Ab2251, Millipore
COX4	1/4 000	mouse	ab 14744, Abcam
COPA	1/500	rabbit	ab104710, Abcam
PLCH1	1/500	rabbit	19143-1-AP, Proteintech
SYT17	1/500	rabbit	154113-1-AP, Proteintech
TST	1/500	rabbit	16311-1-AP, Proteintech
CACNA1A	1/200	rabbit	ACC-001, Alomone labs
GRM1	1/250	rabbit	Ab1551, Millipore
ITPR1	1/500	goat	Sc-6093, Santa Cruz biotechnology
KCNC3	1/200	rabbit	APC-102, Alomone labs

II. Additional data

1. Skeletal muscle

When mitochondrial respiration and glycolysis were assessed in myoblasts, a focus was put on trying to validate deregulated transcripts found by RNA-sequencing in quadriceps. Indeed, if the deregulated transcript levels could also be found in Coq8a$^{-/-}$ myoblasts, it would have been a proof that these primary cultures are a good model to assess deregulated pathways. By an Ingenuity Pathway Analysis (Quiagen), lipid metabolism was one of the molecular and cellular function coming out in RNA-sequencing of quadriceps (Table 8). Primers, for genes implicated in this pathway, were therefore designed. Transcripts levels were assessed in 30 weeks old Coq8a$^{-/-}$ and WT mice quadriceps, by qRT-PCR. None of the transcriptional deregulation assessed could be validated (Table 9).

Molecular and Cellular Functions

Name	p-value	Number of genes
Lipid Metabolism	4,05E-03 - 9,18E-11	37
Molecular Transport	4,39E-03 - 9,18E-11	46
Small Molecule Biochemistry	4,39E-03 - 9,18E-11	44
Cell Morphology	3,96E-03 - 5,71E-09	44
Carbohydrate Metabolism	3,96E-03 - 1,07E-07	27

Table 8 : Ingenuity Pathway Analysis of RNA-sequencing of quadriceps.

Molecular and cellular functions predicted to be affected are depicted in the first column; the p-value corresponds to the confidence in this prediction and the number of genes is the number of genes implicated in this pathway, not the one deregulated in the RNA-sequencing dataset.

	Quadriceps 30 weeks			
	RNA-sequencing		qRT-PCR	
Gene name	KO /WT	Adjusted P-value (KO vs WT)	KO / WT	P-value (KO vs WT)
Adipoq	2,36	1,06E-07	1,015	9,42E-01
ApoE	1,27	4,56E-02	1,298	3,89E-01
Cebpa	2,06	3,41E-03	1,071	8,00E-01
COPA	0,70	5,72E-07	0,508	1,53E-01
Dusp10	0,63	2,70E-03	1,109	6,27E-01
Enah	0,77	2,87E-02	1,240	1,85E-01
Fos	0,37	2,64E-02	0,918	8,03E-01
Gas5	0,50	4,19E-05	0,893	2,71E-01
Mt1	0,45	1,09E-12	0,846	7,11E-01
Nnat	3,22	3,04E-11	1,438	3,82E-01
Sncg	2,34	7,67E-06	1,206	6,10E-01
Tuba1a	1,43	9,00E-03	1,223	3,61E-01

Table 9 : Gene coming up in quadriceps by RNA-sequencing of 30 weeks old Coq8a$^{-/-}$ mice and assessed by qRT-PCR.

RNA sequencing: n=3, qRT-PCR: n=6; KO/WT: fold change between KO and WT.

2. Cerebellum

	Cerebellum							
	RNA-sequencing		qRT-PCR					
	30 weeks		30 weeks		5 weeks		1 week	
Gene name	KO/WT	Adjusted P-value (KO vs WT)	KO/WT	P-value (KO vs WT)	KO/WT	P-value (KO vs WT)	KO/WT	P-value (KO vs WT)
Apoa2	0,010	1,18E-03	0,166	2,34E-05	0,127	1,24E-05	0,235	3,77E-03
Copa	0,688	1,89E-08	0,713	2,45E-05	0,804	1,88E-03	0,820	1,35E-02
Hsd17b7	0,739	3,54E-02			0,873	7,55E-02	1,269	3,97E-02
Slc7a3	0,117	4,56E-38			0,222	1,82E-08	0,811	1,46E-01
Syt17	1,868	6,86E-01	1,623	7,56E-05	1,613	2,94E-06	0,995	9,61E-01
Snhg11	1,417	5,25E-08	1,217	2,21E-02	1,251	1,06E-04	0,989	9,19E-01
Asns	0,701	1,00E-04	0,651	3,05E-07	0,760	1,37E-04	0,940	4,46E-01
Plch1	1,324	7,46E-02	1,399	1,45E-03	1,384	2,13E-04	0,815	9,57E-02
Kcnab3	1,721	7,21E-10	1,559	5,39E-06	1,476	2,71E-04	0,907	2,16E-01
Ret	1,601	5,29E-08			1,658	8,32E-04	0,952	6,65E-01
Slc24a3	1,418	1,05E-05	1,363	1,35E-03	1,237	1,48E-03	0,915	2,67E-01
B3galt2	1,519	7,19E-04	1,502	5,86E-04	1,256	3,07E-03	1,052	5,65E-01
Sesn2	0,572	4,66E-07			0,681	3,86E-03	0,904	4,73E-01
Kcnj10	1,164	6,86E-01			1,540	4,54E-03	0,975	8,74E-01
Sccpdh	0,850	8,27E-01			0,843	9,06E-03	0,899	1,22E-01
Hpca	1,513	1,27E-06			1,433	9,19E-03	0,861	2,79E-01
Cplx1	1,235	4,69E-02	1,138	2,73E-02	1,147	1,14E-02	0,919	4,29E-01
Slc6a7	1,946	7,15E-08			1,569	1,21E-02	0,842	3,07E-01
Faim2	1,223	8,54E-02			1,217	1,95E-02	0,865	2,94E-01
Ache	1,188	5,13E-01			1,182	2,36E-02	0,995	9,33E-01
Srebp1c	0,955	1,00E+00			0,906	2,88E-02	1,039	5,52E-01
Nrsn1	1,256	1,46E-01			1,249	3,02E-02	0,958	5,24E-01
Cars	0,800	8,66E-02			0,814	3,13E-02	0,986	8,60E-01
Atf4	0,824	1,46E-01	0,673	5,55E-03	0,780	3,64E-02	0,822	2,31E-01
Trpm2	1,275	1,94E-01			1,197	3,65E-02	0,861	1,17E-01
Grin2d	1,400	8,18E-02			1,291	3,68E-02	0,975	8,02E-01
ApoA1	1,565	1,00E+00			0,758	3,75E-02	0,286	3,32E-01
Gas5	0,611	4,56E-02	0,878	1,19E-02	0,966	5,31E-01		
Lyplal1	2,765	7,21E-10	1,028	7,51E-01				
Myoc	0,279	6,03E-24			1,009	9,49E-01		
Irf7	0,485	1,63E-03			1,161	6,63E-01		
Nos1ap	1,383	1,21E-02	1,103	3,34E-01	1,160	8,68E-02	1,033	7,89E-01
Plxna4	1,281	2,24E-02			0,933	5,27E-01		
Slc7a5	0,779	5,62E-02			0,795	5,94E-02	0,983	8,64E-01

	Cerebellum							
	RNA-sequencing		qRT-PCR					
	30 weeks		30 weeks		5 weeks		1 week	
Gene name	KO/WT	Adjusted P-value (KO vs WT)	KO/WT	P-value (KO vs WT)	KO/WT	P-value (KO vs WT)	KO/WT	P-value (KO vs WT)
Ncs1	1,198	3,29E-01			1,069	5,23E-01		
Slc8a3	1,300	4,80E-01			1,051	5,44E-01		
Pcp4	0,848	5,76E-01			0,958	6,02E-01		
Kcnk2	0,701	6,24E-01			1,017	8,74E-01		
Atp1a3	1,155	6,86E-01			1,128	8,40E-02	0,950	6,01E-01
Ckmt1	1,172	8,11E-01			1,132	7,57E-02	0,990	8,94E-01
Kcnh2	1,216	8,41E-01			1,159	2,53E-01		
Tmem25	1,171	8,97E-01			1,085	2,66E-01		
Cox8a	1,225	9,49E-01			1,053	5,38E-01		
Srebp1a	0,955	1,00E+00			0,976	4,54E-01	1,073	2,60E-01
Srebp2	0,941	1,00E+00			1,021	7,59E-01	0,974	7,55E-01
Synj1	1,041	1,00E+00			0,917	2,56E-01	1,065	4,23E-01
ApoE	0,948	1,00E+00			1,007	8,74E-01	0,932	3,87E-01
ApoJ	0,974	1,00E+00			1,054	3,39E-01	0,867	2,75E-01
Abca1	1,015	1,00E+00			0,950	4,23E-01	0,860	3,24E-01
Abcg1	1,005	1,00E+00			1,008	8,56E-01	0,963	7,60E-01
Pltp	1,043	1,00E+00			0,971	5,14E-01	0,953	4,63E-01
Acox	1,002	1,00E+00			0,965	5,71E-01	0,954	6,76E-01
Cpt1a	0,978	1,00E+00			1,014	7,40E-01	0,990	8,99E-01
Nr1h2	0,996	1,00E+00			1,017	7,87E-01	1,074	3,69E-01
Scd1	0,976	1,00E+00			1,025	6,24E-01	0,921	6,02E-01
Dgat2	1,093	1,00E+00			0,980	7,34E-01	1,016	8,77E-01
Ldlr	0,866	1,00E+00			1,011	9,05E-01	1,053	6,36E-01
Lrp1	0,972	1,00E+00			1,023	8,19E-01	0,950	7,89E-01
Hmgcr	0,928	1,00E+00			1,009	8,36E-01	0,952	7,33E-01

Table 10 : RNA-sequencing and qRT-PCR results from Coq8a$^{-/-}$ and WT mice cerebellum.

Gene tested by qRT-PCR in cerebellum of Coq8a$^{-/-}$ and WT mice and results of RNA-sequencing for these genes, RNA sequencing: n=3, qRT-PCR: n=6; KO/WT: fold change.

	Cerebellum		
Gene Name	Fold change (KO/WT)	P-Value	Q-Value
Apoa2	0,33	2,01E-06	8,75E-03
Cars	0,89	4,62E-03	4,10E-01
Nudt3	0,81	2,56E-02	6,33E-01
Sccpdh	0,90	4,83E-02	7,02E-01
Cplx1	1,21	6,28E-02	7,25E-01
Kcnj10	1,18	7,87E-02	7,90E-01
Asns	0,89	1,45E-01	8,23E-01
Faim2	1,07	1,55E-01	8,28E-01
Copa	0,94	3,10E-01	8,76E-01

Table 11 : Results of proteomic analysis of 30 weeks old Coq8a$^{-/-}$ and WT mice cerebellum obtained for proteins for which deregulated transcripts levels were observed.

Data obtained by proteomic analysis in Dr. David Pagliarini's laboratory using 30 weeks old Coq8a$^{-/-}$ and WT mice cerebellum. Q-value: adjusted P-value; Fold change: Coq8a$^{-/-}$ protein expression divided by WT expression obtained. n=3.

3. Hydrogen sulfide

Gene Names	Cerebellum (KO/WT)	Cerebellum P-Value	Muscle (KO/WT)	Muscle P-Value	Kidney (KO/WT)	Kidney P-Value	Heart (KO/WT)	Heart P-Value
Sqrdl	1,01	9,06E-01	1,30	6,98E-04	1,39	1,64E-04	1,20	4,55E-03
Tst	0,90	2,17E-01	1,18	1,96E-02	1,00	9,53E-01	0,99	9,34E-01
Suox	1,04	7,21E-01	0,94	3,57E-01	1,01	7,28E-01	1,01	9,07E-01
Ethe1	1,07	1,84E-01	-	-	1,09	2,33E-02	0,95	6,56E-01

Table 12 : Results of proteomic analysis of 30 weeks old Coq8a$^{-/-}$ and WT mice cerebellum obtained for proteins implicated in hydrogen sulfide catabolism

Data obtained by proteomic analysis in Dr. David Pagliarini's laboratory using 30 weeks old Coq8a$^{-/-}$ and WT mice cerebellum. Q-value: adjusted P-value; Fold change: Coq8a$^{-/-}$ protein expression divided by WT expression obtained. n=3.

BIBLIOGRAPHY

Bibliography

Åberg, F., Appelkvist, E.L., Dallner, G., and Ernster, L. (1992). Distribution and redox state of ubiquinones in rat and human tissues. Arch. Biochem. Biophys. *295*, 230–234.

Ackermann, M., Kubitza, M., Maier, K., Brawanski, A., Hauska, G., and Pi??a, A.L. (2011). The vertebrate homolog of sulfide-quinone reductase is expressed in mitochondria of neuronal tissues. Neuroscience *199*, 1–12.

Aeby, A., Sznajer, Y., Cavé, H., Rebuffat, E., Van Coster, R., Rigal, O., and Van Bogaert, P. (2007). Cardiofaciocutaneous (CFC) syndrome associated with muscular coenzyme Q10 deficiency. J. Inherit. Metab. Dis. *30*, 827.

Afri, M., Ehrenberg, B., Talmon, Y., Schmidt, J., Cohen, Y., and Frimer, A.A. (2004). Active oxygen chemistry within the liposomal bilayer: Part III: Locating Vitamin E, ubiquinol and ubiquinone and their derivatives in the lipid bilayer. Chem. Phys. Lipids *131*, 107–121.

Aguer, C., Gambarotta, D., Mailloux, R.J., Moffat, C., Dent, R., McPherson, R., and Harper, M.E. (2011). Galactose enhances oxidative metabolism and reveals mitochondrial dysfunction in human primary muscle cells. PLoS One *6*.

Akbar, U., and Ashizawa, T. (2015). Ataxia. Neurol. Clin. *33*, 225–248.

Akizu, N., Cantagrel, V., Zaki, M.S., Al-Gazali, L., Wang, X., Rosti, R.O., Dikoglu, E., Gelot, A.B., Rosti, B., Vaux, K.K., et al. (2015). Biallelic mutations in SNX14 cause a syndromic form of cerebellar atrophy and lysosome-autophagosome dysfunction. Nat. Genet. *47*, 528–534.

Alcázar-Fabra, M., Navas, P., and Brea-Calvo, G. (2016). Coenzyme Q biosynthesis and its role in the respiratory chain structure. Biochim. Biophys. Acta - Bioenerg. *1857*, 1073–1078.

Alexander, E.T., and Phillips, M.C. (2013). Influence of apolipoprotein A-I and apolipoprotein A-II availability on nascent HDL heterogeneity. J. Lipid Res. *54*, 3464–3470.

Allan, C.M., Awad, A.M., Johnson, J.S., Shirasaki, D.I., Wang, C., Blaby-Haas, C.E., Merchant, S.S., Loo, J.A., and Clarke, C.F. (2015). Identification of Coq11, a new coenzyme Q biosynthetic protein in the CoQ-synthome in saccharomyces cerevisiae. J. Biol. Chem. *290*, 7517–7534.

Amado, M., Almeida, R., Carneiro, F., Levery, S.B., Holmes, E.H., Nomoto, M., Hollingsworth, M.A., Hassan, H., Schwientek, T., Nielsen, P.A., et al. (1998). A family of human beta3-galactosyltransferases. Characterization of four members of a UDP-galactose:beta-N-acetyl-glucosamine/beta-nacetyl-galactosamine beta-1,3-galactosyltransferase family. J. Biol. Chem. *273*, 12770–12778.

Ameri, K., and Harris, A.L. (2008). Activating transcription factor 4. Int. J. Biochem. Cell Biol. *40*, 14–21.

Aminlari, M., Malekhusseini, A., Akrami, F., and Ebrahimnejad, H. (2007). Cyanide-metabolizing enzyme rhodanese in human tissues: Comparison with domestic animals. Comp. Clin. Path. *16*, 47–51.

Amiri, K., RJ, H., and PJ, H. (2008). Fragile x–associated tremor/ataxia syndrome: An aging face of the fragile x gene. Arch. Neurol. *65*, 19–25.

Andersen, B.B., Korbo, L., and Pakkenberg, B. (1992). A quantitative study of the human cerebellum with unbiased stereological techniques. J. Comp. Neurol. *326*, 549–560.

Andersen, L.W., Mackenhauer, J., Roberts, J.C., Berg, K.M., Cocchi, M.N., and Donnino, M.W. (2013). Etiology and therapeutic approach to elevated lactate levels. Mayo Clin. Proc. *88*, 1127–1140.

Anheim, M., Tranchant, C., and Koenig, M. (2012). The autosomal recessive cerebellar ataxias. N. Engl. J. Med. *366*, 636–646.

Anttonen, A.-K., Mahjneh, I., Hämäläinen, R.H., Lagier-Tourenne, C., Kopra, O., Waris, L., Anttonen, M., Joensuu, T., Kalimo, H., Paetau, A., et al. (2005). The gene disrupted in Marinesco-Sjögren syndrome encodes SIL1, an HSPA5 cochaperone. Nat. Genet. *37*, 1309–1311.

Apps, R., and Garwicz, M. (2005). Anatomical and physiological foundations of cerebellar information processing. Nat. Rev. Neurosci. *6*, 297–311.

Armstrong, D.M. (1974). Functional significance of connections of the inferior olive. Physiol. Rev. *54*, 358–417.

Artuch, R., Salviati, L., Jackson, S., Hirano, M., and Navas, P. (2009). Coenzyme Q10 deficiencies in neuromuscular diseases. In Advances in Experimental Medicine and Biology, pp. 117–128.

Asencio, C., Navas, P., Cabello, J., Schnabel, R., Cypser, J.R., Johnson, T.E., and Rodríguez-Aguilera, J.C. (2009). Coenzyme Q supports distinct developmental processes in Caenorhabditis elegans. Mech. Ageing Dev. *130*, 145–153.

Ashby, M.N., Kutsunai, S.Y., Ackerman, S., Tzagoloff, A., and Edwards, P.A. (1992). COQ2 is a candidate for the structural gene encoding para-hydroxybenzoate:polyprenyltransferase. J. Biol. Chem. *267*, 4128–4136.

Ashraf, S., Gee, H.Y., Woerner, S., Xie, L.X., Vega-Warner, V., Lovric, S., Fang, H., Song, X., Cattran, D.C., Avila-Casado, C., et al. ADCK4 mutations promote steroid-resistant nephrotic syndrome through CoQ 10 biosynthesis disruption. J. Clin. Invest. *123*.

Ashraf, S., Gee, H.Y., Woerner, S., Xie, L.X., Vega-Warner, V., Lovric, S., Fang, H., Song, X., Cattran, D.C., Avila-Casado, C., et al. (2013). ADCK4 mutations promote steroid-Resistant nephrotic syndrome through CoQ10 biosynthesis disruption. J. Clin. Invest. *123*, 5179–5189.

Assoum, M., Salih, M.A., Drouot, N., Hnia, K., Martelli, A., and Koenig, M. (2013). The salih ataxia mutation impairs rubicon endosomal localization. Cerebellum *12*, 835–840.

Aussel, L., Pierrel, F., Loiseau, L., Lombard, M., Fontecave, M., and Barras, F. (2014). Biosynthesis and physiology of coenzyme Q in bacteria. Biochim. Biophys. Acta - Bioenerg. *1837*, 1004–1011.

Baines, C.P., Kaiser, R.A., Purcell, N.H., Blair, N.S., Osinska, H., Hambleton, M.A., Brunskill, E.W., Sayen, M.R., Gottlieb, R.A., Dorn, G.W., et al. (2005). Loss of cyclophilin D reveals a critical role for mitochondrial permeability transition in cell death. Nature *434*, 658–662.

Barca, E., Musumeci, O., Montagnese, F., Marino, S., Granata, F., Nunnari, D., Peverelli, L., DiMauro, S., Quinzii, C.M., and Toscano, A. (2016). Cerebellar ataxia and severe muscle CoQ10 deficiency in a patient with a novel mutation in ADCK3. Clin. Genet. *90*, 156–160.

Beaudin, M., Klein, C.J., Rouleau, G.A., and Dupré, N. (2017). Systematic review of autosomal recessive ataxias and proposal for a classification. Cerebellum & Ataxias *4*, 3.

Beier, C.P. (2005). FasL (CD95L/APO-1L) Resistance of Neurons Mediated by Phosphatidylinositol 3-Kinase-Akt/Protein Kinase B-Dependent Expression of Lifeguard/Neuronal Membrane Protein 35. J. Neurosci. *25*, 6765–6774.

Bekri, S., Kispal, G., Lange, H., Fitzsimons, E., Tolmie, J., Lill, R., and Bishop, D.F. (2000). Human ABC7 transporter: gene structure and mutation causing X-linked sideroblastic anemia with ataxia with disruption of cytosolic iron-sulfur protein maturation. Blood *96*, 3256–3264.

Belliere, J., Devun, F., Cottet-Rousselle, C., Batandier, C., Leverve, X., and Fontaine, E. (2012). Prerequisites for ubiquinone analogs to prevent mitochondrial permeability transition-induced cell death. J. Bioenerg. Biomembr. *44*, 207–212.

Bentinger, M., Dallner, G., Chojnacki, T., and Swiezewska, E. (2003). Distribution and breakdown of labeled coenzyme Q10 in rat. Free Radic. Biol. Med. *34*, 563–575.

Bentinger, M., Tekle, M., and Dallner, G. (2010). Coenzyme Q - Biosynthesis and functions. Biochem. Biophys. Res. Commun. *396*, 74–79.

Beyer, R.E., Segura-Aguilar, J., Di Bernardo, S., Cavazzoni, M., Fato, R., Fiorentini, D., Galli, M.C., Setti, M., Landi, L., and Lenaz, G. (1996). The role of DT-diaphorase in the maintenance of the reduced antioxidant form of coenzyme Q in membrane systems. Proc. Natl. Acad. Sci. U. S. A. *93*, 2528–2532.

Bhavya, S., Lew, P.S., and Mizuno, T.M. (2016). Central action of xenin affects the expression of lipid metabolism-related genes and proteins in mouse white adipose tissue. Neuropeptides *63*, 67–73.

Biagini, G., Benini, R., de Guzman, P., Longo, D., Avoli, M., Di Maio, R., and Capogna, M. (2013a). Perirhinal cortex and temporal lobe epilepsy.

Biagini, G., D'Antuono, M., Benini, R., de Guzman, P., Longo, D., and Avoli, M. (2013b). Perirhinal cortex and temporal lobe epilepsy. Front. Cell. Neurosci. *7*, 130.

Biebl, M., Cooper, C.M., Winkler, J., and Kuhn, H.G. (2000). Analysis of neurogenesis and programmed cell death reveals a self-renewing capacity in the adult rat brain. Neurosci. Lett. *291*, 17–20.

Bird, T.D. (2016). Hereditary Ataxia Overview - Review. Genet. Couns. 1–39.

Blanco-Vaca, F., Escolà-Gil, J.C., Martín-Campos, J.M., and Julve, J. (2001). Role of apoA-II in lipid metabolism and atherosclerosis: advances in the study of an enigmatic protein. J. Lipid Res. *42*, 1727–1739.

Blumkin, L., Leshinsky-Silver, E., Zerem, A., Yosovich, K., Lerman-Sagie, T., and Lev, D. (2014). Heterozygous Mutations in the ADCK3 Gene in Siblings with Cerebellar Atrophy and Extreme Phenotypic Variability. JIMD Rep. *12*, 103–107.

Bockenhauer, D., Feather, S., Stanescu, H.C., Bandulik, S., Zdebik, A.A., Reichold, M., Tobin, J., Lieberer, E., Sterner, C., Landoure, G., et al. (2009). Epilepsy, ataxia, sensorineural deafness, tubulopathy, and KCNJ10 mutations. N. Engl. J. Med. *360*, 1960–1970.

Bolk, L. (1906). Das Cerebellum der Säugetiere: eine verglichende anatomische Untersuchung.

Böning, D., Lindinger, M.I., Bailey, D.M., Berczi, I., Kalsi, K., González-Alonso, J., Dyck, D.J., Robinson, L.E., Wright, D.C., Docherty, J.R., et al. (2012). Aerobic Metabolism. In Encyclopedia of Exercise Medicine in Health and Disease, (Berlin, Heidelberg: Springer Berlin Heidelberg), pp. 29–32.

Braga Neto, P., Pedroso, J.L., Kuo, S.-H., Marcondes Junior, C.F., Teive, H.A.G., and Barsottini, O.G.P. (2016). Current concepts in the treatment of hereditary ataxias. Arq. Neuropsiquiatr. *74*, 244–252.

Braissant, O., Gotoh, T., Loup, M., Mori, M., and Bachmann, C. (1999). L-arginine uptake, the citrulline-NO cycle and arginase II in the rat brain: An in situ hybridization study. Mol. Brain Res. *70*, 231–241.

Brandt, U. (1999). Proton translocation in the respiratory chain involving ubiquinone - A hypothetical semiquinone switch mechanism for complex I. BioFactors *9*, 95–101.

Brüning, A., Rahmeh, M., and Friese, K. (2013). Nelfinavir and bortezomib inhibit mTOR activity via ATF4-mediated sestrin-2 regulation. Mol. Oncol. *7*, 1012–1018.

Buchkremer, S., González Coraspe, J.A., Weis, J., and Roos, A. (2016). Sil1-Mutant Mice Elucidate Chaperone Function in Neurological Disorders. J. Neuromuscul. Dis. *3*, 169–181.

Burazin, T.C.D., and Gundlach, A.L. (1999). Localization of GDNF/neurturin receptor (c-ret, GFR??-1 and ??-2) mRNAs in postnatal rat brain: Differential regional and temporal expression in hippocampus, cortex and cerebellum. Mol. Brain Res. *73*, 151–171.

Burman, J.L., Bourbonniere, L., Philie, J., Stroh, T., Dejgaard, S.Y., Presley, J.F., and McPherson, P.S. (2008). Scyl1, mutated in a recessive form of spinocerebellar neurodegeneration, regulates COPI-mediated retrograde traffic. J. Biol. Chem. *283*, 22774–22786.

Calvo, S.E., Julien, O., Clauser, K.R., Shen, H., Kamer, K.J., Wells, J.A., and Mootha, V.K. (2017). Comparative Analysis of Mitochondrial N-Termini from Mouse, Human, and Yeast. Mol. Cell. Proteomics *16*, 512–523.

Campuzano, V., Montermini, L., Moltò, M.D., Pianese, L., Cossée, M., Cavalcanti, F., Monros, E., Rodius, F., Duclos, F., Monticelli, A., et al. (1996). Triplet Repeat Expansion Friedreich â€™s Ataxia : Autosomal Recessive Disease Caused by an Intronic GAA Triplet Repeat Expansion. Science (80-.). *271*, 1423–1427.

Cerminara, N.L., Lang, E.J., Sillitoe, R. V, and Apps, R. (2015). Redefining the cerebellar cortex as an assembly of non-uniform Purkinje cell microcircuits. Nat. Rev. Neurosci. *16*, 79–93.

Chan, D.C., Ng, T.W.K., and Watts, G.F. (2012). Apolipoprotein A-II: Evaluating its significance in dyslipidaemia, insulin resistance, and atherosclerosis. Ann. Med. *44*, 313–324.

Chang, T.-Y., Yamauchi, Y., Hasan, M.T., Chang, C.C.Y., and Chang, T.-Y. (2017). Cellular Cholesterol Homeostasis and Alzheimer's Disease. Dartmouth Coll.

Chang, Y.-F., Imam, J.S., and Wilkinson, M.F. (2007). The Nonsense-Mediated Decay RNA Surveillance Pathway. Annu. Rev. Biochem. *76*, 51–74.

Chen, H., Pan, Y.X., Dudenhausen, E.E., and Kilberg, M.S. (2004). Amino acid deprivation induces the transcription rate of the human asparagine synthetase gene through a timed program of expression and promoter binding of nutrient-responsive basic region/leucine zipper transcription factors as well as localized histone . J. Biol. Chem. *279*, 50829–50839.

Chow, V.T., and Quek, H.H. (1997). Alpha coat protein COPA (HEP-COP): presence of an Alu repeat in cDNA and identity of the amino terminus to xenin. Ann. Hum. Genet. *61*, 369–373.

Chung, W.K., Martin, K., Jalas, C., Braddock, S.R., Juusola, J., Monaghan, K.G., Warner, B., Franks, S., Yudkoff, M., Lulis, L., et al. (2015). Mutations in *COQ4* , an essential component of coenzyme Q biosynthesis, cause lethal neonatal mitochondrial encephalomyopathy. J. Med. Genet. *52*, 627–635.

Clarkson, Y.L., Gillespie, T., Perkins, E.M., Lyndon, A.R., and Jackson, M. (2010). B-III spectrin mutation L253P associated with spinocerebellar ataxia type 5 interferes with binding to Arp1 and protein trafficking from the Golgi. Hum. Mol. Genet. *19*, 3634–3641.

Colin, F., Martelli, A., Clémancey, M., Latour, J.M., Gambarelli, S., Zeppieri, L., Birck, C., Page, A., Puccio, H., and Ollagnier De Choudens, S. (2013). Mammalian frataxin controls sulfur production and iron entry during de novo Fe4S4 cluster assembly. J. Am. Chem. Soc. *135*, 733–740.

Cortez, D., Wang, Y., Qin, J., and Elledge, S.J. (1999). Requirement of ATM-dependent phosphorylation of brca1 in the DNA damage response to double-strand breaks. Science *286*, 1162–1166.

Costanzo, V., Robertson, K., Bibikova, M., Kim, E., Grieco, D., Gottesman, M., Carroll, D., and Gautier, J. (2001). Mre11 protein complex prevents double-strand break accumulation during chromosomal DNA replication. Mol. Cell *8*, 137–147.

Crabtree, G.W., Park, A.J., Gordon, J.A., and Gogos, J.A. (2016). Cytosolic Accumulation of L-Proline Disrupts GABA-Ergic Transmission through GAD Blockade. Cell Rep. *17*, 570–582.

Crane, F.L., Hatefi, Y., Lester, R.L., and Widmer, C. (1957). Isolation of a quinone from beef heart mitochondria. Biochim. Biophys. Acta *25*, 220–221.

Crane, F.L., Sun, I.L., Barr, R., and L??w, H. (1991). Electron and proton transport across the plasma membrane. J. Bioenerg. Biomembr. *23*, 773–803.

Crawley, J.N., Belknap, J.K., Collins, A., Crabbe, J.C., Frankel, W., Henderson, N., Hitzemann, R.J., Maxson, S.C., Miner, L.L., Silva, A.J., et al. (1997). Behavioral phenotypes of inbred mouse strains: Implications and recommendations for molecular studies. Psychopharmacology (Berl). *132*, 107–124.

Dallner, G., and Sindelar, P.J. (2000). Regulation of ubiquinone metabolism. Free Radic. Biol. Med. *29*, 285–294.

Davidson, E., Caffarella, J., Vitseva, O., Hou, Y.M., and King, M.P. (2001). Isolation of two cDNAs encoding functional human cytoplasmic cysteinyl-tRNA synthetase. Biol. Chem. *382*, 399–406.

Dean, C., Dunning, F.M., Liu, H., Bomba-Warczak, E., Martens, H., Bharat, V., Ahmed, S., and Chapman, E.R. (2012). Axonal and dendritic synaptotagmin isoforms revealed by a pHluorin-syt functional screen. Mol. Biol. Cell *23*, 1715–1727.

Devun, F., Walter, L., Belliere, J., Cottet-Rousselle, C., Leverve, X., and Fontaine, E. (2010). Ubiquinone analogs: A mitochondrial permeability transition pore-dependent pathway to selective cell death. PLoS One *5*, e11792.

Dimova, R. (2014). Recent developments in the field of bending rigidity measurements on membranes. Adv. Colloid Interface Sci. *208*, 225–234.

Diomedi-Camassei, F., Di Giandomenico, S., Santorelli, F.M., Caridi, G., Piemonte, F., Montini, G., Ghiggeri, G.M., Murer, L., Barisoni, L., Pastore, A., et al. (2007). COQ2 nephropathy: a newly described inherited mitochondriopathy with primary renal involvement. J. Am. Soc. Nephrol. *18*, 2773–2780.

Divakaruni, A.S., Rogers, G.W., and Murphy, A.N. (2014). Measuring mitochondrial function in permeabilized cells using the seahorse XF analyzer or a clark-type oxygen electrode. Curr. Protoc. Toxicol. *2014*, 25.2.1-25.2.16.

Do, T.Q., Hsu, A.Y., Jonassen, T., Lee, P.T., and Clarke, C.F. (2001). A Defect in Coenzyme Q Biosynthesis is Responsible for the Respiratory Deficiency in Saccharomyces cerevisiae abc1 Mutants. J. Biol. Chem. *276*, 18161–18168.

Doetschman, T. (2009). Influence of genetic background on genetically engineered mouse phenotypes. Methods Mol. Biol. *530*, 423–433.

Doi, H., Yoshida, K., Yasuda, T., Fukuda, M., Fukuda, Y., Morita, H., Ikeda, S.I., Kato, R., Tsurusaki, Y., Miyake, N., et al. (2011). Exome sequencing reveals a homozygous SYT14 mutation in adult-onset, autosomal-recessive spinocerebellar ataxia with psychomotor retardation. Am. J. Hum. Genet. *89*, 320–327.

Douillard-Guilloux, G., Mouly, V., Caillaud, C., and Richard, E. (2009). Immortalization of murine muscle cells from lysosomal a-glucosidase deficient mice: A new tool to study pathophysiology and assess therapeutic strategies for Pompe disease.

Duarri, A., Jezierska, J., Fokkens, M., Meijer, M., Schelhaas, H.J., Den Dunnen, W.F.A., Van Dijk, F., Verschuuren-Bemelmans, C., Hageman, G., Van De Vlies, P., et al. (2012). Mutations in potassium channel KCND3 cause spinocerebellar ataxia type 19. Ann. Neurol. *72*, 870–880.

Duncan, A.J., Bitner-Glindzicz, M., Meunier, B., Costello, H., Hargreaves, I.P., López, L.C., Hirano, M., Quinzii, C.M., Sadowski, M.I., Hardy, J., et al. (2009). A Nonsense Mutation in COQ9 Causes Autosomal-Recessive Neonatal-Onset Primary Coenzyme Q10 Deficiency: A Potentially Treatable Form of Mitochondrial Disease. Am. J. Hum. Genet. *84*, 558–566.

Duncan, E.J., Larivière, R., Bradshaw, T.Y., Longo, F., Sgarioto, N., Hayes, M.J., Romano, L.E.L., Nethisinghe, S., Giunti, P., Bruntraeger, M.B., et al. (2017). Altered organisation of the intermediate filament cytoskeleton and relocalisation of proteostasis modulators in cells lacking the ataxia protein sacsin. Hum. Mol. Genet. *26*, 3130–3143.

Durr, A. (2010). Autosomal dominant cerebellar ataxias: Polyglutamine expansions and beyond. Lancet Neurol. *9*, 885–894.

Echtay, K.S., Winkler, E., and Klingenberg, M. (2000). Coenzyme Q is an obligatory cofactor for uncoupling protein function. Nature *408*, 609–613.

Echtay, K.S., Winkler, E., Frischmuth, K., and Klingenberg, M. (2001). Uncoupling proteins 2 and 3 are highly active H+ transporters and highly nucleotide sensitive when activated by coenzyme Q (ubiquinone). Proc. Natl. Acad. Sci. *98*, 1416–1421.

El-Khamisy, S.F., Saifi, G.M., Weinfeld, M., Johansson, F., Helleday, T., Lupski, J.R., and Caldecott, K.W. (2005). Defective DNA single-strand break repair in spinocerebellar ataxia with axonal neuropathy-1. Nature *434*, 108–113.

Elkalaf, M., Anděl, M., and Trnka, J. (2013). Low Glucose but Not Galactose Enhances Oxidative Mitochondrial Metabolism in C2C12 Myoblasts and Myotubes. PLoS One *8*.

Elrick, M.J., Pacheco, C.D., Yu, T., Dadgar, N., Shakkottai, V.G., Ware, C., Paulson, H.L., and Lieberman, A.P. (2010). Conditional Niemann-Pick C mice demonstrate cell autonomous Purkinje cell neurodegeneration. Hum. Mol. Genet. *19*, 837–847.

Ernster, L., and Dallner, G. (1995). Biochemical, physiological and medical aspects of ubiquinone function. BBA - Mol. Basis Dis. *1271*, 195–204.

Ernster, L., and Forsmark-Andrée, P. (1993). Ubiquinol: an endogenous antioxidant in aerobic organisms. Clin. Investig. *71*, S60-5.

Esclapez, M., and Houser, C.R. (1999). Up-regulation of GAD65 and GAD67 in remaining hippocampal GABA neurons in a model of temporal lobe epilepsy. J. Comp. Neurol. *412*, 488–505.

Eugster, A., Frigerio, G., Dale, M., and Duden, R. (2000). COP I domains required for coatomer integrity, and novel interactions with ARF and ARF-GAP. EMBO J. *19*, 3905–3917.

Evans, D.R., and Guy, H.I. (2004). Mammalian pyrimidine biosynthesis: Fresh insights into an ancient pathway. J. Biol. Chem. *279*, 33035–33038.

Farlow, M.R., DeMyer, W., Dlouhy, S.R., and Hodes, M.E. (1987). X-linked recessive inheritance of ataxia and adult-onset dementia: clinical features and preliminary linkage analysis. Neurology *37*, 602–607.

Fernández, M., Segura, M.F., Solé, C., Colino, A., Comella, J.X., and Ceña, V. (2007). Lifeguard/neuronal membrane protein 35 regulates Fas ligand-mediated apoptosis in neurons via microdomain recruitment. J. Neurochem. *103*, 190–203.

Festenstein, G., Heaton, F., Lowe, J., and Morton, R. (1955). A Constituent of the Unsaponifiable Portion of Animal Tissue Lipids (λmax. 272 mμ.). Biochem. J. *4*, 558–566.

Filla, A., and De Michele, G. (2011). Overview of autosomal recessive ataxias. Handb. Clin. Neurol. *103*, 265–274.

Finkel, T., and Holbrook, N.J. (2000). Oxidants, oxidative stress and the biology of ageing. Nature *408*, 239–247.

Fiskerstrand, T., H'Mida-Ben Brahim, D., Johansson, S., M'Zahem, A., Haukanes, B.I., Drouot, N., Zimmermann, J., Cole, A.J., Vedeler, C., Bredrup, C., et al. (2010). Mutations in ABHD12 cause the neurodegenerative disease PHARC: An inborn error of endocannabinoid metabolism. Am. J. Hum. Genet. *87*, 410–417.

Floyd, B.J., Wilkerson, E.M., Veling, M.T., Minogue, C.E., Xia, C., Beebe, E.T., Wrobel, R.L., Cho, H., Kremer, L.S., Alston, C.L., et al. (2016). Mitochondrial Protein Interaction Mapping Identifies Regulators of Respiratory Chain Function. Mol. Cell *63*, 621–632.

Fontaine, E., Ichas, F., and Bernardi, P. (1998). A ubiquinone-binding site regulates the mitochondrial permeability transition pore. J. Biol. Chem. *273*, 25734–25740.

Freeman, W., and Morton, A.J. (2004). Differential messenger RNA expression of complexins in mouse brain. Brain Res. Bull. *63*, 33–44.

Freyer, C., Stranneheim, H., Naess, K., Mourier, A., Felser, A., Maffezzini, C., Lesko, N., Bruhn, H., Engvall, M., Wibom, R., et al. (2015). Rescue of primary ubiquinone deficiency due to a novel COQ7 defect using 2,4-dihydroxybensoic acid. J. Med. Genet. *52*, 779–783.

Fried, N.T., Moffat, C., Seifert, E.L., and Oshinsky, M.L. (2014). Functional mitochondrial analysis in acute brain sections from adult rats reveals mitochondrial dysfunction in a rat model of migraine. AJP Cell Physiol. *307*, C1017–C1030.

Furutama, D., Morita, N., Takano, R., Sekine, Y., Sadakata, T., Shinoda, Y., Hayashi, K., Mishima, Y., Mikoshiba, K., Hawkes, R., et al. (2010). Expression of the IP3R1 promoter-driven nls-LacZ transgene in Purkinje cell parasagittal arrays of developing mouse cerebellum. J. Neurosci. Res. *88*, 2810–2825.

Van Gaalen, J., Kerstens, F.G., Maas, R.P.P.W.M., Härmark, L., and Van De Warrenburg, B.P.C. (2014). Drug-induced cerebellar ataxia: A systematic review. CNS Drugs *28*, 1139–1153.

Galassi, V.V., and Arantes, G.M. (2015). Partition, orientation and mobility of ubiquinones in a lipid bilayer. Biochim. Biophys. Acta - Bioenerg. *1847*, 1560–1573.

Garaeva, A.A., Kovaleva, I.E., Chumakov, P.M., and Evstafieva, A.G. (2016). Mitochondrial dysfunction induces SESN2 gene expression through activating transcription factor 4. Cell Cycle *15*, 64–71.

Garcia, V., Phelps, S.E.L., Gray, S., and Neale, M.J. (2011). Bidirectional resection of DNA double-strand breaks by Mre11 and Exo1. Nature *479*, 241–244.

García-Corzo, L., Luna-Sánchez, M., Doerrier, C., García, J.A., Guarás, A., Acín-Pérez, R., Bullejos-Peregrín, J., López, A., Escames, G., Enríquez, J.A., et al. (2013). Dysfunctional coq9 protein causes predominant encephalomyopathy associated with CoQ deficiency. Hum. Mol. Genet. *22*, 1233–1248.

García-Corzo, L., Luna-Sánchez, M., Doerrier, C., Ortiz, F., Escames, G., Acuña-Castroviejo, D., and López, L.C. (2014). Ubiquinol-10 ameliorates mitochondrial encephalopathy associated with CoQ deficiency. Biochim. Biophys. Acta - Mol. Basis Dis. *1842*, 893–901.

Garcia-Diaz, B., Barca, E., Balreira, A., Lopez, L.C., Tadesse, S., Krishna, S., Naini, A., Mariotti, C., Castellotti, B., and Quinzii, C.M. (2015). Lack of aprataxin impairs mitochondrial functions via downregulation of the APE1/NRF1/NRF2 pathway. Hum. Mol. Genet. *24*, 4516–4529.

Gempel, K., Topaloglu, H., Talim, B., Schneiderat, P., Schoser, B.G.H., Hans, V.H., Pálmafy, B., Kale, G., Tokatli, A., Quinzii, C., et al. (2007). The myopathic form of coenzyme Q10 deficiency is caused by mutations in the electron-transferring-flavoprotein dehydrogenase (ETFDH) gene. Brain *130*, 2037–2044.

Gerards, M., van den Bosch, B., Calis, C., Schoonderwoerd, K., van Engelen, K., Tijssen, M., de Coo, R., van der Kooi, A., and Smeets, H. (2010). Nonsense mutations in CABC1/ADCK3 cause progressive cerebellar ataxia and atrophy. Mitochondrion *10*, 510–515.

Gille, L., and Nohl, H. (2000). The existence of a lysosomal redox chain and the role of ubiquinone. Arch. Biochem. Biophys. *375*, 347–354.

Glickstein, M., Strata, P., and Voogd, J. (2009). Cerebellum: history. Neuroscience *162*, 549–559.

Goldstein, J.L., and Brown, M.S. (1990). Regulation of the mevalonate pathway. Nature *343*, 425–430.

Gómez-Díaz, C., Rodríguez-Aguilera, J.C., Barroso, M.P., Villalba, J.M., Navarro, F., Crane, F.L., and Navas, P. (1997). Antioxidant ascorbate is stabilized by NADH-Coenzyme Q10 reductase in the plasma membrane. J. Bioenerg. Biomembr. *29*, 251–257.

Gómez-Herreros, F., Schuurs-Hoeijmakers, J.H.M., McCormack, M., Greally, M.T., Rulten, S., Romero-Granados, R., Counihan, T.J., Chaila, E., Conroy, J., Ennis, S., et al. (2014). TDP2 protects transcription from abortive topoisomerase activity and is required for normal neural function. Nat. Genet. *46*, 516–521.

Gravel, C., and Hawkes, R. (1990). Parasagittal organization of the rat cerebellar cortex: Direct comparison of purkinje cell compartments and the organization of the spinocerebellar projection. J. Comp. Neurol. *291*, 79–102.

Green, D., and Tzagoloff, A. (1966). The Mitochondrial Electron Transfer Chain. Arch. Biochem. Biophys. *116*, 293–304.

Grienberger, C., and Konnerth, A. (2012). Imaging Calcium in Neurons. Neuron *73*, 862–885.

Grimaldi, G., Argyropoulos, G.P., Bastian, A., Cortes, M., Davis, N.J., Edwards, D.J., Ferrucci, R., Fregni, F., Galea, J.M., Hamada, M., et al. (2016). Cerebellar Transcranial Direct Current Stimulation (ctDCS): A Novel Approach to Understanding Cerebellar Function in Health and Disease. Neuroscientist *22*, 1073858414559409-.

Groh, M., Lufino, M.M.P., Wade-Martins, R., and Gromak, N. (2014). R-loops Associated with Triplet Repeat Expansions Promote Gene Silencing in Friedreich Ataxia and Fragile X Syndrome. PLoS Genet. *10*, e1004318.

Grudzien-Nogalska, E., Jiao, X., Song, M.-G., Hart, R.P., and Kiledjian, M. (2016). Nudt3 is an mRNA decapping enzyme that modulates cell migration. RNA *22*, 773–781.

Grünler, J., Ericsson, J., and Dallner, G. (1994). Branch-point reactions in the biosynthesis of cholesterol, dolichol, ubiquinone and prenylated proteins. Biochim. Biophys. Acta (BBA)/Lipids Lipid Metab. *1212*, 259–277.

Guergueltcheva, V., Azmanov, D.N., Angelicheva, D., Smith, K.R., Chamova, T., Florez, L., Bynevelt, M., Nguyen, T., Cherninkova, S., Bojinova, V., et al. (2012). Autosomal-recessive congenital cerebellar ataxia is caused by mutations in metabotropic glutamate receptor 1. Am. J. Hum. Genet. *91*, 553–564.

Guissart, C., Li, X., Leheup, B., Drouot, N., Montaut-Verient, B., Raffo, E., Jonveaux, P., Roux, A.F., Claustres, M., Fliegel, L., et al. (2015). Mutation of SLC9A1, encoding the major Na+/H+ exchanger, causes ataxia-deafness Lichtenstein-Knorr syndrome. Hum. Mol. Genet. *24*, 463–470.

Habas, C., Kamdar, N., Nguyen, D., Prater, K., Beckmann, C.F., Menon, V., and Greicius, M.D. (2009). Distinct cerebellar contributions to intrinsic connectivity networks. J. Neurosci. *29*, 8586–8594.

Hallen, A., Jamie, J.F., and Cooper, A.J.L. (2013). Lysine metabolism in mammalian brain: An update on the importance of recent discoveries. Amino Acids *45*, 1249–1272.

Hartzell, H.C., Yu, K., Xiao, Q., Chien, L.-T., and Qu, Z. (2009). Anoctamin/TMEM16 family members are Ca 2+ -activated Cl − channels. J Physiol *58710*, 2127–2139.

Hauß, T., Dante, S., Haines, T.H., and Dencher, N.A. (2005). Localization of coenzyme Q10 in the center of a deuterated lipid membrane by neutron diffraction. Biochim. Biophys. Acta - Bioenerg. *1710*, 57–62.

Häusser, M., Clark, B.A., Abbott, L.F., Varela, J.A., Sen, K., Nelson, S.B., Abeles, M., Albus, J.S., Alger, B.E., Nicoll, R.A., et al. (1997). Tonic Synaptic Inhibition Modulates Neuronal Output Pattern and Spatiotemporal Synaptic Integration. Neuron *19*, 665–678.

Hawkes, R., Blyth, S., Chockkan, V., Tano, D., Ji, Z., and Mascher, C. (1993). Structural and molecular compartmentation in the cerebellum. Can.J.Neurol.Sci. *20 Suppl 3*, S29–S35.

Hayano, M., Yang, W.S., Corn, C.K., Pagano, N.C., and Stockwell, B.R. (2016). Loss of cysteinyl-tRNA synthetase (CARS) induces the transsulfuration pathway and inhibits ferroptosis induced by cystine deprivation. Cell Death Differ. *23*, 270–278.

He, C.H., Xie, L.X., Allan, C.M., Tran, U.C., and Clarke, C.F. (2014). Coenzyme Q supplementation or over-expression of the yeast Coq8 putative kinase stabilizes multi-subunit Coq polypeptide complexes in yeast coq null mutants. Biochim. Biophys. Acta - Mol. Cell Biol. Lipids *1841*, 630–644.

He, C.H., Black, D.S., Nguyen, T.P.T., Wang, C., Srinivasan, C., and Clarke, C.F. (2015). Yeast Coq9 controls deamination of coenzyme Q intermediates that derive from para-aminobenzoic acid. Biochim. Biophys. Acta - Mol. Cell Biol. Lipids *1851*, 1227–1239.

Heckroth, J.A., and Abbott, L.C. (1994). Purkinje cell loss from alternating sagittal zones in the cerebellum of leaner mutant mice. Brain Res. *658*, 93–104.

Heeringa, S.F., Chernin, G., Chaki, M., Zhou, W., Sloan, A.J., Ji, Z., Xie, L.X., Salviati, L., Hurd, T.W., Vega-Warner, V., et al. (2011). COQ6 mutations in human patients produce nephrotic syndrome with sensorineural deafness. J. Clin. Invest. *121*, 2013–2024.

Herebian, D., Seibt, A., Smits, S.H.J., Bünning, G., Freyer, C., Prokisch, H., Karall, D., Wredenberg, A., Wedell, A., López, L.C., et al. (2017). Detection of 6-demethoxyubiquinone in CoQ10 deficiency disorders: Insights into enzyme interactions and identification of potential therapeutics. Mol. Genet. Metab. *121*, 216–223.

Herrup, K., and Wilczynski, S.L. (1982). Cerebellar cell degeneration in the leaner mutant mouse. Neuroscience *7*, 2185–2196.

Hess, S.D., Daggett, L.P., Deal, C., Lu, C.C., Johnson, E.C., and Veliçelebi, G. (1998). Functional characterization of human N-methyl-D-aspartate subtype 1A/2D receptors. J. Neurochem. *70*, 1269–1279.

Hikmat, O., Tzoulis, C., Knappskog, P.M., Johansson, S., Boman, H., Sztromwasser, P., Lien, E., Brodtkorb, E., Ghezzi, D., and Bindoff, L.A. (2016). ADCK3 mutations with epilepsy, stroke-like episodes and ataxia: a POLG mimic? Eur. J. Neurol. *23*, 1188–1194.

Hills, L.B., Masri, A., Konno, K., Kakegawa, W., Lam, A.T.N., Lim-Melia, E., Chandy, N., Hill, R.S., Partlow, J.N., Al-Saffar, M., et al. (2013). Deletions in GRID2 lead to a recessive syndrome of cerebellar ataxia and tonic upgaze in humans. Neurology *81*, 1378–1386.

Hirano, M., Garone, C., and Quinzii, C.M. (2012). CoQ10 deficiencies and MNGIE: Two treatable mitochondrial disorders. Biochim. Biophys. Acta - Gen. Subj. *1820*, 625–631.

Horton, J.D., Goldstein, J.L., and Brown, M.S. (2002). SREBPs: Activators of the complete program of cholesterol and fatty acid synthesis in the liver. J. Clin. Invest. *109*, 1125–1131.

Horvath, R. (2012). Update on clinical aspects and treatment of selected vitamin-responsive disorders II (riboflavin and CoQ 10). J. Inherit. Metab. Dis. *35*, 679–687.

Horvath, R., Czermin, B., Gulati, S., Demuth, S., Houge, G., Pyle, A., Dineiger, C., Blakely, E.L., Hassani, A., Foley, C., et al. (2012). Adult-onset cerebellar ataxia due to mutations in CABC1/ADCK3. J. Neurol. Neurosurg. Psychiatry *83*, 174–178.

Hosokawa, H., Ninomiya, H., Sawamura, T., Sugimoto, Y., Ichikawa, A., Fujiwara, K., and Masaki, T. (1999). Neuron-specific expression of cationic amino acid transporter 3 in the adult rat brain. Brain Res. *838*, 158–165.

Hsieh, E.J., Gin, P., Gulmezian, M., Tran, U.C., Saiki, R., Marbois, B.N., and Clarke, C.F. (2007). Saccharomyces cerevisiae Coq9 polypeptide is a subunit of the mitochondrial coenzyme Q biosynthetic complex. Arch. Biochem. Biophys. *463*, 19–26.

Huang, Y., Kang, B.N., Tian, J., Liu, Y., Luo, H.R., Hester, L., and Snyder, S.H. (2007). The cationic amino acid transporters CAT1 and CAT3 mediate NMDA receptor activation-dependent changes in elaboration of neuronal processes via the mammalian target of rapamycin mTOR pathway. J. Neurosci. *27*, 449–458.

Hutson, R.G., and Kilberg, M.S. (1994). Cloning of rat asparagine synthetase and specificity of the amino acid-dependent control of its mRNA content. Biochem J *304 (Pt 3*, 745–750.

Hwang, J.-I., Oh, Y.-S., Shin, K.-J., Kim, H., Ryu, S.H., and Suh, P.-G. (2005). Molecular cloning and characterization of a novel phospholipase C , PLC-ŋ. Biochem. J *186*, 181–186.

Ichas, F., and Mazat, J.P. (1998). From calcium signaling to cell death: Two conformations for the mitochondrial permeability transition pore. Switching from low- to high-conductance state. Biochim. Biophys. Acta - Bioenerg. *1366*, 33–50.

IMPC Gene details for coenzyme Q4 | International Mouse Phenotyping Consortium.

Infante, R.E., Wang, M.L., Radhakrishnan, A., Kwon, H.J., Brown, M.S., and Goldstein, J.L. (2008). NPC2 facilitates bidirectional transfer of cholesterol between NPC1 and lipid bilayers, a step in cholesterol egress from lysosomes. Proc. Natl. Acad. Sci. U. S. A. *105*, 15287–15292.

Irie, T., Matsuzaki, Y., Sekino, Y., and Hirai, H. (2014). Kv3.3 channels harbouring a mutation of spinocerebellar ataxia type 13 alter excitability and induce cell death in cultured cerebellar Purkinje cells. J. Physiol. *592*, 229–247.

Ishii, S., Iizuka, K., Miller, B.C., and Uyeda, K. (2004). Carbohydrate response element binding protein directly promotes lipogenic enzyme gene transcription. Proc. Natl. Acad. Sci. U. S. A. *101*, 15597–15602.

Ito, M. (2008). Control of mental activities by internal models in the cerebellum. Nat. Rev. Neurosci. *9*, 304–313.

Ito, K., and Groudine, M. (1997). A new member of the cationic amino acid transporter family is preferentially expressed in adult mouse brain. J. Biol. Chem. *272*, 26780–26786.

Jaatinen, P., and Rintala, J. (2008). Mechanisms of ethanol-induced degeneration in the developing, mature, and aging cerebellum. Cerebellum *7*, 332–347.

Jansen, G.A., Ofman, R., Ferdinandusse, S., Ijlst, L., Muijsers, A.O., Skjeldal, O.H., Stokke, O., Jakobs, C., Besley, G.T.N., Wraith, J.E., et al. (1997). Refsum disease is caused by mutations in the phytanoyl-CoA hydroxylase gene. Nat. Genet. *15*, 57–61.

Janssen, A., van der Burg, M., Szuhai, K., Kops, G.J.P.L., and Medema, R.H. (2011). Chromosome Segregation Errors as a Cause of DNA Damage and Structural Chromosome Aberrations. Science (80-.). *333*, 1895–1898.

Jemiola-Rzeminska, M., Kruk, J., Skowronek, M., and Strzalka, K. (1996). Location of ubiquinone homologues in liposome membranes studied by fluorescence anisotropy of diphenyl-hexatriene and trimethylammonium-diphenyl-hexatriene. Chem. Phys. Lipids *79*, 55–63.

Jobling, R.K., Assoum, M., Gakh, O., Blaser, S., Raiman, J.A., Mignot, C., Roze, E., Dürr, A., Brice, A., Lévy, N., et al. (2015). PMPCA mutations cause abnormal mitochondrial protein processing in patients with non-progressive cerebellar ataxia. Brain *138*, 1505–1517.

Kalen, A., Appelkvist, E.L., Chojnacki, T., and Dallner, G. (1990). Nonaprenyl-4-hydroxybenzoate transferase, an enzyme involved in ubiquinone biosynthesis, in the endoplasmic reticulum-Golgi system of rat liver. J. Biol. Chem. *265*, 1158–1164.

Kalén, A., Norling, B., Appelkvist, E.L., and Dallner, G. (1987). Ubiquinone biosynthesis by the microsomal fraction from rat liver. Biochim. Biophys. Acta *926*, 70–78.

Karten, B., Campenot, R.B., Vance, D.E., and Vance, J.E. (2006). Expression of ABCG1, but not ABCA1, correlates with cholesterol release by cerebellar astroglia. J. Biol. Chem. *281*, 4049–4057.

Khatun, I., Walsh, M.T., and Hussain, M.M. (2013). Loss of both phospholipid and triglyceride transfer activities of microsomal triglyceride transfer protein in abetalipoproteinemia. J. Lipid Res. *54*, 1541–1549.

Kiedrowski, L., Czyz, A., Li, X.-F., and Lytton, J. (2002). Preferential expression of plasmalemmal K-dependent Na+/Ca2+ exchangers in neurons versus astrocytes. Neuroreport *13*, 1529–1532.

Kim, E.R., Lew, P.S., Spirkina, A., and Mizuno, T.M. (2016). Xenin-induced feeding suppression is not mediated through the activation of central extracellular signal-regulated kinase signaling in mice. Behav. Brain Res. *312*, 118–126.

Kim, J.K., Choi, J.W., Lim, S., Kwon, O., Seo, J.K., Ryu, S.H., and Suh, P.G. (2011). Phospholipase C-η1 is activated by intracellular Ca2+ mobilization and enhances GPCRs/PLC/Ca2+ signaling. Cell. Signal. *23*, 1022–1029.

King, S.J., Nowak, K., Suryavanshi, N., Holt, I., Shanahan, C.M., and Ridley, A.J. (2014). Nesprin-1 and nesprin-2 regulate endothelial cell shape and migration. Cytoskeleton *71*, 423–434.

Kishi, T., Morré, D.M., and Morré, D.J. (1999). The plasma membrane NADH oxidase of HeLa cells has hydroquinone oxidase activity. Biochim. Biophys. Acta - Bioenerg. *1412*, 66–77.

Kiyonaga-Endou, K., Oshima, M., Sugimoto, K., Thomas, M., Taketani, S., and Araki, M. (2016). Localization of Neurensin1 in cerebellar Purkinje cells of the developing chick and its possible function in dendrite formation. Brain Res. *1635*, 113–120.

Klein, P., Müller-Rischart, A.K., Motori, E., Schönbauer, C., Schnorrer, F., Winklhofer, K.F., and Klein, R. (2014). Ret rescues mitochondrial morphology and muscle degeneration of Drosophila Pink1 mutants. EMBO J. *33*, 341–355.

Klingenberg, M., and Huang, S.-G.G. (1999). Structure and function of the uncoupling protein from brown adipose tissue. Biochim. Biophys. Acta *1415*, 271–296.

Klockgether, T. (2007). Ataxias. Parkinsonism Relat. Disord. *13*, 391–394.

Klockgether, T. (2010). Sporadic ataxia with adult onset: classification and diagnostic criteria. Lancet Neurol. *9*, 94–104.

Klockgether, T., Schroth, G., Diener, H.C., and Dichgans, J. (1990). Idiopathic cerebellar ataxia of late onset: natural history and MRI morphology. J. Neurol. Neurosurg. Psychiatry *53*, 297–305.

Kobayashi, M., Masaki, T., Hori, K., Masuo, Y., Miyamoto, M., Tsubokawa, H., Noguchi, H., Nomura, M., and Takamatsu, K. (2005). Hippocalcin-deficient mice display a defect in cAMP response element-binding protein activation associated with impaired spatial and associative memory. Neuroscience *133*, 471–484.

Kocak, O., Kilic Yildirim, G., Yarar, C., Durmus Aydogdu, S., and Carman, K.B. (2015). Primary coenzyme Q10 deficiency-type 4: A case report. J. Inherit. Metab. Dis. *38*, S223–S224.

Koeleman, B.P.C. (2016). What do genetic studies tell us about the heritable basis of common epilepsy? Polygenic or complex epilepsy? Neurosci. Lett.

Kolbinger, F., Streiff, M.B., and Katopodis, A.G. Cloning of a Human UDP-galactose:2-Acetamido-2-deoxy-D-glucose 3[illegible]-Galactosyltransferase Catalyzing the Formation of Type 1 Chains*.

Kono, N., Ohto, U., Hiramatsu, T., Urabe, M., Uchida, Y., Satow, Y., and Arai, H. (2013). Impaired -TTP-PIPs Interaction Underlies Familial Vitamin E Deficiency. Science (80-.). *340*, 1106–1110.

Korkmaz, E., Lipska-Zi tkiewicz, B.S., Boyer, O., Gribouval, O., Fourrage, C., Tabatabaei, M., Schnaidt, S., Gucer, S., Kaymaz, F., Arici, M., et al. (2015). ADCK4-Associated Glomerulopathy Causes Adolescence-Onset FSGS. J. Am. Soc. Nephrol. *27*, 1–6.

Kowsky, S., Pöppelmeyer, C., Kramer, E.R., Falkenburger, B.H., Kruse, A., Klein, R., and Schulz, J.B. (2007). RET signaling does not modulate MPTP toxicity but is required for regeneration of dopaminergic axon terminals. Proc. Natl. Acad. Sci. U. S. A. *104*, 20049–20054.

Kraev, A., Quednau, B.D., Leach, S., Li, X.F., Dong, H., Winkfein, R., Perizzolo, M., Cai, X., Yang, R., Philipson, K.D., et al. (2001). Molecular cloning of a third member of the potassium-dependent sodium-calcium exchanger gene family, NCKX3. J. Biol. Chem. *276*, 23161–23172.

Lagier-Tourenne, C., Tazir, M., López, L.C., Quinzii, C.M., Assoum, M., Drouot, N., Busso, C., Makri, S., Ali-Pacha, L., Benhassine, T., et al. (2008). ADCK3, an Ancestral Kinase, Is Mutated in a Form of Recessive Ataxia Associated with Coenzyme Q10 Deficiency. Am. J. Hum. Genet. *82*, 661–672.

Lalouette, A., Lohof, A., Sotelo, C., Guénet, J.L., and Mariani, J. (2001). Neurobiological effects of a null mutation depend on genetic context: Comparison between two hotfoot alleles of the delta-2 ionotropic glutamate receptor. Neuroscience *105*, 443–455.

Lapointe, J., Wang, Y., Bigras, E., and Hekimi, S. (2012). The submitochondrial distribution of ubiquinone affects respiration in long-lived Mclk1+/- mice. J. Cell Biol. *199*, 215–224.

Laredj, L.N., Licitra, F., and Puccio, H.M. (2014). The molecular genetics of coenzyme Q biosynthesis in health and disease. Biochimie *100*, 78–87.

Larsell, O. (1952). The morphogenesis and adult pattern of the lobules and fissures of the cerebellum of the white rat. J. Comp. Neurol. *97*, 281–356.

Lascano, A.M., Lemkaddem, A., Granziera, C., Korff, C.M., Boex, C., Jenny, B., Schmitt-Mechelke, T., Thiran, J.P., Garibotto, V., Vargas, M.I., et al. (2013). Tracking the source of cerebellar epilepsy: Hemifacial seizures associated with cerebellar cortical dysplasia. Epilepsy Res. *105*, 245–249.

Latasa, M.-J., Griffin, M.J., Moon, Y.S., Kang, C., and Sul, H.S. (2003). Occupancy and function of the -150 sterol regulatory element and -65 E-box in nutritional regulation of the fatty acid synthase gene in living animals. Mol. Cell. Biol. *23*, 5896–5907.

Ledesma, F.C., El Khamisy, S.F., Zuma, M.C., Osborn, K., and Caldecott, K.W. (2009). A human 5'-tyrosyl DNA phosphodiesterase that repairs topoisomerase-mediated DNA damage. Nature *461*, 674–678.

Lee, J., and Hegele, R.A. (2014). Abetalipoproteinemia and homozygous hypobetalipoproteinemia: A framework for diagnosis and management. J. Inherit. Metab. Dis. *37*, 333–339.

Leicher, T., Bähring, R., Isbrandt, D., and Pongs, O. (1998). Coexpression of the KCNA3B gene product with Kv1.5 leads to a novel A-type potassium channel. J. Biol. Chem. *273*, 35095–35101.

Lemeer, S., Gholami, A.M., Wu, Z., and Kuster, B. (2015). Quantitative proteome profiling of human myoma and myometrium tissue reveals kinase expression signatures with potential for therapeutic intervention. Proteomics *15*, 356–364.

Lenaz, G., and Genova, M.L. (2010). Structure and Organization of Mitochondrial Respiratory Complexes: A New Understanding of an Old Subject. Antioxid. Redox Signal. *12*, 961–1008.

Lenaz, G., Samorì, B., Fato, R., Battino, M., Parenti Castelli, G., and Domini, I. (1992). Localization and preferred orientations of ubiquinone homologs in model bilayers. Biochem. Cell Biol. *70*, 504–514.

Lenaz, G., Fato, R., Castelluccio, C., Genova, M.L., Bovina, C., Estornell, E., Valls, V., Pallotti, F., Parenti Castelli, G., and Estornell Valls V, E.X. (1993). The function of coenzyme Q in mitochondria. [Review]. Clin. Investig. *71*, S66–S70.

Leonard, C.J., Aravind, L., and Koonin, E. V (1998). Novel families of putative protein kinases in bacteria and archaea: Evolution of the “eukaryotic” protein kinase superfamily. Genome Res. *8*, 1038–1047.

Lester, R.L., and Crane, F.L. (1959). The natural occurrence of coenzyme Q and related compounds. J. Biol. Chem. *234*, 2169–2175.

Levavasseur, F., Miyadera, H., Sirois, J., Tremblay, M.L., Kita, K., Shoubridge, E., and Hekimi, S. (2001). Ubiquinone is necessary for mouse embryonic development but is not essential for mitochondrial respiration. J. Biol. Chem. *276*, 46160–46164.

Li, H., and Capetanaki, Y. (1993). Regulation of the mouse desmin gene: Transactivation by MyoD, myogenin, MRF4 and Myf5. Nucleic Acids Res. *21*, 335–343.

Licitra, F. (2013). Pathophysiological and molecular characterization of a mouse model of ARCA2, a recessive cerebellar ataxia associated to Coenzyme Q10 deficiency. Http://www.theses.fr.

Licitra, F., and Puccio, H. (2014). An overview of current mouse models recapitulating coenzyme Q10 deficiency syndrome. Mol. Syndromol. *5*, 180–186.

Van Liefferinge, J., Jensen, C.J., Albertini, G., Bentea, E., Demuyser, T., Merckx, E., Aronica, E., Smolders, I., and Massie, A. (2015). Altered vesicular glutamate transporter expression in human temporal lobe epilepsy with hippocampal sclerosis. Neurosci. Lett. *590*, 184–188.

Littarru, G.P., and Langsjoen, P. (2007). Coenzyme Q10 and statins: Biochemical and clinical implications. Mitochondrion *7*, S168-74.

Liu, Y.-T., Hersheson, J., Plagnol, V., Fawcett, K., Duberley, K.E.C., Preza, E., Hargreaves, I.P., Chalasani, A., Laurá, M., Wood, N.W., et al. (2014). Autosomal-recessive cerebellar ataxia caused by a novel ADCK3 mutation that elongates the protein: clinical, genetic and biochemical characterisation. J. Neurol. Neurosurg. Psychiatry *85*, 493–498.

Lobo, A.C., Gomes, J.R., Catarino, T., Mele, M., Fernandez, P., Inácio, A.R., Bahr, B.A., Santos, A.E., Wieloch, T., Carvalho, A.L., et al. (2011). Cleavage of the vesicular glutamate transporters under excitotoxic conditions. Neurobiol. Dis. *44*, 292–303.

López, L.C., Schuelke, M., Quinzii, C.M., Kanki, T., Rodenburg, R.J.T., Naini, A., DiMauro, S., and Hirano, M. (2006). Leigh Syndrome with Nephropathy and CoQ10 Deficiency Due to decaprenyl diphosphate synthase subunit 2 (PDSS2) Mutations (Elsevier).

López, L.C., Quinzii, C.M., Area, E., Naini, A., Rahman, S., Schuelke, M., Salviati, L., Dimauro, S., and Hirano, M. (2010). Treatment of CoQ10 deficient fibroblasts with ubiquinone, CoQ analogs, and vitamin C: Time-and compound-dependent effects. PLoS One *5*.

López, L.C., Luna-Sánchez, M., García-Corzo, L., Quinzii, C.M., and Hirano, M. (2014). Pathomechanisms in coenzyme q10-deficient human fibroblasts. Mol. Syndromol. *5*, 163–169.

Louet, J.-F.F., Hayhurst, G., Gonzalez, F.J., Girard, J., and Decaux, J.-F.F. (2002). The coactivator PGC-1 is involved in the regulation of the liver carnitine palmitoyltransferase I gene expression by cAMP in combination with HNF4?? and cAMP-response element-binding protein (CREB). J. Biol. Chem. *277*, 37991–38000.

Loureiro, J.R., Oliveira, C.L., and Silveira, I. (2016). Unstable repeat expansions in neurodegenerative diseases: Nucleocytoplasmic transport emerges on the scene. Neurobiol. Aging *39*, 174–183.

Löw, H., Crane, F.L., and Morré, D.J. (2012). Putting together a plasma membrane NADH oxidase: A tale of three laboratories. Int. J. Biochem. Cell Biol. *44*, 1834–1838.

Lowe, J.S., Morton, R.A., and Vernon, J. (1957). Unsaponifiable constituents of kidney in various species. Biochem. J. *67*, 228.

Lu, S., Lu, L.Y., Liu, M.F., Yuan, Q.J., Sham, M.H., Guan, X.Y., and Huang, J.D. (2012). Cerebellar defects in Pdss2 conditional knockout mice during embryonic development and in adulthood. Neurobiol. Dis. *45*, 219–233.

Luca Colucci-D 'amato, G., D 'alessio, A., Filliatreau, G., Flono, T., Giamberardino, L. Di, Chiappetta, G., Vecchio, G., Fusco, A., Santoro, M., and De Franciscis3, V. (1996). Presence of Physiologically Stimulated RET in Adult Rat Brain: Induction of RET Expression during Nerve Regeneration1. Cell Growth Differ. *7*, 1081–1086.

Luna-Sánchez, M., Hidalgo-Gutiérrez, A., Hildebrandt, T.M., Chaves-Serrano, J., Barriocanal-Casado, E., Santos-Fandila, Á., Romero, M., Sayed, R.K., Duarte, J., Prokisch, H., et al. (2017). CoQ deficiency causes disruption of mitochondrial sulfide oxidation, a new pathomechanism associated with this syndrome. EMBO Mol. Med. *9*, 78–95.

Lundquist, P.K., Poliakov, A., Giacomelli, L., Friso, G., Appel, M., McQuinn, R.P., Krasnoff, S.B., Rowland, E., Ponnala, L., Sun, Q., et al. (2013). Loss of Plastoglobule Kinases ABC1K1 and ABC1K3 Causes Conditional Degreening, Modified Prenyl-Lipids, and Recruitment of the Jasmonic Acid Pathway. Plant Cell *25*, 1818–1839.

Luo, H., Chan, D.W., Yang, T., Rodriguez, M., Chen, B.P.-C., Leng, M., Mu, J.-J., Chen, D., Songyang, Z., Wang, Y., et al. (2004). A new XRCC1-containing complex and its role in cellular survival of methyl methanesulfonate treatment. Mol. Cell. Biol. *24*, 8356–8365.

Maïga, S.F., Kalopissis, A.D., and Chabert, M. (2014). Apolipoprotein A-II is a key regulatory factor of HDL metabolism as appears from studies with transgenic animals and clinical outcomes. Biochimie *96*, 56–66.

Di Maio, R., Mastroberardino, P.G., Hu, X., Montero, L., and Greenamyre, J.T. (2011). Pilocapine alters NMDA receptor expression and function in hippocampal neurons: NADPH oxidase and ERK1/2 mechanisms. Neurobiol. Dis. *42*, 482–495.

Malgireddy, K., Thompson, R., and Torres-Russotto, D. (2016). A novel CABC1/ADCK3 mutation in adult-onset cerebellar ataxia. Park. Relat. Disord. *33*, 151–152.

Malhas, A., Goulbourne, C., and Vaux, D.J. (2011). The nucleoplasmic reticulum: form and function. Trends Cell Biol. *21*, 362–373.

Mancuso, M., Orsucci, D., Volpi, L., Calsolaro, V., and Siciliano, G. (2010). Coenzyme Q10 in neuromuscular and neurodegenerative disorders. Curr. Drug Targets *11*, 111–121.

Manning, G., Whyte, D.B., Martinez, R., Hunter, T., and Sudarsanam, S. (2002). The Protein Kinase Complement of the Human Genome. Science (80-.). *298*, 1912–1934.

Manto, M., and Marmolino, D. (2009). Cerebellar ataxias. Curr. Opin. Neurol. *22*, 419–429.

Manto, M., Bower, J.M., Conforto, A.B., Delgado-García, J.M., Da Guarda, S.N.F., Gerwig, M., Habas, C., Hagura, N., Ivry, R.B., Marien, P., et al. (2012). Consensus paper: Roles of the cerebellum in motor control-the diversity of ideas on cerebellar involvement in movement. In Cerebellum, (Springer-Verlag), pp. 457–487.

Marbois, B., Gin, P., Faull, K.F., Poon, W.W., Lee, P.T., Strahan, J., Shepherd, J.N., and Clarke, C.F. (2005). Coq3 and Coq4 define a polypeptide complex in yeast mitochondria for the biosynthesis of coenzyme Q. J. Biol. Chem. *280*, 20231–20238.

Marbois, B., Gin, P., Gulmezian, M., and Clarke, C.F. (2009). The yeast Coq4 polypeptide organizes a mitochondrial protein complex essential for coenzyme Q biosynthesis. Biochim. Biophys. Acta - Mol. Cell Biol. Lipids *1791*, 69–75.

Marbois, B., Xie, L.X., Choi, S., Hirano, K., Hyman, K., and Clarke, C.F. (2010). para-aminobenzoic acid is a precursor in coenzyme Q6 biosynthesis in Saccharomyces cerevisiae. J. Biol. Chem. *285*, 27827–27838.

Martinis, J., Glauser, G., Valimareanu, S., Stettler, M., Zeeman, S.C., Yamamoto, H., Shikanai, T., and Kessler, F. (2014). ABC1K1/PGR6 kinase: A regulatory link between photosynthetic activity and chloroplast metabolism. Plant J. *77*, 269–283.

Mast, N., Anderson, K.W., Lin, J.B., Li, Y., Turko, I. V., Tatsuoka, C., Bjorkhem, I., and Pikuleva, I.A. (2017). Cytochrome P450 27A1 deficiency and regional differences in brain sterol metabolism cause preferential cholestanol accumulation in the cerebellum. J. Biol. Chem. *292*, 4913–4924.

Mauger, J.-P. (2012). Role of the nuclear envelope in calcium signalling. Biol. Cell *104*, 70–83.

Mazarati, A.M., Lewis, M.L., and Pittman, Q.J. (2017). Neurobehavioral comorbidities of epilepsy: Role of inflammation. Epilepsia *58*, 48–56.

McDonough, M.A., Kavanagh, K.L., Butler, D., Searls, T., Oppermann, U., and Schofield, C.J. (2005). Structure of human phytanoyl-CoA 2-hydroxylase identifies molecular mechanisms of Refsum disease. J. Biol. Chem. *280*, 41101–41110.

McLennan, H.R., and Esposti, M.D. (2000). The contribution of mitochondrial respiratory complexes to the production of reactive oxygen species. J. Bioenerg. Biomembr. *32*, 153–162.

McMahon, A., Fowler, S.C., Perney, T.M., Akemann, W., Knöpfel, T., and Joho, R.H. (2004). Allele-dependent changes of olivocerebellar circuit properties in the absence of the voltage-gated potassium channels Kv3.1 and Kv3.3. Eur. J. Neurosci. *19*, 3317–3327.

Mead, J.R., Irvine, S.A., and Ramji, D.P. (2002). Lipoprotein lipase: Structure, function, regulation, and role in disease. J. Mol. Med. *80*, 753–769.

de Mello Serrano, G.C., e Silva Figueira, T.R., Kiyota, E., Zanata, N., and Arruda, P. (2012). Lysine degradation through the saccharopine pathway in bacteria: LKR and SDH in bacteria and its relationship to the plant and animal enzymes. FEBS Lett. *586*, 905–911.

Mellors, A., and Tappel, A.L. (1966). The Inhibition of Mitochondrial Peroxidation by Ubiquinone and Ubiquinole. J. Biol. Chem. *241*, 4353–4356.

Mignot, C., Apartis, E., Durr, A., Marques Lourenço, C., Charles, P., Devos, D., Moreau, C., de Lonlay, P., Drouot, N., Burglen, L., et al. (2013). Phenotypic variability in ARCA2 and identification of a core ataxic phenotype with slow progression. Orphanet J. Rare Dis. *8*, 173.

Mikhaleva, A., Kannan, M., Wagner, C., Yalcin, B., Mikhaleva, A., Kannan, M., Wagner, C., and Yalcin, B. (2016). Histomorphological Phenotyping of the Adult Mouse Brain. In Current Protocols in Mouse Biology, (Hoboken, NJ, USA: John Wiley & Sons, Inc.), pp. 307–332.

Milagre, I., Olin, M., Nunes, M.J., Moutinho, M., Lövgren-Sandblom, A., Gama, M.J., Björkhem, I., and Rodrigues, E. (2012). Marked change in the balance between CYP27A1 and CYP46A1 mediated elimination of cholesterol during differentiation of human neuronal cells. Neurochem. Int. *60*, 192–198.

Mitchell, P. (1961). Coupling of phosphorylation to electron and hydrogen transfer by a chemi-osmotic type of mechanism. Nature *191*, 144–148.

Mitchell, P. (1976). Possible molecular mechanisms of the protonmotive function of cytochrome systems. J. Theor. Biol. *62*, 327–367.

Mollet, J., Giurgea, I., Schlemmer, D., Dallner, G., Chretien, D., Delahodde, A., Bacq, D., De Lonlay, P., Munnich, A., and Rötig, A. (2007). Prenyldiphosphate synthase, subunit 1 (PDSS1) and OH-benzoate polyprenyltransferase (COQ2) mutations in ubiquinone deficiency and oxidative phosphorylation disorders. J. Clin. Invest. *117*, 765–772.

Mollet, J., Delahodde, A., Serre, V., Chretien, D., Schlemmer, D., Lombes, A., Boddaert, N., Desguerre, I., de Lonlay, P., Ogier de Baulny, H., et al. (2008). CABC1 Gene Mutations Cause Ubiquinone Deficiency with Cerebellar Ataxia and Seizures. Am. J. Hum. Genet. *82*, 623–630.

Monaghan, R.M., Barnes, R.G., Fisher, K., Andreou, T., Rooney, N., Poulin, G.B., and Whitmarsh, A.J. (2015). A nuclear role for the respiratory enzyme CLK-1 in regulating mitochondrial stress responses and longevity. Nat. Cell Biol. *17*, 782–792.

Montarras, D., Chelly, J., Bober, E., Arnold, H., Ott, M.O., Gros, F., and Pinset, C. (1991). Developmental patterns in the expression of Myf5, MyoD, myogenin, and MRF4 during myogenesis. New Biol. *3*, 592–600.

Morré, D.J., and Morré, D.M. (2011). Non-mitochondrial coenzyme Q. BioFactors *37*, 355–360.

Mugoni, V., Postel, R., Catanzaro, V., De Luca, E., Turco, E., Digilio, G., Silengo, L., Murphy, M.P., Medana, C., Stainier, D.Y.R., et al. (2013). Ubiad1 is an antioxidant enzyme that regulates eNOS activity by CoQ10 synthesis. Cell *152*, 504–518.

Nachbauer, W., Eigentler, A., and Boesch, S. (2015). Acquired ataxias: the clinical spectrum, diagnosis and management. J. Neurol. *262*, 1385–1393.

Narayan, V., Landré, V., Ning, J., Hernychova, L., Muller, P., Verma, C., Walkinshaw, M.D., Blackburn, E.A., and Ball, K.L. (2015). Protein-Protein Interactions Modulate the Docking-Dependent E3-Ubiquitin Ligase Activity of Carboxy-Terminus of Hsc70-Interacting Protein (CHIP). Mol. Cell. Proteomics *14*, 2973–2987.

Naukkarinen, J., Surakka, I., Pietilainen, K.H., Rissanen, A., Salomaa, V., Ripatti, S., Yki-Jarvinen, H., Duijn, C.M., Wichmann, H.E., Kaprio, J., et al. (2010). Use of genome-wide expression data to mine the "gray zone" of GWA studies leads to novel candidate obesity genes. PLoS Genet. *6*, 1–10.

Nava, C., Rupp, J., Boissel, J.-P., Mignot, C., Rastetter, A., Amiet, C., Jacquette, A., Dupuits, C., Bouteiller, D., Keren, B., et al. (2015). Hypomorphic variants of cationic amino acid transporter 3 in males with autism spectrum disorders. Amino Acids *47*, 2647–2658.

Nedergaard, J., Golozoubova, V., Matthias, A., Asadi, A., Jacobsson, A., and Cannon, B. (2001). UCP1: The only protein able to mediate adaptive non-shivering thermogenesis and metabolic inefficiency. Biochim. Biophys. Acta - Bioenerg. *1504*, 82–106.

Nwaobi, S.E., Lin, E., Peramsetty, S.R., and Olsen, M.L. (2014). DNA methylation functions as a critical regulator of Kir4.1 expression during CNS development. Glia *62*, 411–427.

Ogata, K., and Volini, M. (1990). Mitochondrial rhodanese: membrane-bound and complexed activity. J. Biol. Chem. *265*, 8087–8093.

Ohkuma, A., Noguchi, S., Sugie, H., Malicdan, M.C. V, Fukuda, T., Shimazu, K., López, L.C., Hirano, M., Hayashi, Y.K., Nonaka, I., et al. (2009). Clinical and genetic analysis of lipid storage myopathies. Muscle Nerve *39*, 333–342.

Okada, K., Suzuki, K., Kamiya, Y., Zhu, X., Fujisaki, S., Nishimura, Y., Nishino, T., Nakagawa, T., Kawamukai, M., and Matsuda, H. (1996). Polyprenyl diphosphate synthase essentially defines the length of the side chain of ubiquinone. Biochim. Biophys. Acta - Lipids Lipid Metab. *1302*, 217–223.

Olschowka, J.A., and Vijayan, V.K. (1980). Postnatal development of cholinergic neurotransmitter enzymes in the mouse cerebellum. Biochemical, light microscopic and electron microscopic cytochemical investigations. J. Comp. Neurol. *191*, 77–101.

Olson, R.E., and Rudney, H. (1983). Biosynthesis of ubiquinone. Vitam. Horm. *40*, 1–43.

Oostra, B.A., and Willemsen, R. (2009). FMR1: A gene with three faces. Biochim. Biophys. Acta - Gen. Subj. *1790*, 467–477.

Ortiz de Montellano, P.R., Wei, J.S., Vinson, W.A., Castillo, R., and Boparai, A.S. (1977). Substrate selectivity of squalene synthetase. Biochemistry *16*, 2680–2685.

Oscarsson, O. (1979). Functional units of the cerebellum - sagittal zones and microzones. Trends Neurosci. *2*, 144–145.

Ozeir, M., Mühlenhoff, U., Webert, H., Lill, R., Fontecave, M., and Pierrel, F. (2011). Coenzyme Q biosynthesis: Coq6 is required for the C5-hydroxylation reaction and substrate analogs rescue Coq6 deficiency. Chem. Biol. *18*, 1134–1142.

Ozol, K., Hayden, J.M., Oberdick, J., and Hawkes, R. (1999). Transverse zones in the vermis of the mouse cerebellum. J. Comp. Neurol. *412*, 95–111.

Pagliarini, D.J., Calvo, S.E., Chang, B., Sheth, S.A., Vafai, S.B., Ong, S.E., Walford, G.A., Sugiana, C., Boneh, A., Chen, W.K., et al. (2008). A Mitochondrial Protein Compendium Elucidates Complex I Disease Biology. Cell *134*, 112–123.

Pandya, C., Uzilov, A. V, Bellizzi, J., Lau, C.Y., Moe, A.S., Strahl, M., Hamou, W., Newman, L.C., Fink, M.Y., Antipin, Y., et al. (2017). Genomic profiling reveals mutational landscape in parathyroid carcinomas. JCI Insight *2*, 1–14.

Papa, S., and Skulachev, V.P. (1997). Reactive oxygen species, mitochondria, apoptosis and aging. Mol. Cell. Biochem. *174*, 305–319.

Papucci, L., Schiavone, N., Witort, E., Donnini, M., Lapucci, A., Tempestini, A., Formigli, L., Zecchi-Orlandini, S., Orlandini, G., Carella, G., et al. (2003). Coenzyme Q10 prevents apoptosis by inhibiting mitochondrial depolarization independently of its free radical scavenging property. J. Biol. Chem. *278*, 28220–28228.

Parfitt, D.A., Michael, G.J., Vermeulen, E.G.M., Prodromou, N. V., Webb, T.R., Gallo, J.M., Cheetham, M.E., Nicoll, W.S., Blatch, G.L., and Chapple, J.P. (2009). The ataxia protein sacsin is a functional co-chaperone that protects against polyglutamine-expanded ataxin-1. Hum. Mol. Genet. *18*, 1556–1565.

Parrado-Fernández, C., López-Lluch, G., Rodríguez-Bies, E., Santa-Cruz, S., Navas, P., Ramsey, J.J., and Villalba, J.M. (2011). Calorie restriction modifies ubiquinone and COQ transcript levels in mouse tissues. Free Radic. Biol. Med. *50*, 1728–1736.

Patel, A.B., De Graaf, R.A., Martin, D.L., Battaglioli, G., and Behar, K.L. (2006). Evidence that GAD65 mediates increased GABA synthesis during intense neuronal activity in vivo. J. Neurochem. *97*, 385–396.

Paull, T.T., and Gellert, M. (1998). The 3′ to 5′ Exonuclease Activity of Mre11 Facilitates Repair of DNA Double-Strand Breaks. Mol. Cell *1*, 969–979.

Paulson, H.L. (2009). The spinocerebellar ataxias. J. Neuroophthalmol. *29*, 227–237.

Pelletier, M., Billingham, L.K., Ramaswamy, M., and Siegel, R.M. (2014). Extracellular flux analysis to monitor glycolytic rates and mitochondrial oxygen consumption. Methods Enzymol. *542*, 125–149.

Perdomini, M., Belbellaa, B., Monassier, L., Reutenauer, L., Messaddeq, N., Cartier, N., Crystal, R.G., Aubourg, P., and Puccio, H. (2014). Prevention and reversal of severe mitochondrial cardiomyopathy by gene therapy in a mouse model of Friedreich's ataxia. Nat. Med. *20*, 542–547.

Peter, C.J., Evans, M., Thayanithy, V., Taniguchi-Ishigaki, N., Bach, I., Kolpak, A., Bassell, G.J., Rossoll, W., Lorson, C.L., Bao, Z.Z., et al. (2011). The COPI vesicle complex binds and moves with survival motor neuron within axons. Hum. Mol. Genet. *20*, 1701–1711.

Pierrel, F., Hamelin, O., Douki, T., Kieffer-Jaquinod, S., Mühlenhoff, U., Ozeir, M., Lill, R., and Fontecave, M. (2010). Involvement of mitochondrial ferredoxin and para-aminobenzoic acid in yeast coenzyme q biosynthesis. Chem. Biol. *17*, 449–459.

De Pinieux, G., Chariot, P., Ammi-Saïd, M., Louarn, F., Lejonc, J.L., Astier, A., Jacotot, B., and Gherardi, R. (1996). Lipid-lowering drugs and mitochondrial function: effects of HMG-CoA reductase inhibitors on serum ubiquinone and blood lactate/pyruvate ratio. Br. J. Clin. Pharmacol. *42*, 333–337.

Pink, D.B.S., Gatrell, S.K., Elango, R., Turchinsky, J., Kiess, A.S., Blemings, K.P., Dixon, W.T., and Ball, R.O. (2011). Lysine α-ketoglutarate reductase, but not saccharopine dehydrogenase, is subject to substrate inhibition in pig liver. Nutr. Res. *31*, 544–554.

Pitkänen, A., Roivainen, R., and Lukasiuk, K. (2016). Development of epilepsy after ischaemic stroke. Lancet Neurol. *15*, 185–197.

Poon, W.W., Barkovich, R.J., Hsu, A.Y., Frankel, A., Lee, P.T., Shepherd, J.N., Myles, D.C., and Clarke, C.F. (1999). Yeast and rat Coq3 and Escherichia coli UbiG polypeptides catalyze both O-methyltransferase steps in coenzyme Q biosynthesis. J. Biol. Chem. *274*, 21665–21672.

Poon, W.W., Davis, D.E., Ha, H.T., Jonassen, T., Rather, P.N., and Clarke, C.F. (2000). Identification of Escherichia coli ubiB, a gene required for the first monooxygenase step in ubiquinone biosynthesis. J. Bacteriol. *182*, 5139–5146.

Poopalasundaram, S., Knott, C., Shamotienko, O.G., Foran, P.G., Dolly, J.O., Ghiani, C.A., Gallo, V., and Wilkin, G.P. (2000). Glial heterogeneity in expression of the inwardly rectifying K+ channel, Kir4.1, in adult rat CNS. Glia *30*, 362–372.

Popoff, V., Adolf, F., Brügge, B., and Wieland, F. (2011). COPI budding within the Golgi stack. Cold Spring Harb. Perspect. Biol. *3*.

Punga, T., and Bühler, M. (2010). Long intronic GAA repeats causing Friedreich ataxia impede transcription elongation. EMBO Mol. Med. *2*, 120–129.

Quinzii, C., Naini, A., Salviati, L., Trevisson, E., Navas, P., DiMauro, S., and Hirano, M. (2006). A Mutation in Para-Hydroxybenzoate-Polyprenyl Transferase (COQ2) Causes Primary Coenzyme Q10 Deficiency. Am. J. Hum. Genet. *78*, 345–349.

Quinzii, C.M., Kattah, A.G., Naini, A., Akman, H.O., Mootha, V.K., DiMauro, S., and Hirano, M. (2005). Coenzyme Q deficiency and cerebellar ataxia associated with an aprataxin mutation. Neurology *64*, 539–541.

Quinzii, C.M., Emmanuele, V., and Hirano, M. (2014). Clinical presentations of coenzyme Q10 deficiency syndrome. Mol. Syndromol. *5*, 141–146.

Radons, J. (2016). The human HSP70 family of chaperones: where do we stand? Cell Stress Chaperones *21*, 379–404.

Rahman, S., Clarke, C.F., and Hirano, M. (2012). 176th ENMC International Workshop: Diagnosis and treatment of coenzyme Q 10 deficiency. Neuromuscul. Disord. *22*, 76–86.

Ramasamy, S., Singh, S., Taniere, P., Langman, M.J.S., and Eggo, M.C. (2006). Sulfide-detoxifying enzymes in the human colon are decreased in cancer and upregulated in differentiation. Am. J. Physiol. Gastrointest. Liver Physiol. *291*, G288-96.

Ramnani, N. (2006). The primate cortico-cerebellar system: anatomy and function. Nat. Rev. Neurosci. *7*, 511–522.

Reeber, S.L., Otis, T.S., and Sillitoe, R. V (2013). New roles for the cerebellum in health and disease. Front. Syst. Neurosci. *7*, 83.

Rhee, H.-W., Zou, P., Udeshi, N.D., Martell, J.D., Mootha, V.K., Carr, S.A., and Ting, A.Y. (2013). Proteomic mapping of mitochondria in living cells via spatially restricted enzymatic tagging. Science *339*, 1328–1331.

Richards, N.G., and Schuster, S.M. (1998). Mechanistic issues in asparagine synthetase catalysis. Adv. Enzymol. Relat. Areas Mol. Biol. *72*, 145–198.

Robert, K., Vialard, F., Thiery, E., Toyama, K., Sinet, P.-M., Janel, N., and London, J. (2003). Expression of the cystathionine beta synthase (CBS) gene during mouse development and immunolocalization in adult brain. J. Histochem. Cytochem. *51*, 363–371.

Ropp, P.A., and Copeland, W.C. (1996). Cloning and characterization of the human mitochondrial DNA polymerase, DNA polymerase gamma. Genomics *36*, 449–458.

Rötig, A., Appelkvist, E.-L., Geromel, V., Chretien, D., Kadhom, N., Edery, P., Lebideau, M., Dallner, G., Munnich, A., Ernster, L., et al. (2000). Quinone-responsive multiple respiratory-chain dysfunction due to widespread coenzyme Q10 deficiency. Lancet *356*, 391–395.

Ruano, L., Melo, C., Silva, M.C., and Coutinho, P. (2014). The global epidemiology of hereditary ataxia and spastic paraplegia: A systematic review of prevalence studies. Neuroepidemiology *42*, 174–183.

Sadakata, T., Kakegawa, W., Mizoguchi, A., Washida, M., Katoh-Semba, R., Shutoh, F., Okamoto, T., Nakashima, H., Kimura, K., Tanaka, M., et al. (2007). Impaired cerebellar development and function in mice lacking CAPS2, a protein involved in neurotrophin release. J. Neurosci. *27*, 2472–2482.

Saiki, R., Nagata, A., Kainou, T., Matsuda, H., and Kawamukai, M. (2005). Characterization of solanesyl and decaprenyl diphosphate synthases in mice and humans. FEBS J. *272*, 5606–5622.

Sailer, A., and Houlden, H. (2012). Recent advances in the genetics of cerebellar ataxias. Curr. Neurol. Neurosci. Rep. *12*, 227–236.

Saitoh, S., Takamatsu, K., Kobayashi, M., and Noguchi, T. (1993). Distribution of hippocalcin mRNA and immunoreactivity in rat brain. Neurosci. Lett. *157*, 107–110.

Sala-Rabanal, M., Kucheryavykh, L.Y., Skatchkov, S.N., Eaton, M.J., and Nichols, C.G. (2010). Molecular mechanisms of EAST/SeSAME syndrome mutations in Kir4.1 (KCNJ10). J. Biol. Chem. *285*, 36040–36048.

Salviati, L., Trevisson, E., Rodriguez Hernandez, M.A., Casarin, A., Pertegato, V., Doimo, M., Cassina, M., Agosto, C., Desbats, M.A., Sartori, G., et al. (2012). Haploinsufficiency of COQ4 causes coenzyme Q10 deficiency. J. Med. Genet. *49*, 187–191.

Sano, Y., Date, H., Igarashi, S., Onodera, O., Oyake, M., Takahashi, T., Hayashi, S., Morimatsu, M., Takahashi, H., Makifuchi, T., et al. (2004). Aprataxin, the causative protein for EAOH is a nuclear protein with a potential role as a DNA repair protein. Ann. Neurol. *55*, 241–249.

Sarna, J.R., Larouche, M., Marzban, H., Sillitoe, R. V., Rancourt, D.E., and Hawkes, R. (2003). Patterned Purkinje cell degeneration in mouse models of Niemann-Pick type C disease. J. Comp. Neurol. *456*, 279–291.

Sarnat, H.B., and Flores-Sarnat, L. (2013). Neuropathology of pediatric epilepsy. Handb. Clin. Neurol. *111*, 399–416.

Scheeff, E.D., and Bourne, P.E. (2005). Structural evolution of the protein kinase-like superfamily.

Scherzer, C.R., Landwehrmeyer, G.B., Kerner, J.A., Standaert, D.G., Hollingsworth, Z.R., Daggett, L.P., Veliçelebi, G., Penney, J.B., and Young, A.B. (1997). Cellular distribution of NMDA glutamate receptor subunit mRNAs in the human cerebellum. Neurobiol. Dis. *4*, 35–46.

Schindelin, J., Arganda-Carreras, I., Frise, E., Kaynig, V., Longair, M., Pietzsch, T., Preibisch, S., Rueden, C., Saalfeld, S., Schmid, B., et al. (2012). Fiji: an open-source platform for biological-image analysis. Nat. Methods *9*, 676–682.

Schinzel, A.C., Takeuchi, O., Huang, Z., Fisher, J.K., Zhou, Z., Rubens, J., Hetz, C., Danial, N.N., Moskowitz, M.A., and Korsmeyer, S.J. (2005). Cyclophilin D is a component of mitochondrial permeability transition and mediates neuronal cell death after focal cerebral ischemia. Proc. Natl. Acad. Sci. U. S. A. *102*, 12005–12010.

Schmahmann, J.D. (2007). Chapter 1 Cerebellum and Spinal Cord: Principles of Development, Anatomic Organization, and Functional Relevance. Blue Books Neurol. *31*, 1–60.

Schmidley, J.W., Levinsohn, M.W., and Manetto, V. (1987). Infantile X-linked ataxia and deafness: a new clinicopathologic entity? Neurology *37*, 1344–1349.

Schmidt, W.M., Rutledge, S.L., Schüle, R., Mayerhofer, B., Züchner, S., Boltshauser, E., and Bittner, R.E. (2015). Disruptive SCYL1 Mutations Underlie a Syndrome Characterized by Recurrent Episodes of Liver Failure, Peripheral Neuropathy, Cerebellar Atrophy, and Ataxia. Am. J. Hum. Genet. *97*, 855–861.

Schmucker, S., Martelli, A., Colin, F., Page, A., Wattenhofer-Donz??, M., Reutenauer, L., and Puccio, H. (2011). Mammalian frataxin: An essential function for cellular viability through an interaction with a preformed ISCU/ NFS1/ISD11 iron-sulfur assembly complex. PLoS One *6*, e16199.

Schoolmeesters, A., Brown, D.D., and Fedorov, Y. (2012). Kinome-Wide functional genomics screen reveals a novel mechanism of TNFalpha-induced nuclear accumulation of the HIF-1alpha transcription factor in cancer cells. PLoS One *7*.

Schultz, B.E., and Chan, S.I. (2001). Structures and Proton-Pumping Strategies of Mitochondrial Respiratory Enzymes. Annu. Rev. Biophys. Biomol. Struct. *30*, 23–65.

Schweitzer, B., Suter, U., and Taylor, V. (2002). Neural membrane protein 35/Lifeguard is localized at postsynaptic sites and in dendrites. Mol. Brain Res. *107*, 47–56.

Scott, T.G. (1964). A unique pattern of localization within the cerebellum of the mouse. J. Comp. Neurol. *122*, 1–7.

Sen, D., Nandakumar, D., Tang, G.Q., and Patel, S.S. (2012). Human mitochondrial DNA helicase TWINKLE is both an unwinding and annealing helicase. J. Biol. Chem. *287*, 14545–14556.

Sergaki, M.C., López-Ramos, J.C., Stagkourakis, S., Gruart, A., Broberger, C., Delgado-García, J.M., and Ibáñez, C.F. (2017). Compromised Survival of Cerebellar Molecular Layer Interneurons Lacking GDNF Receptors GFRα1 or RET Impairs Normal Cerebellar Motor Learning. Cell Rep. *19*, 1977–1986.

Sha, Y., Rao, L., Settembre, C., Ballabio, A., and Eissa, N.T. (2017). STUB1 regulates TFEB-induced autophagy–lysosome pathway. EMBO J. e201796699.

Shakkottai, V.G., do Carmo Costa, M., Dell'orco, J.M., Sankaranarayanan, A., Wulff, H., and Paulson, H.L. (2011). Early changes in cerebellar physiology accompany motor dysfunction in the polyglutamine disease spinocerebellar ataxia type 3. J. Neurosci. *31*, 13002–13014.

Sillitoe, R. V. (2012). An introduction to journal club in the Cerebellum. Cerebellum *11*, 828.

Sillitoe, R. V., Fu, Y., and Watson, C. (2012). Cerebellum.

Siu, F., Bain, P.J., Leblanc-Chaffin, R., Chen, H., and Kilberg, M.S. (2002). ATF4 is a mediator of the nutrient-sensing response pathway that activates the human asparagine synthetase gene. J. Biol. Chem. *277*, 24120–24127.

Slater, E.C. (1983). The Q cycle, an ubiquitous mechanism of electron transfer. Trends Biochem. Sci. *8*, 239–242.

Šmidák, R., Mayer, R.L., Bileck, A., Gerner, C., Mechtcheriakova, D., Stork, O., Lubec, G., and Li, L. (2016). Quantitative proteomics reveals protein kinases and phosphatases in the individual phases of contextual fear conditioning in the C57BL/6J mouse. Behav. Brain Res. *303*, 208–217.

Smirnov, A., Comte, C., Mager-Heckel, A.M., Addis, V., Krasheninnikov, I.A., Martin, R.P., Entelis, N., and Tarassov, I. (2010). Mitochondrial enzyme rhodanese is essential for 5 S ribosomal RNA import into human mitochondria. J. Biol. Chem. *285*, 30792–30803.

Soba, P., Han, C., Zheng, Y., Perea, D., Miguel-Aliaga, I., Jan, L.Y., and Jan, Y.N. (2015). The ret receptor regulates sensory neuron dendrite growth and integrin mediated adhesion. Elife *2015*.

Sokolov, A.A., Miall, R.C., and Ivry, R.B. (2017). The Cerebellum: Adaptive Prediction for Movement and Cognition. Trends Cogn. Sci. *21*, 313–332.

Somia, N. V, Schmitt, M.J., Vetter, D.E., Van Antwerp, D., Heinemann, S.F., and Verma, I.M. (1999). LFG: an anti-apoptotic gene that provides protection from Fas-mediated cell death. Proc. Natl. Acad. Sci. U. S. A. *96*, 12667–12672.

Stefely, J.A., Reidenbach, A.G., Ulbrich, A., Oruganty, K., Floyd, B.J., Jochem, A., Saunders, J.M., Johnson, I.E., Minogue, C.E., Wrobel, R.L., et al. (2015). Mitochondrial ADCK3 employs an atypical protein kinase-like fold to enable coenzyme Q Biosynthesis. Mol. Cell *57*, 83–94.

Stefely, J.A., Licitra, F., Laredj, L., Reidenbach, A.G., Kemmerer, Z.A., Grangeray, A., Jaeg-Ehret, T., Minogue, C.E., Ulbrich, A., Hutchins, P.D., et al. (2016). Cerebellar Ataxia and Coenzyme Q Deficiency through Loss of Unorthodox Kinase Activity. Mol. Cell *63*, 608–620.

Stoodley, C.J., and Schmahmann, J.D. (2009). Functional topography in the human cerebellum: A meta-analysis of neuroimaging studies. Neuroimage *44*, 489–501.

Stukas, S., Robert, J., and Wellington, C.L. (2014). High-density lipoproteins and cerebrovascular integrity in Alzheimer's disease. Cell Metab. *19*, 574–591.

Sun, Q., Westphal, W., Wong, K.N., Tan, I., and Zhong, Q. (2010). Rubicon controls endosome maturation as a Rab7 effector. Proc. Natl. Acad. Sci. U. S. A. *107*, 19338–19343.

Sun, W., Winseck, A., Vinsant, S., Park, O., Kim, H., and Oppenheim, R.W. (2004). Programmed Cell Death of Adult-Generated Hippocampal Neurons Is Mediated by the Proapoptotic Gene Bax. J. Neurosci. *24*.

Suraweera, A., Lim, Y.C., Woods, R., Birrell, G.W., Nasim, T., Becherel, O.J., and Lavin, M.F. (2009). Functional role for senataxin, defective in ataxia oculomotor apraxia type 2, in transcriptional regulation. Hum. Mol. Genet. *18*, 3384–3396.

Suzuki, H., Tohyama, K., Nagata, K., Taketani, S., and Araki, M. (2007). Regulatory expression of Neurensin-1 in the spinal motor neurons after mouse sciatic nerve injury. Neurosci. Lett. *421*, 152–157.

Sykora, P., Wilson, D.M., and Bohr, V.A. (2012). Repair of persistent strand breaks in the mitochondrial genome. Mech. Ageing Dev. *133*, 169–175.

Synofzik, M., Gonzalez, M.A., Lourenco, C.M., Coutelier, M., Haack, T.B., Rebelo, A., Hannequin, D., Strom, T.M., Prokisch, H., Kernstock, C., et al. (2014). PNPLA6 mutations cause Boucher-Neuhäuser and Gordon Holmes syndromes as part of a broad neurodegenerative spectrum. Brain *137*, 69–77.

Takumi, T., Ishii, T., Horio, Y., Morishige, K., Takahashi, N., Yamada, M., Yamashita, T., Kiyama, H., Sohmiya, K., Nakanishi, S., et al. (1995). A novel ATP-dependent inward rectifier potassium channel expressed predominantly in glial cells. J. Biol. Chem. *270*, 16339–16346.

Tansey, T.R., and Shechter, I. (2000). Structure and regulation of mammalian squalene synthase. Biochim. Biophys. Acta *1529*, 49–62.

Tansey, M.G., Baloh, R.H., Milbrandt, J., and Johnson, E.M. (2000). GFRalpha-mediated localization of RET to lipid rafts is required for effective downstream signaling, differentiation, and neuronal survival. Neuron *25*, 611–623.

Tauche, A., Krause-Buchholz, U., and Rödel, G. (2008). Ubiquinone biosynthesis in Saccharomyces cerevisiae: The molecular organization of O-methylase Coq3p depends on Abc1p/Coq8p. FEMS Yeast Res. *8*, 1263–1275.

Teclebrhan, H., Jakobsson-Borin, A., Brunk, U., and Dallner, G. (1995). Relationship between the endoplasmic reticulum-Golgi membrane system and ubiquinone biosynthesis. Biochim. Biophys. Acta (BBA)/Lipids Lipid Metab. *1256*, 157–165.

Tekle, M., Bentinger, M., Nordman, T., Appelkvist, E.-L., Chojnacki, T., and Olsson, J.M. (2002). Ubiquinone biosynthesis in rat liver peroxisomes. Biochem. Biophys. Res. Commun. *291*, 1128–1133.

Terracciano, A., Renaldo, F., Zanni, G., D'Amico, A., Pastore, A., Barresi, S., Valente, E.M., Piemonte, F., Tozzi, G., Carrozzo, R., et al. (2012). The use of muscle biopsy in the diagnosis of undefined ataxia with cerebellar atrophy in children. Eur. J. Paediatr. Neurol. *16*, 248–256.

Todd, A.G., Lin, H., Ebert, A.D., Liu, Y., and Androphy, E.J. (2013). COPI transport complexes bind to specific RNAs in neuronal cells. Hum. Mol. Genet. *22*, 729–736.

Todorov, B., Kros, L., Shyti, R., Plak, P., Haasdijk, E.D., Raike, R.S., Frants, R.R., Hess, E.J., Hoebeek, F.E., De Zeeuw, C.I., et al. (2012). Purkinje cell-specific ablation of CaV2.1 Channels is sufficient to cause cerebellar ataxia in mice. Cerebellum *11*, 246–258.

Tong, L. (2005). Acetyl-coenzyme A carboxylase: Crucial metabolic enzyme and attractive target for drug discovery. Cell. Mol. Life Sci. *62*, 1784–1803.

Tran, U.C., and Clarke, C.F. (2007). Endogenous synthesis of coenzyme Q in eukaryotes. Mitochondrion *7*, S62-71.

Trouche, D., Grigoriev, M., Lenormand, J.L., Robin, P., Leibovitch, S.A., Sassone, C.P., and Harel, B.A. (1993). Repression of c-fos promoter by MyoD on muscle cell differentiation. Nature *363*, 79–82.

Trumpower, B.L. (1981). New concepts on the role of ubiquinone in the mitochondrial respiratory chain. J. Bioenerg. Biomembr. *13*, 1–24.

Tucci, S., Herebian, D., Sturm, M., Seibt, A., and Spiekerkoetter, U. (2012). Tissue-Specific Strategies of the Very-Long Chain Acyl-CoA Dehydrogenase-Deficient (VLCAD-/-) Mouse to Compensate a Defective Fatty Acid ??-Oxidation. PLoS One *7*, e45429.

Turunen, M., Olsson, J., and Dallner, G. (2004). Metabolism and function of coenzyme Q. Biochim. Biophys. Acta - Biomembr. *1660*, 171–199.

Uusisaari, M., and Knöpfel, T. (2013). Neurons of the Deep Cerebellar Nuclei. Handb. Cerebellum Cerebellar Disord. 1101–1110.

Vance, J.E. (2006). Lipid imbalance in the neurological disorder, Niemann-Pick C disease. FEBS Lett. *580*, 5518–5524.

Vega, R.B., Huss, J.M., and Kelly, D.P. (2000). The Coactivator PGC-1 Cooperates with Peroxisome Proliferator-Activated Receptor alpha in Transcriptional Control of Nuclear Genes Encoding Mitochondrial Fatty Acid Oxidation Enzymes. Mol. Cell. Biol. *20*, 1868–1876.

Velaz-Faircloth, M., Guadaño-Ferraz, A., Henzi, V.A., and Fremeau, R.T. (1995). Mammalian brain-specific L-proline transporter. Neuronal localization of mRNA and enrichment of transporter protein in synaptic plasma membranes. J. Biol. Chem. *270*, 15755–15761.

Vermeer, S., van de Warrenburg, B.P.C., Willemsen, M.A.A.P., Cluitmans, M., Scheffer, H., Kremer, B.P., and Knoers, N.V. a. M. (2011). Autosomal recessive cerebellar ataxias: the current state of affairs. J. Med. Genet. *48*, 651–659.

Voogd, J., and Glickstein, M. (1998). The anatomy of the cerebellum. Trends Neurosci. 370–375.

Walker, E.H., Perisic, O., Ried, C., Stephens, L., and Williams, R.L. (1999). Structural insights into phosphoinositide 3-kinase catalysis and signalling. Nature *402*, 313–320.

Walter, L., Nogueira, V., Leverve, X., Heitz, M.P., Bernardi, P., and Fontaine, E. (2000). Three classes of ubiquinone analogs regulate the mitochondrial permeability transition pore through a common site. J. Biol. Chem. *275*, 29521–29527.

Wang, Y., and Hekimi, S. (2013a). Molecular genetics of ubiquinone biosynthesis in animals. Crit. Rev. Biochem. Mol. Biol. *48*, 69–88.

Wang, Y., and Hekimi, S. (2013b). Mitochondrial respiration without ubiquinone biosynthesis. Hum. Mol. Genet. *22*, 4768–4783.

Wang, Y., Smith, C., Parboosingh, J.S., Khan, A., Innes, M., and Hekimi, S. (2017). Pathogenicity of two COQ7 mutations and responses to 2,4-dihydroxybenzoate bypass treatment. J. Cell. Mol. Med.

Wassef, M., Sotelo, C., Cholley, B., Brehier, A., and Thomasset, M. (1987). Cerebellar mutations affecting the postnatal survival of Purkinje cells in the mouse disclose a longitudinal pattern of differentially sensitive cells. Dev. Biol. *124*, 379–389.

Watmough, N.J., and Frerman, F.E. (2010). The electron transfer flavoprotein: Ubiquinone oxidoreductases. Biochim. Biophys. Acta - Bioenerg. *1797*, 1910–1916.

Weng, W., and Breslow, J.L. (1996). Dramatically decreased high density lipoprotein cholesterol, increased remnant clearance, and insulin hypersensitivity in apolipoprotein A-II knockout mice suggest a complex role for apolipoprotein A-II in atherosclerosis susceptibility. Proc Natl Acad Sci U S A *93*, 14788–14794.

White, J.J., and Sillitoe, R. V. (2013). Development of the cerebellum: From gene expression patterns to circuit maps. Wiley Interdiscip. Rev. Dev. Biol. *2*, 149–164.

Williams, M.J., Almén, M.S., Fredriksson, R., and Schiöth, H.B. (2012). What model organisms and interactomics can reveal about the genetics of human obesity. Cell. Mol. Life Sci. *69*, 3819–3834.

Williams, M.J., Eriksson, A., Shaik, M., Voisin, S., Yamskova, O., Paulsson, J., Thombare, K., Fredriksson, R., and Schiöth, H.B. (2015). The Obesity-Linked Gene Nudt3 Drosophila Homolog Aps Is Associated With Insulin Signaling. Mol. Endocrinol. *29*, 1303–1319.

Wittmann, M., Queisser, G., Eder, A., Wiegert, J.S., Bengtson, C.P., Hellwig, A., Wittum, G., and Bading, H. (2009). Synaptic Activity Induces Dramatic Changes in the Geometry of the Cell Nucleus: Interplay between Nuclear Structure, Histone H3 Phosphorylation, and Nuclear Calcium Signaling. J. Neurosci. *29*, 14687–14700.

Wu, G., and Morris Jr., S.M. (1998). Arginine metabolism: nitric oxide and beyond. Biochem. J *336 (Pt 1*, 1–17.

Xia, L., Björnstedt, M., Nordman, T., Eriksson, L.C., and Olsson, J.M. (2001). Reduction of ubiquinone by lipoamide dehydrogenase. An antioxidant regenerating pathway. Eur. J. Biochem. *268*, 1486–1490.

Xie, L.X., Hsieh, E.J., Watanabe, S., Allan, C.M., Chen, J.Y., Tran, U.C., and Clarke, C.F. (2011). Expression of the human atypical kinase ADCK3 rescues coenzyme Q biosynthesis and phosphorylation of Coq polypeptides in yeast coq8 mutants. Biochim. Biophys. Acta - Mol. Cell Biol. Lipids *1811*, 348–360.

Xie, L.X., Ozeir, M., Tang, J.Y., Chen, J.Y., Jaquinod, S.K., Fontecave, M., Clarke, C.F., and Pierrel, F. (2012). Overexpression of the Coq8 kinase in Saccharomyces cerevisiae coq null mutants allows for accumulation of diagnostic intermediates of the coenzyme Q6 biosynthetic pathway. J. Biol. Chem. *287*, 23571–23581.

Xie, Y.-F., Macdonald, J.F., and Jackson, M.F. (2010). TRPM2, calcium and neurodegenerative diseases. Int. J. Physiol. Pathophysiol. Pharmacol. *2*, 95–103.

Xue, M., Reim, K., Chen, X., Chao, H.-T., Deng, H., Rizo, J., Brose, N., and Rosenmund, C. (2007). Distinct domains of complexin I differentially regulate neurotransmitter release. Nat. Struct. Mol. Biol. *14*, 949–958.

Yang, L., Yang, Q., Zhang, K., Li, Y.-J., Wu, Y.-M., Liu, S.-B., Zheng, L.-H., and Zhao, M.-G. (2014). Neuroprotective Effects of Daphnetin against NMDA Receptor-Mediated Excitotoxicity. Molecules *19*, 14542–14555.

Ye, J., Palm, W., Peng, M., King, B., Lindsten, T., Li, M.O., Koumenis, C., and Thompson, C.B. (2015). GCN2 sustains mTORC1 suppression upon amino acid deprivation by inducing Sestrin2. Genes Dev. *29*, 2331–2336.

Yu, C.A., Zhang, L., Deng, K.P., Tian, H., Xia, D., Kim, H., Deisenhofer, J., and Yu, L. (1999). Structure and reaction mechanisms of multifunctional mitochondrial cytochrome bc1 complex. Biofactors *9*, 103–109.

Yubero, D., Montero, R., Armstrong, J., Espinós, C., Palau, F., Santos-Ocaña, C., Salviati, L., Navas, P., and Artuch, R. (2015). Molecular diagnosis of coenzyme Q10 deficiency. Expert Rev. Mol. Diagn. *15*, 1–11.

Zabezhinsky, D., Slobodin, B., Rapaport, D., and Gerst, J.E. (2016). An Essential Role for COPI in mRNA Localization to Mitochondria and Mitochondrial Function Cell Reports Report An Essential Role for COPI in mRNA Localization to Mitochondria and Mitochondrial Function. Cell Rep. *15*, 540–549.

Zammit, P.S. (2006). Pax7 and myogenic progression in skeletal muscle satellite cells. J. Cell Sci. *119*, 1824–1832.

Zanni, G., Calì, T., Kalscheuer, V.M., Ottolini, D., Barresi, S., Lebrun, N., Montecchi-Palazzi, L., Hu, H., Chelly, J., Bertini, E., et al. (2012). Mutation of plasma membrane Ca2+ ATPase isoform 3 in a family with X-linked congenital cerebellar ataxia impairs Ca2+ homeostasis. Proc. Natl. Acad. Sci. U. S. A. *109*, 14514–14519.

Zhao, D.Y., Gish, G., Braunschweig, U., Li, Y., Ni, Z., Schmitges, F.W., Zhong, G., Liu, K., Li, W., Moffat, J., et al. (2015). SMN and symmetric arginine dimethylation of RNA polymerase II C-terminal domain control termination. Nature *529*, 48–53.

Zhou, H., Lin, Z., Voges, K., Ju, C., Gao, Z., Bosman, L.W.J., Ruigrok, T.J., Hoebeek, F.E., De Zeeuw, C.I., and Schonewille, M. (2014). Cerebellar modules operate at different frequencies. Elife *2014*.

Ziosi, M., Di Meo, I., Kleiner, G., Gao, X.-H., Barca, E., Sanchez-Quintero, M.J., Tadesse, S., Jiang, H., Qiao, C., Rodenburg, R.J., et al. (2017). Coenzyme Q deficiency causes impairment of the sulfide oxidation pathway. EMBO Mol. Med. *9*, 96–111.

Zoratti, M., and Szabò, I. (1995). The mitochondrial permeability transition. Biochim. Biophys. Acta *1241*, 139–176.

FRENCH SUMMARY

Exploration du fonctionnement mitochondrial dans le muscle et des dérégulations moléculaires dans le cervelet d'un modèle murin d'ARCA2, une ataxie récessive associée à un déficit en coenzyme Q_{10}

I. Introduction

ARCA2, Autosomal Recessive Cerebellar Ataxia type 2, est une ataxie cérébelleuse caractérisée par une atrophie du cervelet et un léger déficit en Coenzyme Q_{10}. Outre des problèmes de coordination fine et des troubles de l'équilibre, propres à l'ataxie, certains patients présentent des signes neurologiques supplémentaires comme de l'épilepsie et un léger retard mental ainsi que d'autres symptômes comme une intolérance à l'exercice (Lagier-Tourenne et al., 2008). Les mutations responsables d'ARCA2 sont localisées dans le gène *COQ8A* (aussi appelé *ADCK3* ou *CABC1*) et induisent une perte de fonction. *COQ8A* code pour une kinase mitochondriale putative, homologue à Coq8p chez S.*cerevisiae* et à UbiB chez les bactéries, toutes deux nécessaires à la biosynthèse du coenzyme Q (CoQ, aussi appelé ubiquinone). La protéine Coq8p chez la levure a deux homologues chez l'homme et la souris : COQ8A (ADCK3) et COQ8B (ADCK4), qui sont des paralogues. Au cours de ma thèse, il a été montré que COQ8A est une protéine kinase-like non-orthodoxe (se liant à des lipides), qui participe à la biosynthèse du CoQ et semble améliorer l'activité du complexe Q (par son activité ATPase), même si les mécanismes d'action restent encore à élucider (Stefely et al., 2016).

Le CoQ, une molécule lipophile présente dans toutes les membranes, possède de nombreuses fonctions. Il a notamment un rôle de transport des électrons dans la chaîne respiratoire mitochondriale (Yu et al., 1999), d'antioxydant (Frei et al., 1990) et contribue à la structure des membranes (Turunen et al., 2004). De plus, la biosynthèse du CoQ est liée à celle du cholestérol par la voie métabolique du mévalonate.

Pour comprendre les mécanismes pathologiques d'ARCA2 et étudier la fonction de COQ8A, un mutant Coq8a knock-out constitutif ($Coq8a^{-/-}$) murin a été généré. Les souris $Coq8a^{-/-}$ récapitulent la plupart des symptômes observés chez les patients atteints d'ARCA2, ce sont donc de bons modèles pour étudier la physiopathologie de cette maladie (thèse Licitra, 2013; Stefely et al., 2016).

Il a précédemment été montré au laboratoire que les souris mutantes présentent un déficit en CoQ_9 (l'équivalent du CoQ_{10} chez l'homme) dans certains tissus, ainsi qu'une ataxie (débutant entre 5 et 10 semaines chez la souris) mais sans atrophie du cervelet. De plus ces souris présentent également une élévation de certains lipides sanguins (cholestérol total, HDL, LDL et acides gras saturés), une intolérance à l'exercice, ainsi qu'une susceptibilité accrue à l'épilepsie. Dans le muscle, seul l'analyse ultrastructurale de quadriceps de souris de 7 mois a montré une anomalie mitochondriale dans certaines fibres. Néanmoins, dans des souris du même âge la respiration mitochondriale musculaire reste inchangée, même après exercice (Licitra, 2013; Stefely et al., 2016).

Lors de ma thèse je me suis intéressée aux différents phénotypes observés chez la souris, et pour certains retrouvés chez l'homme, en essayant de comprendre les voies physiopathologiques impliquées. Le but étant de mieux comprendre la maladie et à terme pouvoir soulager certains symptômes des patients.

Mon projet de thèse c'est divisé en plusieurs parties. Pendant ma première année, j'ai tenté d'explorer deux aspects du phénotype chez la souris : élucider les causes de la dyslipidémie et voir s'il pouvait y avoir un lien avec le déficit en CoQ ; et identifier les causes de l'épilepsie, notamment au niveau de l'hippocampe. Les résultats sur ces deux projets n'étant pas concluant, et après discussion avec mon comité de mi-thèse, je me suis ensuite tournée vers la compréhension de la dégénérescence des cellules de Purkinje dans le cervelet et vers la potentielle altération de la chaîne respiratoire mitochondriale, surtout dans les muscles.

Afin d'étudier ces défauts, j'ai généré des modèles cellulaires (culture organotypiques de cervelets et cultures primaires d'hippocampe, de cervelet et de muscles), ce qui m'a permis d'effectuer des expériences difficiles *in vivo*. Les cultures organotypiques ont l'avantage de conserver la structure du cervelet et donc l'organisation des cellules tout en étant un système *in vitro*. Les cultures primaires permettent quant à elles d'avoir des neurones ou cellules musculaires isolés.

II. Résultats

1. Dyslipidémie

Un des buts de ma thèse était d'élucider les causes de la dyslipidémie et l'éventuel lien avec le déficit en CoQ, en sachant que les voies de biosynthèse du CoQ et du cholestérol sont liées. Ces 2 molécules sont produites à partir du farnésyl-pyrophosphate (FPP) par la voie métabolique du mévalonate. Je me suis donc intéressée à la dérégulation potentielle de gènes de cette voie métabolique. La quantité de transcrits de différents gènes a été évaluée par qRT-PCR sur des foies de souris WT (Wild type) et Coq8a$^{-/-}$ de 27 semaines (âge où la dyslipidémie est observée chez les souris Coq8a$^{-/-}$). Les résultats non significatifs et la grande variabilité entre les contrôles m'ont conduit à répéter ces expériences dans des souris ayant jeûnés. Aucune différence significative n'a tout de même pu être constatée. Des analyses ultra-structurale du foie ont confirmé l'absence de phénotype clair au niveau de cet organe malgré le taux réduit en CoQ dans celui-ci.

Aux vues des taux de CoQ réduits dans certains organes chez les souris Coq8a$^{-/-}$ et de nouveaux résultats obtenus au laboratoire et par des collaborateurs, qui semblaient plus prometteurs, je me suis ensuite orienté vers l'identification des interacteurs de COQ8A.

2. Interactions

COQ8A, par homologie avec Coq8p chez S.*cerevisiae* (Lagier-Tourenne et al., 2008), semble avoir un rôle dans la biosynthèse du CoQ et Coq8p a été décrit comme phosphorylant certaines protéines Coq: Coq3p, Coq5p, Coq7p (Xie et al., 2011). De plus, par analyse protéomique de tissus des souris Coq8a$^{-/-}$, il a été observé que certaines protéines COQ sont sous-exprimées. Nous avons pu confirmer ces résultats pour COQ7, par Western blot, dans plusieurs tissus et nous avons montré que cette dérégulation apparait très tôt (déjà à l'état embryonnaire). Nous avons donc cherché à savoir si COQ8A interagit directement avec certaines de ces protéines COQ, par immunoprécipitation, et si cette interaction varie en fonction du sucre utilisé (glucose/galactose) et du substrat (ADP/ATP). J'ai répété l'expérience dans des cellules COS par surexpression des protéines avec un tag Flag (COQ8A) et HA (COQ4, 5 ou 9). Lors de ces expériences, les protéines apparaissent avec un poids moléculaire plus élevé en Western blot pour les fractions d'immunoprécipitations. Malgré les optimisations (dilution des échantillons et changement de tampon d'élution), les résultats restent inchangés. Cependant ces expériences ont tout de même permis de confirmer l'interaction de COQ8A avec COQ5 dans

différentes conditions (absence ou présence d'ADP ou d'ATP) et de confirmer les résultats de l'interaction de COQ8A avec COQ4 et COQ5 mais pas COQ9 (Figure 66), pour la publication réalisé en collaboration (Stefely et al., 2016).

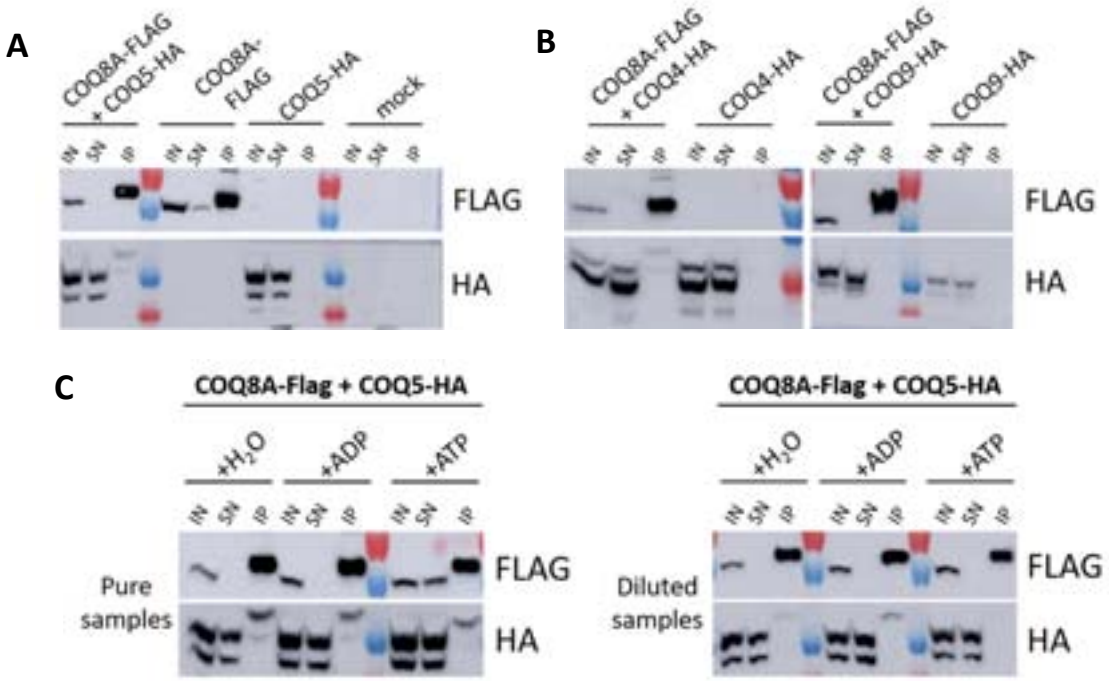

Figure 66 : COQ8A interagit avec COQ5 and COQ4, et l'interaction avec COQ5 est plus forte en présence d'ADP.

Western blots des immunoprécipitations de COQ8A-FLAG et COQ-HA transfectés dans des cellules COS et immunoprécipité avec des billes anti-FLAG. Détection réalisée grâce aux anticorps contre les tags FLAG et HA. IN : mélange initial, SN : surnageant, IP : immunoprécipitation. A) COQ8A-FLAG et COQ5-HA transfectés dans des cellules COS. COQ8A-FLAG seul, ou COQ5-HA ou mock (addition uniquement de Fugene) servent de contrôle pour l'immunoprécipitation. B) COQ8A-FLAG et COQ4-HA ou COQ9-HA, transfectés dans des cellules COS. C) COQ8A-FLAG et COQ5-HA transfectés dans des cellules COS. Additiion d'ATP ou d'ADP aux lysats avant et pendant l'immunoprécipitation (H_2O pris comme contrôle). Gauche : échantillons purs, droite : échantillons dilués avant chargement sur gel.

3. Respiration mitochondriale

L'absence de COQ8A dérégulant certaines protéines COQ et entrainant un léger déficit de CoQ, nous avons testé la respiration mitochondriale, puisque le CoQ est nécessaire au transport des électrons du complexe I et II vers le complexe III de la chaîne respiratoire. Une étude précédemment menée au laboratoire (par Leïla Laredj, postdoctorante) avait montré que les cellules musculaires semblaient affectées (altération de la chaîne respiratoire mitochondriale). J'ai donc cherché à savoir si les mitochondries peuvent fonctionner normalement avec un niveau réduit de certaines protéines de la biosynthèse du CoQ, surtout dans les cellules ayant un besoin énergétique plus important (neurones

et muscles). La respiration mitochondriale, si elle est affectée, devrait l'être tôt, puisqu'au stade embryonnaire dans les souris Coq8a$^{-/-}$ le niveau protéique de COQ7 est déjà diminué. Nous avons donc choisi d'utiliser des modèles cellulaires pour étudier la respiration mitochondriale (cultures primaires de muscles : myoblastes).

Après avoir vérifié que la morphologie des myoblastes et leur différentiation est similaire entre les deux génotypes, j'ai optimisé les différents paramètres (densité cellulaire et concentration des composés) nécessaires pour la mesure de cette respiration avec la technologie Seahorse (BD Bioscience). Les respirations mitochondriales mesurées étant similaires dans les cultures de muscles Coq8a$^{-/-}$ par rapport aux cultures WT, j'ai cherché à exacerber un phénotype en obligeant les cellules à utiliser leurs mitochondries, en remplaçant le glucose du milieu par du galactose. Les résultats restent inchangés dans ces nouvelles conditions.

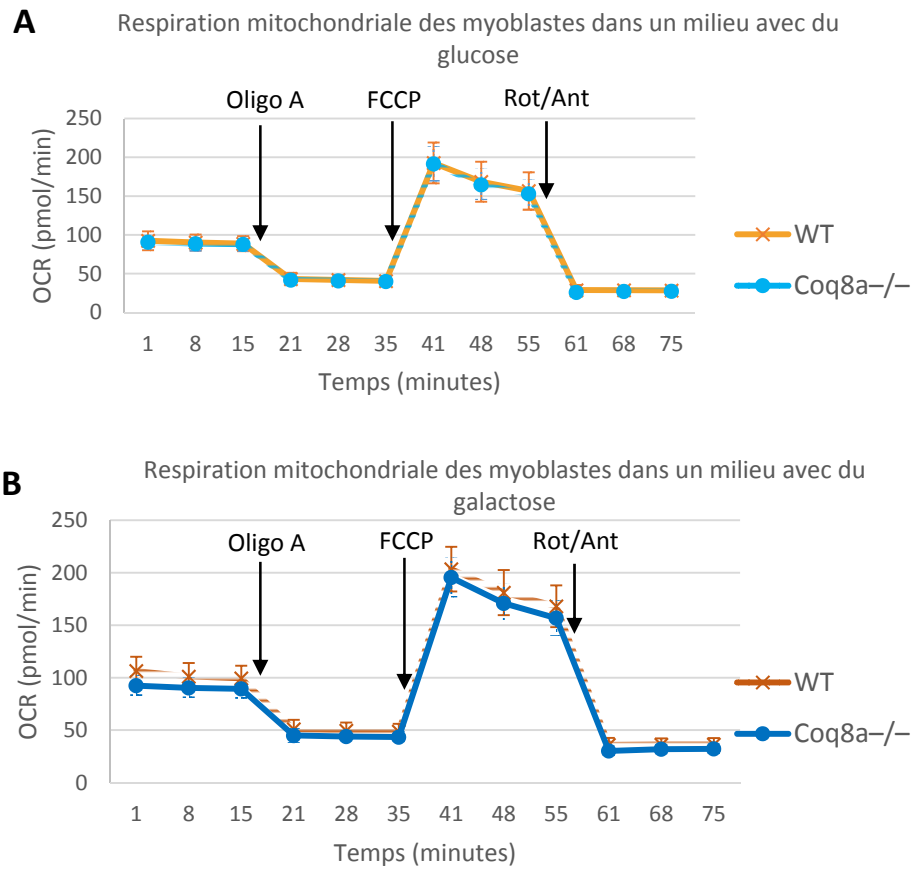

Figure 67 : La respiration mitochondriale n'est pas affectée dans les myoblasts Coq8a$^{-/-}$.

Taux de consommation d'oxygène (OCR: Oxygen Consumption Rate) mesuré avec un appareil Seahorse, en pmol O_2/min. Données normalisées avec le nombre de cellules. Moyenne ± déviation standard. n=6. A) Respiration des myoblastes dans un milieu avec glucose, avec injection pour une concentration finale de 1,5 µM d'oligomycin A (OligoA), 1 µM de FCCP et 0,5 µM de rotenone/antimycin A (Rot/Ant). B) Respiration des myoblastes dans un milieu avec galactose, avec injection pour une concentration finale de 2 µM d'oligomycin A (OligoA), 1 µM de FCCP et 0,5 µM de rotenone/antimycin A (Rot/Ant).

Nous savons que les souris Coq8a$^{-/-}$ ont un niveau basal de glucose circulant dans le sang plus élevé que les WT. Il est donc possible que les cellules des souris mutantes favorisent la glycolyse pour produire l'énergie nécessaire et compenser un défaut mitochondrial. J'ai donc mesuré la glycolyse dans les mêmes lignées que précédemment, toujours avec la technologies Seahorse. Comme auparavant les myoblastes des 2 génotypes ont des niveaux de glycolyse comparables. Contrairement à ce attendu, les mitochondries mutantes ne présentent aucun défaut de phosphorylation oxydative, ni de glycolyse.

4. Atteinte neuronale

Les souris Coq8a$^{-/-}$, comme les patients ARCA2, présentent deux atteintes au niveau du cerveau, à savoir de l'épilepsie et l'ataxie.

a. Epilepsie

Certains patients ARCA2 présentent une épilepsie et un faible retard mental. Les souris mutantes reproduisent ce phénotype avec une susceptibilité à l'épilepsie et une mémoire spatiale légèrement retardée (test de la piscine de Morris). L'hippocampe jouant un rôle dans la mémoire spatiale et pouvant être l'épicentre de l'épilepsie, j'ai étudié cette région du cerveau en histologie et par la culture de neurones primaires d'hippocampe.

Après avoir perfusé des souris de 25 semaines (âge du test de la susceptibilité à l'épilepsie), j'ai fixé et coupé les tissus avant de les colorer au Luxol et Crésyl violet. L'histologie, grâce à une analyse morphométrique de l'hippocampe m'a permis d'observer que les cerveaux des souris Coq8a$^{-/-}$ sont similaires à ceux des WT. Il en est de même pour les cultures de neurones primaires d'hippocampes.

Par Western blot, le niveau de récépteurs GABAergiques et glutamatergiques, connus pour induire de l'épilepsie, ont été testés mais les résultats divergent entre deux cohortes de souris.

L'analyse ultrastructurale de cette même région, a révélé une dégénérescence de certains neurones, autant présente dans les hippocampes de souris mutantes que sauvages. Toutefois la microscopie électronique a révélé des invaginations nucléaires plus importantes dans certains neurones de l'hippocampe des souris Coq8a$^{-/-}$ (Figure 68). Pour l'instant aucune hypothèse expliquant ces résultats n'a été trouvée, mais cela pourrait être dû à une dérégulation calcique (Wittmann et al., 2009). Cela reste incertain si ce phénomène est pathologique ou physiologique.

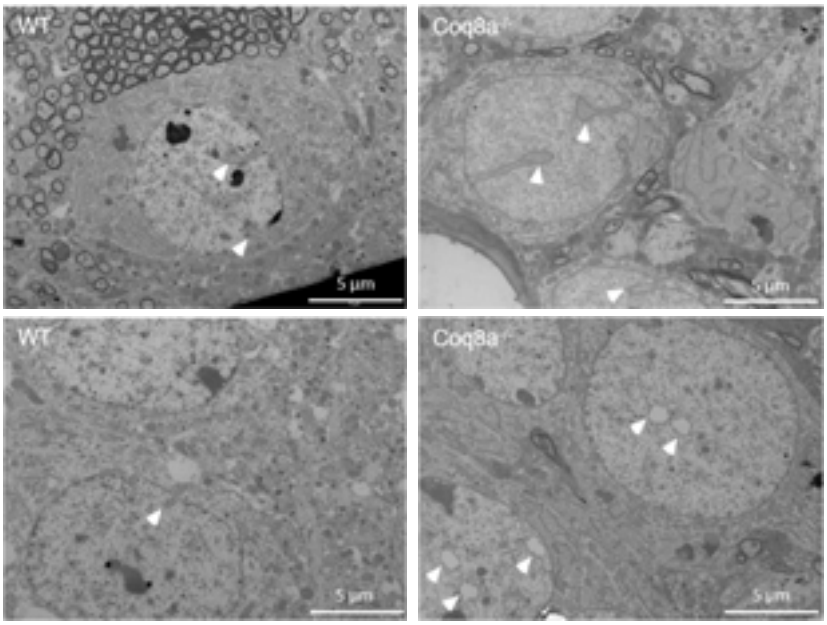

Figure 68 : Invaginations nucléaires de neurones de l'hippocampe observées par microscopie électronique dans des souris Coq8a$^{-/-}$ de 30 semaines.

Microscopie électronique à transmission d'hippocampes de souris de 30 semaines. Invaginations nucléaires (flèches). Echelle : 5 µM. Gauche : WT, droite : Coq8a$^{-/-}$. n=2.

L'épilepsie n'est pas retrouvée chez tous les patients et elle peut émaner d'autres régions du cerveau, comme du cortex. N'ayant pas assez de pistes pour continuer d'explorer cette voie, je me suis concentrée sur le phénotype ataxique, lié à un défaut dans le cervelet.

b. Ataxie-dégénérescence des cellules de Purkinje

La maladie se caractérise par le phénotype ataxique, dû à un dysfonctionnement du cervelet. Cette atteinte du cervelet, observée chez les patients, est retrouvée chez les souris Coq8a$^{-/-}$ avec notamment une dégénérescence des cellules de Purkinje, ainsi que des anomalies ultra-structurales et électrophysiologiques (mais sans atrophie contrairement aux patients) (Stefely et al., 2016).

Mon sujet de thèse s'est donc orienté vers l'identification de la cause de cette ataxie, et de la dégénérescence des cellules de Purkinje. Pour cela j'ai notamment étudié certains canaux ioniques, qui sont connus comme étant responsables d'ataxies et induisant un phénotype similaire en électrophysiologie. En parallèle de multiples optimisations d'immuno-marquage infructueuses (notamment divers démasquages), l'analyse de ces canaux par western blot a été étudié mais sans dérégulation de ceux-ci au niveau protéique. De plus, des cultures organotypiques et primaires ont

révélés un branchement et une morphologie des cellules de Purkinje normal, qui laisse à penser que le phénotype n'apparait que plus tardivement, malgré le stress des cellules par la mise en culture.

Par une approche de RNA-sequencing, effectuée notamment dans le muscle et le cervelet de souris Coq8a$^{-/-}$ et WT de 30 semaines, un certain nombre de gènes apparaissent dérégulés. Il semble qu'une partie de ces gènes soit impliquée notamment dans le métabolisme des lipides et le transport des ions. Ces fonctions sont intéressantes aux vues de la fonction de COQ8A et des phénotypes observés chez les souris mutantes (Stefely et al., 2016). Nous voulions savoir si cette dérégulation est précoce et si elle est retrouvée dans nos cultures. Pour cela, j'ai validé par qRT-PCR la dérégulation de certains gènes, dans les cervelets de souris de 30, 20, 10, 5 et 1 semaines. De la cinquantaine de gènes testés, vingt-sept transcrits sont déjà dérégulés à 5 semaines dans les cervelets de souris Coq8a$^{-/-}$, et deux à 1 semaine : ApoAII (Figure 69), un gène codant pour une apolipoprotéine présente dans les HDL (High Density Lipoprotein) et COPA (Figure 70), codant pour une protéine de transport de l'appareil de Golgi vers le réticulum endoplasmique. Par Western blot, j'ai commencé à vérifier si ces dérégulations induisent également un changement protéique. Seule SYT17, une synaptotagmin, jouant un rôle potentiel dans la formation de dendrites, a pour l'instant été observée comme surexprimée au niveau transcriptionnel et protéique dans des cervelets de souris mutantes de 5 semaines (Figure 71). Une étude histologique est en cours et les voies métaboliques validées comme dérégulées qui semblent les plus pertinentes vont être explorées.

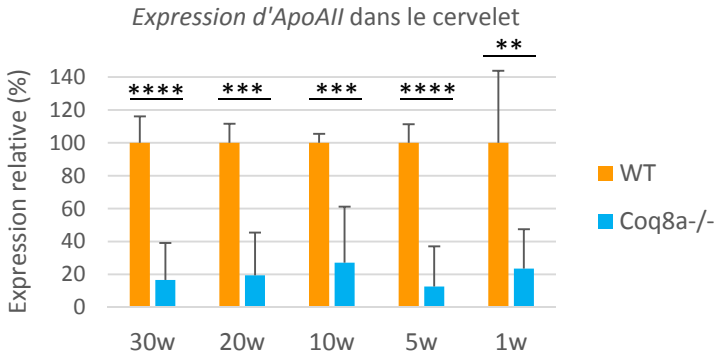

Figure 69 : Les souris Coq8a$^{-/-}$ ont un niveau de transcrits d'ApoAII réduit de 1 à 30 semaines dans le cervelet.

Expression relative des transcrits d'*ApoAII* dans le cervelet de souris Coq8a$^{-/-}$ et WT de 30, 20, 10, 5 et 1 semaines. n=6. Pour toutes les expériences : normalisation du niveau de transcrits sur le niveau de transcrits d'*Hprt* (gène contrôle). Barres d'erreurs : déviation standard, ** = p<0.005, ***=p<0.0005, ****=p<0.00005.

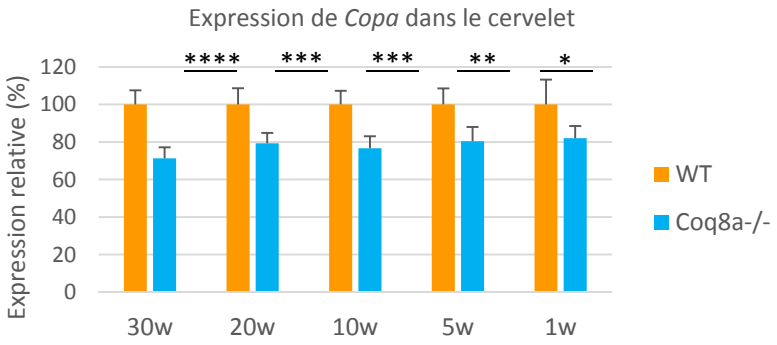

Figure 70 : Les souris Coq8a$^{-/-}$ ont un niveau de transcrits de COPA réduit de 1 à 30 semaines dans le cervelet.

Expression relative des transcrits de COPA dans le cervelet de souris Coq8a$^{-/-}$ et WT de 30, 20, 10, 5 et 1 semaines. n=6. Pour toutes les expériences : normalisation du niveau de transcrits sur le niveau de transcrits d'*Hprt* (gène contrôle). Barres d'erreurs : déviation standard, *=p<0.05, ** = p<0.005, ***=p<0.0005, ****=p<0.00005.

Figure 71 : La protéine SYT17 est plus exprimée dans le cervelet des souris Coq8a$^{-/-}$ de 5 semaines que dans les WT.

Expression de SYT17 observée par Western blots dans les cervelets de souris de 5 semaines. GAPDH pris comme protéine contrôle.

III. Conclusions-perspectives

Les modèles cellulaires utilisés n'ont, jusqu'à présent, pas permis de mieux comprendre la maladie, ni la fonction de COQ8A. Il se pourrait que les cultures soient effectuées avec des cellules trop jeunes et que le phénotype mette plus de temps à s'exprimer. Il pourrait être envisagé de stresser les cultures (notamment avec de l'H_2O_2) et de mesurer le taux de ROS cellulaire et mitochondrial grâce à des sondes fluorescentes (CM-H_2-DCFDA et mitoSOX respectivement) pour voir si un phénotype peut être exacerbé.

Concernant le cervelet, il avait précédemment été montrée au laboratoire, sur des coupes histologiques de cervelets de souris de 30 semaines, que des cellules de Purkinje dégénèrent. Cependant nous ne savons pas si ce phénomène est étendu à tout le cervelet ou restreint à certaines zones (lobules, vermis, hémisphères…). De plus, il a été montré dans certaines pathologies affectant

le cervelet, que la dégénérescence suit un motif bien défini correspondant aux bandes zebrin-II-positives et négatives. Il serait intéressant de savoir si cela est également le cas dans les souris *Coq8a*$^{-/-}$. Suivant les résultats obtenus, et si un lien est établi, nous saurons si un motif protège les neurones de la dégénérescence et s'il existe une différence de métabolisme qui pourrait les rendre plus ou moins susceptibles. De plus si la dérégulation de certains canaux est confirmée à un stade précoce, nous pourrions avoir recourt à l'électrophysiologie pour confirmer leur implication.

Au travers de cette thèse, j'ai ainsi pu montrer : que la voie de biosynthèse du mévalonate ne semble pas être dérégulée et ne peut donc pas expliquer la dyslipidémie des souris Coq8a$^{-/-}$; que l'interaction de COQ8A avec COQ4 et COQ5 est confirmée, ce qui renforce l'idée que COQ8A fait partie du la biosynthèse du CoQ, même si son rôle est encore à explorer ; que l'altération du niveau de certaines protéines COQ n'affecte pas la respiration mitochondriale, ni ne promeut la glycolyse ; que l'épilepsie pourrait ne pas provenir de l'hippocampe ; et enfin que des dérégulations moléculaires apparaissent précocement dans le cervelet des souris mutantes. Il reste à élucider si ces dernières dérégulations induisent l'ataxie ou si elles n'en sont qu'une résultante. Les voies métaboliques dérégulés restent encore à explorer pour mieux comprendre ce qu'il se passe lors du développement de la maladie, et essayer de clarifier le rôle de COQ8A dans les différents tissus.

Références :

Frei, B., Kim, M.C., and Ames, B.N. (1990). Ubiquinol-10 is an effective lipid-soluble antioxidant at physiological concentrations. Proc. Natl. Acad. Sci. U. S. A. *87*, 4879–4883.

Lagier-Tourenne, C., Tazir, M., López, L.C., Quinzii, C.M., Assoum, M., Drouot, N., Busso, C., Makri, S., Ali-Pacha, L., Benhassine, T., et al. (2008). ADCK3, an ancestral kinase, is mutated in a form of recessive ataxia associated with coenzyme Q10 deficiency. Am. J. Hum. Genet. *82*, 661–672.

Licitra, F. (2013). Pathophysiological and molecular characterization of a mouse model of ARCA2, a recessive cerebellar ataxia associated to Coenzyme Q10 deficiency. Http://www.theses.fr.

Stefely, J.A., Licitra, F., Laredj, L., Reidenbach, A.G., Kemmerer, Z.A., Grangeray, A., Jaeg-Ehret, T., Minogue, C.E., Ulbrich, A., Hutchins, P.D., et al. (2016). Cerebellar Ataxia and Coenzyme Q Deficiency through Loss of Unorthodox Kinase Activity. Mol. Cell *63*, 608–620.

Turunen, M., Olsson, J., and Dallner, G. (2004). Metabolism and function of coenzyme Q. Biochim. Biophys. Acta - Biomembr. *1660*, 171–199.

Wittmann, M., Queisser, G., Eder, A., Wiegert, J.S., Bengtson, C.P., Hellwig, A., Wittum, G., and Bading, H. (2009). Synaptic Activity Induces Dramatic Changes in the Geometry of the Cell Nucleus: Interplay between Nuclear Structure, Histone H3 Phosphorylation, and Nuclear Calcium Signaling. J. Neurosci. *29*, 14687–14700.

Xie, L.X., Hsieh, E.J., Watanabe, S., Allan, C.M., Chen, J.Y., Tran, U.C., and Clarke, C.F. (2011). Expression of the human atypical kinase ADCK3 rescues coenzyme Q biosynthesis and phosphorylation of Coq polypeptides in yeast coq8 mutants. Biochim. Biophys. Acta - Mol. Cell Biol. Lipids *1811*, 348–360.

Yu, C.A., Zhang, L., Deng, K.P., Tian, H., Xia, D., Kim, H., Deisenhofer, J., and Yu, L. (1999). Structure and reaction mechanisms of multifunctional mitochondrial cytochrome bc1 complex. Biofactors *9*, 103–109.

Tiphaine JAEG

Exploration du fonctionnement mitochondrial dans le muscle et des dérégulations moléculaires dans le cervelet d'un modèle murin d'ARCA2, une ataxie récessive associée à un déficit en coenzyme Q_{10}

Résumé

ARCA2 est une ataxie autosomique récessive rare, caractérisée par une atrophie du cervelet et un léger déficit en Coenzyme Q_{10} (CoQ). La majorité des patients présentent des signes neurologiques supplémentaires comme l'épilepsie ou l'intolérance à l'exercice. La maladie est due à des mutations dans le gène *COQ8A* qui semble encoder une protéine kinase-like atypique, impliquée dans la biosynthèse du CoQ. Pour comprendre les mécanismes physiopathologiques, une souris Coq8a knock-out (KO) constitutif a été générée et récapitule les symptômes observés chez les patients. Le but de ce travail de thèse était de mieux comprendre certains aspects, notamment l'intolérance à l'exercice et l'ataxie. Malgré un déficit en CoQ dans les muscles, aucun défaut de respiration mitochondriale n'a été détecté dans un modèle cellulaire de muscle. Néanmoins, dans le cervelet, les niveaux de transcrits de 27 gènes sont dérégulés, précocement dans l'apparition de la pathologie chez les souris KO. Les voies métaboliques vont être explorées, ce qui devrait permettre de relier la fonction de COQ8A au taux de CoQ et aux symptômes observés chez les patients.

Mots-clés : Ataxie, ARCA2, ADCK3/COQ8A, Coenzyme Q, respiration mitochondriale, dérégulation moléculaire

Résumé en anglais

ARCA2, a rare form of recessive ataxia, is characterized by early onset progressive ataxia, cerebellar atrophy and a mild Coenzyme Q_{10} deficiency. Most of the patients show additional neurological signs such as epilepsy and exercise intolerance. Mutations in the *COQ8A* gene lead to ARCA2. COQ8A is suggested as being an unorthodox protein kinase like, with a regulatory role in CoQ biosynthesis, in mammals. To better understand ARCA2, a constitutive Coq8a knock-out (KO) mouse model was generated, which recapitulates most of the patient's symptoms. Here we report the use of cellular models and the affected tissues to uncover the molecular signature of COQ8A loss and CoQ deficit. Despite CoQ deficit in the muscle, no mitochondrial bioenergetics defect was uncovered. In parallel, we have identified, by RT-qPCR, a key set of genes that are dysregulated in cerebellum, very early on in the pathology. We are currently investigating these pathways to uncover the link with COQ8A function. Altogether, our experiments will shed light on the early molecular events that lead to ARCA2 and may help draw a link between COQ8A function, CoQ pools and the symptoms observed in patients.

Keywords: Ataxia, ARCA2, ADCK3/COQ8A, Coenzyme Q, mitochondrial respiration, molecular dysregulation